ANALYTICAL APPLICATIONS OF ION/MOLECULE REACTIONS USING A TRIPLE QUADRUPOLE MASS SPECTROMETER

By

Timothy Gordon Heath

A DISSERTATION

Submitted to
Michigan State University
in partial fulfillment of the requirements
for the degree of

DOCTOR OF PHILOSOPHY

Department of Chemistry

1990

ABSTRACT

ANALYTICAL APPLICATIONS OF ION/MOLECULE REACTIONS USING A TRIPLE QUADRUPOLE MASS SPECTROMETER

By

Timothy Gordon Heath

Tandem mass spectrometry (MS/MS) has been a valuable tool in the study of gas-phase ion chemistry. Triple quadrupole mass spectrometers have proven to be versatile instruments for MS/MS studies, in both fundamental and analytical applications. The second quadrupole collision chamber (Q_2) provides a region where low-energy ion/molecule interactions may probe structural features of gaseous ions. Evaluation of the ionic products detected following the second stage of mass analysis provides insight into the gas-phase chemistry occurring within Q_2, and may lead to innovative analytical applications based on selective chemistry.

Utilization of a triple quadrupole mass spectrometer for exploring ion/molecule reactions has resulted in novel analytical applications. Studies of ion/molecule reactions involving aryl cations led to applications for detection of aromatic ions which contain a vacant charged site on the ring. The reactivity of $C_7H_7^+$ isomers with selected neutral reagents has been investigated and, as predicted by the thermochemistry, only the tolyl cation undergoes ring addition reactions with nucleophilic reagents while benzyl and tropylium cations do not.

Ion/molecule reactions are not limited to positive ions. A reaction involving molecular anions of abscisic acid methyl ester (ABA-Me) and molecular oxygen was elucidated. Oxygen-activated fragmentation results in the formation of structurally diagnostic ions. This ion/molecule reaction

approach was used to analyze ABA-Me in ^{18}O-labeling studies, and the results provided insight into the biosynthetic pathway of abscisic acid.

Not all the studies involve reactions carried out in the collision cell. Ion/molecule reactions may occur in the ion source, with ionic products then being subjected to collision-induced dissociation (CID). This approach was used extensively in the study of reactions involving protonated carbonyl compounds and alcohols. Comparison of the CID daughter ion mass spectra derived from known ion structures with those of unknown product ions suggests alkylation occurs on the carbonyl oxygen. In addition, the inherent selectivity of conventional MS/MS using CID is demonstrated in the analysis of dexamethasone. Finally, ion/molecule reactions of protonated molecules with hexamethyldisilazane were studied. Whereas, the gas-phase silylation reaction was demonstrated, its selectivity for protonated molecules remains unknown.

To my darling Melissa.

ACKNOWLEDGMENTS

I would like to thank my research advisor, Dr. J. Throck Watson for his support and encouragement throughout my graduate school career. I would also like to thank the rest of my guidance committee, especially Dr. John Allison, who continually emphasized the importance of evaluating the experimental mass spectral results in terms of the thermochemistry of the reaction.

There are many people to whom I am grateful for having the opportunity to work with, and whose assistance contributed to my successful completion of the degree requirements. Thanks to Dr. J.A.D. Zeevaart, Doug Gage, Chris Rock, Greg Dolnikowski, and Kathleen Kayganich for their efforts in enjoyable collaborative projects. I would also like to thank Curt Heine, Paul O'Connor, Ron Lopshire, Mark Cole, Mike Davenport, Mel Micke along with the rest of the crew at the Michigan State Mass Spectrometry Facility, for their assistance in my research efforts.

I am also grateful for the love, encouragement, and support I received from my family, especially from my parents, while I was pursuing my degree. Also, I would like to thank fellow 'Hags', Kurt Kooyer and Kevin Heath, for their tremendous friendship. I have many fond memories of; spring training drills in March, softball with "The Goats" (and SBC), "Prairie Home..." barbecues in the summer evenings, football in September, and the annual UM-MSU battle in October. And to Kevin and Greg Heath, I will never forget the two-day, thousand-mile, four-state expedition to see (in 24 hours) ball games at Municipal, Three-Rivers and Riverfront Stadiums.

I am very grateful to my wife, Melissa. I feel blessed to have married someone as wonderful as you. Thanks for your continued love, support, and encouragement throughout these past few years while I have been a student. At last, I think I am done.

And finally, I would like to thank my heavenly father for his grace and kindness shown to me. I echo the psalmist's words, *"Praise the Lord, O my soul, and forget not all his benefits."* (Psalm 103:2).

TABLE OF CONTENTS

LIST OF TABLES

LIST OF FIGURES

CHAPTER I

INTRODUCTION AND OBJECTIVES

A. Introduction

Mass spectrometry has provided the capability for studying ion/molecule chemistry in a solvent-free environment. Tandem mass spectrometry (MS/MS) has extended this capability, enabling further exploration of gas-phase ion/molecule phenomena. The primary focus of the research described in this dissertation involves the investigation of gas-phase ion/molecule reactions using a triple quadrupole mass spectrometer (TQMS). The principal intent has been to develop novel analytical methodology which utilizes gas-phase ion/molecule reactions of a selected mass-analyzed reactant ion with a reagent gas which is introduced into the collision cell of a TQMS for a tandem MS analysis.

There are numerous avenues by which this goal of developing the analytical utility of ion/molecule reactions may be realized. Some of the experimental results could have obvious analytical implications, as in the study of an ion/molecule reaction which leads to development of an MS/MS assay for a biologically important compound. However, the analytical implications of other experimental results may be more subtle. Perhaps studying ion/molecule reactions in a TQMS will reveal alternative methods which would assist in the elucidation of ion/molecule reaction mechanisms, or in the probing of ionic or neutral structures. Various applications are discussed in this dissertation and all serve to demonstrate the continued

flexibility and diversity of a triple quadrupole mass spectrometer for studying gas-phase ion/molecule chemistry.

The objective of this first chapter is to: (i) introduce the instrumentation used in this research, that being the triple quadrupole mass spectrometer, (ii) discuss the different modes of ion activation in an analysis by MS/MS using TQMS and, (iii) lay out the rationale for pursuing the investigation of ion/molecule reactions with a TQMS. Towards the end of this chapter, the effort extended by other researchers in studying ion/molecule reactions with triple quadrupole mass spectrometry, will be reviewed. This section provides an overview of the published successes, which serves to demonstrate the analytical value of a TQMS in studying ion/molecule reactions and the types of experiments accessed by a TQMS. Finally this chapter will conclude with a guideline to the research objectives.

B. Triple quadrupole mass spectrometry

1. *Instrumentation*

The ability to mass-select an ion of a specific mass-to-charge ratio (m/z) in the first stage of analysis, for introduction into a spatially-separated reaction chamber, which is followed by a second stage of mass analysis, provides a powerful tool for studying gas-phase ion chemistry. This technique is referred to as tandem mass spectrometry, mass spectrometry/mass spectrometry, or just MS/MS (1,2). With the development of the triple quadrupole mass spectrometer by Yost and Enke (3-5), a new and relatively straightforward approach emerged for studying low energy (1-200 eV_{Lab}) ion/molecule interactions.

A schematic of a triple quadrupole mass spectrometer is shown in Figure 1-1. Following ionization in the ion source, the ions are focussed and passed into the first mass analyzer, Q_1. After the first stage of mass analysis, the ions continue their flight path into the second quadrupole, Q_2, which does not function as a mass analyzer, but as a reaction (or collision) chamber and an ion transmission device. Introduction of a collision gas in this region (Q_2) provides the mass-selected reactant ion with a reagent molecule for interaction. The reaction products generated in Q_2 may then pass to the second mass analyzer in a TQMS, which is the third quadrupole, Q_3. With detection of the ionic products, the researcher may infer the reaction processes that are occurring in the second quadrupole reaction chamber. Currently, triple quadrupole mass spectrometers provide the capability of analyzing gaseous ions up to 4000 mass units, although resolution of the ions suffers beyond 2000 mass units.

a) Operating principles of quadrupoles

The core of the triple quadrupole instrument is the three sets of quadrupole rods. The triple quadrupole mass spectrometer consists of two quadrupole mass analyzers, Q_1 and Q_3, and one set of rods, Q_2, which acts as a reaction chamber, and an ion transmission device. With the proper combination of direct-current (DC) and radio-frequency (RF) potentials applied to the rods, the four quadrupole rods act as a mass filter. Ideal performance is obtained with rods having hyperbolic geometry (6-8), however, cylindrical rods are most often used and provide satisfactory results.

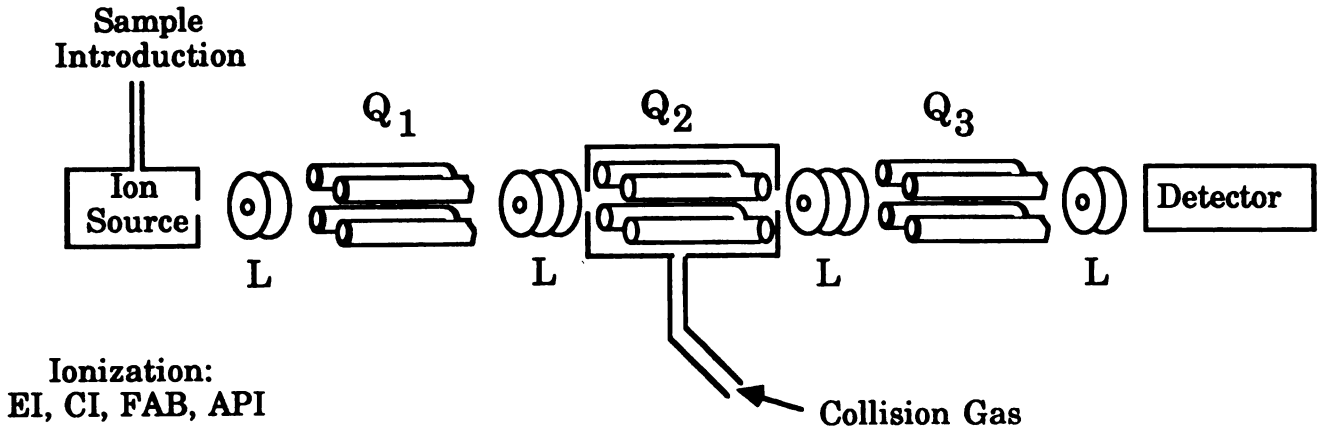

Q_1 : First mass analyzer
Q_2 : Collision chamber
Q_3 : Second mass analyzer

L : Focussing lens assemblies

Figure 1-1: Schematic diagram of a triple quadrupole mass spectrometer (TQMS).

The function of the first and third quadrupole rod sets is to mass-analyze the ions. As the ions travel through the central longitudinal space between the rods, their motion in the X-Y plane is influenced by the combined DC and RF fields and is described by the Mathieu equation with a_x and q_x parameters defined as follows:

$$a_x = -a_y = 4zeU / m\omega^2 r_0^2$$
$$q_x = -q_y = 2zeV / m\omega^2 r_0^2$$

where m/z represents the mass-to-charge ratio of the ionic species, r_0 is the distance from the center of the quadrupolar field to the closest surface of any rod, ω is the alternating RF frequency, U is the magnitude of the DC field, and V is the amplitude of the RF field. Figure 1-2 represents the **a-q** stability diagram, and the tip of this region, which is the bound area where the mass scan line intersects the stability diagram, represents coordinates of those ions which will have stable trajectories through the quadrupole field. The slope of the mass scan line is defined by the ratio 2U/V. Altering the slope of the mass scan line changes the mass-resolution of the ions. Typically, in TQMS experiments, the voltages selected by the researcher provide unit mass resolution. There are certain applications, however, where it may be desirable to either increase or decrease the mass resolution of the ions. In any case, if the voltage applied to the rods is swept while maintaining a constant slope of the mass scan line, the mass of ions with stable trajectories within the field changes, thus one is able to obtain a mass spectrum with uniform mass resolution over the mass range.

In contrast to the mass filtering capabilities of Q_1 and Q_3 is the RF-only second quadrupole. There is no DC potential applied to the second

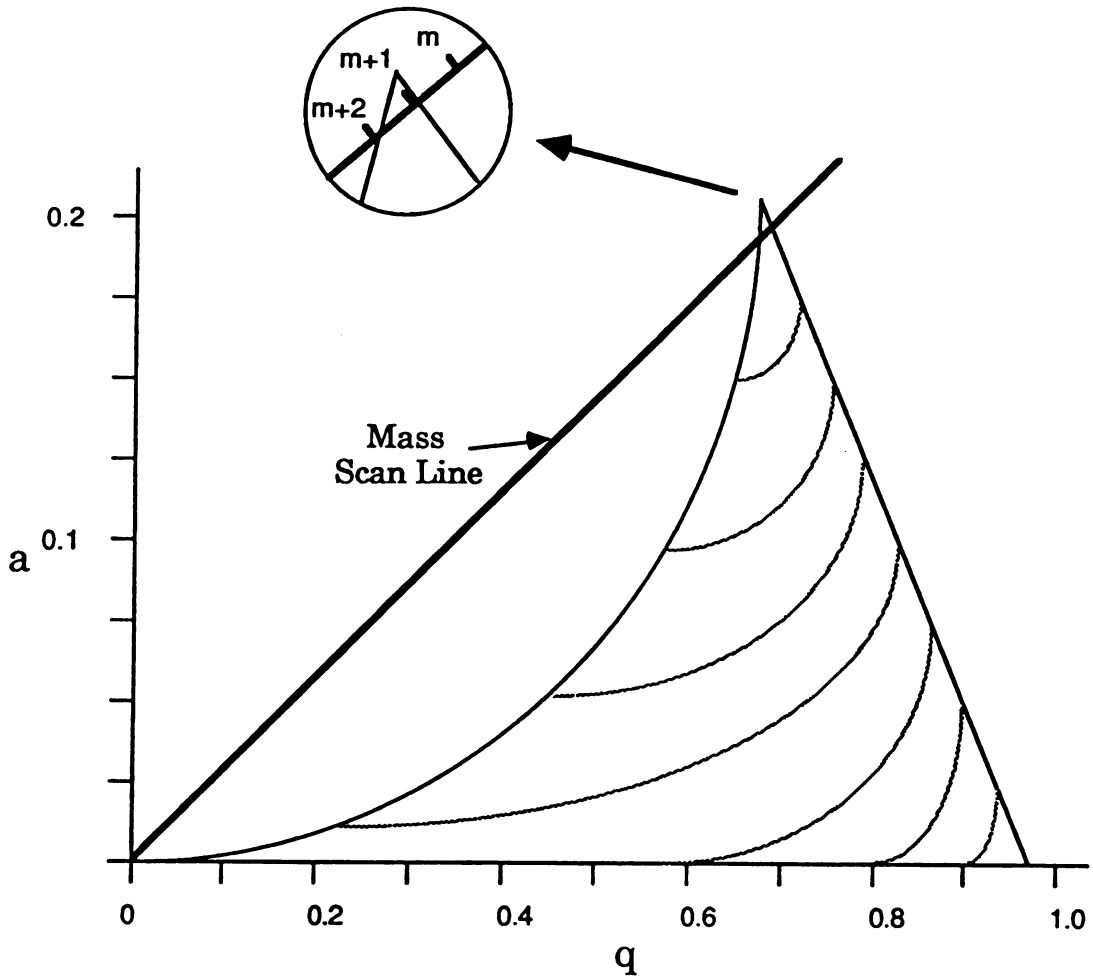

Figure 1-2: The a-q stability diagram indicating region which corresponds to stable ion trajectories; **a** relates to the RF-only field and **q** relates to the DC field.

quadrupole, which implies theoretically that ions of all m/z ratios will have stable trajectories within the field, thus RF-only quadrupoles have commonly been referred to as total ion transmission devices. However, as suggested by Miller and Denton (9), the transmission efficiency for ions of all m/z values is not 100% in an RF-only quadrupole. Not only is the transmission of ions through a quadrupole influenced by the stability of the ions as defined by the Mathieu stability diagram, but by (i) the acceptance aperture of the quadrupole and (ii) the spatial focusing conditions that arise due to the trajectory of the ions through the quadrupole (9). Therefore, mass discrimination effects are apparent, which implies that RF-only quadrupoles are not strictly total ion transmission chambers, that is, ions of different m/z ratios are transmitted through RF-only quadrupole rod assemblies with different degrees of efficiency. It should also be noted that most of the experimental work reported in this dissertation was performed on a Finnigan TSQ-70 triple quadrupole mass spectrometer. This TQMS instrument is unique in that the axis of the second quadrupole collision cell is non-linear, which helps minimize the detection of chemical noise arising from fast neutrals in fast atom bombardment (FAB) experiments. Recently, the transmission characteristics of non-linear RF quadrupole collision cells were investigated (10). The authors of this study concluded that the transmission of the ions in a non-linear device was not measurably different than the transmission of ions in a linear quadrupole collision cell (10).

b) Ionization modes

Several ionization modes are available with triple quadrupole mass spectrometers. These include but are not limited to electron impact (EI), chemical ionization (both positive and negative CI) (11), fast atom

bombardment (FAB) (12,13), and atmospheric pressure ionization (API) techniques (14-16). In addition, triple quadrupole instruments are well suited to interfacing with a gas chromatograph (GC) or liquid chromatograph (LC). In many MS/MS experiments, it is desirable to use a 'soft' ionization technique, such as CI or FAB, where most of the ion current is concentrated at one particular m/z value, usually representing the protonated species, which reflects the molecular weight of the compound of interest while maintaining the structural integrity of the molecule. Structural information supplied by fragmentation of the ion can then be obtained by subjecting the ionic species to an analysis by MS/MS.

c) Detection

An electron multiplier is often used as the detector in triple quadrupole mass spectrometry. Ions strike the electron multiplier, causing electrons to be ejected. These electrons then strike the walls of the multiplier creating a cascade of electrons which finally results in a measurable current at the base of the multiplier. The typical gain of an electron multiplier is 10^5 (17). With recent advances in the ionization efficiency of large biomolecules, post-acceleration conversion dynodes are more frequently being used in the detection scheme providing more uniform detection of ions within a large mass range. The conversion dynode is located before the electron multiplier. Ions strike this dynode which is biased with a large positive or negative potential depending on the polarity of the detected ions. After the ions strike this conversion dynode, charged particles are ejected and accelerated, with energy in the kV range, towards the electron multiplier.

2. *MS/MS scan modes with TQMS*

There are four different MS/MS scan modes available with a triple quadrupole mass spectrometer, the daughter ion scan, parent ion scan, functional relationship scan and the selected reaction monitoring (SRM) mode (18,19). Recently, details of the various scan modes possible for a MS^n system have been described (18,19). The TQMS may also be operated as a single stage quadrupole mass spectrometer by scanning only one of the two mass analyzers while the other two quadrupole rod assemblies in the RF-only mode, function as ion transmission devices. The role of the rods in the different scan modes is illustrated in Table 1-1.

a) Daughter ion scan

The most familiar and commonly used MS/MS scan mode is the daughter ion scan. In this mode, the first mass analyzer, Q_1, is set to pass ion current of a particular mass-to-charge (m/z) ratio which is referred to as the parent ion or reactant ion. Parent ions chosen by Q_1 interact with the collision gas in Q_2 generating product ions, referred to as daughter ions when the process is collision-induced dissociation (CID). These fragment ions formed in the collision cell enter the third quadrupole which is scanned to obtain a daughter ion mass spectrum. Throughout this dissertation, the term **daughter ion mass spectrum** will be used when the collision gas introduced is inert, such as the case with argon. However, if a reagent gas is introduced, the term **product ion mass spectrum** will be used. It should be noted that use of a reagent gas does not preclude the formation of ions formed by CID.

Table 1-1: Function of the quadrupoles in various TQMS scan modes.

Q_1	Q_2	Q_3	Mode
Scan	RF-only	RF-only	MS
RF-only	RF-only	Scan	MS
Fixed	RF-only	RF-only	SIM (MS)
RF-only	RF-only	Fixed	SIM (MS)
Fixed	RF-only	Scan	Daughter Ion Scan (MS/MS)
Scan	RF-only	Fixed	Parent Ion Scan (MS/MS)
Scan	RF-only	Scan	Functional Relationship Scan (MS/MS)
Fixed	RF-only	Fixed	SRM (MS/MS)

MS= single stage analysis SIM= selected ion monitoring,
MS/MS=tandem analysis, SRM= selected reaction monitoring,

b) Parent ion scan

A parent ion mass spectrum is obtained if Q_3 is set to pass a selected daughter (or product) ion, while the first mass analyzer, Q_1, is scanned sequentially passing parent ions with different mass into Q_2. This resulting spectrum will indicate all those ions generated in the source which upon reaction with collision gas in Q_2, yield a specific m/z value as chosen by the second mass analyzer, Q_3.

c) Functional relationship scan

In a functional relationship scan, both Q_1 and Q_3 are scanned with a mass offset. The most familiar functional relationship scan is a neutral loss or neutral gain scan, where the mass offset remains constant. Neutral loss scans are used when examining dissociation reactions in the collision cell. A neutral gain scan may be utilized if a reactive collision gas is introduced into the collision cell for associative ion/molecule reactions. In a neutral loss/gain experiment, ions will be detected provided that the parent ion eliminates (or gains) a neutral moiety prior to entering the second stage of mass analysis; the mass lost or gained being equal to the constant mass offset of Q_1 and Q_3.

A second example of a functional relationship scan is in the search for proton-bound dimers; an anticipated fragment would be the protonated monomer (18). To search for symmetric proton-bound dimers, a scan mode such that $m_2^+ = (m_1^+ + 1)/2$ could be implemented, where m_1^+ is the parent mass and m_2^+ is the daughter mass (18). In this case the mass offset is not constant. Functional relationship scans could get quite complex, but at times may be useful.

d) Selected reaction monitoring (SRM)

Selected reaction monitoring refers to the MS/MS mode in which Q_1 and Q_3 are set to pass ions of only one m/z value. Neither of the mass analyzers is scanned, a feature which provides greater sensitivity at the expense of selectivity. Selected reaction monitoring (SRM) is analogous to a selected ion monitoring (SIM) experiment which is employed with a single mass analyzer, and is most often used in the targeted detection of a low-level analyte.

3. *Methods of ion activation*

The heart of the MS/MS technique is the ion activation step. This section summarizes the more prominent ion activation methods which have been used in tandem MS. These include: collisional activation (CA) (20) with a collision gas resulting in either charge permutation reactions, collisionally-induced dissociation (CID), or associative ion/molecule reactions; photodissociation, and surface-induced dissociation (SID). Activation of the parent ion by collision with a gas was the first activation method to be used for analytical MS/MS analyses, and currently is the most popular method (1). Table 1-2 lists the various activation methods used in tandem MS, and the following section discusses in more detail those methods most prominent in TQMS studies.

Table 1-2: Methods of ion activation in a TQMS.

A. Collisional Activation With a Gas:

$M^- + N \text{-------} > M^+ + N + 2e^-$	Charge Inversion (1)
$M^+ + N \text{-------} > M^{2+} + N + e^-$	Charge Stripping (2)
$M^+ + N \text{-------} > M + N^+$	Charge Exchange (3)
$M^+ + N \text{-------} > M^{+*} + N \text{-------} > M_2^+ + M_3 + N$	Collision Induced Dissociation (4)
$M^+ + N \text{-------} > MN^{+*} \text{--------} > M_4^+ + M_5$	Ion/Molecule Reaction (5)

B. Surface Induced Dissociation:

$M^+ + S \text{-------} > M^{+*} \text{----------} > M_6^+ + M_7$

C. Photodissociaton:

$M^+ + h\upsilon \text{------} > M^{+*} \text{----------} > M_8^+ + M_9$

N = neutral collision gas
M^{+*} = ion with excess internal energy.
MN^{+*} = adduct ion with excess internal energy.

S = solid surface
$h\upsilon$= photon

a) Collisional activation (CA)

Efficient transfer of the parent ion's translational kinetic energy to internal vibrational energy can occur when an ion collides with a neutral gas with kinetic energy in the eV range. This first step, termed collisional activation (CA), produces an ion with excess vibrational energy. The maximum energy available for conversion from kinetic to internal energy distributed within the incident ion, is described by the expression:

$$E_{CM} = E_{Lab} \times M_g/(M_p+M_g) \qquad \text{Equation 1-1}$$

where E_{Lab} is the potential difference between the ion source and Q_2 which determines the kinetic energy of the parent ion, M_g is the mass of the target gas, and M_p is the mass of the parent ion. The important variable is the collision energy in the center of mass system, E_{CM}, as this represents the energy available for conversion to internal energy within the ion (21). The energy in the laboratory frame may be varied by changing the DC offset potential applied to the second quadrupole rod assembly, which is in addition to the ramping DC voltage. Following collisional activation, the excited ion depicted as M^{+*} may either be collisionally stabilized by third-body collisions or if the collisionally-excited ion has sufficient internal energy, it can undergo unimolecular decomposition forming fragment ions. This latter process is termed collisionally induced dissociation (CID).

The mathematical expression of Equation 1-1 suggests a massive target gas is preferred as a collision gas for CID experiments because there is more efficient conversion of kinetic energy to internal energy relative to that in a lighter target. However, the use of heavy mono or polyatomic target

gases has not always been found to be advantageous in low-energy collisionally induced dissociation studies (22). With polyatomic targets, for example, significant amounts of kinetic energy may be transferred to internal modes of the target gas (22) robbing the parent ion of this available kinetic energy. In CID studies the ionization potential of a target gas also needs to be considered so that charge exchange does not effectively compete with CID. The expression for conversion of kinetic energy to internal energy is ideal, and does not exactly indicate the conversion efficiency. Studies have shown that at very low ion kinetic energies, the fraction of the theoretical maximum energy E_{CM} transferred into internal energy is high, but levels off as the collision energy (E_{Lab}) is increased (23).

Not only does the nature of the target gas affect the collisional activation results (22,24), but the pressure of the target gas influences the average internal energy deposited into the parent ion (23,25,26). In a study by Cooks' group (23), they reported that in the collision of $(C_2H_5)_4Si^{+\cdot}$ ions with argon in Q_2 of a triple quadrupole instrument, the calculated amount of internal energy deposited in this parent ion was 3.5 times greater for roughly 15 collisions with argon than for a single collision with argon at collision energy of 28 eV_{Lab} for both experiments. Multiple collisions increases the energy deposited in a stepwise fashion. The use of multiple collisions, although increasing the average internal energy deposition, may lead to complications in characterizing an ion structure as (i) both parent and fragment ions may undergo a collision, thereby complicating the CID daughter ion mass spectrum, and (ii) isomerization may occur between collisions (23,27-29). Furthermore, although multiple collisions increases the average energy imparted, these conditions broaden the range of internal energy deposited in the incident ion. The energetics of fragmentation

processes in CID is dependant on the nature of the collision gas and the pressure of the collision gas, and these factors must be considered, especially in fundamental studies.

b) Surface induced dissociation (SID)

In recent years, research pioneered primarily by Cooks' group at Purdue University has demonstrated the feasibility of dissociating a parent ion via its collision with a surface, usually made of stainless steel (30-32). In triple quadrupole surface induced dissociation (SID) studies (32), a stainless steel target was placed at a fixed 90 degree scattering angle following the second quadrupole. The parent ion was selected by Q_1, passed through the lens system and the Q_2 focussing chamber, and collided with the target surface. Following activation of the ion due to collision with the surface, the extracted ions were mass-analyzed by Q_3. The collision energy was changed by maintaining the ion source at ground while applying a potential of -10 to -100 eV to the steel target. If collision with the surface supplied sufficient internal energy for the ion, the activated ion may undergo unimolecular dissociation, hence the term SID. Recently, in-line SID was demonstrated in a triple quadrupole mass spectrometer (33). The advantages to the SID method include: (i) improved vacuum as no collision gas is introduced, (ii) narrow and very high internal energy deposition into the parent ion, and (iii) highly reproducible spectra. Interestingly, with the SID technique, ion/molecule reactions occur, usually for radical ions, even at collision energies up to 50 eV (30-32). The most common reactions observed include reduction by addition of hydrogen to the parent ion. This phenomenon is attributed to hydrocarbon impurities which are adsorbed on the metal surface, so that the ion collides with an organic molecule rather than a clean

stainless steel surface. Greater vacuum requirements are necessary to ensure a clean surface, free of any adsorbant. SID techniques appear promising in that greater internal energy is deposited into the parent ion than in CA methods with a target gas, although it is not known the extent to which this conversion of kinetic energy to internal energy takes place.

c) Photodissociation

Excitation of an ion by photon absorption is another means of activating an ion and promoting dissociation. One of the great advantages is that, in principle, photoexcitation can impart a wide range of energies to the ion, assuming the ion is able to absorb the light. Of all the ion activation methods, photodissociation is most capable of depositing a well defined energy into the ion. Where photodissociation suffers compared to collisional activation is that the cross sections are on the order of 10^{-2} A^2, whereas typical CID cross sections are 10-100 A^2 (1). Mass spectrometers with the capability to trap ions are best suited for photodissociation experiments as ions may be irradiated by light for varying lengths of time. Most experiments have been performed in an ion cyclotron resonance (ICR) instrument or in an ion trap mass spectrometer, but photodissociation studies have been performed on fast ion beams, and a recent review addresses the analytical utility of this technique (34). A tandem quadrupole Fourier transform instrument has also been built for studying laser photodissociation (35,36). Interestingly enough, the first triple quadrupole mass spectrometer was constructed with the intent of studying photodissociation of organic ions with the RF-only quadrupole (37).

d) Ion/molecule reactions

All of the previously described activation methods result in fragmentation of the parent ion. In contrast, ion activation may be promoted by exploiting the reactivity of the parent ion with a neutral reagent gas leading to associative ion/molecule reactions. Associative ion/molecule reactions do not imply, however, that the product ions are always of higher mass than the reactant ion. Associative ion/molecule reactions produce product ions which are attributed to the ion/molecule chemistry that occurs with the interaction, not just the unimolecular decomposition process following CA. Ion/molecule reactions most often have been studied in ICR instruments (38,39), flowing afterglow instruments (40), or drift tubes (41-43) with most of the attention in these studies directed towards determining the kinetics of ion/molecule reactions, reaction cross-sections, and gas-phase basicities. The study of ion/molecule reactions with a triple quadrupole mass spectrometer has remained largely underutilized.

Ion/molecule reactions proceed via the initial formation of a collision-complex. If an ion collides with a reagent gas, a collision-complex may form. This collision-complex intermediate may then undergo one of four processes indicated in Table 1-3. The complex may: (i) fall apart back to the original reactants, (ii) undergo collisions with a third body, thereby stabilizing the intermediate, (iii) proceed to yield reaction products through one or more reaction channels, or (iv) emit a photon in a radiative emission process (44).

The formation of a collision-complex may occur following the ion/molecule interaction in the second quadrupole of a TQMS, and under kinetically and thermodynamically favorable conditions, reaction products, as reflected by (iii) in Table 1-3, can be detected. Generally, only exothermic or

Table 1-3: Low-energy ion/molecule reaction collision processes.

(i) $M_1^+ + R \text{ -----> } M_1R^{+*} \text{ -----> } M_1^+ + R$

(ii) $M_1^+ + R \text{ -----> } M_1R^{+*} \text{ ---}^{+R}\text{----> } M_1R^+$ Collisional Stabilization

(iii) $M_1^+ + R \text{ -----> } M_1R^{+*} \text{ -----> } M_2^+ + M_3$ Ion/molecule reactions

(iv) $M_1^+ + R \text{ -----> } M_1R^{+*} \text{ -----> } M_1R^+ + h\upsilon$ Radiative Emission
where $h\upsilon$ is a photon

thermoneutral ion/molecule reaction products are observed from ion/molecule reactions occurring in the collision cell of a TQMS, although by increasing the collision energy of the reactant ion, it is possible to deposit more internal energy into the collision complex thereby driving the formation of endothermic reactions. However, increasing the kinetic energy of the reactant ion decreases the lifetime of the collision-complex, consequently the lifetime of the collision complex may become too short to form reaction products. Increasing the collision energy decreases the cross-section of the reaction (45), thereby decreasing the likelihood of detecting product ions. Finally, raising the collision energy increases the abundance of products arising from collisionally-induced dissociation which complicates the product ion mass spectrum. For these reasons, the collision energy is usually very low (<5 eV_{Lab}) for studying ion/molecule reactions in the reaction chamber of a TQMS.

4. *Analytical utility of TQMS*

Triple quadrupole mass spectrometry has proved to be a versatile analytical instrument capable of selectively detecting a targeted compound to levels of 10^{-12} to 10^{-15} moles. Some of the recent applications of TQMS include: screening for trace levels of environmental pollutants and contaminants (46-49), detection of carcinogenic compounds in foods (50), drug metabolism studies for structural characterization and identification of unknowns (51-55), quantification of drugs in biological matrices (56-60), analysis and sequencing of peptides and small proteins (61-65), and on-line characterization of products produced by electrochemical oxidation/reduction reactions of uric acid (66) and purines (67). Advances in the analysis of large

biomolecules has been proceeding rapidly. Recent studies have shown that for some ionization methods (thermospray and electrospray techniques, in particular) multiply charged ions are formed (14,63,68). This provides two significant advantages to analysis by triple quadrupole techniques, the first being that the mass range of the quadrupole analyzer is extended. For example, a quadrupole mass analyzer with a range of 2000 u, will theoretically be able to detect ions with eight charges up to 16000 u. The second advantage offered by multiply charged ions is that the effective collision energy in the laboratory frame of reference (E_{Coll}), is equal to the number of charges present on the ion multiplied by the collision energy in the laboratory frame of reference (E_{Lab}), $E_{Coll} = E_{Lab}$ x number of charges. This multiplication of the kinetic energy should result in greater amounts of internal energy being deposited into the parent ion. Finally, triple quadrupole mass spectrometry continues to be useful for CID studies of ion/molecule reactions that occur in the ion source (69-71).

5. *Limitations to dissociation (CID, SID) methods*

Despite the many successes of triple quadrupole mass spectrometry with conventional ion activation techniques, collisional activation resulting in fragmentation does not always offer solutions to analytical problems. With the advent of desorption ionization, and the API techniques, larger and larger biomolecules can be introduced into the gas phase and ionized, often producing a protonated molecular species. Minimal structural information is obtained so tandem MS analysis is required. Coupling these ionization methods with a quadrupole mass spectrometer generally is preferred. However, with larger ionic species, there are more internal vibrational modes

for which the internal energy is distributed following CA and with low-energy triple quadrupole methods, this may result in insufficient energy being available for bond fragmentation. This is especially apparent in collisional activation with a gas, whereas in SID, larger relative amounts of internal energy are deposited. Additional work is required before one may assess the utility of SID in fragmenting larger ions.

Poor fragmentation efficiencies is not only limited to larger ions. In certain cases, ions of low mass (<500 u) may not fragment very readily due to the high stability of the parent ion. In these cases, low collision energy CID does not impart sufficient energy for bond cleavage. Highly cyclic aromatic compounds are a class of compounds for which this holds true. In addition, dissociation methods may not always provide the specificity necessary to distinguish between isomeric species. Reaction channels by which two isomers fragment may proceed through an identical intermediate, thereby eliminating variances in the CID daughter ion mass spectrum of the two isomers. Finally, there may not always be diagnostic fragment ions from dissociation methods which would supply the necessary structural or compositional information of the analyte. These limitations point to the need of alternative activation methods other than dissociation techniques. The approach being investigated and reported on in the bulk of this dissertation involves the use of low-energy reactive collisions. These reactions have occurred in the second quadrupole, although for some applications it is useful to perform the ion/molecule chemistry in the ion source, thereby generating the ionic species for conventional CID MS/MS analysis.

C. Ion/molecule reactions in a TQMS

The triple quadrupole mass spectrometer has some unique features which make it an attractive tool for the study of gas-phase ion/molecule reactions. Ion/molecule reactions may be studied in an ion source, and the reaction products may be analyzed by collisional activation. An alternative approach for using a TQMS for studying ion/molecule reactions is to select an individual parent ion by Q_1 and introduce it into the collision chamber filled with the reagent gas. Provided that the kinetics and thermodynamics are favorable, interaction of the ion and neutral molecule may result in the formation of reaction products. The ion/molecule reaction conditions, including target gas pressure and collision energy, may influence which reaction pathway is available.

1. *Advantages of using TQMS for studying ion / molecule reactions*

There are several features of a TQMS which are advantageous for the study of ion/molecule reactions. First, quadrupole mass spectrometers are versatile in that a wide range of ionization techniques is available for use, including those which involve relatively high source pressure, such as FAB, CI and API. This feature makes quadrupoles amenable to GC and LC interfacing. The quadrupoles are able to tolerate relatively high pressures without significant degradation of performance. Second, with a tandem quadrupole instrument, both the reactant ion and product ions may be mass-selected with unit resolution. Third, the reactant ion and neutral reagent gas are separated spatially which likely eliminates mixing of the reactants prior

to reaction in the collision cell. Finally, the researcher has some control over the energetics of the reaction as the collision energy may be adjusted. This enables ion/molecule reactions to be examined in crude energy-resolved studies. Also, by raising the collision energy, CID products may be observed. On one hand, this may complicate the product ion spectrum, but it does enable one to observe both reactive and dissociative collisions within the same experiment.

2. *Disadvantages of using a TQMS for studying ion/molecule reactions*

There are some undesirable characteristics of a triple quadrupole mass spectrometer that need to be considered when studying ion/molecule reactions. First, it is difficult to determine exactly the collision energy in current triple quadrupole mass spectrometers. The potential difference between the ion source and the second quadrupole provides most of the kinetic energy to the reactant ion, but additional kinetic energy arises from other sources. The radio frequency voltage applied to the quadrupole rods imparts an undetermined amount of radial kinetic energy to ions within the field. In addition, the voltages applied to the set of focusing lenses located just prior to and after the second quadrupole will affect the kinetic energy of the ion. This makes accurate thermochemical measurements difficult due to the uncertainty of the kinetic energy of the reactant ion. However, the focus of this research is not in determining thermochemical measurements, so this limitation should not interfere with the intent of this research project.

As discussed previously, one advantage of the triple quadrupole mass spectrometer is the capability to examine both reactive collision and dissociation product ions. However, this may complicate the product ion

mass spectrum and it is necessary to determine reaction channels accessed by each reactant ion. One way that this dilemma may be overcome is by comparing interaction of the reactant ion with reagent gas to the interaction of the ion with an inert gas under identical collision conditions. Comparison of the daughter ion mass spectrum with the product ion mass spectrum should be useful in determining the competitive processes that are occurring in the ion/molecule interaction.

A final disadvantage with studying ion/molecule reactions in the TQMS is that it is difficult to control the residence time in the collision chamber. If there is insufficient residence time, it would be expected that the yield of reaction products may be low for slower reactions. There has been some successes with ion trapping techniques in a TQMS which effectively increase the residence time of the ions in Q_2 (72). The ions are trapped in the reaction chamber by applying a positive potential to the Q_2 exit lens so that the ions are confined in the collision cell. Following this trapping, the lenses are pulsed with a large negative potential which serves to extract the ions. This method enhances the signal of reaction product ions generated in the collision because (i) the residence time was increased so that more product ions were formed from slower ion/molecule reactions and (ii) product ions that had low kinetic energy were extracted from the second quadrupole.

D. Literature review of ion/molecule reactions in TQMS

There have been a limited number of reports in the literature where ion/molecule reactions were investigated in the second quadrupole and the following section summarizes this work. Although the distinction is somewhat arbitrary, this section has been divided into two subsections: i)

fundamental studies and ii) analytical applications of ion/molecule reactions in a TQMS.

1. *Fundamental studies*

a) Ion/molecule reactions of $C_2H_5O^+$ isomers with NH_3 (73)

Two isomers of $C_2H_5O^+$ composition were reacted with NH_3 and N_2 at single collision conditions and the energy-resolved results were discussed in relation to the thermochemistry of the reactions. Thresholds for the formation of CH_3^+ in CID studies with N_2 as the target gas were determined from the energy-resolved plots to be 3.8 eV and 6.5 eV for $CH_3OCH_2^+$ and CH_3CHOH^+, respectively. These values correlated to thresholds predicted by the thermochemical calculations of the reaction enthalpies. Thresholds were then experimentally determined for the formation of the same ion, in this case CH_3^+, in the ion/molecule reaction with NH_3. It was found that the reaction threshold, which is the energy at which product ions of m/z 15 were detected, with NH_3 as the target gas was 3.0 eV and 4.2 eV for $CH_3OCH_2^+$ and CH_3CHOH^+, respectively. The lower observed threshold energy in the ion/molecule reaction with ammonia was attributed to reaction-induced fragmentation (RIF). The lower threshold values obtained experimentally are in agreement with calculated enthalpies of reaction. The formation of stable neutral NH_2CH_2OH leads to the shift of the CH_3^+ threshold, as shown in Table 1-4.

The authors illustrated the use of ion/molecule reactions for inducing the formation of product ions at a lower energy than was required for unimolecular decomposition occurring with CID. Similar values for the

Table 1-4: Reaction enthalpies for dissociation of $C_2H_5O^+$ isomers in collision with N_2 and NH_3.

CID $CH_3\text{-}O{=}CH_2^+ \text{ ----> } CH_3^+ + H_2CO$

ΔH_f 6.7eV 11.4 eV -1.2eV ΔH_r= 3.5 eV

observed threshhold = 3.8 eV

CID $CH_3\text{-}CH{=}OH^+ \text{ ----> } CH_3^+ + HCOH$

ΔH_f 6.1eV 11.4eV 1.2eV ΔH_r=6.5 eV

observed threshhold = 6.5 eV

RIF $CH_3\text{-}O{=}CH_2^+ + NH_3 \text{ ----> } CH_3^+ + NH_2CH_2OH$

ΔH_f 6.7eV -0.5eV 11.4eV -2.1eV ΔH_r=3.1 eV

observed threshhold = 3.5 eV

RIF $CH_3\text{-}CH{=}OH^+ + NH_3 \text{ ----> } CH_3^+ + NH_2CH_2OH$

ΔH_f 6.1eV -0.5eV 11.4eV -2.1eV ΔH_r=3.7 eV

observed threshhold = 4.2 eV

experimental thresholds for reactions and calculated reaction enthalpies lent support to the suggested reaction mechanisms.

b) Endothermic proton transfer reactions (74)

A triple quadrupole was used to determine the proton affinities of the conjugate bases $[C_6H_5]\cdot$ of the following acids: benzene molecular ion, 2,4-hexadiyne molecular ion, and 1,5-hexadiyne molecular ion. The $C_6H_6^+$ ion was reacted with dimethylamine, ammonia, methanol, and water under single collision conditions. Proton affinities for $[C_6H_5]\cdot$ radicals were established from the kinetic energy at which the onset of proton transfer to less basic species occurs within the second quadrupole rod assembly. The values obtained by this method were compared with proton affinities obtained using bracketing methods, involving exothermic proton transfer reactions. In the TQMS used for this study, the lateral motion of ions in the second quadrupole did not appreciably influence the kinetic energy of the parent ion. A second report by Bursey's group discussed the difficulties that need to be addressed when measuring onset potentials for proton transfer reactions in a triple quadrupole (75).

c) Reaction of benzoyl ions with ammonia (76)

In this study, the reaction of the $C_6H_5O^+$ ion with ammonia was investigated. The authors were interested in determining the affect of multiple collision conditions on the determination of thermochemical information. Onset potentials, determined experimentally, for endothermic processes under multiple collision conditions were not in agreement with calculated enthalpies and the authors concluded that information on the energetics of reactions could not be obtained when the parent ion undergoes

more than one collision. However, they stated that multiple collision conditions may be useful analytically for maximizing the formation of product ions.

d) Formation of ammonium ions in reaction of protonated carbonyls with NH_3 (77)

Ammonia was introduced into the collision cell, and the dependence of the protonation of neutral ammonia on the axial kinetic energy of protonated carbonyl reactant ions was investigated. Evaluation of the resultant energy curves led to the postulation that formation of protonated ammonia may occur via two non-competitive reaction channels. The ammonium ion, NH_4^+, may be generated by either a very low-energy direct proton exchange reaction, or by fragmentation of an initially formed adduct ion.

2. *Analytical applications*

a) Reaction of $C_3H_3^+$ ions with acetylene (78)

The first demonstration that reactive collisions in the center quadrupole can be analytically useful was demonstrated by the reaction of $C_3H_3^+$ ions with acetylene (C_2H_2). These $C_3H_3^+$ ions were generated by charge exchange of propargyl halides (C_3H_3X where X=Cl, Br or I). ICR experiments indicated that the linear $C_3H_3^+$ ion was reactive with acetylene, forming a $C_5H_5^+$ ion, whereas the cyclic structure was not. The experiments on the triple quadrupole corroborated those on the ICR indicating that the reactive linear $C_3H_3^+$ structure is generated from C_3H_3I, and that the structure of $C_3H_3^+$ ions may be probed by ion/molecule reactions with acetylene.

b) Reactions of $C_2H_5O^+$ isomers with reagent molecules (79)

In this work, reactive collisions with either benzene or 1,3, butadiene distinguished two $C_2H_5O^+$ isomers, the 1-hydroxyethyl cation and the methoxymethyl cation. These two isomers can be distinguished by conventional CID methods, but the distinction is based on differences in relative intensities of fragment ion peaks. In ion/molecule reactions of these isomers with benzene, both isomeric ions transferred a proton to benzene resulting in a peak at m/z 79 representing protonated benzene. However, only the methoxymethyl cation reacted with benzene to give a peak at m/z 91 which probably represents an ion with the benzyl structure.

c) Reactions of cations with hydrocarbons (80-82)

This series of papers described research in which, small cations, including CH_3^+, $CH_4^{+\cdot}$, and $C_2H_4^{+\cdot}$, were reacted with hydrocarbons. Reaction pathways were elucidated by selecting the particular parent ion and reacting it with the neutral reagent gas in the collision cell of a TQMS. Much of the work was done to confirm earlier experiments performed with an ICR instrument or in high pressure CI studies. They demonstrated that the triple quadrupole was an elegant instrument by which ion/molecule reactions could be studied.

d) Reaction of protonated esters with ammonia (83)

The authors in this study investigated the formation of adduct ions when a series of protonated esters was reacted with ammonia. They proposed that the loss of H_2O from the protonated ester increased when ammonia was the collision gas rather than nitrogen due to reaction-induced fragmentation (RIF). Elimination of water from the initially formed protonated ester-ammonia collision complex yields stable neutral products, which effectively decreases the reaction enthalpy of the dehydration reaction. The structure of this collision complex adduct ion was discussed, and they proposed that it was a covalently bound tetrahedral structure rather than a hydrogen bound structure. Formation of an adduct ion was not observed when the molecular ion of the esters was reacted with ammonia.

e) Protonated natural products reacting with ethyl vinyl ether (84)

This report describes ion/molecule reactions in ethyl vinyl ether of protonated natural products, including quabalactones, psorospermins, and diterpene dilactone compounds. The reaction channels accessed by these protonated compounds were explained by proton affinity differences, delocalization of the charge within the compound, along with structural differences amongst the natural products. In some compounds, ion/molecule reactions resulted in product ion peaks which were larger than any of the CID daughter ion peaks, implying that the TQMS is well suited for sensitive analytical techniques employing ion/molecule reactions.

f) Reaction of protonated hexachlorobiphenyl molecules with ammonia (85)

The ion/molecule reaction between six hexachlorobiphenyl protonated molecules and ammonia was investigated in the TQMS. The product ion $(M+NH_3-HCl)^{+\cdot}$ was detected in all six cases, yet under uniform conditions, the abundance of this reaction induced fragment ion varied by at least an order of magnitude depending on which compound was being analyzed, thereby offering a method for distinguishing these isomers.

g) Discrimination of 1,2-cyclopentanediol isomers (86,87)

The *cis* and *trans* isomers of 1,2-cyclopentanediols were distinguished by ion/molecule reactions with ammonia (86). These isomers could be differentiated by isobutane positive CI or by comparison of the CID daughter ion mass spectrum of the protonated molecule, yet the distinction was based on the differences of the relative abundances of some fragment ions. However, due to proton affinity differences of the isomers, in collisions with ammonia in a TQMS, the protonated *trans* isomer transferred the proton to ammonia yielding a peak at m/z 18, whereas proton transfer with the *cis* isomer was minimal. There also was a significant abundance of the $(M+NH_4)^+$ adduct formed in the reaction of the *trans* isomer with ammonia, whereas no adduct was observed with the protonated *cis* isomer.

In contrast to this work just described, the authors reported an alternative approach for discriminating the stereoisomers of 1,2-cyclopentanediols (87). Rather than distinguish the isomers in their protonated form, a method was developed by which the neutral isomeric compounds could be differentiated. In this case, 1,2-cyclopentanediols were individually introduced into the second quadrupole reaction chamber. When

$[Si(CH_3)_3]^+$ and 1,2-cyclopentanediol were reacted, a $(M+Si(CH_3)_3)^+$ adduct was formed for both isomers, but there were significant differences in the subsequent decomposition behavior of the two isomeric adducts. The *cis* isomer favored decomposition of the $(M+Si(CH_3)_3)^+$ adduct to the hydrated trimethylsilyl ion $[Si(CH_3)_3OH_2]^+$ ion with m/z 91. The formation of the hydrated trimethylsilyl ion from the *trans* isomer adduct is endothermic, and a definite ion kinetic energy threshold was observed.

h) Reactions in a double quadrupole mass spectrometer (88)

Although this work was not done in a triple quadrupole instrument, it deserves mention as it demonstrated the capability of studying ion/molecule reactions when two quadrupole mass analyzers were utilized. In this double quadrupole instrument, a collision-cell was located between the two quadrupole mass analyzers. Within this region, reagent gases were introduced, and Glish demonstrated that ion/molecule reactions could supply structural information for ionic species. Isomers of $C_2H_5O^+$ were studied by reaction with 2-propanol. Fragment ions of n-hexane reacting with n-hexane itself were also investigated in the double quadrupole instrument.

i) Quantitative analysis using reactions in ammonia (89)

Ion/molecule reactions with NH_3 were used for developing a selected reaction monitoring (SRM) method in a GC/MS/MS analysis. The targeted analytes were 2-methoxyethanol and chlorobenzene in methanol and in urine. A fragment ion from electron impact of 2-methoxyethanol, and the molecular ion from chlorobenzene were chosen to react with ammonia forming an addition product ion. The authors demonstrated an increase in sensitivity

and selectivity compared to the conventional SRM analysis in which a CID daughter ion fragment was monitored.

j) Reactions of protonated trichothecenes with ammonia (90,91)

Characterization of trichothecenes, *Fusarium* mycotoxins produced by a variety of fungi and found in food, grain, and feed, was done utilizing a TQMS and reactive collisions with ammonia. Reactions between the protonated molecule with ammonia were highly specific for structural features in this class of compounds. Good detection limits (20-300 pg) and good reproducibility was obtained (relative standard deviation, 5-10%) by means of reactive collisions with ammonia.

k) Reaction of CH_3CO^+ with 1-methylcyclopentene (92)

The authors were interested in the functional group interaction in the fragmentation of protonated 2,7-octanedione. Over the course of this elegant study, reactive collisions of CH_3CO^+ with 1-methylcyclopentene and deuterated analogues of 1-methylcyclopentene, were performed in the collision cell. The study of these reactions was used to lend further support to the reaction mechanisms proposed for the fragmentation of 2,7-octanedione. The use of ion/molecule reactions in the TQMS complemented their CID fragmentation studies.

l) Reactions of tetrachlorodibenzo-*p*- dioxins with O_2 (93,94)

An isomer-specific determination method of tetrachlorodibenzo-*p*-dioxins (TCDD) utilizing reactions of the molecular anion with O_2 was developed by Kostiainen. Low-energy collisions of the molecular anion with molecular oxygen result in an oxidative ether cleavage reaction yielding an

abundant phenoxide ion at $(M-19)^-$ which is formed by the addition of O_2 and elimination of OCl·. Variations in the abundance of this ion was dependent on the specific isomer, and these variations were used to distinguish them. When the isotope ion $(M+2)^-$ is selected, the isotope ratio pattern of the product ions provides information concerning the chlorine distribution in the rings. A second paper (94) dealt with the effect of collision gas pressure and collision energy on this reaction. They concluded that it was desirable to use high pressures of oxygen (3-6 mtorr) and a low collision energy (0.1-7 eV_{Lab}). Here at Michigan State, a similar approach has been used successfully by Ron Lopshire for sensitive detection of polychlorinated biphenyls (PCBs). Molecular anions of PCBs are reacted with oxygen in the collision cell yielding the $(M-19)^-$ anion.

m) Tetraethylsilane molecular ion reacting with air (95)

Reaction of a selected parent ion, either the tetraethylsilane molecular ion with m/z 144 or the molecular ion of argon, was used to probe the 'purity' of air. If the tetraethylsilane molecular ion reacted with dry air, only CID product ions were observed. If the air present in the collision cell contained moisture, products were detected which were explained by ion/molecule reactions with water. Similarly, when $Ar^{+\cdot}$ was chosen to react with air which had been intentionally contaminated with organics, charge exchange product ions were observed in the MS/MS spectrum, provided that the neutral molecules had a recombination energy lower than that of argon.

n) Charge exchange and proton transfer reactions (96)

This paper reports on the advantages of first mass-selecting a reactant ion, which then is used to ionize sample molecules in the center quadrupole.

It was demonstrated that control of the energetics of a specific charge-exchange or proton-transfer reaction could be achieved with mass selection of the reactant ions, whereas the energetics of these processes were not as well defined when they were done in the ion source due to interfering reactions. For these studies, n-butyl benzene was used as the energy required to form the ions with m/z 91 and m/z 92 is well established and reflects the internal energy imparted during ionization of the molecule. Different reactant ions were chosen for charge exchange (CE) experiments with n-butylbenzene, and through comparison of the relative abundances of the peaks at m/z 91 and m/z 92, it was possible to assess the energy imparted by CE. The results were in good agreement with values predicted theoretically.

o) Reactions of selected ions with GC effluent (97)

Perhaps the most novel study involving ion/molecule reactions in a triple quadrupole mass spectrometer is this study from Yost's group. The effluent from a GC column was introduced into the collision cell, so that reactions of a selected reactive ion with components in a mixture could be investigated. Charge exchange reactions and chemical ionization reactions were studied. This approach allowed the control of the energetics involved in the ionization of the eluting GC components. By alternating the reactant ion, different internal energies could be imparted to the neutral reagent enabling both structural information and molecular weight information to be obtained during the same chromatogram. A search of EI library spectra using the charge exchange spectrum was found to be generally reliable, with CH_3^+ charge exchange spectra yielding the most reliable match. This method is being evaluated for selectively detecting aromatics in jet fuels. Detection

limits for benzophenone with this method were achieved at the low picogram level.

E. Low-energy ion/molecule reactions in a four sector instrument (98-101)

Recently, a series of papers has been published which describes endothermic ion/molecule reactions that occur between protonated molecules and ammonia; of particular interest is the reaction of protonated leu-enkephalin and ammonia. A second report describes reactions of N,N dimethyl myristamide and monomethyl amine (102). Remote site fragmentation is observed at very low center-of-mass energies (102). Although these experiments were not done with a TQMS, this type of experiment is well suited for a TQMS, and the results are interesting and deserve mention. These experiments were done in a hybrid instrument of BEQQ geometry and in a HX110/HX110 four sector (EBEB configuration) tandem mass spectrometer equipped with a collision cell on which large potentials could be applied. This allows the study of very low beam collision energy ion/molecule reactions. The authors report on the increase in fragment ion abundances of protonated leucine enkephalin (m/z 556) when ammonia is the target gas compared to a neutral gas such as helium, for collision energies on the order of 5-10 eV_{Lab} (98-100). This is attributed to reaction induced fragmentation, and results in an overall fragmentation efficiency that is even greater than high-energy CID. For their experiments, the ion beam was attenuated up to 99% in some cases, yet they correlate their results with predicted energetics of the endothermic reaction and report energy-resolved curves. As discussed earlier in this chapter, thermochemical

information cannot be obtained under multiple collision conditions, which surely are occurring with these beam attenuations. In spite of what is perceived as certain flaws and that according to one of the investigators, difficult to reproduce (103), these experiments are intriguing, and demonstrate the power of increasing the fragmentation efficiency for large ionized molecules by utilizing ion/molecule reactions. These studies led to the development of a new technique, called neutralization chemical reionization mass spectrometry (101) where deprotonation of the reactant ion, followed by *reprotonation*, occurs in the collision cell.

This report described above merits some additional attention. As mentioned, it seems as if a TQMS is more suited to these types of experiments, so a preliminary attempt was made exploring this reaction using the TQMS. Protonated leu-enkephalin was produced in the ion source by FAB, and the ion (m/z 556) was passed into the collision cell containing ammonia. A target gas pressure was chosen which resulted in 80% attenuation of the primary beam at a collision energy of 10 eV_{Lab}. In the TQMS study, the $(M+H+NH_3)^+$ adduct was most abundant at 1-2 eV_{Lab} collision energy. Beyond 2 eV_{Lab}, no adduct ion was observed in the TQMS. This is in contrast to their study where 6 eV_{Lab} collision energy provided maximum formation of the $(M+H+NH_3)^+$ adduct as seen Figure 1-3. They also report that fragment ion abundances for ions with m/z 425, 397 and 279 reached a maximum at a slightly higher collision energy, and then leveled off. They believe that forming the $(M+H+NH_3)^+$ adduct, via an endothermic ion/molecule reaction, provides internal energy for this adduct ion which induces fragmentation. In preliminary studies done in our laboratory using the TQMS, this fragmentation behavior was not observed. Additional investigations are required before one may assess the utility of this reaction

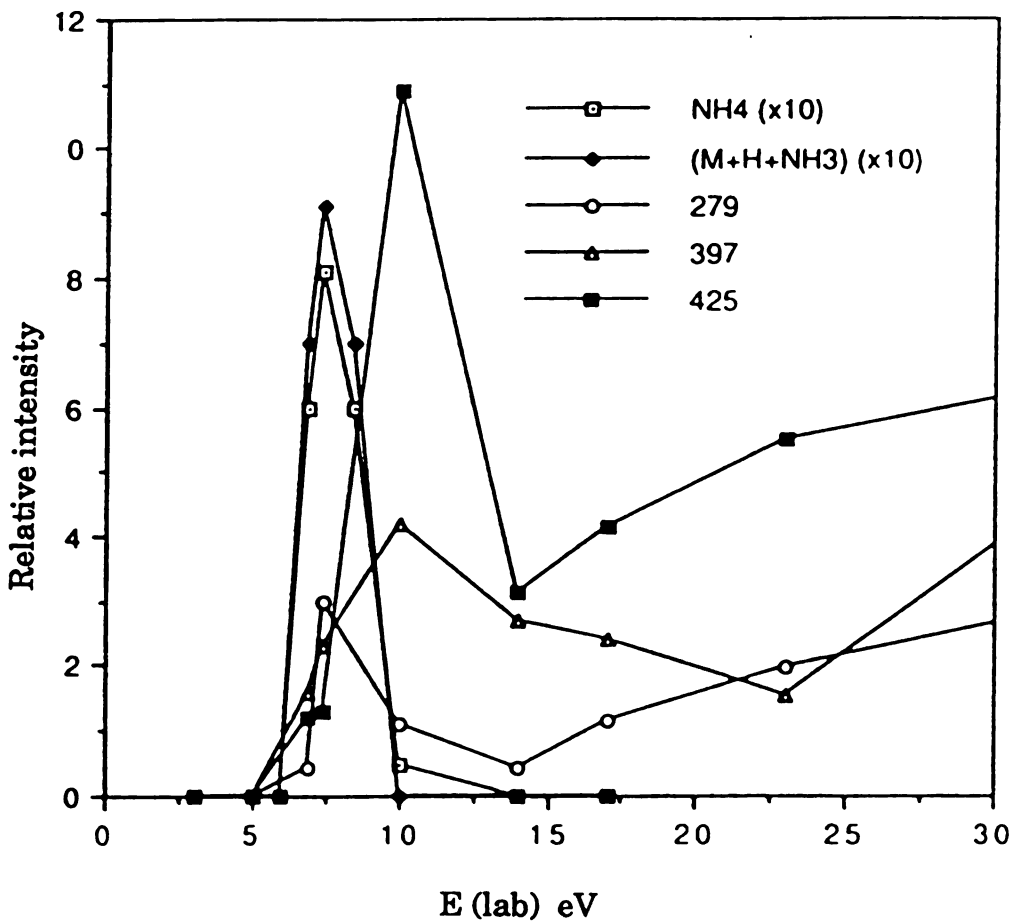

Figure 1-3: Relative abundances of various ions in reaction of protonated leu-enkephalin with ammonia as function of ion kinetic energy. (Adapted from reference 100).

when utilizing a TQMS, and this may be a fruitful area of research considering the interest in peptide sequencing at Michigan State University.

F. Research objectives

A primary goal of this investigative research is to use a triple quadrupole mass spectrometer for developing novel applications of gas-phase ion/molecule reactions. Manifestation of this goal may be realized by a variety of diverse applications. The following guidelines were used as an aid in directing this research to the overall objective:

(i) Apply reactions which have been previously characterized, either in a TQMS or another instrument, and seek to develop methodology which exploits the unique intermolecular activity of specific ionized functional groups present in a molecule. The chemistry of the ionized species with a reagent molecule may provide selective detection of a class of compounds.

(ii) Commit to understanding the mass spectrometric results in terms of the chemistry that is occurring in the gas-phase. This may lead to intensive study of a specific ion/molecule reaction, perhaps in an attempt to unravel mechanisms of ion formation or fragmentation. Where possible, the reaction will be evaluated in terms its thermochemistry. At times, calculating the reaction enthalpies may prove valuable in directing the future course of the research.

(iii) Being observant to the chemistry that is occurring in the ion source of the mass spectrometer may prompt ideas for ion/molecule reactive collisions which could occur in the second quadrupole collision cell. This would allow a specific reaction to be examined in an environment free of any

interfering reaction, and may help in understanding the chemistry that is happening within the ion source.

(iv) Realizing that ion/molecule reactions are not a panacea for all analytical problems involving mass spectrometry, but instead just a complement to the more conventional MS/MS techniques. Some of the work reported in this dissertation does not involve ion/molecule reactions, but new applications for the traditional collisionally induced dissociation methodology.

Mass spectrometry is a tool used for studying isolated ions in the gas-phase. Understanding the chemistry of these ions in their interaction with neutral molecules is critical in the evolution of analytical methodology. This dissertation is the culmination of the effort to further demonstrate the capabilities of a triple quadrupole mass spectrometer in studying ion/molecule reactions, and reveals some novel applications for this unique instrument.

CHAPTER II

ION/MOLECULE REACTIONS OF ARYL CATIONS

A. Introduction

Ion/molecule reactions involving aromatic cations, especially those ions which contain the six-membered benzene ring, have been widely studied in the gas-phase (104-106). The impetus behind the research that is described in this chapter arises from the previous effort put forth by Dr. Gregory Dolnikowski while he was a graduate student at Michigan State University (106). In his ion/molecule reaction studies utilizing a TQMS, he demonstrated that aryl cations which are even-electron ions with a vacant charged site on an aromatic ring, react with methanol to form a hydroxylated product ion. In the case of the $C_6H_5^+$ phenyl cation with m/z 77, reaction with methanol vapor was shown to produce a product ion with m/z 94. This product ion of m/z 94 was shown to have the structure of the molecular ion of phenol as established by their strikingly similar CID daughter ion mass spectra (71). Aryl cations were also found to be reactive with ammonia (106). Once again using the phenyl cation for illustrative purposes, the product ion with m/z 93 was obtained in the reaction with ammonia. This ion was shown to be identical in structure to the molecular ion of aniline based on the similarity of their CID daughter ion mass spectra. Ammonia has also been used as a reagent gas in the collision cell of a TQMS to probe isomeric $XC_6H_4^+$ ions for X= OCH_3, CH_3, F, and CN (107). In these studies, a nucleophilic substitution reaction occurred forming the molecular ion of derivatives of aniline.

The phenyl cation was the model aryl cation used in these earlier studies, and it proved to be very reactive in the gas-phase. This chapter describes the continued investigation of ion/molecule reactions involving aryl cations. For most reactions described in this chapter, the phenyl cation or the $(M-H)^+$ aryl cation generated from napthalene, is the model aryl cation which serves as the reactant ion.

It should be noted that all of the research performed by Dr. Dolnikowski was done on an Extranuclear (now Extrel) triple quadrupole mass spectrometer which was located in the NIH Michigan State University Mass Spectrometry Facility. Following his departure, a new triple quadrupole mass spectrometer was purchased, that being a Finnigan TSQ-70. Some of the initial experiments performed on the newly acquired Finnigan TQMS were done in the attempt to reproduce the experiments performed on the Extrel TQMS. As mentioned in chapter one, the Finnigan TQMS instrument contains a non-linear second quadrupole rod assembly, and all three sets of quadrupole rods are physically much smaller than the quadrupole rods in the Extrel instrument. Therefore, it was necessary to attempt initially experiments on the Finnigan TSQ-70 that had been characterized previously with the Extrel TQMS, so the feasibility of performing ion/molecule reactions in the TSQ-70 could be determined. These investigations led to the further study and elucidation of the hydroxylation ion/molecule reaction between the phenyl cation and methanol, establishing in more detail the reaction mechanism. Furthermore, additional experiments of aryl cations with different reagent gases were performed.

This chapter is divided into three broad sections following this introductory section. In the first section, the chemistry of the reaction of aryl cations, predominantly the ion/molecule reaction of the phenyl cation with

various reagent gases is described. The intent was not to perform an exhaustive study for each reagent gas investigated, but rather to examine reactions with some neutral reagent candidates and comment on the ion/molecule reaction products in terms of the computed thermochemistry. Unless otherwise indicated, all of the reaction enthalpies reported for the ion/molecule reactions, were calculated based on ionic and neutral heats of formation obtained from reference 108. The latter sections of this chapter describe two analytical applications for an ion/molecule reaction with dimethyl ether which appears to be selective for aryl cations. One application demonstrates the potential for using neutral gain experiments in screening for aromatic compounds present in mixtures. The second application described in this chapter involves probing the structure of $C_7H_7^+$ isomers utilizing low-energy ion/molecule reactions in the center quadrupole of a TQMS.

B. Survey of ion/molecule reactions involving the phenyl cation

1. *Experimental*

The experiments described in this chapter were performed on the Finnigan TSQ-70 triple quadrupole mass spectrometer. The phenyl cation was generated by electron impact of benzene which was introduced directly into the ion source via a variable leak. A direct inlet system was constructed by the machine shop which fitted onto the flange mounted for use with the GC transfer line. This set-up enabled the CI reagent gas lines to be utilized simultaneously which provides the capability of mixing neutral vapor molecules in the ion source. Solid samples analyzed were dissolved in a

suitable solvent and introduced into the ion source via the direct insertion probe. When the ion/molecule reactions were performed in the collision cell, the reagent vapors were introduced through the CID gas lines.

For liquid reagents, the sample was introduced into a glass bulb which was constructed at the Department of Chemistry's glass blowing shop. These bulbs were fitted with 1/8" stainless steel tubes which enabled them to be connected directly to the gas lines via Swagelok^{TM} connections. The bulb also was fitted with a rubber stopper which permitted an efficient vacuum seal to be created when the bulb was exposed to the pumping system of the TSQ-70. After connecting the empty glass bulb to the collision gas inlet line of the TSQ-70, the gas line valves were opened which served to purge the bulb prior to the introduction of the liquid reagent. Once the bulb was purged, the valves were closed and the liquid was introduced via an injection by a syringe through the rubber stopper. Provided that there was sufficient vapor pressure, the gaseous molecules diffused into the second quadrupole collision cell (or into the ion source) and the pressure could be regulated by the needle valves connected to the gas lines. The pressures in the collision cell and in the ion source were measured by a convectron gauge, and are not indicative of the actual pressure. An ion gauge is located towards the rear of the manifold region of the TSQ-70, and the pressure readings indicated by the ion gauge generally remain stable throughout the duration of an experiment. The pressure reading indicated by the convectron gauge fluctuates often, even while the ion gauge reading remains steady. For all of the experiments reported in this chapter, the temperature of the ion source was maintained at 150°C, while the manifold region was held at 70°C. Figure 2-1 is a representation of the vacuum system of the Finnigan TSQ-70.

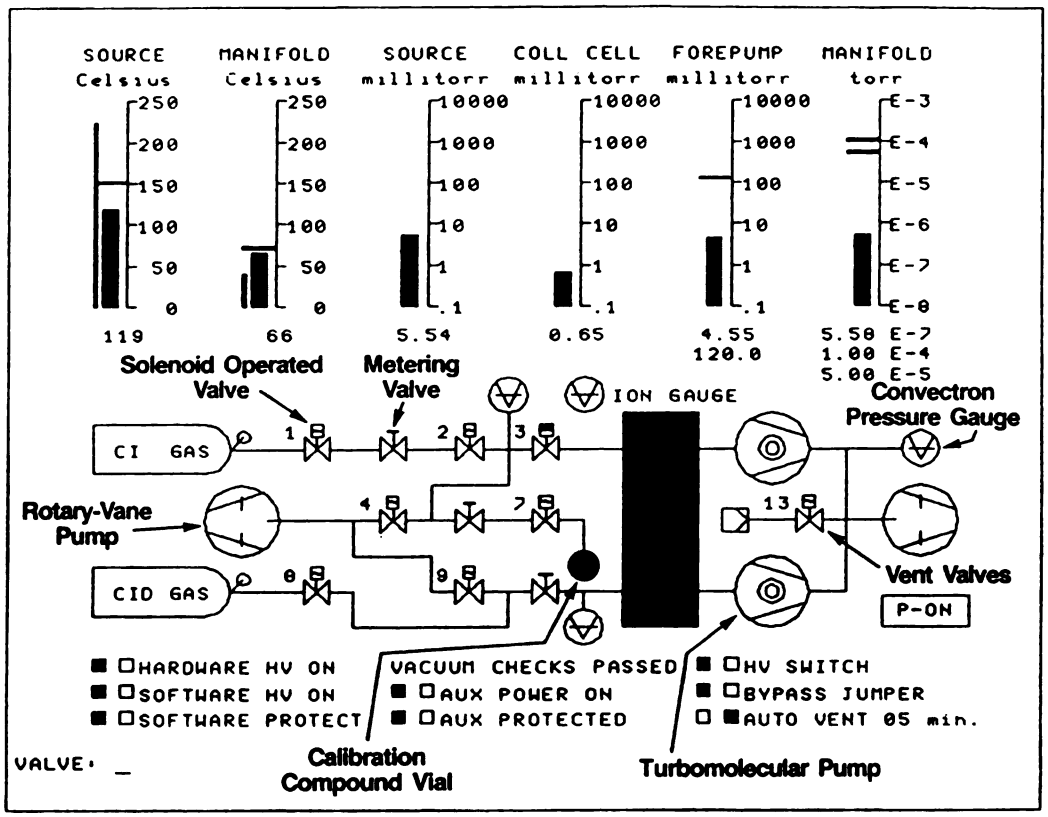

Figure 2-1: Schematic diagram of the vacuum system of the Finnigan TSQ-70 triple quadrupole mass spectrometer. (Adapted from reference 17).

2. *Reaction with alcohols*

a) Methanol

The first ion/molecule reaction investigated in the collision cell of the Finnigan TSQ-70 was the reaction of the phenyl cation with m/z 77 and methanol. The product ion mass spectrum is shown in Figure 2-2, along with the product ion mass spectrum obtained on the Extrel triple quadrupole prior to this instrument being transported to the Chemistry Building. In both cases, the pressure in the collision cell was approximately 1 mtorr and the collision energy was 2 eV_{Lab}. Considering the vast differences in the physical dimensions of the Q_2 collision cells, the product ion mass spectra obtained with the two TQMS instruments appear remarkably similar. Based on the results of this initial experiment, it did not appear that the physical dimensions of the rods in the TSQ-70 would deter the formation of low-energy ion/molecule reaction products and subsequent detection.

It had been demonstrated by Dolnikowski that the reaction product ion of m/z 94 was identical in structure to the molecular ion of phenol (71). This determination was made by comparing the CID daughter ion mass spectrum of the molecular ion of authentic phenol with the CID daughter ion mass spectrum of the reaction product ion of m/z 94 generated when benzene and methanol were simultaneously introduced into the ion source. It seems likely that the structure of the intermediate collision-complex preceding the formation of the product ion of m/z 94, is identical to the structure of protonated anisole as shown in Figure 2-3. However, no experimental evidence had been obtained on the Extrel which would support this hypothesis. To verify this premise, methanol and benzene were simultaneously introduced into the ion source, and the product ion which

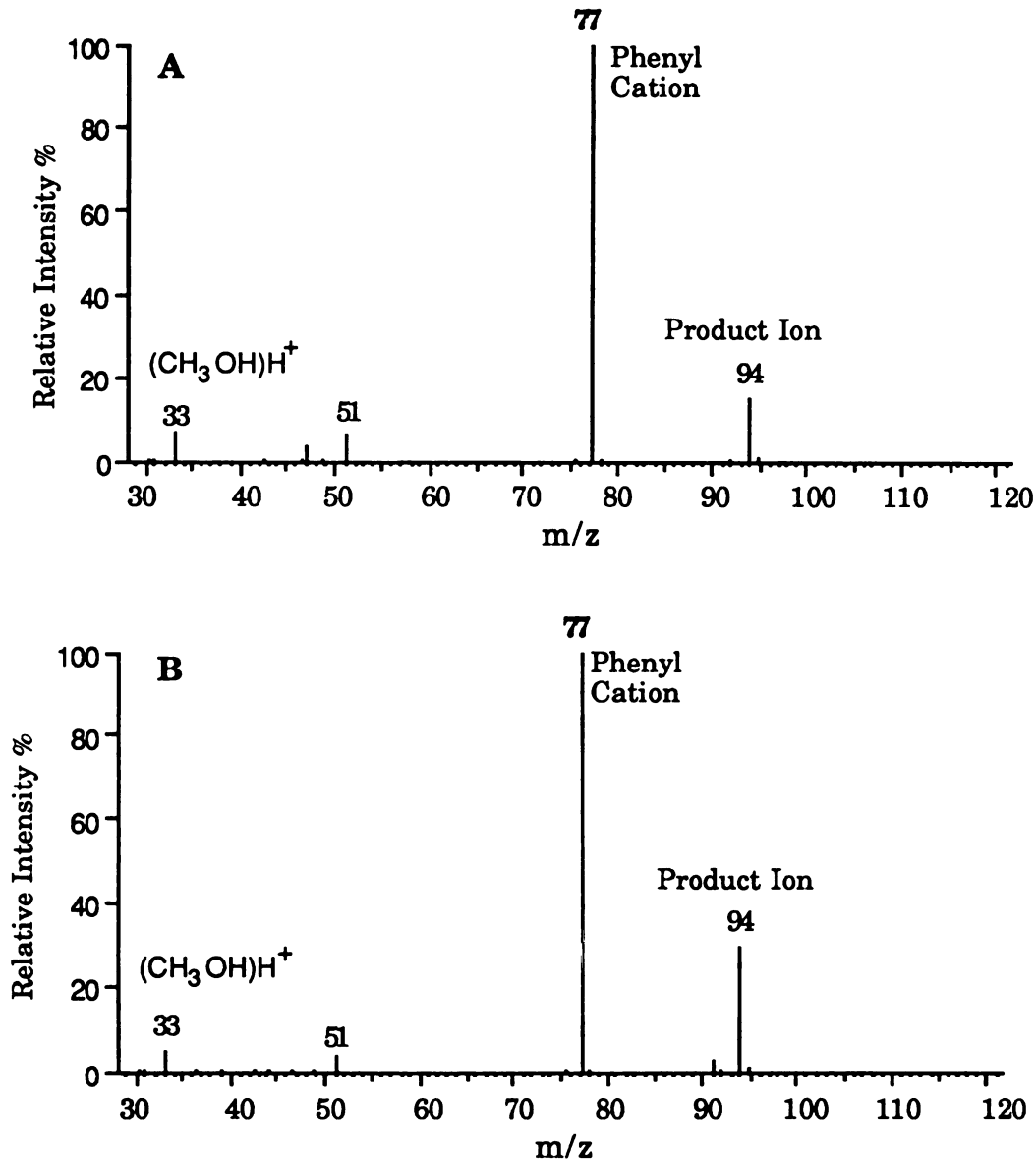

Figure 2-2: Product ion mass spectra of the phenyl cation and methanol obtained with the A) Extrel TQMS and B) Finnigan TSQ-70.

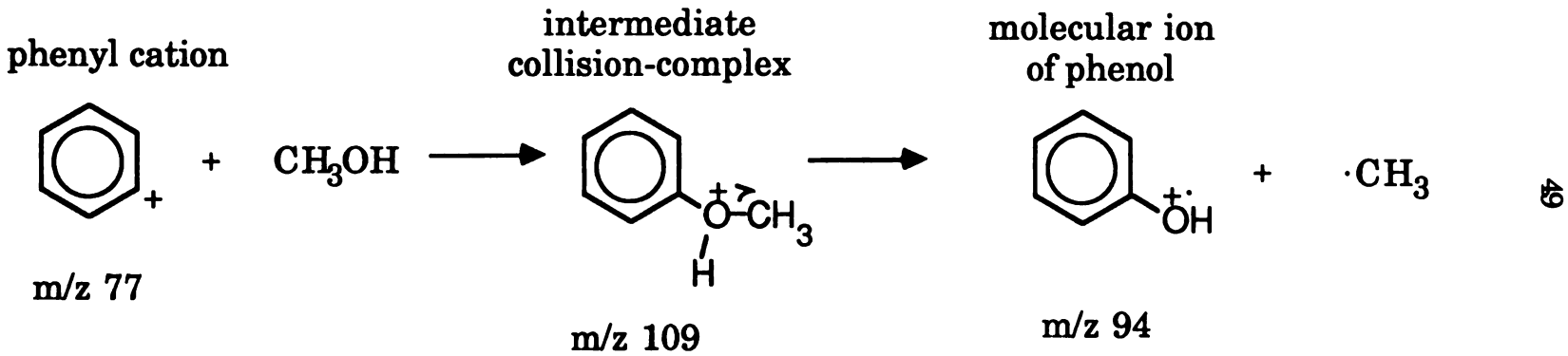

Figure 2-3: Ion/molecule reaction mechanism to form the molecular ion of phenol from the reaction of the phenyl cation and methanol.

appeared with m/z 109 was subjected to CID. The CID daughter ion mass spectrum of the proposed intermediate ion of m/z 109 is shown in Figure 2-4. Protonated isomers of cresol along with protonated anisole were all viewed as possible structural candidates for the intermediate with m/z 109. All of these ions have the $C_7H_9O^+$ composition. The CID daughter ion mass spectrum of protonated anisole, along with the CID spectra of the protonated forms of two cresol isomers, are shown in Figure 2-5. All of the daughter ion mass spectra show a fragment peak at m/z 94, therefore it appears that all of these isomeric ions with m/z 109 give rise to the phenol molecular ion upon CID. The CID daughter ion mass spectrum of protonated anisole, however, is nearly identical to the CID daughter ion mass spectrum of the product ion produced from the phenyl cation and methanol reaction (Figure 2-4). The distinguishing feature is the presence of peaks at m/z 66 and m/z 77 in the CID daughter ion mass spectra of both protonated anisole and the reaction product ion of m/z 109. These peaks at m/z 66 and m/z 77 are absent in the CID daughter ion mass spectra of the *o*-and *p*-isomers of cresol. This clearly establishes that the molecular ion of phenol is formed via the initially-formed intermediate collision-complex which has the structure of protonated anisole. These experiments demonstrate how CID and ion/molecule reaction experiments complement each other. The isolated reactants of a product ion may be determined by examining the ion/molecule reaction in the center quadrupole, while mechanisms of the product ion formation may be verified by CID studies following the formation of the reaction products in the ion source. The formation of the product ions in the ion source does not preclude the possibility of other isomeric product ions being formed with identical m/z values, however, to generate the product ion in the second quadrupole, it would be necessary to have a second collision chamber and a third mass

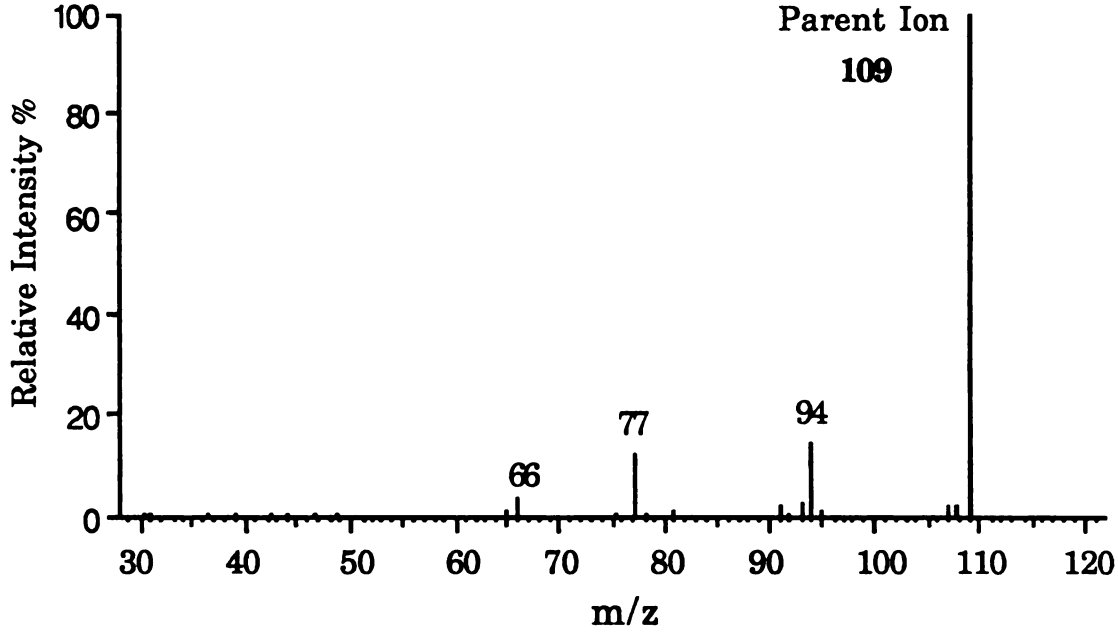

Figure 2-4: CID daughter ion mass spectrum of product ion of m/z 109 formed when benzene and methanol were simultaneously introduced into the ion source. Collision energy was 30 eV_{Lab} at single collision conditions.

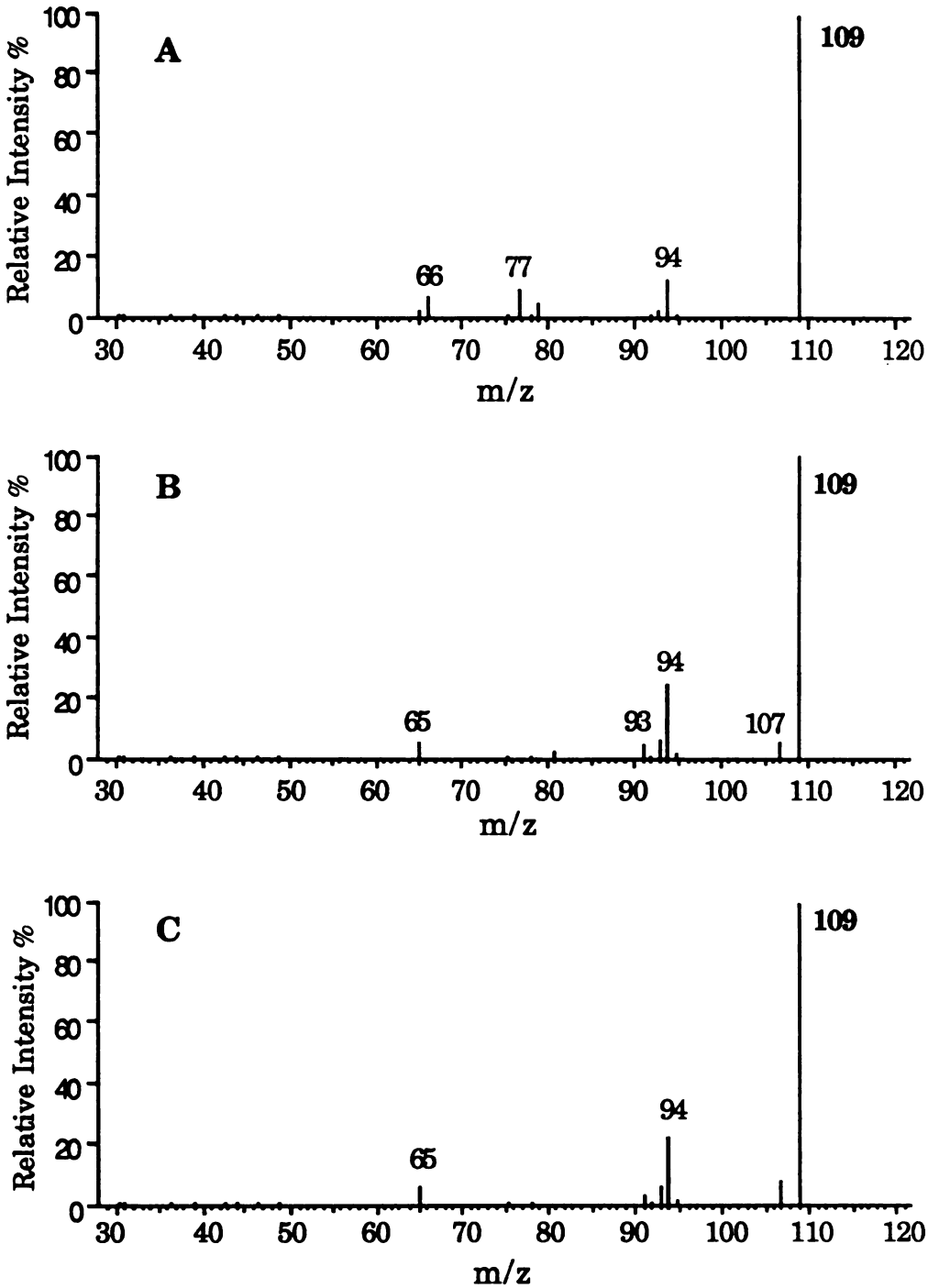

Figure 2-5: CID daughter ion mass spectra of the protonated forms of A) anisole, B) o-cresol and C) p-cresol. Collision energy was 30 eV_{Lab} at single collision conditions.

analyzer for the subsequent CID. This would require a penta-quadrupole mass spectrometer which is not available at Michigan State University. An alternative approach would be to perform an MS/MS/MS experiment in an ion-trap mass spectrometer.

One of the interesting features of this ion/molecule reaction is that the initial reactant ion, $C_6H_5^+$, is an even-electron ion, while the product ion with m/z 94 contains an odd number of electrons. The even-electron rule, often applied as a basic principle in organic mass spectrometry, is usually applied to fragmentation of ions following ionization by EI (109,110). It states that odd-electron cations may eliminate a radical or an even-electron neutral species, but even-electron ions generally will not lose a radical to form an odd-electron cation. In our case, an even-electron ion reacts with methanol to form protonated anisole, an even-electron intermediate collision-complex. This intermediate ion (m/z 109) eliminates a radical, which is in violation of the 'rule' used for interpreting mass spectra generated by EI. The question of an even-electron reactant ion forming an odd-electron product ion was posed by a referee who reviewed a manuscript (71), and additional experimental work was performed to verify our claims concerning this hydroxylation reaction. The referee thought that perhaps the reactant ion was not the phenyl cation, but rather the molecular ion of benzene, which is a much more intense peak in the EI mass spectrum. If the benzene radical cation, $C_6H_6^{+\cdot}$, is chosen to react with methanol in the collision cell, there is no peak detected at m/z 94, but rather at m/z 95. This product ion with m/z 95 presumably represents protonated phenol. Formation of protonated phenol and the methyl radical from $C_6H_6^{\cdot+}$ and methanol is 16.2 kJ/mol exothermic. On the other hand, the reaction enthalpy for the production of the molecular ion of phenol along with a methyl radical and hydrogen radical from $C_6H_6^{\cdot+}$ and

methanol is 311.6 kJ/mol endothermic. If methane were the neutral product along with the phenol molecular ion in the reaction of $C_6H_6^{\cdot+}$ and methanol, the reaction enthalpy would be 126.7 kJ/mol exothermic. This exothermic sequence, however, would require extensive hydrogen rearrangement and does not appear to occur as suggested by the absence of a peak at m/z 94 in the product ion mass spectrum. Although our experimental results of the reaction of the even-electron phenyl cation with methanol violate the so called 'even-electron rule', thermochemical data support the experimental claims. The reaction of the phenyl cation with methanol to form the molecular ion of phenol and a methyl radical is 54 kJ/mol exothermic. Additional reaction products may be expected based on the calculated exothermic heats of reactions, however, these product ions are either absent or present only as minor peaks in the product ion mass spectrum. This is attributed to unfavorable kinetic conditions, that is, the residence time within the collision cell is too short for these reactions to occur.

b) Ethanol

Following the success of the hydroxylation reaction with methanol, the reaction of the phenyl cation with a higher order alcohol was investigated. It was anticipated, rather naively, that in similar fashion to the reaction with methanol, the reaction with ethanol would yield the hydroxylation product ion with the structure of phenol. However, as shown in Figure 2-6, the predominant product ion appears as a peak at m/z 95, which represents protonated phenol. Once again, examination of the reaction enthalpies provides insight into the chemistry by clearly indicating that the formation of protonated phenol is favored thermodynamically over the formation of the molecular ion of phenol. In fact, as shown in Table 2-1, methanol is unique in

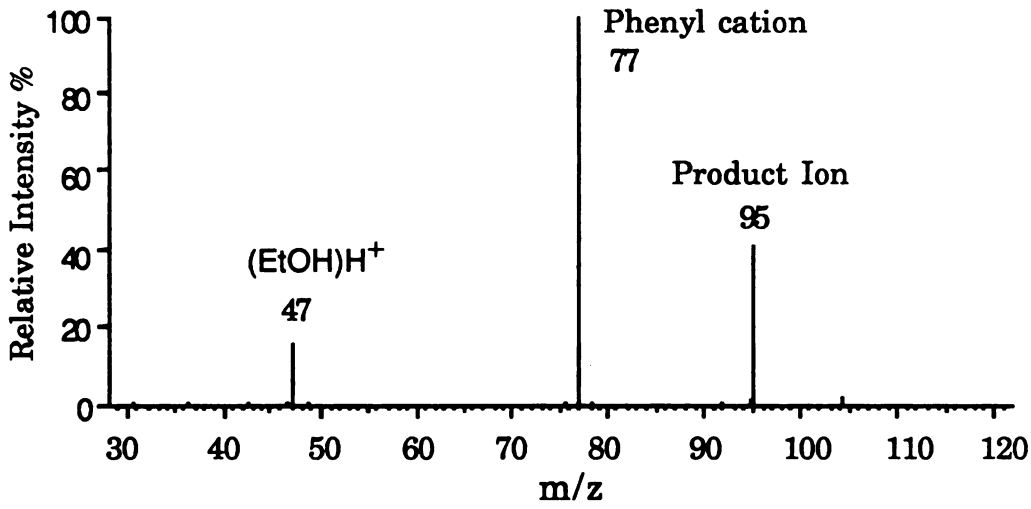

Figure 2-6: Product ion mass spectrum of the phenyl cation reacting with ethanol at a pressure of 1.5 mtorr and with a collision energy of 1 eV_{Lab}.

Table 2-1: Calculated enthalpies for reactions of phenyl cation with alcohols[a]

	ΔH_{rxn} (kJ/mol)
$C_6H_5^+ + CH_3OH \longrightarrow C_6H_5OH^{+\cdot} + \cdot CH_3$	-54
$C_6H_5^+ + CH_3OH \longrightarrow C_6H_5OH_2^+ + CH_2$	+77
$C_6H_5^+ + C_2H_5OH \longrightarrow C_6H_5OH^{+\cdot} + \cdot C_2H_5$	- 52
$C_6H_5^+ + C_2H_5OH \longrightarrow C_6H_5OH_2^+ + C_2H_4$	- 227
$C_6H_5^+ + C_3H_7OH \longrightarrow C_6H_5OH^{+\cdot} + \cdot C_3H_7$	- 50
$C_6H_5^+ + C_3H_7OH \longrightarrow C_6H_5OH_2^+ + C_3H_6$	-239
$C_6H_5^+ + i\text{-}C_3H_7OH \longrightarrow C_6H_5OH^{+\cdot} + \cdot C_3H_7$	-39
$C_6H_5^+ + i\text{-}C_3H_7OH \longrightarrow C_6H_5OH_2^+ + C_3H_6$	-221

a Ionic and heats of formation found in reference 108.

that the thermodynamically-favored reaction product is the molecular ion of phenol and ***not*** the protonated form. For reactions of the phenyl cation with alcohols which contain more than one carbon, the formation of the molecular ion of phenol and a radical species is exothermic, however, the elimination of a neutral olefin along with the formation of protonated phenol, provides neutral products with increased stability. This significantly increases the exothermicity of the reaction. During the course of formation of protonated phenol, hydrogen located on an ethanol carbon atom apparently may undergo rearrangement, transferring to the oxygen atom prior to elimination of the olefin. If this transfer can also readily occur for higher order alcohols and proceed rapidly, the thermochemistry suggests, as indicated in Table 2-1, that protonated phenol would be the expected ionic reaction product of the phenyl cation with alcohols other than methanol.

3. *Reaction with amines*

a) Ammonia

The reaction of the phenyl cation with ammonia was previously shown to result in the formation of reaction product ions with m/z 93 and m/z 94 (106). Based on the similarity of the respective CID daughter ion mass spectra, the ion with m/z 93 was shown to be identical in structure to the molecular ion of aniline (106). The ion with m/z 94 may either represent protonated aniline or a non-covalently bound phenyl cation-ammonia adduct. This reaction was performed in the second quadrupole of the TSQ-70 and the product ion mass spectrum shown in Figure 2-7 appears similar to that obtained on the Extrel TQMS. The reactions forming ionic aniline and protonated aniline are exothermic as indicated in Table 2-2.

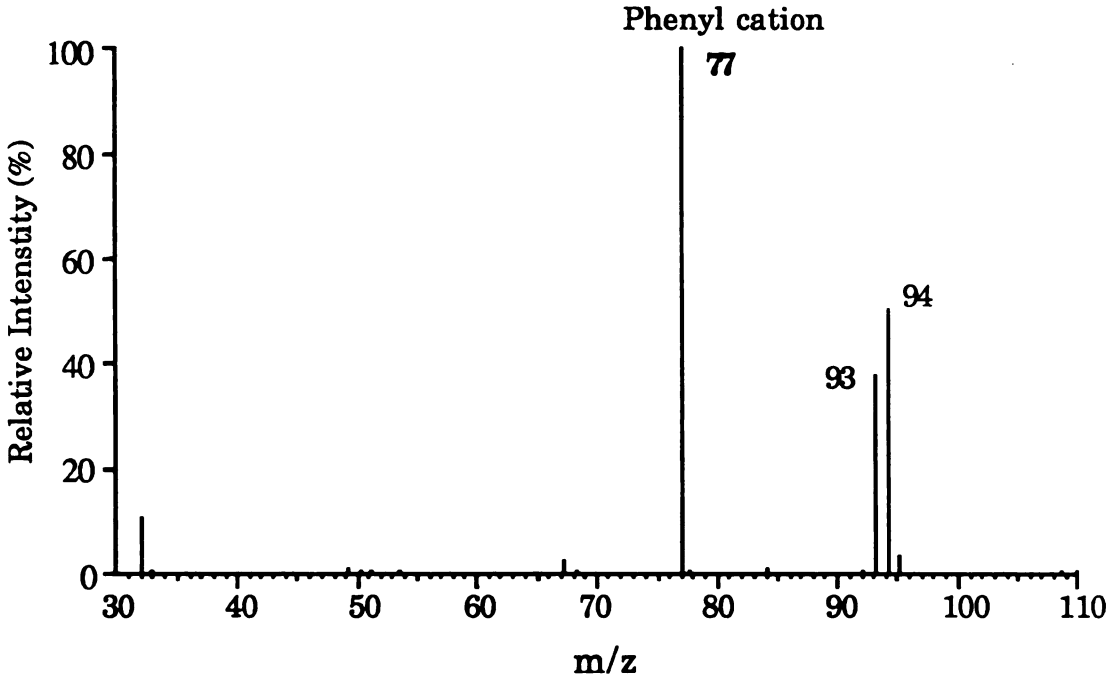

Figure 2-7: Product ion mass spectrum of the phenyl cation and ammonia. Collision pressure ~ 2 mtorr and collision energy is 2 eV_{Lab}.

Table 2-2: Reaction enthalpies for the phenyl cation reacting with ammonia.

$C_6H_5^+ + NH_3 \text{ ----------> } C_6H_5NH_2^{+\cdot} + \cdot H \qquad \Delta H_{rxn} = -34 \text{ kJ/mol}$

$C_6H_5^+ + NH_3 \text{ ----------> } C_6H_5NH_3^+ \qquad \Delta H_{rxn} = -341 \text{ kJ/mol}$

It is interesting to examine the energy-resolved curve for the reaction of the phenyl cation with ammonia as shown in Figure 2-8. At collision energies greater than 5 eV_{Lab}, the product ions obtained in the interaction of the reactant ion of m/z 77 and ammonia are a result of CID. At collision energies nearer to 0 eV_{Lab}, the abundance of the ion/molecule reaction products increases, while the CID products decrease in intensity. Of considerable importance is the maximum abundance of the ion/molecule reaction product of m/z 93, which represents the formation of a covalently-bound product ion as compared to the maximum abundance of the CID product ion of m/z 51 over the range of collision energies examined. The intensity of the CID peak at m/z 51 representing the elimination of ethyne, at optimal fragmenting conditions is only one-fourth that of the maximum abundance of the covalently bound ion/molecule reaction product ion (m/z 93) formed at low-collision energy. The implication of this observation is important. Here is a case where the inherent stability of the parent ion impedes fragmentation in CID, whereas with the ion/molecule reaction, the formation of more stable products results in an abundant product ion being detected. The formation of the $C_4H_3^+$ ion and C_2H_2 from the $C_6H_5^+$ phenyl cation is 318 kJ/mol endothermic. By taking advantage of the exothermic reactivity of the phenyl cation with ammonia, an ion/molecule reaction sequence occurs which forms the molecular ion of aniline and ·H; the reaction enthalpy is -34 kJ/mol. As discussed in chapter one, a possible disadvantage with the ion/molecule reaction approach using a TQMS is the potential difficulty in detecting product ions formed at low collision energy due to insufficient kinetic energy. At low collision energies, this can lead to poor transmission efficiency. However, in this case, the detectability of the low-

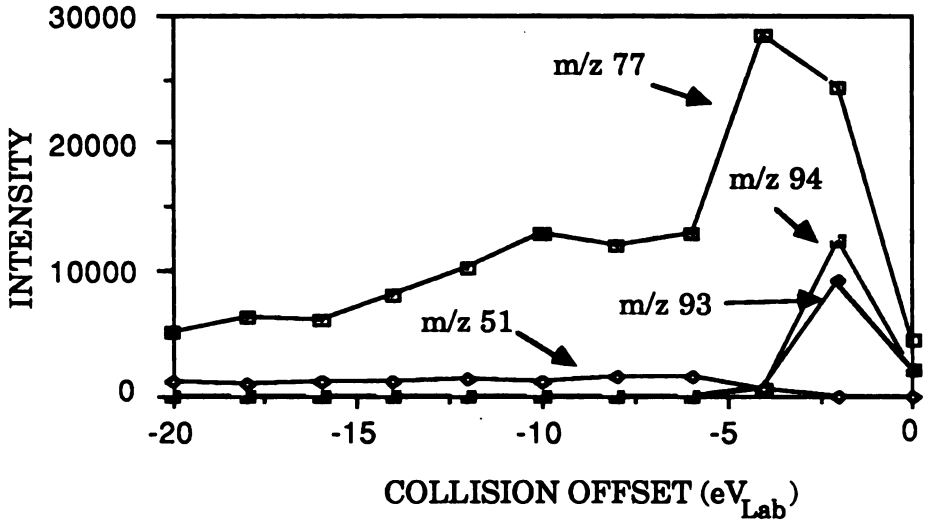

Figure 2-8: Energy-resolved curve of the reaction products generated from reaction of the phenyl cation and ammonia. Collision pressure is 1 mtorr.

energy ion/molecule reaction product ion is greater than the detectability of CID fragments. These results imply that ion/molecule reactions may be useful in analytical applications where the formation of a product ion in high yield is critical for the development of MS/MS methodology which could provide low detection limits.

b) Methyl amine

Methyl amine was introduced into the collision cell and the phenyl cation was selected as the reactant ion. The product ion mass spectrum at a collision energy of 1 eV_{Lab}, obtained when methylamine was present in Q_2 at a pressure of 1.5 mtorr, is shown in Figure 2-9A. The spectrum obtained under multiple collision conditions, indicates a peak at m/z 93 which again represents the molecular ion of aniline, and a peak at m/z 32 representing protonated methyl amine. Protonated methyl amine is formed by ion/molecule reactions in methyl amine occurring in Q_2. If the collision energy is raised to 20 eV_{Lab}, the product ion mass spectrum, as seen in Figure 2-9B, lacks the peaks at m/z 93 and m/z 32, but the CID peak at m/z 51 is more prominent. The enthalpy of the reaction forming the aniline molecular ion and the methyl radical is 129.1 kJ/mol exothermic. If the $(M-H)^+$ of napthalene is generated by EI ionization and chosen to react with methylamine, once again a product ion at 16 u (corresponding to NH_2) higher than the parent ion is detected in the product ion mass spectrum as shown in Figure 2-10.

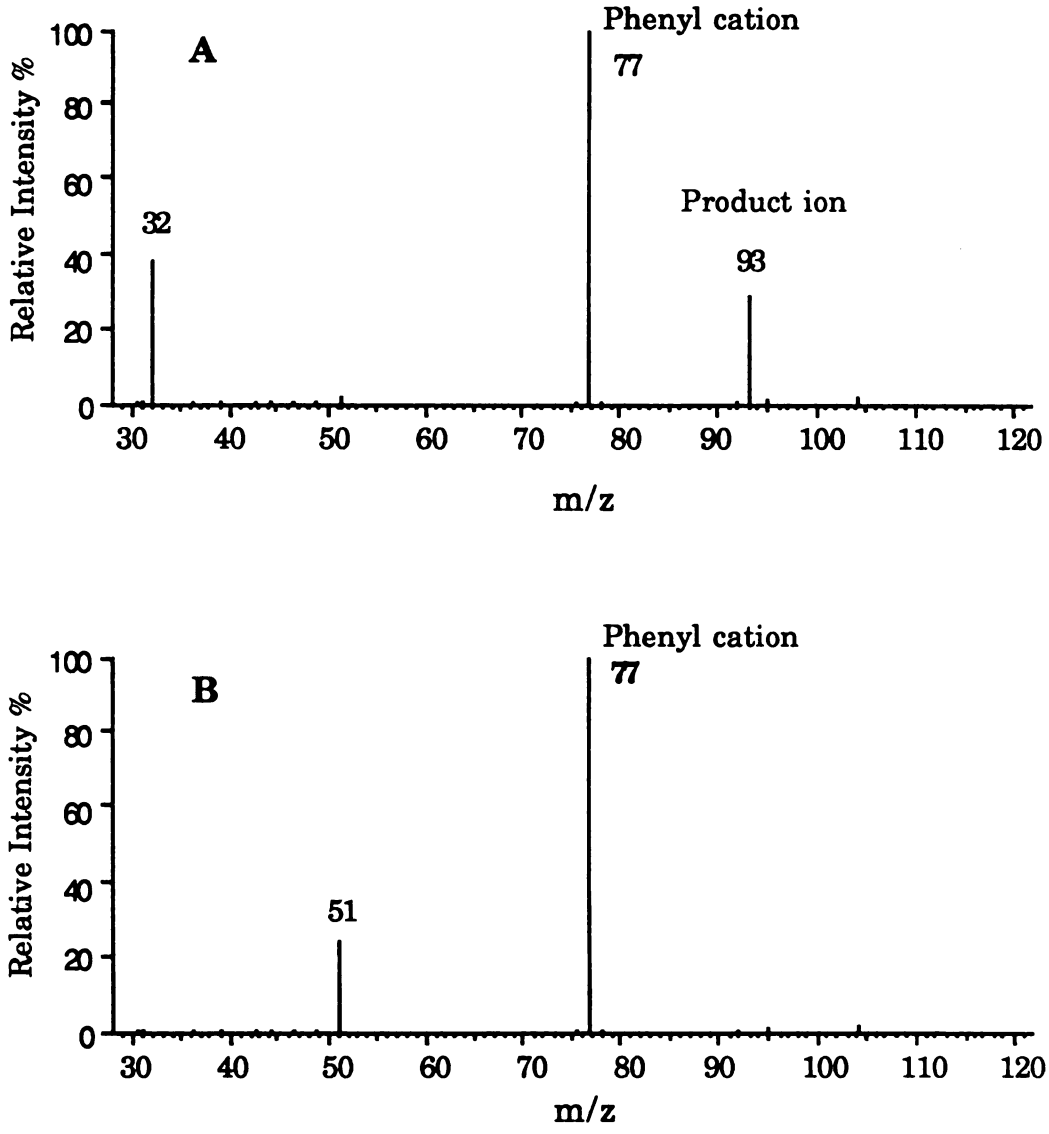

Figure 2-9: Product ion mass spectrum of the phenyl cation and methyl amine at collision energy of A) 1 eV_{Lab} and B) 20 eV_{Lab}. Methyl amine pressure is 1.5 mtorr.

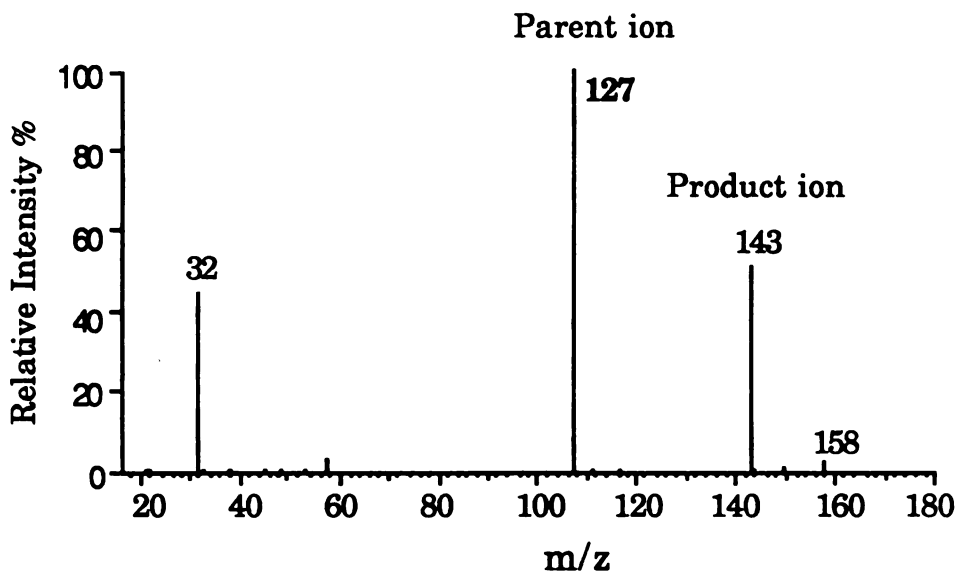

Figure 2-10: Product ion mass spectrum of the $(M-H)^+$ of napthalene with methyl amine at a pressure of 1.5 mtorr and collision energy of 1 eV_{Lab}.

4. *Reaction with CH_3CN*

In contrast to the previous reagents described in reaction with the phenyl cation, the computed thermochemistry suggests that a covalently bound addition product ion would not be formed when the phenyl cation reacts with acetonitrile. The reaction enthalpy for the formation of the $C_6H_5CN^+$ cation and a methyl radical from the phenyl cation and acetonitrile is 392 kJ/mol endothermic. The CH_3-CN bond strength is 507 kJ/mol, and is not overcome by the formation of a new bond with a ring carbon in the phenyl cation. Although this reaction was not examined with the phenyl cation, the analogous reaction was performed with the $(M-H)^+$ aryl cation of napthalene. In the studies being described in this chapter, ion/molecule reaction with the $(M-H)^+$ ion of napthalene always parallels a successful reaction of the reagent with the phenyl cation. Therefore, reaction of the napthyl cation with acetonitrile should be indicative of the reactivity of the phenyl cation with CH_3CN. The product ion mass spectrum of the napthyl cation with m/z 127 and acetonitrile is shown in Figure 2-11. A peak at m/z 168 representing the non-covalently bound adduct ion is the only product ion detected. There is no product ion detected which represents covalent bond formation during a ring addition reaction.

5. *Reaction with ethers*

a) Dimethyl ether

The product ion mass spectrum of the phenyl cation with dimethyl ether at a pressure of 1 mtorr and a collision energy of $1eV_{Lab}$ shows a

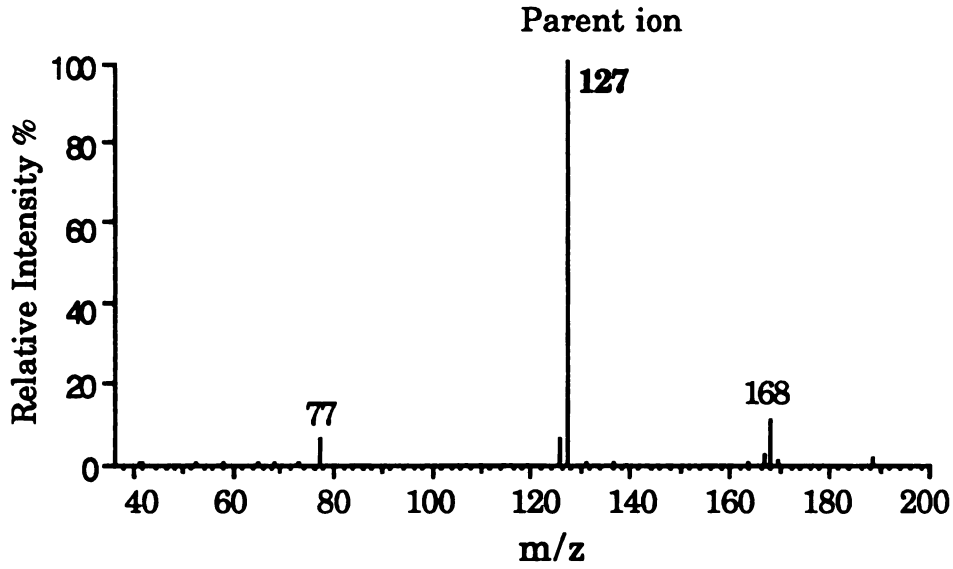

Figure 2-11: Product ion mass spectrum of $(M-H)^+$ of napthalene with acetonitrile at a pressure of 2 mtorr and a collision energy of 1 eV_{Lab}

product ion peak at m/z 108 which represents the addition of $\cdot OCH_3$ (Figure 2-12). Calculation of the reaction enthalpy indicates that this reaction forming the molecular ion of anisole is 73.1 kJ/mol exothermic. Dimethyl ether has been used as a reagent gas in chemical ionization studies, yet there were no peaks detected at $(M+31)^+$ in the chemical ionization (CI) mass spectrum for either benzene or napthalene (111). Perhaps with CI being a soft ionization method, there is not sufficient internal energy in the protonated ion to eliminate H_2 forming the aryl cation for subsequent reaction with dimethyl ether. Ion/molecule reactions involving dimethyl ether will be discussed in greater detail later in this chapter.

b) Diethyl ether

The product ion mass spectrum of the phenyl cation with diethyl ether at a pressure of 1.2 mtorr and a collision energy of 2 eV_{Lab} is shown in Figure 2-13. Two abundant product ion peaks are observed at m/z 95 and m/z 105. The product ion with m/z 95 may represent protonated phenol; this reaction is 158 kJ/mol exothermic as seen in Table 2-3. This reaction requires consecutive hydrogen rearrangements for the elimination of two ethylene molecules. The second product ion with m/z 105 could represent a $C_8H_9^+$ ion. Generation of this product ion requires a collision-complex intermediate structure which would allow for the formation of a C-C bond and the elimination of ethanol, an ion/molecule reaction which is 279 kJ/mole exothermic.

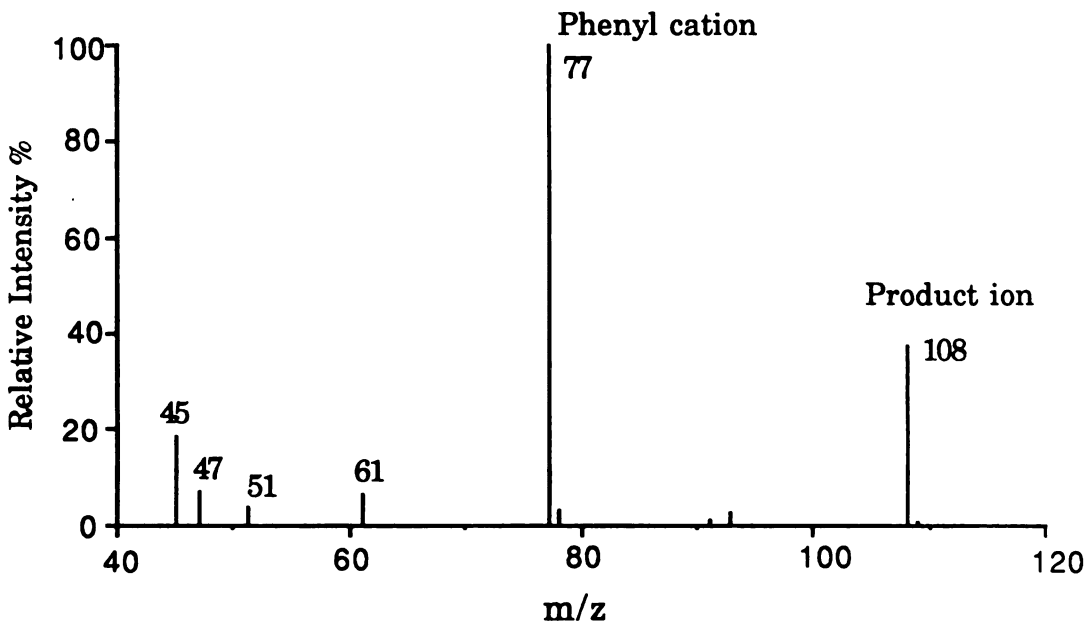

Figure 2-12: Product ion mass spectrum of the phenyl cation and dimethyl ether at a pressure of 1 mtorr and collision energy of 1 eV_{Lab}.

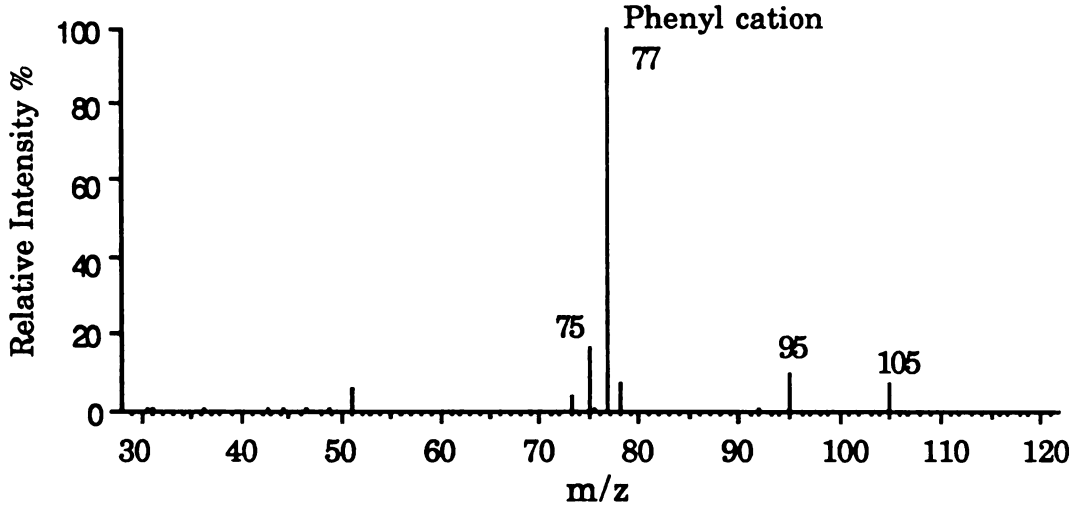

Figure 2-13: Product ion mass spectrum of the phenyl cation and diethyl ether at collision energy of 2 eV_{Lab} and pressure of 1.2 mtorr.

Table 2-3: Reaction enthalpies for the phenyl cation reacting with diethyl ether.

$C_6H_5^+ + (C_2H_5)_2O \rightarrow C_6H_5OH_2^+ + 2C_2H_4 \quad \Delta H_{rxn} = -158$ kJ/mol

$C_6H_5^+ + (C_2H_5)_2O \rightarrow C_6H_5C^+HCH_3 + C_2H_5OH \quad \Delta H_{rxn} = -279$ kJ/mol

c) Vinyl methyl ether

The product ion mass spectrum of the phenyl cation with vinyl methyl ether (VME) at a pressure of 1.2 mtorr is shown in Figure 2-14. The major product ion, although not as intense as product ion peaks derived from other reagents, is observed at m/z 103 which represents the addition of C_2H_2. Minor product ion peaks are detected at m/z 91 and m/z 109. Table 2-4 shows postulated reactions which may account for these product ions.

Table 2-4: Structural candidates of the product ions formed in the reaction of the phenyl cation and VME

	ΔH_{rxn}(kJ/mol)
$C_6H_5^+ + CH_2{=}CHOCH_3 \rightarrow C_6H_5C^+{=}CH_2 + CH_3OH$	*na*
$C_6H_5^+ + CH_2{=}CHOCH_3 \rightarrow C_6H_5CH_2^+ + HOCH{=}CH_2$	- 252
$C_6H_5^+ + CH_2{=}CHOCH_3 \rightarrow (C_6H_5OCH_3)H^+ + C_2H_2$	- 174

na Heat of formation for $C_6H_5C^+{=}CH_2$ not found.

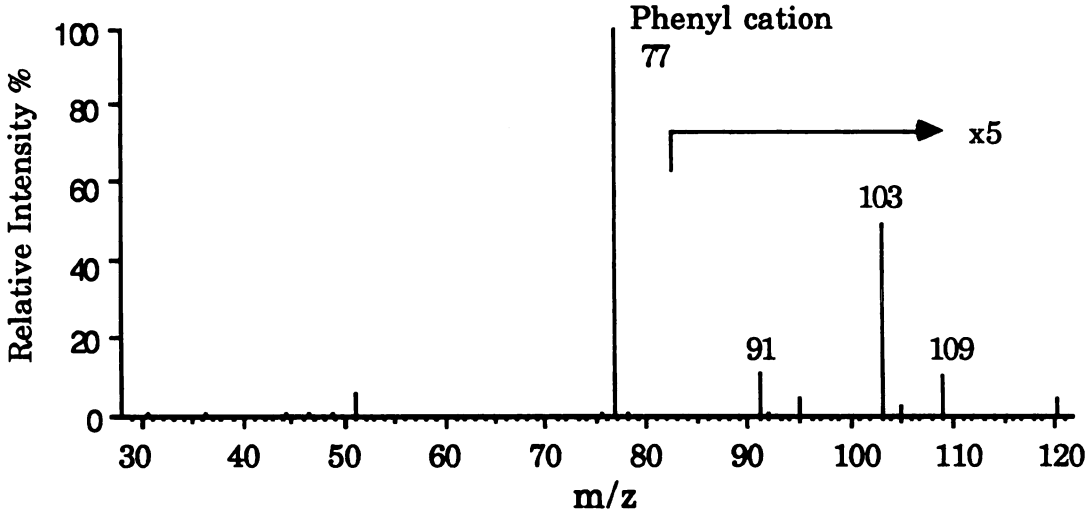

Figure 2-14: Product ion mass spectrum of the phenyl cation and vinyl methyl ether at collision energy of 2 eV_{Lab} and a pressure of 1.2 mtorr.

6. *Summary of reactions*

A variety of neutral reagents are shown to be reactive with the phenyl or napthyl cation forming a nucleophilic addition reaction product ion. In the reactions described, the reaction channels accessed forming covalently bound addition products were all exothermic. For the smallest homologues, such as methanol, dimethyl ether, and methyl amine, simple bond cleavage reactions forming an addition product with the elimination of a radical were the dominant reactions observed. With more complex molecules, hydrogen rearrangement reactions took place. For the analytical applications which were sought for this nucleophilic addition reaction with aryl cations, dimethyl ether was chosen as the reagent gas. There were two reasons for choosing dimethyl ether over other neutral candidates. First, dimethyl ether is a gas at standard temperature and pressure (STP) which makes it easier to handle for introduction into the collision cell of a TQMS. Second, the product ion which is formed, representing the addition of 31 u, is an isolated product ion, that is to say, there is not a non-specific product ion with a mass in close proximity to the mass of this methoxylated product ion. Ammonia satisfies the first criterion in that ammonia is a gas at STP, however, not only is there a product ion representing the addition of NH_2, but there is the potential of a non-specific ion forming at one mass unit greater than the covalently bound ion. This ion could represent the formation of the non-specific ammonia adduct ion. For analytical applications, it was desirable to have a 'clean' region surrounding the peak representing the reaction product ion.

C. Screening for aromatics

As discussed above, the phenyl cation reacts with dimethyl ether to form a methoxylated product ion. Additional experiments were performed to determine the selectivity of this ion/molecule reaction. If this reaction is selective for aromatics with a vacant charged site on an aromatic ring, then perhaps a rapid screening procedure could be developed where aromatics could be detected in a mixture of compounds. Under EI conditions, it would be likely that aromatics, regardless of the substituents located on the ring, would yield ions which satisfy the criteria established for a successful ion/molecule reaction.

Initially, an experiment was performed which demonstrates that the reaction is observed even with up to three substituents on the ring, which might be expected to sterically hinder the ion/molecule reaction. Figure 2-15 indicates that the methoxylation reaction occurs for the $(M\text{-}Cl)^+$ ion of 1,2,4,5 tetrachlorobenzene. The position of the chlorine atoms on the benzene ring ensure that following loss of one Cl, the charge on the ring will be on a carbon atom adjacent to a carbon with a chlorine substituent. The 1,2,4,5 tetrachlorobenzene was introduced into the ion source via the GC, and the $(M\text{-}Cl)^+$ ion was selected for reaction with DME. As shown in Figure 2-15, when the ion with m/z 179 which represents $C_6H_2{}^{35}Cl_3{}^+$, is reacted with dimethyl ether, a product ion is detected at m/z 210. If the ion of m/z 181 is selected ($C_6H_2{}^{35}Cl_2{}^{37}Cl^+$), the product ion is detected as a peak at m/z 212. The presence of three Cl substituents on the aromatic ring does not seem to hinder the reactivity of this $C_6H_2Cl_3{}^+$ aryl cation.

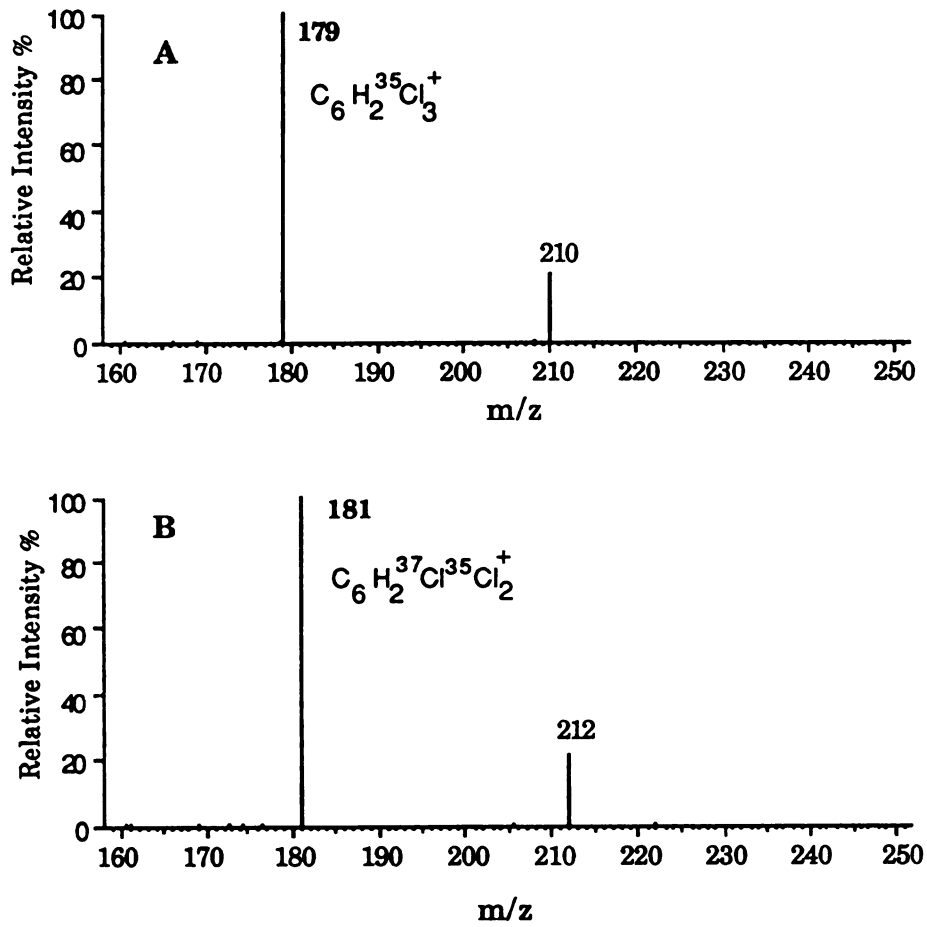

Figure 2-15: Product ion mass spectra of the $(M\text{-}Cl)^+$ ion of 1,2,4,5 tetrachlorobenzene with DME at 1 mtorr. Parent ion is A) $C_6H_2{}^{35}Cl_3^+$ (m/z 179), B) $C_6H_2{}^{37}Cl^{35}Cl_2^+$ (m/z 181).

Over the course of these studies, a variety of compounds were ionized and ions present in the mass spectrum were selected for reaction with dimethyl ether. These compounds included primary, secondary and tertiary alcohols, esters, hydrocarbons, ketones and additional aromatic compounds. A product ion peak 31 u greater than the parent ion mass was only detected for aromatic compounds which contained a vacant charged site on the ring. The product ion mass spectrum of the $(M-H)^+$ ion of pyridine, an aromatic without the benzene ring substructure, is shown in Figure 2-16. The methoxylation product ion peak is seen at m/z 109 following the reaction of the ion with m/z 78 and DME. The peaks at m/z 93 and m/z 124 represent the protonated DME dimer, and the adduct ion of DME and the pyridine ion, respectively.

An experiment was performed which serves to demonstrate the selectivity of this ion/molecule reaction. A simple mixture, with components listed in Table 2-5, was injected into the GC interfaced to the TQMS. Three of the components are aromatic. Figure 2-17 shows the total ion current chromatogram and the reconstructed mass chromatogram of m/z 77, following ionization by EI. The phenyl cation with m/z 77 is indicative of aromatic compounds, however, from this simple mixture, only one of the components gives a peak at m/z 77. There is not an ion formed during EI which is unique to these three aromatic compounds. If the mixture were more complex, it would be even less likely that one ion would characterize the aromatics, yet not be found in the EI mass spectrum of the non-aromatic components. To determine which components are aromatic, it would be necessary to evaluate each individual mass spectrum.

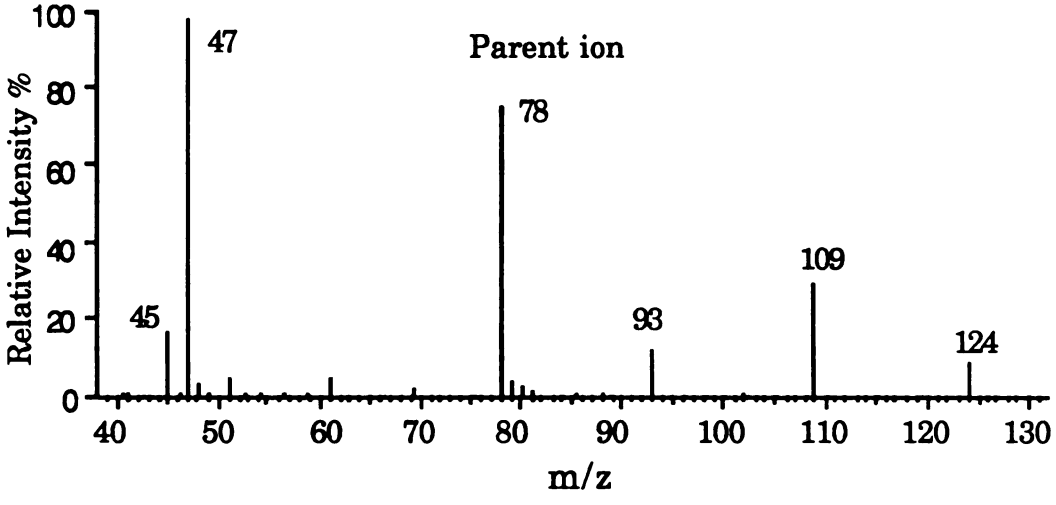

Figure 2-16: Product ion mass spectrum of the $(M-H)^+$ ion of pyridine (m/z 78) with dimethyl ether at a pressure of 2 mtorr and collision energy of 1 eV_{Lab} .

Table 2-5: Components in mixture used to obtain chromatograms shown in Figures 2-17 and 2-18.

1) o-xylene

2) 1,2 dibromopropane

3) 1,2 dichlorobenzene

4) 1,2,4 trichlorobenzene

5) 6-undecanone

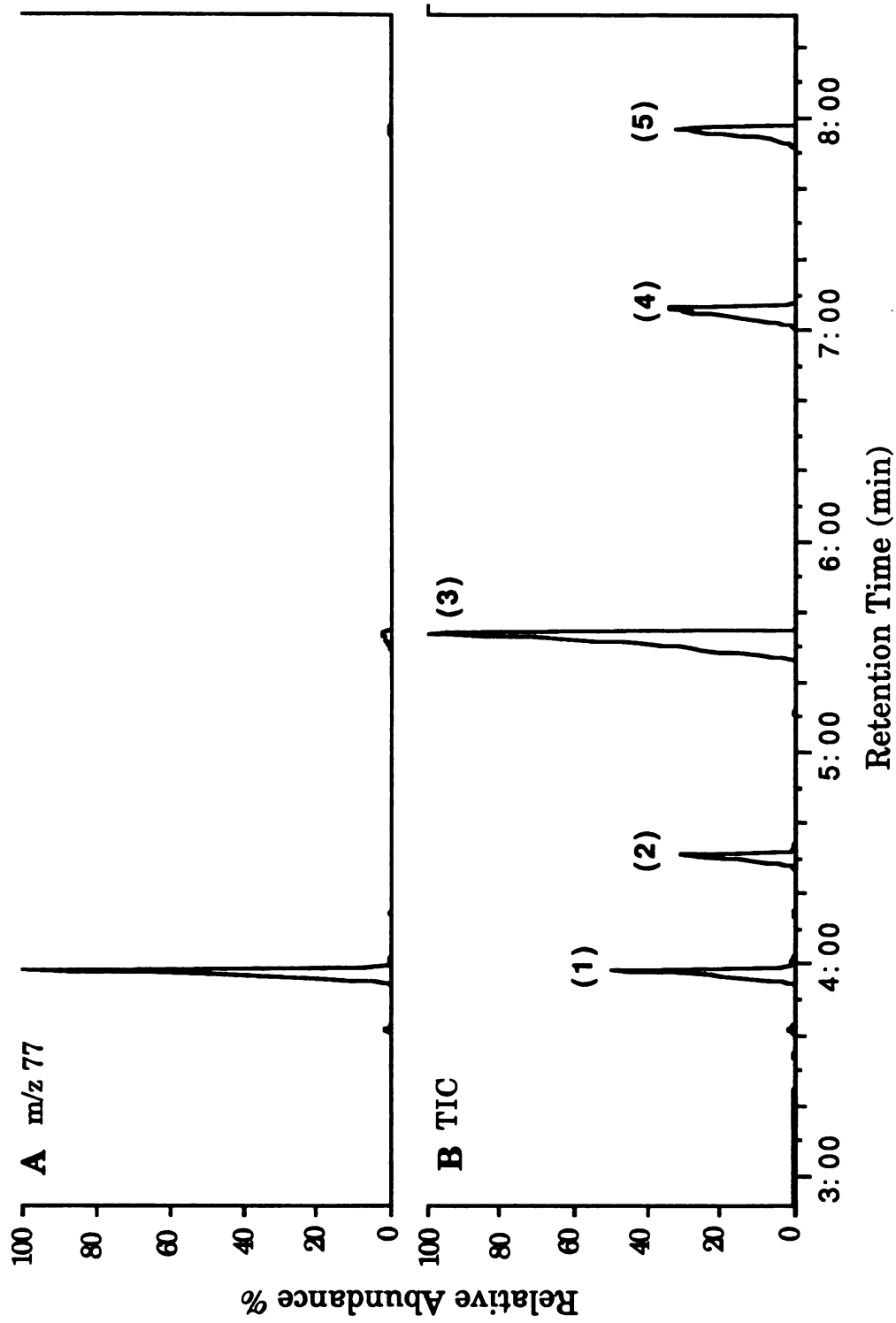

Figure 2-17: A) Reconstructed mass chromatogram of m/z 77 and B) total ion current chromatogram, following EI of mixture introduced through GC.

In contrast, aromatic compounds would be expected to yield at least one ion in the EI mass spectrum which would contain a vacant charged site on the ring. Regardless of the mass of this ion, it would be expected that the aryl cation would react with dimethyl ether to form a methoxylation product ion. A neutral gain experiment of +31 will provide detection of only those ions which are able to undergo an addition of 31 u following reaction with dimethyl ether. Figure 2-18 illustrates the total ion current chromatogram obtained in a +31 neutral gain experiment following injection of this five-component mixture. Only the three aromatic compounds **1**), **3**), and **4**), are detected as peaks in the GC trace. As demonstrated, none of the ions in the EI spectrum of 6-undecanone or 1,2-dibromopropane will form a methoxylation product ion 31 mass units higher than the reactant ion. Electron impact ionization of 6-undecanone offers a slew of ions for reaction with dimethyl ether, yet none undergo the methoxylation ion/molecule reaction with dimethyl ether. Detailed structural information is not obtained with this approach, yet this neutral gain experiment could be used to rapidly identify aromatics within mixtures.

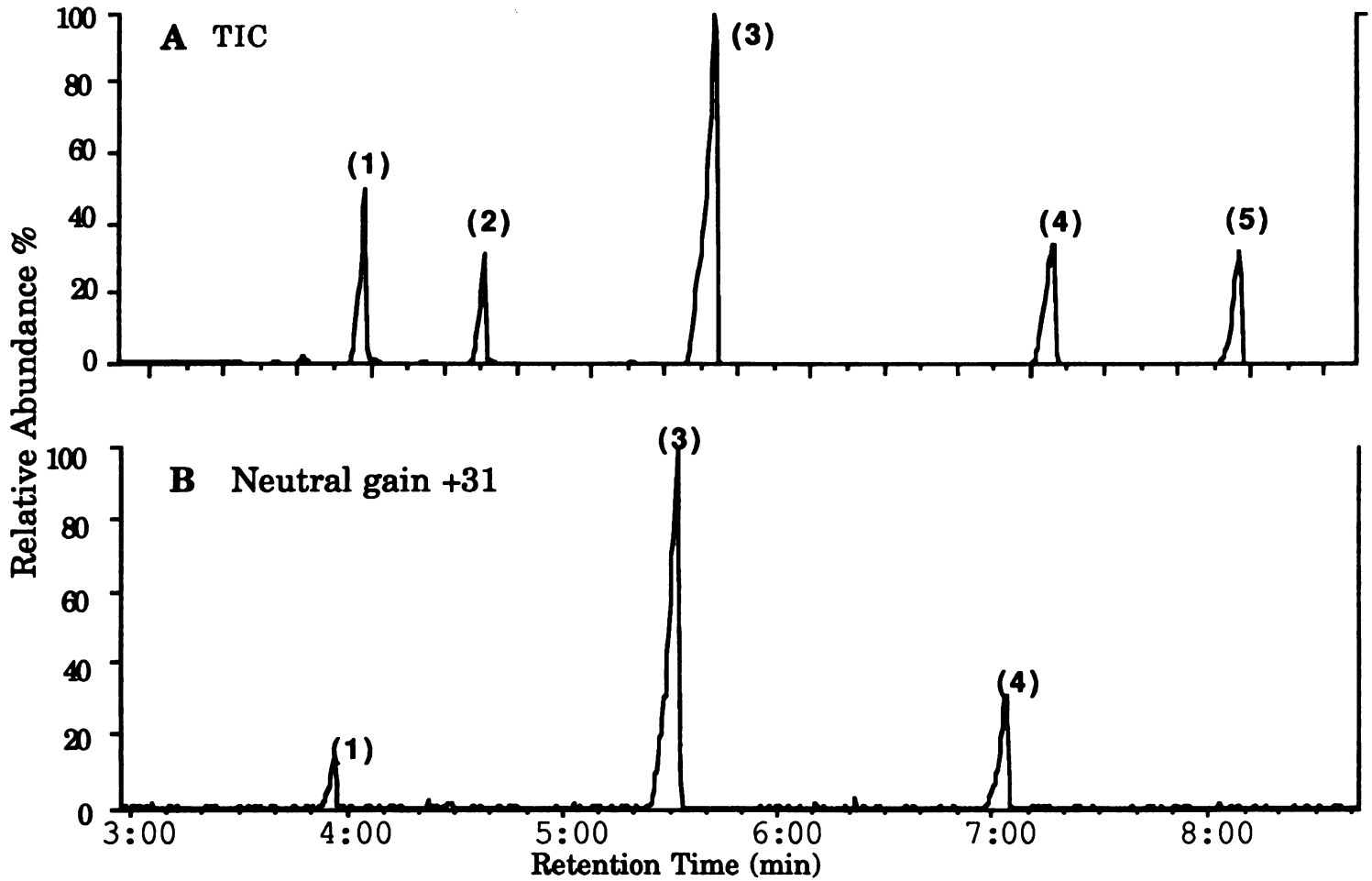

Figure 2-18: A) Total ion current chromatogram, following EI of mixture introduced through GC, and B) total ion current chromatogram from neutral gain experiment (+31) with DME in Q_2 at a pressure of 1.1 mtorr and a collision energy of 1 eV_{Lab}.

D. Ion/molecule reaction of [$C_7H_7^+$] isomers for selective detection of the tolyl cation

1. *Introduction*

Perhaps the most widely investigated series of ionic isomers in the gas-phase are those with $C_7H_7^+$ composition (105). Most of the attention has been directed towards three of these isomers, the benzyl cation (112), the tropylium cation (113), and the tolyl cation (114) which are shown in Figure 2-19. In the effort to distinguish these individual species, high energy collisional activation (CA) mass spectrometry has been utilized with some success (114-118). There are minor differences in the relative abundances of the fragment ions in the m/z 74 to m/z 77 region when the individual ionic species are generated in the ion source and subjected to high-energy collisional activation with a target gas. These variations in relative abundances are indicative of the individual isomers and provide a 'fingerprint' of each ionic species.

Despite the success of the CA methodology, disadvantages exist with this high-energy CA technique. The primary disadvantage being that the capacity to distinguish these isomers is dependant on the reproducibility of specified ratios of fragment ion abundances. The m/z values of the fragment ion peaks in the daughter ion mass spectra are identical; there are no unique daughter ion peaks which unequivocally characterize the individual isomers using the high-energy CA approach. Figure 2-20 indicates the relatively minor differences in the high-energy CA spectra of the benzyl cation and tropylium cation.

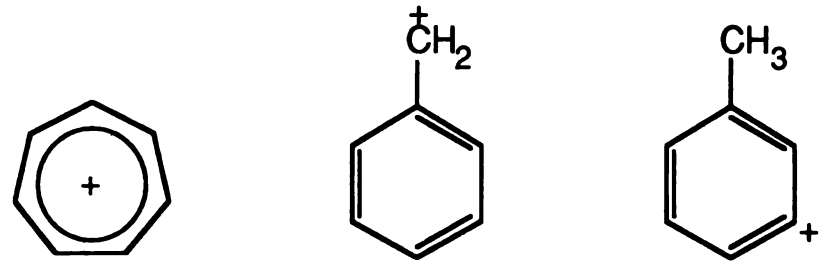

	tropylium (1)	benzyl (2)	3-tolyl (3)
ΔH_f(kJ/mol)	849	897	1054

Figure 2-19: Structures and heats of formation for $C_7 H_7^+$ isomers. Heats of formation taken from references 108 and 125.

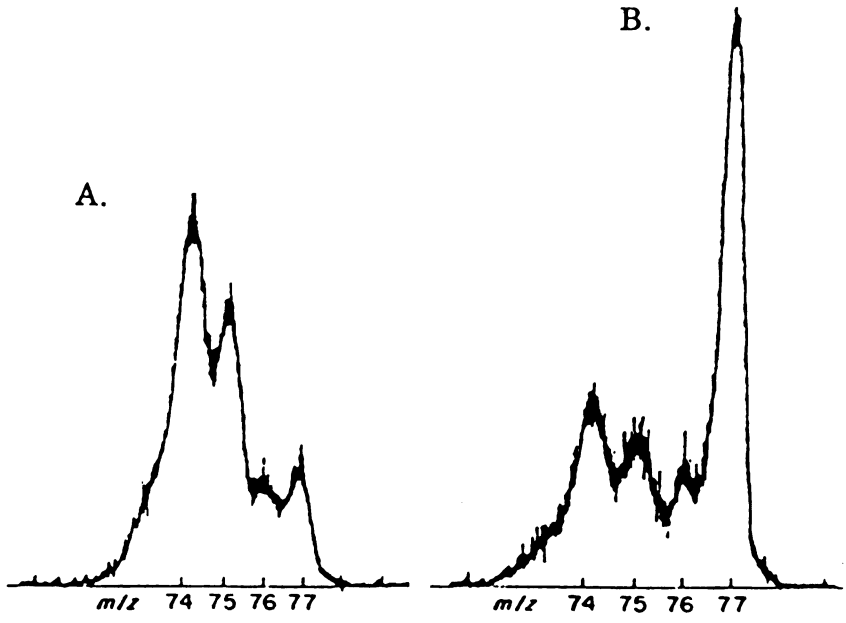

Figure 2-20: CA mass spectrum of A) pure tropylium and B) pure benzyl ions. Accelerating voltage = 8kV. (Adapted from reference 117).

An alternative approach for analysis of $C_7H_7^+$ ions has been to exploit their unique intermolecular reactivity (105). Ion cyclotron resonance (ICR) mass spectrometers are usually chosen for these ion/molecule reaction studies, although some work has been done utilizing high pressure ion sources. Tropylium ions have been found to be non-reactive in the attempts to utilize ion/molecule reactions as structural probes (105). However, both the benzyl and tolyl ions have been shown to be reactive with a variety of neutral reagent molecules, thereby permitting these ions to be characterized via an ion/molecule reaction (11,110,119-124).

Heretofore, little effort has been directed towards differentiating these isomers by low-energy collisions with a reagent gas in a triple quadrupole mass spectrometer. The CID daughter ion mass spectra of these isomers are nearly identical in the collision energy regime accessible with a TQMS. However, based on the results described previously in this chapter, the reactivity of the ions with neutral reagents was investigated in the attempt to selectively detect one or more of these isomeric ions. Only the tolyl ion has the positive charge located on a ring-carbon, therefore, it was expected that this isomer would react with DME whereas the other isomeric ions would not.

2. *Experimental*

a) Instrumentation

All experiments were performed on a Finnigan TSQ-70 triple stage quadrupole mass spectrometer. Following ionization of the aromatic compounds by electron impact, the structurally 'pure' reactant ion of m/z 91 was selected by Q_1 and passed to the collision cell. The reagent gas was introduced into the Q_2 collision cell via stainless steel gas lines at an

indicated pressure of 1E-6 to 8E-6 torr measured by a remote ionization gauge; this corresponds to approximate Q_2 pressures of 0.2 mtorr to 1.5 mtorr, as measured by a convectron gauge. Upon reaction with the neutral vapor, the product ion mass spectrum was obtained by scanning the second mass analyzer, Q_3. This yielded a mass spectrum indicating the m/z for the reaction products formed in the collision cell. The collision energy was always 1-2 eV_{Lab} which optimized the detection of the ion/molecule reaction product ion. For the studies in which the electron energy was varied, the values are reported as indicated by the Finnigan TSQ-70 data system.

b) Generation of 'pure' isomers:

A. Tropylium cation: 'Pure' tropylium ions were generated by 70-eV electron impact of the tropylium tetrafluoroborate salt (118), introduced into the mass spectrometer ion source via the direct insertion probe or by electron impact of toluene at an ion source pressure of ~0.1 torr (114).

B Benzyl cation: The benzyl cation was generated by low electron energy electron impact ionization of benzyl bromide (118). Benzyl bromide was introduced into the ion source via a controlled variable leak valve, or via the gas chromatograph.

C. Tolyl cation: Tolyl cations were initially generated by methane chemical ionization (CI) of 3-fluorotoluene (114). However, later in our investigations, the tolyl cation was generated by low energy EI of 3-nitrotoluene (114,118). To generate a steady production of the tolyl ion of m/z 91, the precursor neutral molecules were introduced into the ion source via a controlled leak valve.

c) GC/MS/MS analyses

The Finnigan TSQ-70 instrument was equipped with a Varian 3700 gas chromatograph which over the course of this study was used to introduce a prepared mixture consisting of substituted aromatics which are known to produce specific isomers or mixtures of isomeric $C_7H_7^+$ ions. The mixture of aromatic compounds (described below), was separated on a DB-5 capillary column (30m x 0.25mm, J&W Scientific, Inc., Rancho Cordova, CA). Helium was used as the carrier gas at a flow rate of 1 ml/min. The column was operated with a splitless injector, and following an injection, the GC oven temperature was held at 60°C for three minutes, ramped to 90°C at 4 deg/min, and then ramped from 90°C to 180°C at 6 deg/min.

3. *Results and discussion*

As described earlier in this chapter, selected hydrocarbons which contain a charged vacant site on an aromatic ring react with various neutral reagents resulting in an addition product ion. The success of these reactions for detection of aryl cations led to the examination of the thermodynamic requirements for selective detection of the tolyl cation among other $C_7H_7^+$ isomers, and to test the hypotheses experimentally using this low-energy ion/molecule reaction approach in a TQMS.

a) Thermochemistry

As shown in Figure 2-19 , the tolyl cation is the least stable of the three isomers under investigation (108,125). The relatively large heat of formation (125) for the tolyl cation contributes to the greater bond strength for [$C_7H_7^+$-X] for a variety of ring substituents (Table 2-6). Conversely, there is more

Table 2-6: Bond strength in kJ/mol [a]

	$D(C_7H_7^+\text{-}X)$ in kJ/mol				
		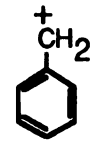	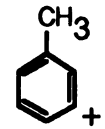	Neutral Molecule	
	D((1)-X)	D((2)-X)	D((3)-X)		D(R-X)
X=H	85	204	371	$R=CH_3$	438
				$R=C_6H_5CH_2$	372
X=OH	-	216	425	$R=CH_3$	386
X=Cl	-	121	305	$R=CH_3$	349
$X=CH_3$	-	168	357	$R=CH_3$	376
$X=OCH_3$	-	132	402	$R=CH_3$	345
$X=NH_2$	-	168	465	$R=CH_3$	358
				R=H	453
X=I	-	71	196	$R=CH_3$	237
X=CN	-	245	405	$R=CH_3$	507
$X=CHCH_2$	-	176	418	R=H	431
$X=COCH_3$	-	132	296	R=H	360

[a] Bond strengths calculated from neutral and ionic heats of formation found in reference 108 and 125 .

energy generated in formation of a bond with a ring carbon (as with the tolyl cation) than with the methyl carbon located on the benzene ring (i.e., benzyl). This thermochemical information aids in our search for a neutral candidate which may selectively react with the tolyl cation. If the energy released in the formation of the ($C_7H_7^+$-X) bond is greater than the R-X bond strength (D(R-X)) for the neutral reactant, the ion/molecule reaction is exothermic. Therefore, a neutral reagent is sought for which the R-X bond strength is greater than D((tropylium)-X) or D((benzyl)-X), yet less than D((tolyl)-X). Satisfying these criteria would yield a thermodynamically favorable ion/molecule reaction for the tolyl cation. It has been our experience in investigating ion/molecule reactions in Q_2, that ionic products formed by ion/molecule reactions are observed only for thermoneutral or exothermic reactions. In considering neutral reagent candidates, methyl iodide, for example, would not be expected to react with any of the $C_7H_7^+$ isomers to form $C_7H_7I^{+\cdot}$, because the reaction would be endothermic in all cases; the CH_3-I bond strength is greater than the D($C_7H_7^+$-I) for the benzyl and tolyl isomers, and based on the trend for R=H, the tropylium isomer. Upon examination of Table 2-6, a few neutral species emerge as reactant candidates which would be selective for the tolyl cation in an low-energy ion/molecule reaction, including methanol, dimethyl ether and ammonia, all of which were reactive with the phenyl cation.

b) Experimental results

To test our hypothesis that the tolyl cation will react selectively with methanol, dimethyl ether, or ammonia, the individual 'pure' isomers with the tolyl, tropylium or benzyl structure were generated in the ion source, and the ion with m/z 91 was chosen for reaction with the reagent gas in the collision

cell. A product ion mass spectrum for each individual isomer upon reaction with methanol was obtained, and only the tolyl cation gave a product ion peak which was detected at m/z 108 representing the addition of ·OH. This same protocol was performed with dimethyl ether as the reagent gas, and the product ion mass spectrum, corresponding to the reaction of the 3-tolyl cation with DME at a pressure of 1mtorr, is shown in Figure 2-21. The dominant ion/molecule reaction product ion is represented by a peak at m/z 122. Minor peaks are observed at m/z 45 which represents $(M-H)^+$ of dimethyl ether formed by hydride abstraction, and at m/z 65 which represents a CID fragment ion (loss of C_2H_2) from the tolyl cation. There are no product ion peaks observed when the benzyl cation or tropylium cations, generated from the appropriate neutral precursor, are individually selected and reacted with DME at the same collision conditions. These results are consistent with predictions from the thermochemistry and suggest that either methanol or dimethyl ether may be used as a reagent gas for selective detection of the tolyl cation. In these studies of the ion/molecule reactions of $C_7H_7^+$ isomers, DME is the preferred reagent gas, primarily due to the ease with which DME is introduced (DME is a gas at STP) into the mass spectrometer.

It is postulated that the product ion with m/z 122 formed by the reaction of the 3-tolyl cation and DME represents an ion structure identical to that of the molecular ion of 3-methyl anisole, as suggested by the proposed reaction mechanism shown in Figure 2-22. This reaction is 57 kJ/mol exothermic. Product ions formed by low energy collisions of the reactant ion with a neutral reagent in the center quadrupole may be detected only if the reaction is exothermic or thermoneutral, and if there is sufficient reaction time. In contrast to the favorable thermochemical conditions for the methoxylation reaction of the tolyl cation with DME, the reaction enthalpy of

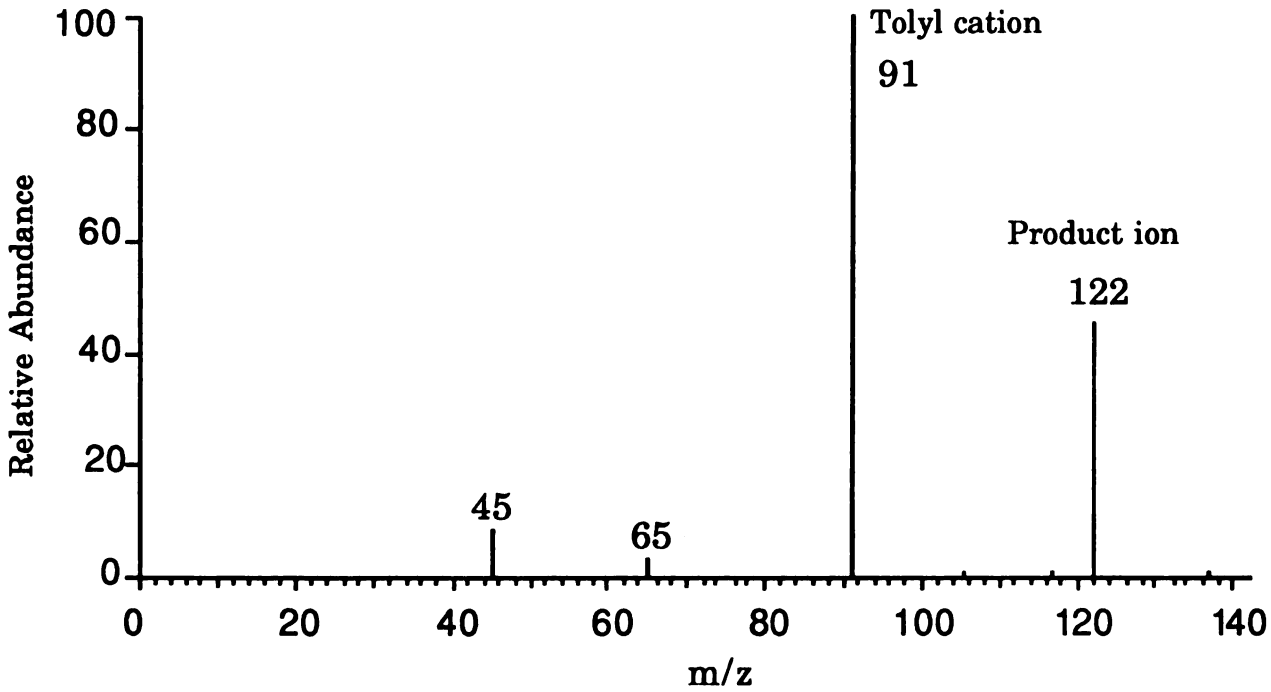

Figure 2-21: Product ion mass spectrum of the tolyl cation with DME at a pressure of 1 mtorr and collision energy of 1 eV_{Lab}.

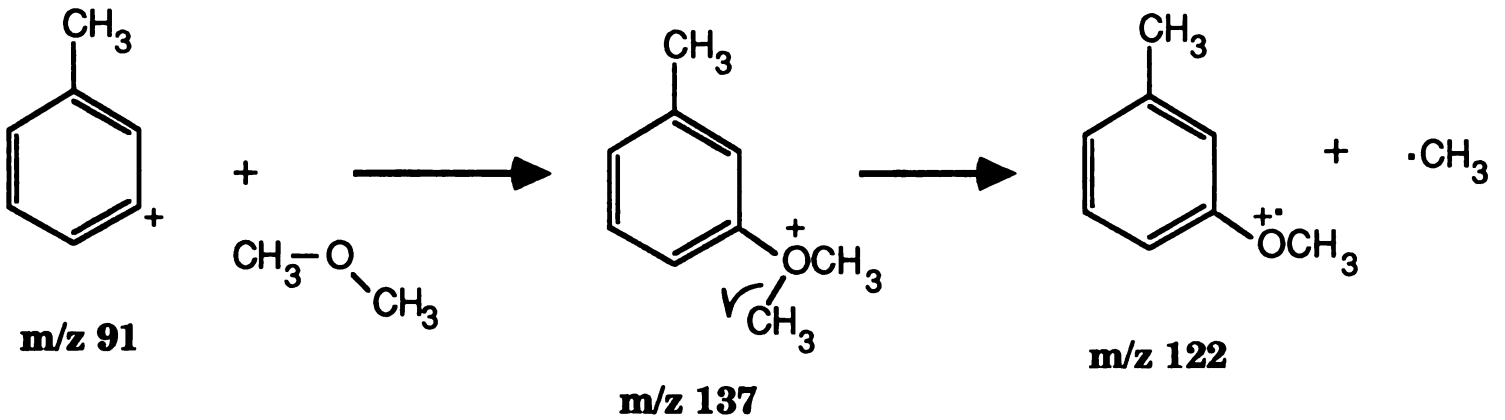

$\Delta H_{rxn.} = -57$ kJ/mol

Figure 2-22: Proposed reaction mechanism for the formation of the product ion of m/z 122 from the reaction of the tolyl cation and dimethyl ether.

the benzyl cation with DME to form a methoxylated product ion is positive 213 kJ/mol, whereas reaction with tropylium would be expected to be more endothermic, due to the even higher stability of the tropylium cation.

Evidence for the structure of the reaction product ion with m/z 122 was obtained by comparing the CID daughter ion mass spectrum of the product ion with the CID daughter ion mass spectrum of the molecular ion of 3-methyl anisole. The product ion with m/z 122 was formed when dimethyl ether was introduced into the ion source simultaneously with 3-nitrotoluene, the source of the tolyl cation. Under low-energy EI conditions, the initially formed tolyl cation reacts with DME in the ion source to give the product ion with m/z 122 which is then subjected to CID. The collision induced dissociation daughter ion mass spectrum of the reaction product of m/z 122 is shown along with the CID daughter ion mass spectrum of the molecular ion of authentic 3-methyl anisole in Figure 2-23. The similarity of these two daughter ion mass spectra provides good evidence for the structure of the product ion being identical to that of the molecular ion of 3-methyl anisole, as shown in Figure 2-22.

C) Analytical utility of the ion/molecule reaction approach

Having established that the ion/molecule reaction of these three $C_7H_7^+$ isomers with DME is selective for detection of the tolyl cation, the analytical utility of this reaction was evaluated. A simple mixture was prepared with components listed in Table 2-7. Each component was present at an approximate concentration of 20 ng/ul. One microliter of the mixture was injected into the GC, and following ionization by 70-eV electrons, the ion current at m/z 91 was selected and passed to Q_2 which contained DME at a pressure of 1 mtorr. If the ion with m/z 91 had the tolyl structure, then a peak

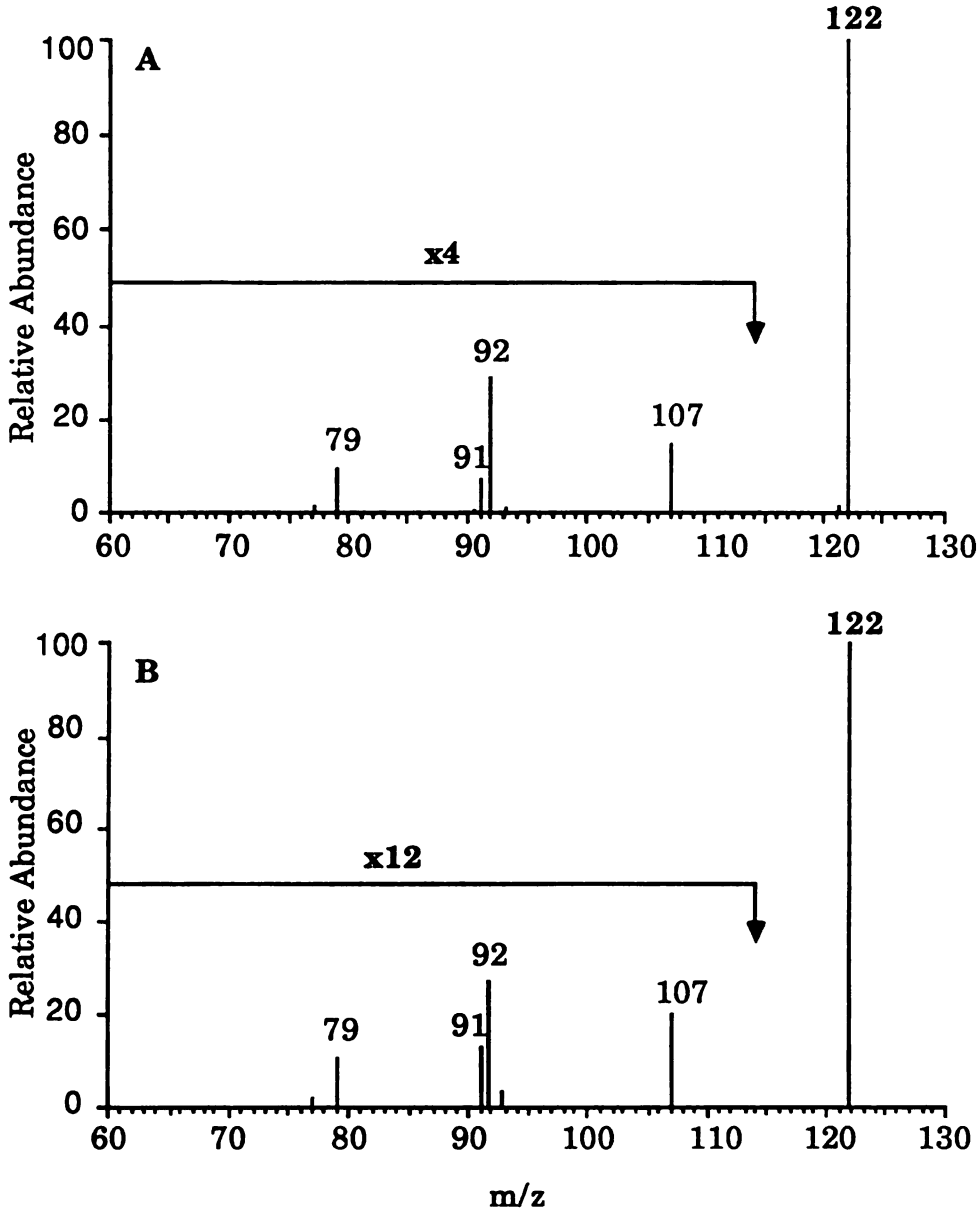

Figure 2-23: CID daughter ion mass spectrum of A) ion/molecule reaction product of mass 122 and B) molecular ion of authentic 3-methyl anisole. Collision energy was 25 eV_{Lab} at single collision conditions.

Table 2-7: Components in test mixture separated by GC to obtain chromatogram shown in Figure 2-24.

	Tolyl (%) 70 eV EI [a.] (CA results)
a) o-chlorotoluene	3
b) m-chlorotoluene	24
c) p-chlorotoluene	3
d) benzyl methyl ether	NR
e) o-bromotoluene	3
f) p-bromotoluene	3
g) benzyl bromide	NR
h) m-iodotoluene	40
i) m-nitrotoluene	57
j) p-nitrotoluene	70

[a.] results taken from reference 118.

NR, not reported.

at m/z 122 was anticipated in the product ion mass spectrum. The results of this experiment are shown in Figure 2-24 which is a composite of the reconstructed mass chromatograms at m/z 91 and at m/z 122. Coincidence of peaks in the two mass chromatograms for **h, i,**and **j** suggest that at least some of those ions with m/z 91 have the tolyl structure; this observation is in agreement with recently published results as summarized in Table 2-7 (118). Lack of reactivity for the ions with m/z 91 generated from the other components to form an ion of m/z 122, suggests that an insignificant portion of these ions have the tolyl structure under these ionization conditions.

The tolyl isomers which have been investigated include the meta and para isomers, and their product ion mass spectra in reaction with dimethyl ether appear identical. The ortho isomer was not investigated, as it is not possible to generate 'pure' tolyl cations by electron impact from *o*-nitrotoluene. However, it is not clear whether the three tolyl isomers are even stable or freely interconvert (125). If the ortho isomer is formed, not only may it interconvert to meta or para isomers, but rearrangement to the benzyl ion which is 1.8 eV more stable, via a simple 1,3-H atom transfer, seems a very likely process (125).

It is interesting to compare the low-energy CID daughter ion mass spectra of m/z 91 representing two predominantly different ionic structures. Figure 2-25 shows the CID daughter ion mass spectra of the ion with m/z 91 from 2-bromotoluene and 3-nitrotoluene, respectively. The collisionally induced daughter ion mass spectra of these two isomeric ions appear nearly identical at a collision energy of 25 eV_{Lab}, yet the difference in reactivity of these two ions with DME as evident from Figure 2-24 is great and can be used to distinguish the ionic structures. The ions of m/z 91 were produced

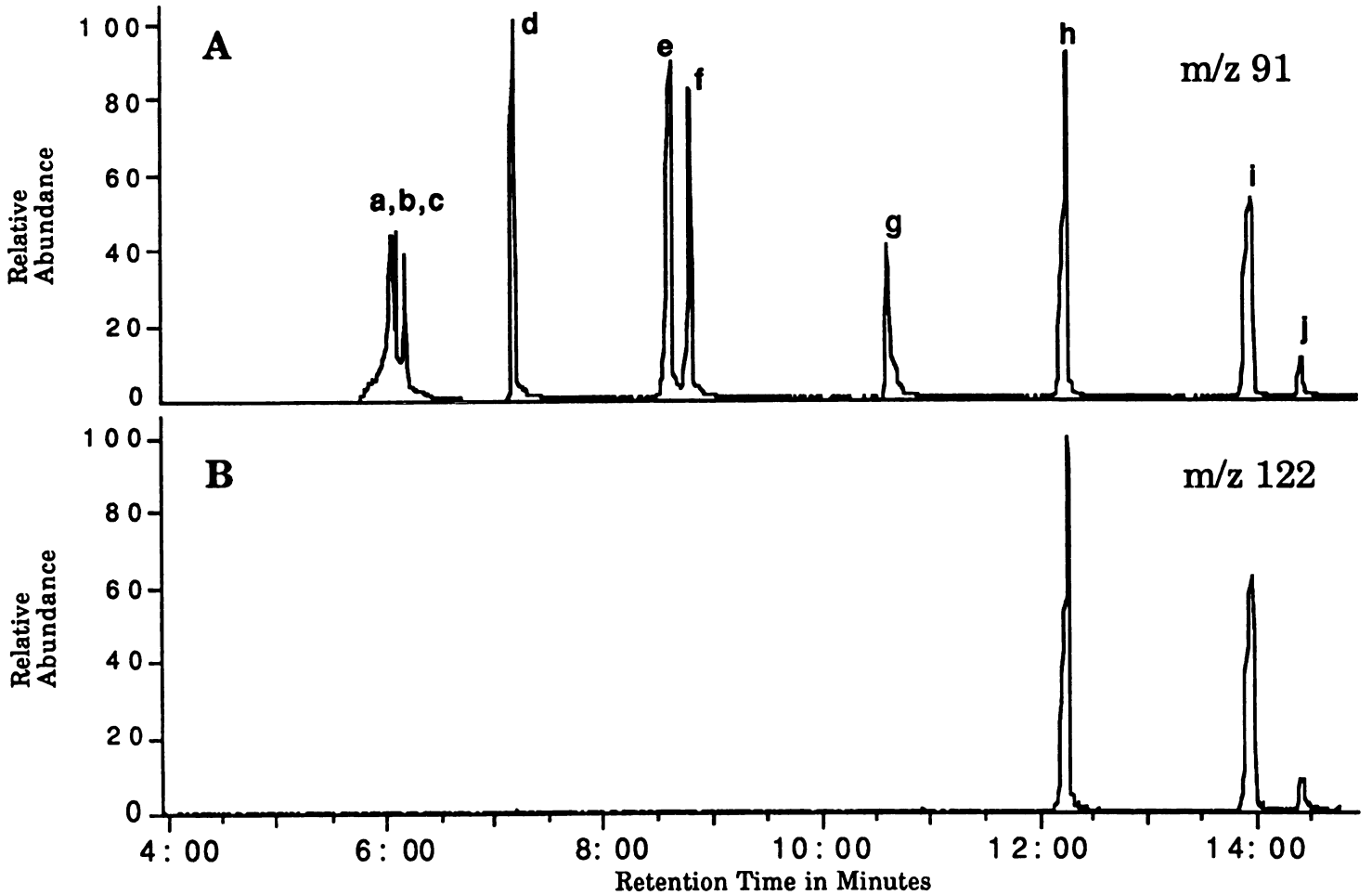

Figure 2-24: Reconstructed mass chromatogram of A) m/z 91 and B) m/z 122 when mixture of components identified in Table 2-7 was injected into the GC and the ion of mass 91 chosen to react with dimethyl ether in the second quadrupole at a pressure of 1 mtorr and collision energy of 2 eV_{Lab}.

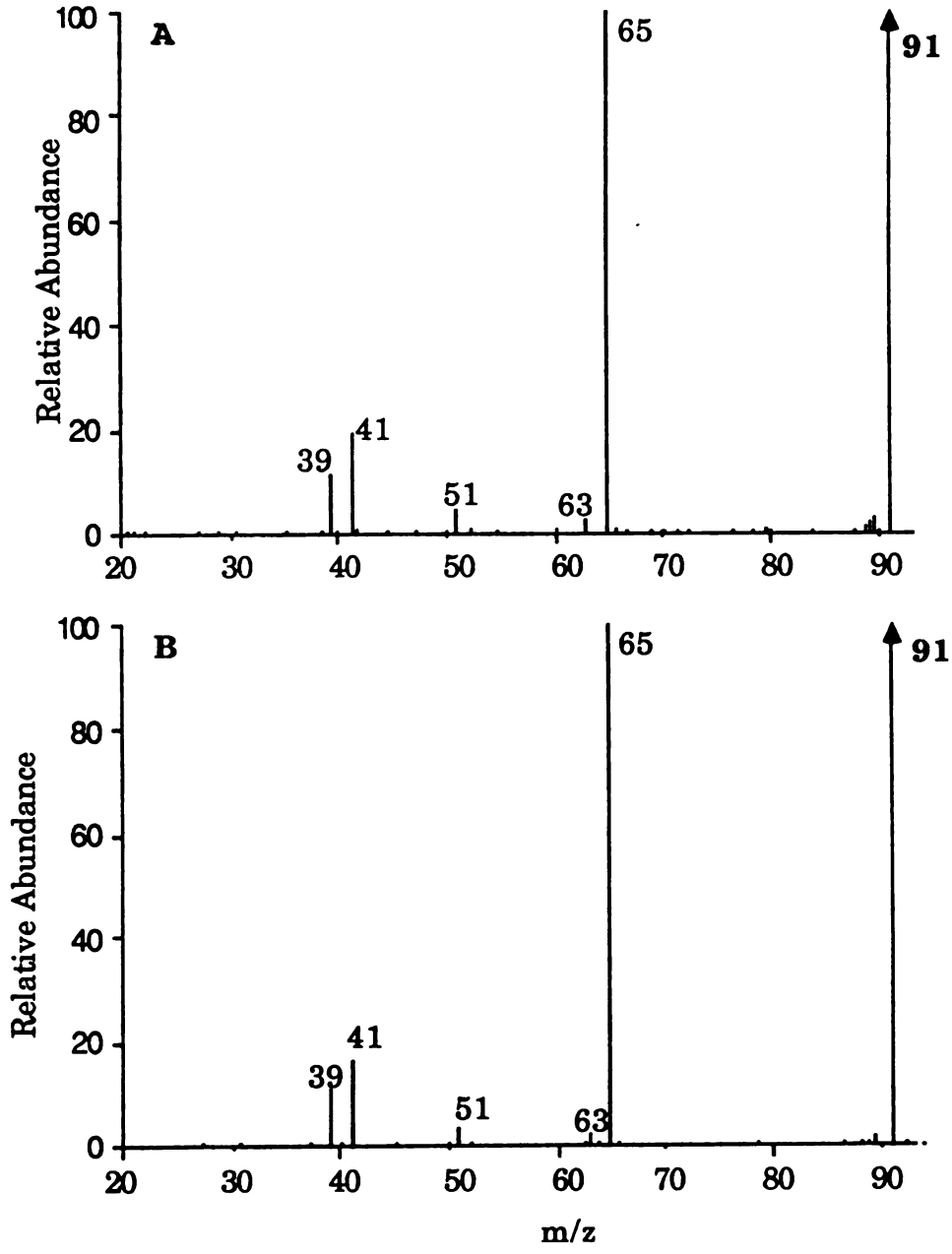

Figure 2-25: CID daughter ion mass spectrum of mass 91 generated by 70 eV EI of A) 2-bromotoluene and B) 3-nitrotoluene. Collision energy was 25 eV_{Lab} and argon was the collision gas at 0.3 mtorr.

under identical conditions for the experiments represented in Figure 2-24 and Figure 2-25.

Another assessment of the selectivity and quantitative nature of the ion/molecule reaction was conducted under conditions which isomerize $C_7H_7^+$ ions in a known manner (118). It is known that during dissociative ionization of 3-nitrotoluene, 'pure' tolyl ions are generated at low electron energy. As the electron energy is increased, isomerization to the more stable benzyl structure occurs in the ion source, prior to sampling in the collision cell. With the straightforward ion/molecule analytical approach, at the very least, a relative assessment of the tolyl composition present in $C_7H_7^+$ mixtures can be established. The ratio of $I_{122}/(I_{122}+I_{91})$, where I_n represents the intensity of the ion current detected at m/z n, should mirror the actual tolyl composition of $C_7H_7^+$ mixtures. The composition of the $C_7H_7^+$ mixture from 3-nitrotoluene as a function of electron energy was investigated by calculating the $I_{122}/(I_{122}+I_{91})$ ratio for three different pressures of dimethyl ether, and the results are depicted in Figure 2-26. Each data point represents the results of 40-50 averaged scans; this is necessary for good ion counting statistics as the intensity of the reactant ion peak at m/z 91 is small at low electron energies. The tolyl content reflected by the $I_{122}/(I_{122}+I_{91})$ ratio, decreases as the electron energy is increased from 12 eV to 20 eV. After 20 eV, the tolyl ion content remains relatively constant. These results suggest, as expected, that the relative amount of tolyl cations in $C_7H_7^+$ mixtures generated by EI of 3-nitrotoluene is greater at low electron energy than at high electron energy.

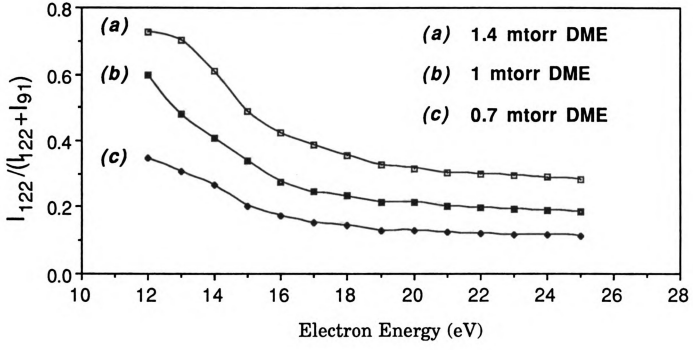

Figure 2-26: Ratio of $I_{122}/I_{(122+91)}$ as a function of electron energy during electron impact of 3-nitrotoluene and transmission of ion current at m/z 91 into Q_2 for reaction with dimethyl ether at indicated pressures.

d) Effect of higher gas pressure

As alluded to earlier in this chapter, the enthalpy of the reaction is not the only factor which determines whether product ions are formed in the second quadrupole with subsequent detection as peaks in the product ion mass spectrum. The ion/molecule reaction kinetics also must be considered. The absence of a peak at m/z 105 in the product ion mass spectra of the $C_7H_7^+$ cations with DME is noteworthy. The ion/molecule reaction of the tolyl cation with DME to yield a methylbenzyl cation with m/z 105 and neutral methanol, is more favored thermodynamically (ΔH_{rxn}=-217 kJ/mol), than is the methoxylation product ion of m/z 122. However, this peak at m/z 105 is very minor in the product ion mass spectrum as seen in Figure 2-21. The thermochemistry also reveals, as shown in Table 2-8, that reactions of benzyl and tropylium cations to form $C_8H_9^+$ ions are favorable, yet product ions with m/z 105 are not detected at a pressure of 1 mtorr DME. If, however, the pressure of dimethyl ether is raised to 3 mtorr, the product ion mass spectrum of all three isomers gives rise to peaks at m/z 105 and at m/z 137 as shown in Figure 2-27. The product ion peak at m/z 122 is still unique to the tolyl cation. In all three cases, the product ion of m/z 137 represents the intermediate collision-complex, $(C_7H_7^+\text{-DME})^+$, which is stabilized at higher gas pressures due to third-body collisions within Q_2. The peak at m/z 105 represents the ion with $C_8H_9^+$ composition, with suggested structures shown in Table 2-8. Since higher reagent gas pressure is required, it follows that, kinetically, the reaction to form the $C_8H_9^+$ cation with m/z 105 proceeds slower than the ion/molecule reaction of the tolyl cation and DME to produce the molecular ion of methyl anisole. Raising the collision pressure increases the lifetime of the collision-complex of m/z 137, as evident by the detection of

Table 2-8: Reaction enthalpies forming $C_8H_9^+$ and methanol from $C_7H_7^+$ and dimethyl ether.[a]

					ΔH_{rxn} (kJ/mol)
(1)	+ CH_3OCH_3	---------->	**[(1)-H]**-CH_3^+	+ CH_3OH	- 7.6
(2)	+ CH_3OCH_3	---------->	$C_6H_5C^+HCH_3$	+ CH_3OH	- 83.6
(3)	+ CH_3OCH_3	---------->	3-$C_6H_4(CH_3)CH_2^+$	+ CH_3OH	- 217

a. Heats of formation found in references 108, 125 and 130.

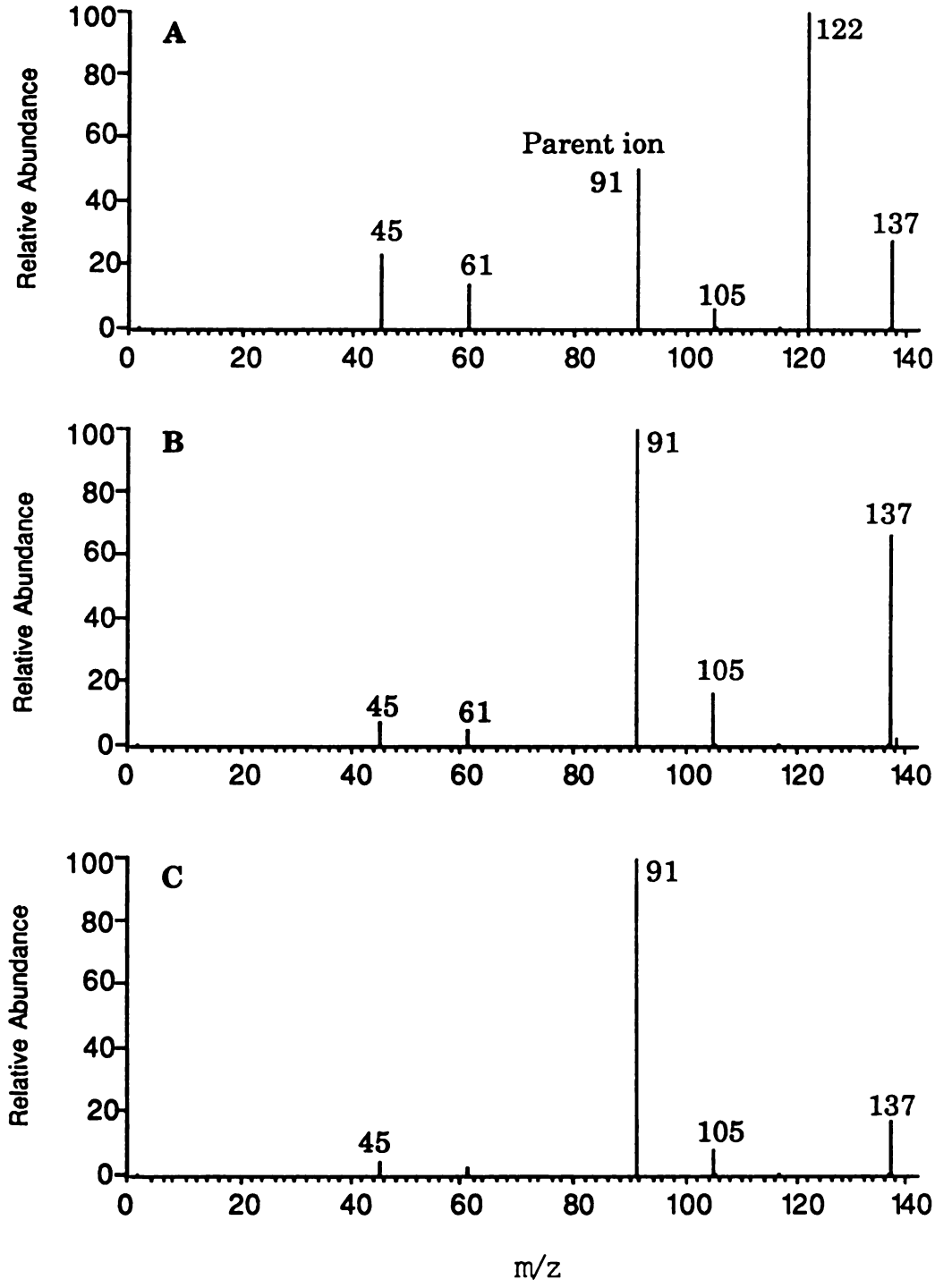

Figure 2-27: Product ion mass spectrum of A) tolyl cation, B) benzyl cation, and C) tropylium cation in reaction with DME at a pressure of ~ 3 mtorr and collision energy of 1.5 eV_{lab}.

peaks at m/z 137, allowing access to slower reaction channels. Hydrogen rearrangement is necessary in the sequence forming $C_8H_9^+$ ions and neutral methanol; this is a slower reaction than the tolyl-DME methoxylation reaction, where only simple bond formation and cleavage are necessary to form the products (Figure 2-22).

e) Reaction with ammonia

Based on the experimental results of the reaction of the phenyl cation with ammonia, and examination of the bond strengths listed in Table 2-6, it was anticipated that the reaction of the tolyl cation with ammonia would yield a product ion with m/z 107, which would represent the addition of NH_2. However, as seen in Figure 2-28, this reaction yields a peak at m/z 93. Neither the benzyl or tropylium cation reacts with ammonia to form a product ion with m/z 93. Once again the thermodynamics of the reaction provides insight into the chemistry that is occurring. Following the formation of the collision-complex, elimination of a methyl radical is thermodynamically more favorable than is the elimination of a hydrogen radical. The enthalpy of the reaction forming the ion with m/z 93 presumably representing the molecular ion of aniline and the methyl radical is 33 kJ/mol exothermic, whereas the reaction enthalpy to form the methyl-substituted aniline molecular ion and H· is only 12 kJ/mol exothermic. It does seem possible, however, that this ion with m/z 93 may be a distonic radical cation (126,127) as the reaction of NH_3 occurs at the charged carbon, and the methyl radical is eliminated at a different site along the ring.

In a study by Tabet (107), reactions of tolyl cations with ammonia produced peaks at m/z 93 and m/z 92. It was suggested that the ion of m/z 92 was $C_6H_4NH_2^+$ (107). Ratios of I_{92} / I_{93} varied for the different ortho, meta,

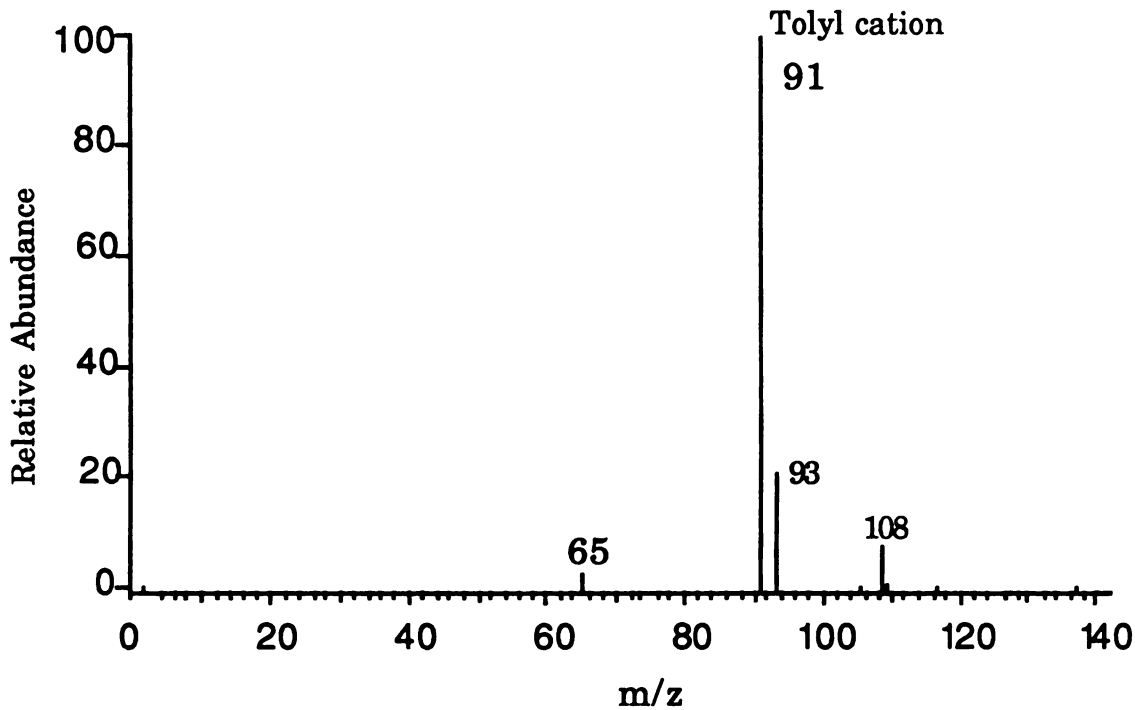

Figure 2-28: Product ion mass spectrum of the 3-tolyl cation and ammonia at a pressure of 1.5 mtorr and a collision energy of 2 eV_{Lab}.

and para isomers. However, it appears from their short report that the authors assumed that the ion with m/z 91, generated from nitrotoluene, was pure tolyl, yet this is not a valid assumption for ionization by electron impact (118), especially in the case of *o*-tolyl. Also, it is likely that the *o*-isomer, as mentioned earlier, could interconvert to either *p*- or *m*- isomers or undergo a rearrangement leading to the benzyl cation (125). Both factors were neglected, which could lead to erroneous results in the reported intensity ratios. In the experimental work performed on the TSQ-70 mass spectrometer, there was no product ion peak detected at m/z 92.

f) Conclusion

A novel approach for selective detection of the tolyl cation among other $C_7H_7^+$ ions has been developed based on its unique reactivity with dimethyl ether. The results recommend the use of triple quadrupole mass spectrometry for detection and quantification of the tolyl cation in isomeric $C_7H_7^+$ mixtures. The search should continue for an ion/molecule reaction utilizing a TQMS which would be selective for the benzyl cation. For an ion/molecule reaction to be thermodynamically favorable for the benzyl cation, but not the tolyl cation, the relative stability of the reaction products formed from the benzyl cation and the neutral reagent must overcome the 157 kJ/mol difference in the ΔH_f of the tolyl and benzyl reactants, thereby providing an exothermic reaction for benzyl, yet endothermic for the tolyl cation. If these reactions can be accomplished in the center quadrupole of a TQMS, then perhaps complete quantification of $C_7H_7^+$ mixtures could be made by this low-energy ion/molecule reaction approach.

E. Conclusion

These series of investigations demonstrate the reactivity of aryl ions, those with a vacant charged site on an aromatic ring, with nucleophilic reagents. In all cases, the thermochemical calculations correlate with experimental observations. Although the thermochemistry may suggest numerous reaction products, the more prominent ionic products observed required only simple bond-cleavage and subsequent covalent bond formation. Ionic products which require rearrangement are in some cases detected, but generally at pressures which are higher than required for the addition reaction.

Two analytical applications are explored which take advantage of the this ion/molecule reaction. The first method described offers an approach for detecting aromatics in mixtures. The presence of aromatics in our environment poses as a real health concern (46,128,129) and this method could perhaps allow aromatics to be identified as such in one GC-MS/MS analysis employing an ion/molecule reaction. The approach takes advantage of the unique reactivity of a class of ions where certain even-electron aromatic ions always gain mass in their reaction with dimethyl ether. It would not be possible to select a neutral loss characteristic of all aromatics. The second application, more fundamental in nature, demonstrates a novel approach to selectively detect the tolyl cation amongst other $C_7H_7^+$ ions. The CID daughter ion mass spectra of the three $C_7H_7^+$ isomers using a TQMS are indistinguishable, yet the reactivity of the tolyl cation with dimethyl ether provides a way to probe for this cation in mixtures.

CHAPTER III

ION/MOLECULE REACTIONS OF ABSCISIC ACID METHYL ESTER WITH MOLECULAR OXYGEN IN ELECTRON CAPTURE NEGATIVE IONIZATION

A. Introduction

1. *Abscisic Acid*

Abscisic acid (ABA), a plant growth regulator, is ubiquitous in higher plants and is also produced by certain algae and several phytopathogenic fungi (131). Abscisic acid has multiple roles during the lifecycle of a plant and the various functions of ABA are determined developmentally and environmentally. A recent review thoroughly addresses the physiological and biochemical responses of this plant hormone (131). Although the structure of ABA, which is shown as the methyl ester in Figure 3-1, has been known since 1965, much of the details concerning the biosynthesis of this plant growth regulator remained obscure. Research has focused on two biosynthetic pathways which may account for ABA production (132). The first of these postulated pathways is termed the direct pathway as this proposed sequence involves the direct formation of a C_{15}-precursor derived from farnesyl pyrophosphate. The second proposed pathway is coined the indirect pathway. It is postulated in this second pathway that ABA is a breakdown product of large C_{40}-carotenoids, following oxidative cleavage reactions. Over the years, the research group of Dr. Jan Zeevart, a Professor at Michigan State

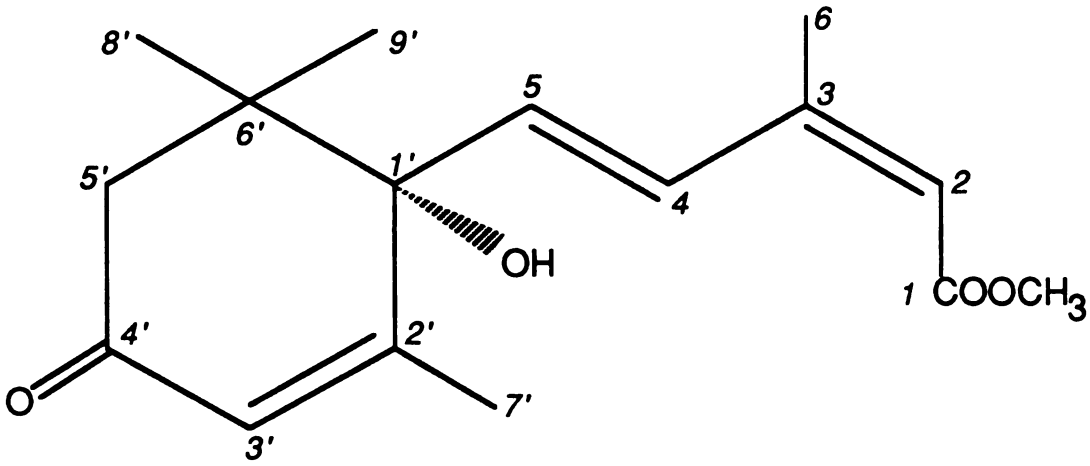

Abscisic Acid Methyl Ester (ABA-Me)
M.W. = 278

Figure 3-1: Structure of abscisic acid methyl ester (ABA-Me)

University in the MSU-DOE Plant Research Laboratory, has been a pioneer in this field and have unraveled numerous details concerning ABA biosynthesis. Mass spectrometry has been a vital tool in their efforts, providing valuable structural information during the course of their studies (132-135).

2. *Mass spectrometry of ABA*

Electron capture negative ionization mass spectrometry (ECNI-MS) has proven to be a highly sensitive technique for detection of the methyl ester derivative of abscisic acid (ABA-Me). The biosynthetic pathway of ABA has been investigated by conducting isotope-labeling studies with $^{18}O_2$ and $H_2{}^{18}O$, and analyzing the samples by mass spectrometry (132-134). ECNI mass spectrometry has been used for the determination of both the enrichment of $^{18}O_2$, and the site of oxygen incorporation in ABA; the latter was possible by observing mass shifts of fragment ions following ECNI. ECNI-MS is preferred over positive ion detection in mass spectrometric analysis of ABA as under ECNI conditions most of the ion current is concentrated in the molecular anion providing the isotopic enrichment information. In addition, there are a few structurally-diagnostic fragment ions which provide the structural information. Finally, the sensitivity using ECNI-MS for this electrophilic compound is superior to that obtained with positive ionization techniques.

Structures and mechanisms for the formation of fragment ions of ABA-Me under ECNI conditions have been suggested by Netting *et al.* (136). However, during the course of our studies, the appearance of certain fragment ion peaks in the mass spectrum, specifically those at m/z 141,

representing the side chain fragment, and at m/z 152, representing the ring, were quite erratic. Figure 3-2 shows two ECNI mass spectra of ABA-Me taken at different times. In Figure 3-2A, intense peaks are observed at m/z 141 and m/z 152, along with several peaks in the m/z 260 region, while in Figure 3-2B, only two fragment peaks are observed, those at m/z 260 (loss of H_2O) and at m/z 245 $(M^{\cdot-}\text{-}H - CH_3OH)^-$ (136). The structures proposed by Netting for the fragment ions, including those 'erratic' ions are shown in Figure 3-3. After the analysis of many ABA-Me samples, it was realized that a peak at m/z 310, $(M+32)^{\cdot-}$, is always observed in conjunction with the peaks at m/z 141 and m/z 152. This peak at m/z 310, apparently representing an adduct ion, was observed by Netting *et al.* when a capillary column was used for introduction of the sample. The origin of the adduct was said to be unknown, although aging of the GC column was offered as a possible cause (136). However, an aging column may be dismissed as the source of the adduct ion with m/z 310, as this ionic species of m/z 310 was observed not only when a gas chromatograph (GC) was used for sample introduction, but also when a direct insertion probe (DIP) was employed. Experiments also ruled out that formation of the ion of m/z 310 was dependent on the buffering gas used to thermalize electrons. The ion represented by a peak at m/z 310 appeared when either ammonia or methane was used. We suspected that formation of this ion was due to the presence of oxygen in the CI gas lines, since rigorous purging of the inlet lines eliminated the peak at m/z 310. However, careful purging of the CI lines also eliminated the fragment ion peaks at m/z 141 and 152. The spectrum, after rigorously purging the gas lines, is shown in Figure 3-2B. The dramatic differences in the appearance of these spectra led us to systematically investigate the role of oxygen in the formation of fragment ions and adduct ions observed in the ECNI mass

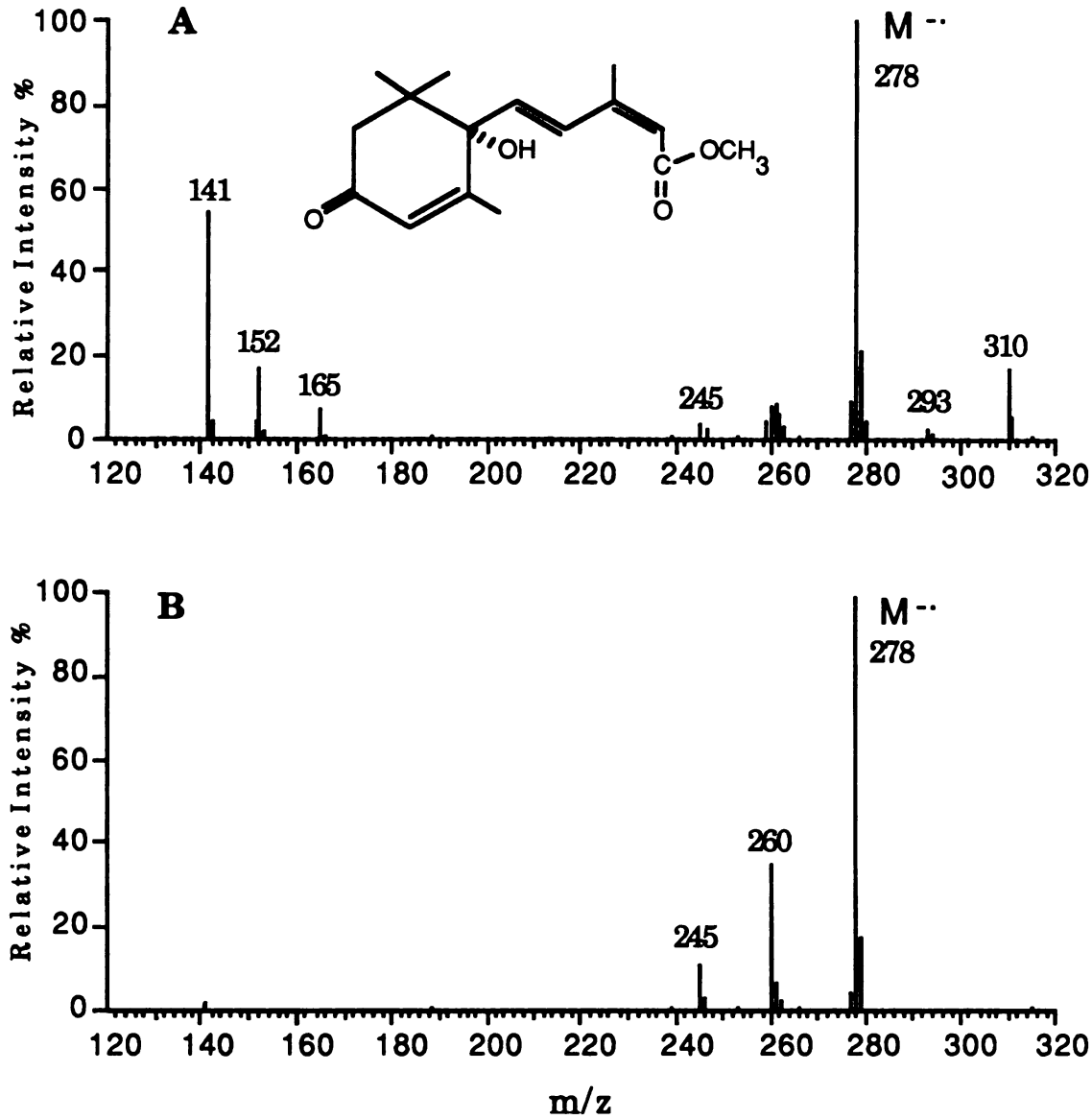

Figure 3-2: ECNI mass spectrum of ABA-Me obtained under conditions in which: (A) no effort was made to purge air from the CI lines and (B) the CI lines were carefully purged free from contamination with air.

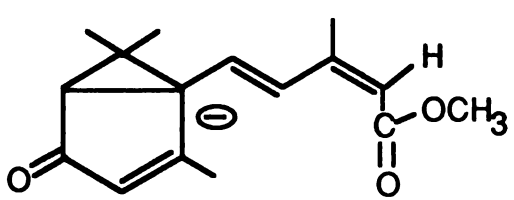

m/z 260

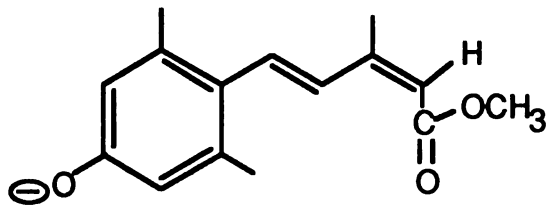

m/z 245

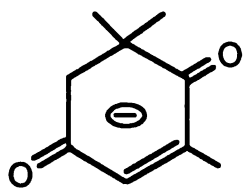

m/z 152

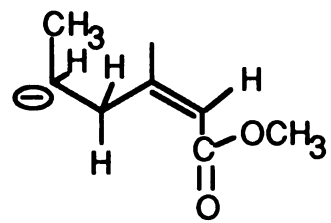

m/z 141

Figure 3-3: Structures of fragment ions of ABA-Me as proposed by Netting *et al.* in reference 136.

spectrum of ABA-Me. It was crucial that the the formation of the fragment ions be elucidated, as the biosynthetic pathway of ABA was inferred from the mass spectrometric results, specifically, from the mass shift of fragment ions under ECNI conditions. The structure of the fragment ions must be known, eliminating the possibility of erroneous conclusions as a result of faulty ionic structural assignments.

3. *Reactions with oxygen in ECNI-MS*

Reactions involving oxygen impurities in the ion source have been reported previously (137,138), with most describing the use of oxygen-enhanced negative chemical ionization for identification of specific congeners of aromatic species (49,139-143). Recently, Stemmler and Buchanan described reactions of polycyclic aromatic hydrocarbons (PAHs) with oxygen-containing impurities (137,138). Mechanisms for the formation of unusual product ions were proposed. These studies of PAHs indicated that gas-phase reactions were not responsible for all the observed product ions, but that wall-catalyzed reactions can occur, and these processes were enhanced by adding oxygen and elevating the ion source temperature (137). In many cases, both ion/molecule reactions and wall-catalyzed reactions with oxygen yield products such as $(M + \cdot O\text{-}2\cdot H)^-$ or $(M + 2O\text{-}2\cdot H)^-$, ions whose mass is higher than that of the molecular anion. However, lower-mass fragment ions also may result from source reactions following subsequent decomposition of the initial reaction products (143). As demonstrated in a recent interlaboratory comparison, rigorous control of the presence of trace gases is required to minimize interfering reactions in ECNI and thus obtain reproducible spectra of compounds at levels near the limits of detection (144).

The use of low-energy collisions in a triple quadrupole mass spectrometer allowed us to investigate reactions of the negative ions observed in the mass spectrum of ABA-Me with molecular oxygen. With selection of the molecular anion by Q_1, gas-phase ion/molecule reactions may be studied in an environment in which the involvement of wall-catalyzed reactions, and pre-ionization reactions between the analyte and neutral reactive species are eliminated. Kostianen and Auriola used analogous reactions of $M^{-\cdot}$ of tetrachlorodibenzo-*p*-dioxins (TCDDs) with oxygen in the collision cell of a TQMS for examining isomer-specific oxidative ether cleavage reactions (93,94). In this chapter, the structure of some of the fragment ions formed under ECNI conditions and the role played by molecular oxygen in inducing their formation is examined. Interpretation of the fragmentation patterns of isotopically-labeled ABA analogues allowed us to propose structures of these fragments, and possible mechanisms to account for these unusual gas-phase ion/molecule reactions. Structurally-similar ABA metabolites were also analyzed, which allowed us to test the proposed mechanisms.

B. Experimental

1. *Instrumentation*

All experiments were performed on a Finnigan triple stage quadrupole (TSQ-70) mass spectrometer equipped with a Varian 3400 gas chromatograph. The samples were introduced through a DB-5 capillary column (30 m x 0.25 mm, film thickness 0.25 μ; J&W Scientific, Inc.) with He as the carrier gas (flow rate 1 ml/min). The GC oven was programmed from 60-210°C degrees at 50°C/min, and 210-280°C at 12°C/min. The analyzing

quadrupole was scanned from m/z 50-330 at a scan rate of 0.5 sec/scan. For samples introduced by the direct insertion probe, the probe was heated from 50-280°C at a rate of 20°C/min. For all the experiments, the ion source temperature was maintained at 150°C. Methane or ammonia at an indicated pressure of approximately 0.8 torr was used as the moderating gas, resulting in the formation of secondary electrons available for capture by the analyte. The electron energy was 100 eV, and the emission current was 0.3 mA.

Molecular anions were generated by electron capture in the ion source, mass-selected by the first quadrupole, Q_1, and passed to the collision chamber, Q_2. Argon or oxygen ($^{16}O_2$ or $^{18}O_2$) was introduced into the Q_2 collision cell at pressures of 0.7-1.4 mtorr, as indicated by a convectron gauge, which provides multiple collisions of the ion with the collision gas. Interaction of the parent ion with the collision gas results in the formation of ionic products which were analyzed by scanning the third quadrupole, Q_3. For low-energy reactions of anions with oxygen, the collision energy, determined by the axial DC-offset voltage of Q_2, was 1-5 eV_{Lab}. Higher collision energies of 10-30 eV_{Lab} were used for the collisionally-induced dissociation (CID) studies, with argon as the target gas.

2. *Materials*

All of the compounds analyzed were extracted and purified from plant tissues by known literature methods (132,134). Labeled analogues were either prepared by known literature procedures (145,146) or prepared biosynthetically (134). In the latter case, confirmation of the location of the isotope labels were made by EI mass spectral measurements (147,148). The deutero methyl ester derivative was prepared with Tri-Deuter-8 ™ (Pierce,

Rockford, IL). The author is grateful to Dr. Jan Zeevart and his graduate student Chris Rock, for the preparation and provision of the samples analyzed over the course of this study.

C.Results and discussion

1. *MS/MS with argon as collision gas*

The preliminary tandem mass spectrometry studies on the molecular anion of ABA-Me were done with argon introduced into Q_2 as the collision gas. Based on the report of Netting and coworkers (136), in which peaks at m/z 141, 152, 245, and 260 were observed in the ECNI mass spectrum, it was anticipated that CID of the molecular anion with m/z 278 would readily yield these corresponding ions as fragments. However, as shown in the CID daughter ion mass spectrum represented in Figure 3-4A, only peaks at m/z 245 and 260 were detected. Collision gas pressure and collision energy adjustments were made in an attempt to increase the formation of the lower-mass fragments, but these adjustments did not result in a significant increase of the desired fragment ion peaks. We did observe, however, that at low energies (<5 eV_{Lab}), ion current at m/z 141, on the order of 2% of the base peak, was detected. At collision energies higher than 5 eV, no ion current at m/z 141 was detected. This observation was attributed to inadequate purging of the CID gas lines. If the gas lines were not rigorously purged, air could be introduced into Q_2 as a contaminant in argon. It was thought that perhaps oxygen present in the collision cell was activating fragmentation at low collision energy. These observations, along with those stated earlier concerning oxygen and the co-occurrence of peaks at m/z 310, 141, and 152 in

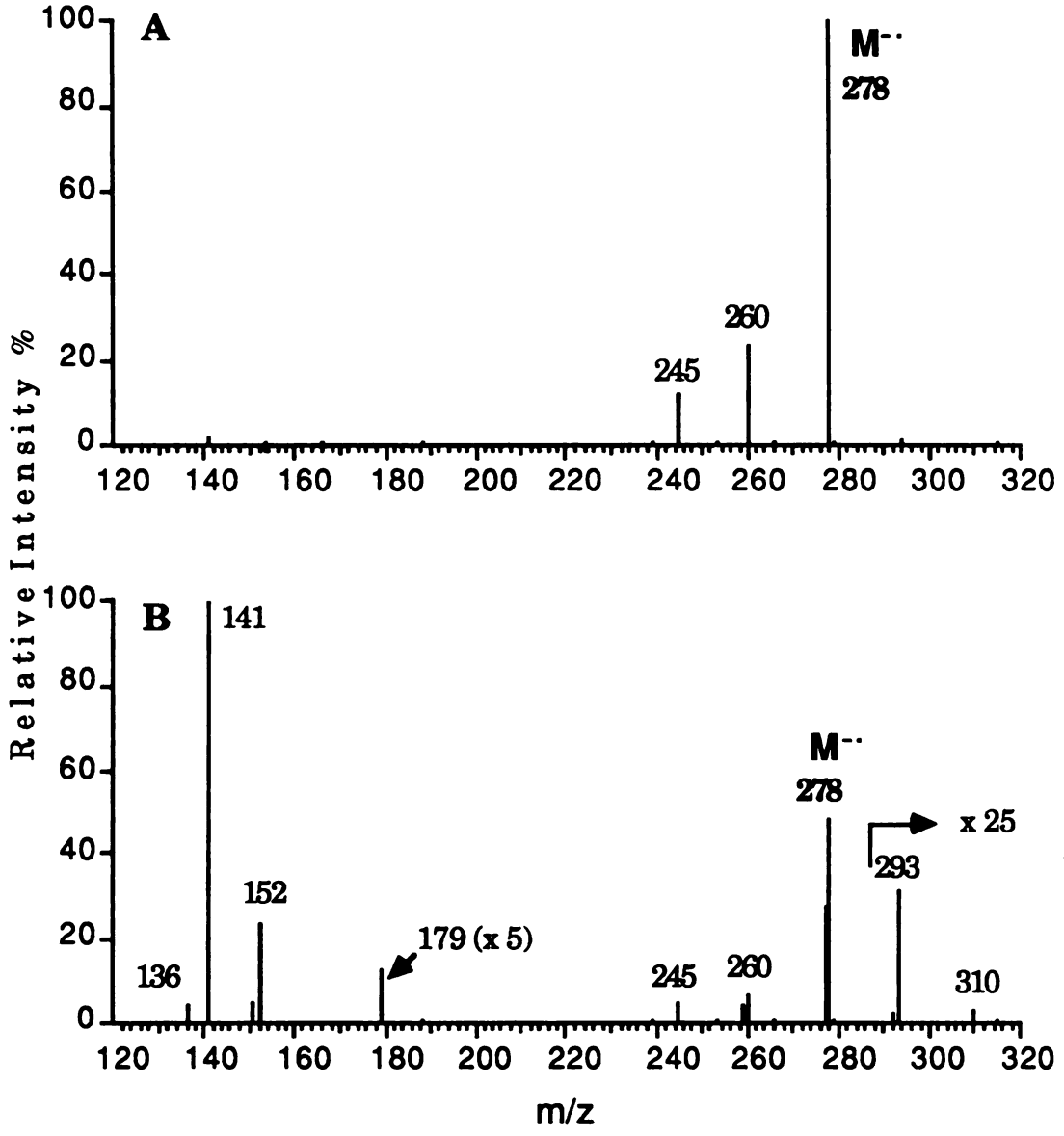

Figure 3-4: Product ion mass spectra (E_{Lab} = 2 eV) of the molecular anion (m/z 278) of ABA-Me obtained with a TQMS following (A) CID with Ar and (B) CID and/or ion/molecule reactions with molecular oxygen.

the mass spectrum suggested that processes other than CID were required to induce fragmentation of the molecular anion.

2. *MS/MS with O_2 as collision gas*

In order to investigate ion/molecule reactions of ABA-Me and oxygen, O_2 was intentionally introduced into Q_2 as the collision gas. The low-energy collisions of $M^{-\cdot}$ of ABA-Me with O_2, as shown in the product ion mass spectrum of Figure 3-4B, results in greatly enhanced peaks at m/z 141 and 152, along with small peaks at m/z 136 and m/z 179 which were not detected in the conventional ECNI mass spectrum. There also are minor, yet discernible, peaks at m/z 310 and m/z 293, presumably representing $(M+O_2)^{-\cdot}$ and $(M+O_2 - \cdot OH)^-$ species, respectively. Low-energy collisions with oxygen also promoted the loss of a hydrogen radical as evident by the increase in ion current at m/z 277. As the collision energy was raised, the lower-mass fragments, along with the peaks at m/z 310 and m/z 293 disappeared, while the fragment ion peaks at m/z 260 and 245 became more intense. The energy-resolved curves for product ions resulting from collision of the molecular anion of ABA-Me with molecular oxygen is shown in Figure 3-5. As indicated by Figure 3-5A, ions represented by peaks at m/z 260 and 245 are formed by direct decompositions of the molecular anion as the intensity of these peaks increases with collision energy, while the product ions represented by peaks at m/z 141 and 152 are formed as result of low-energy ion/molecule reactions of the molecular anion with molecular oxygen. The energy-resolved curves for ions with m/z 136 and 179 are similar to those shown in Figure 3-5B for m/z 141 and 152. Contrary to what had been previously suggested by Netting (136), the biologically active 2-*cis* isomer and

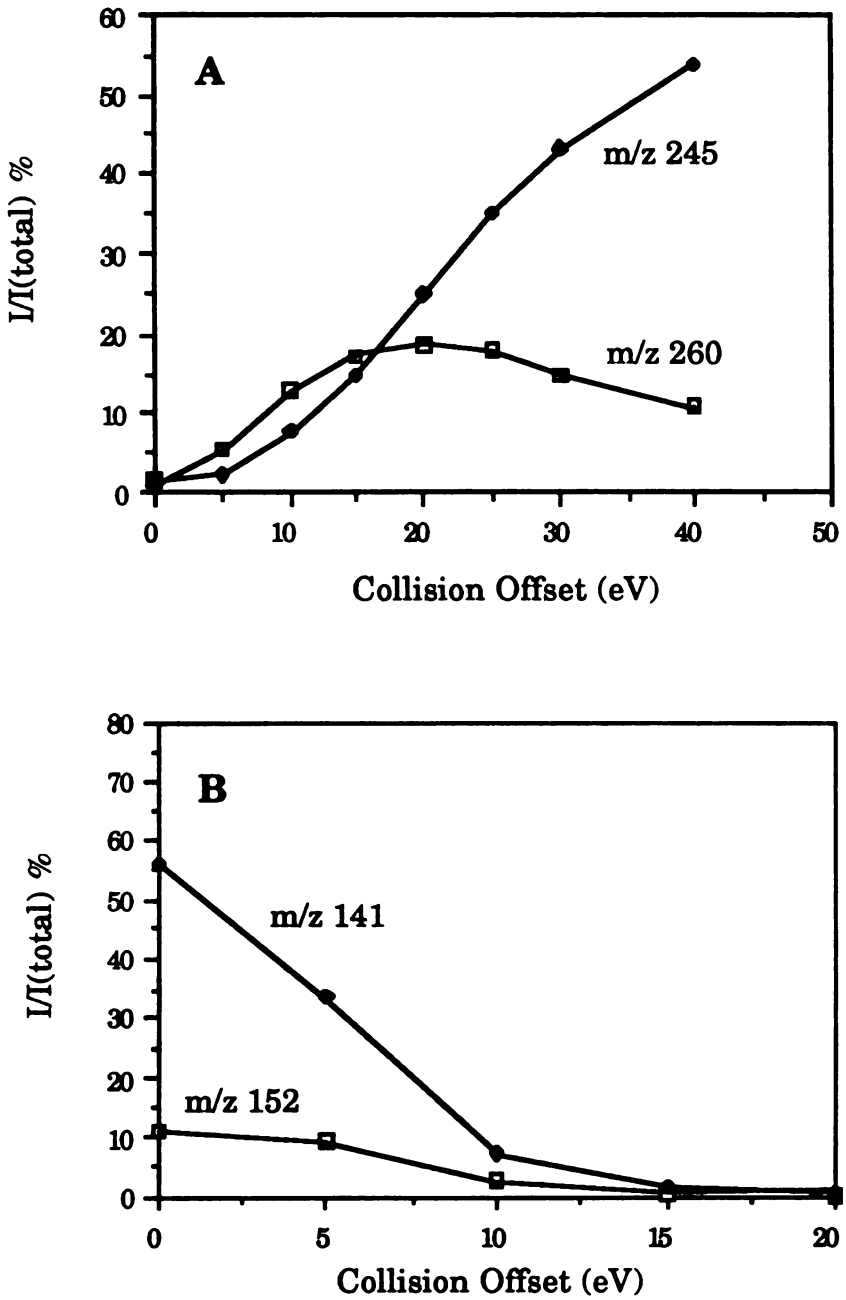

Figure 3-5: Energy-resolved curves in collisions of the molecular anion of ABA-Me with molecular oxygen at a pressure of 1 mtorr. (A) Ions with m/z 260 and 245, and (B) ions with m/z 141 and 152.

the photoisomerized 2-*trans* isomer, which is formed in small amounts during the extraction procedure, have identical fragmentation patterns.

To verify the role of oxygen in the activation process, $^{18}O_2$ was introduced into Q_2 and reacted with the molecular anion of ABA-Me to produce the product ion mass spectrum as shown in Figure 3-6. A peak at m/z 314 replaced the peak at m/z 310, confirming that the $(M+36)^{-\cdot}$ peak represents addition of molecular oxygen ($^{18}O_2$) to the $M^{-\cdot}$ of ABA-Me in the collision cell. Quite unexpectedly, the peak at m/z 141 shifted to m/z 143, and the peak at m/z 179 shifted to m/z 181. It follows that these product ions result from initial reaction of the molecular anion with oxygen to form an intermediate species, which subsequently decomposes with incorporation of an ^{18}O atom from molecular oxygen. The formation of fragment ions with m/z 152 and 136 from the molecular anion requires molecular oxygen, but the peaks at m/z 152 and 136 did not shift when $^{18}O_2$ was introduced into the collision cell.

It is postulated that the ions with m/z 136, 141, 152, and 179 arise from the highly unstable $(M+32)^{-\cdot}$ species. Lack of sufficient third-body collisions to offer stabilization of the O_2 adduct of m/z 310 in the collision cell allows decomposition to give these fragment ions. In contrast, collisional stabilization can occur in a high-pressure CI source. When oxygen was intentionally leaked into the ion source with the buffering reagent gas, formation of the adduct ion of m/z 310 was promoted. A daughter ion scan of m/z 310 following CID with argon was obtained as shown in Figure 3-7. The daughter ion mass spectrum of m/z 310 clearly indicates that the ions with m/z 136, 141, 152, and 179 along with the initial reactant anion $M^{-\cdot}$, with m/z 278, arise from the $(M+O_2)^{-\cdot}$ intermediate adduct species.

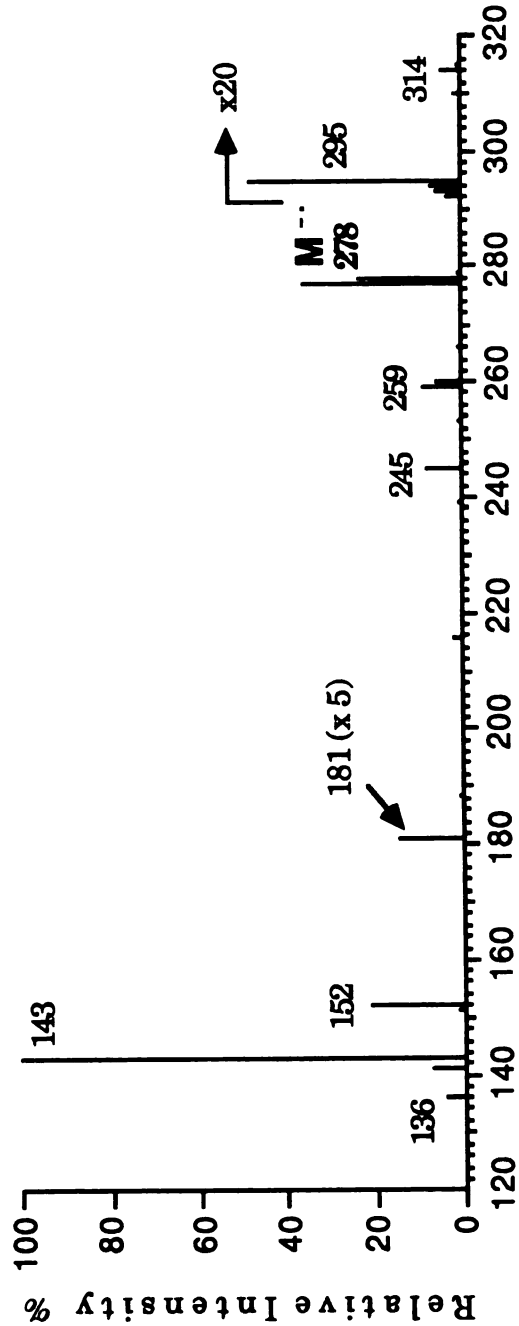

Figure 3-6: Product ion mass spectrum of the molecular anion of ABA-Me (m/z 278) following ion/molecule reactions and/or CID with $^{18}O_2$ in Q_2 at a collision energy of 2 eV_{Lab}

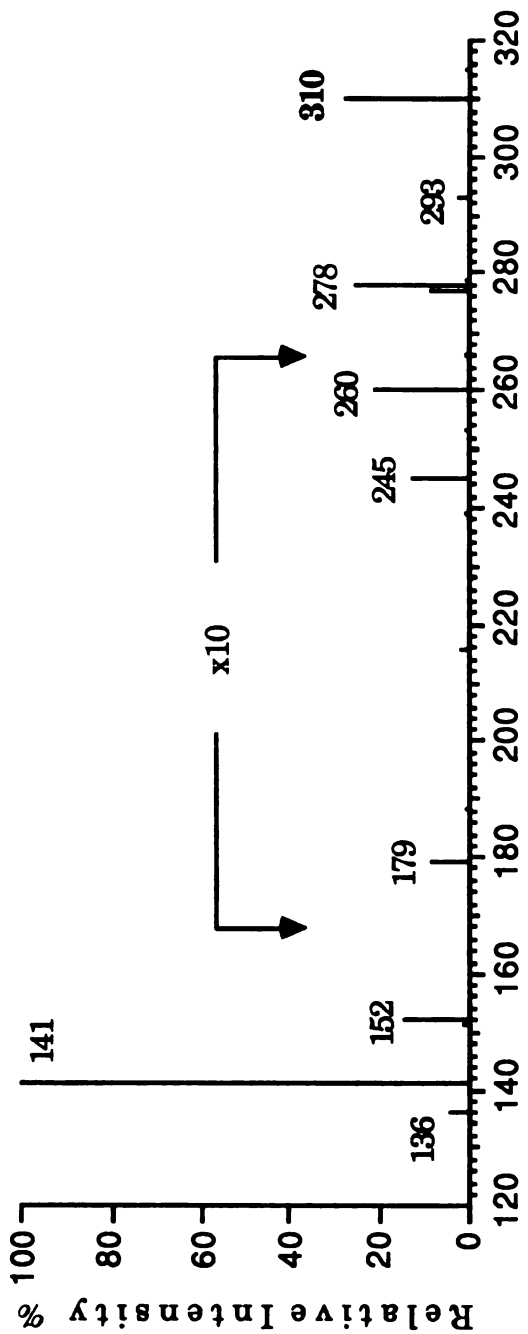

Figure 3-7: The daughter ion mass spectrum following CID with argon at 10 eV_{Lab} collision energy of the adduct ion of m/z 310 formed during ion/molecule reactions of the molecular anion of ABA-Me and O_2 in the ion source.

In an attempt to determine whether the structure of the ion with m/z 310 is a covalent species or a clustering adduct of $M^{-\cdot}$ and O_2, the ion of m/z 310, $(M+^{16}O_2)^{-\cdot}$, formed in the ion source, was chosen as the parent ion and introduced into Q_2, which contained $^{18}O_2$ at a pressure of 1.8 mtorr. If the $(M+O_2)^{-\cdot}$ ion were a non-covalent clustering species, it would be expected that at low collision energy (~0.5 eV_{Lab}) exchange of $^{16}O_2$ with $^{18}O_2$ would occur in Q_2 resulting in formation of some ions of m/z 314, with subsequent decomposition to ions of m/z 143 and m/z 152; that is, if some $^{18}O_2$ were exchanged into the parent ion, one ^{18}O atom would be expected to be retained in the side-chain fragment ion. However, negligible ion currents at m/z 314 and 143 (less than 1% relative to that at m/z 310 and 141) were detected in this experiment suggesting that the $(M+O_2)^{-\cdot}$ ion is predominantly a covalently-bound species or, at the least, a tightly-bound adduct complex.

3. *MS/MS analyses of isotopically labeled compounds*

The availability of stable isotope-labeled analogues of ABA allowed us to re-evaluate the structure of the fragment ions of m/z 141 and m/z 152, and to postulate the structures of ions with m/z 136 and m/z 179. It is evident from these studies that the peak at m/z 141 represents the side chain portion of ABA-Me as was originally proposed by Netting *et al.* (136). However, their suggested structure and mechanism for its formation, where one of the *gem*-dimethyls and one hydrogen from the 5' position transfers to the side chain, are not correct. In the stable isotope labeling studies, expected shifts in the mass of this fragment occur with a number of labeled-analogues including both the deutero methyl-ester derivative and the $[^2H_3]$-C6 analogue (shifts to m/z 144 from m/z 141). Similarly, the analogue containing ^{18}O atoms in the

carbomethoxyl oxygens of the side chain displays a shift from m/z 141 to m/z 143 with one ^{18}O atom, and to m/z 145 with two ^{18}O atoms present. In addition, analysis of the ethyl-ester analogue shows that the side chain fragment ion peak is found at the anticipated m/z 155, as evident by Figure 3-8 which shows the product ion mass spectrum of the molecular anion of ABA-ethyl ester (MW=292) and O_2. However, when the ring positions of ABA-Me are deuterated ([$^2H_3$]-C7', [$^2H_1$]-C3', [$^2H_2$]-C5') or when either one of the ring oxygens is labeled, the fragment ion peak at m/z 141 does not shift.

The ion with m/z 141 contains three oxygen atoms: two in the carbomethoxyl group on the side chain and a third from the reaction with O_2. High pressure flow tube studies have shown that ground-state (triplet) molecular oxygen reacts with negative ions which contain a conjugated diene system, involving incorporation of an oxygen atom, forming enolate anions (149-151). However, these flow tube reactions with oxygen involve even-electron reactant ions; the reaction we describe with ABA-Me is that of an odd-electron molecular anion with molecular oxygen.

In order to account for the observed fragmentation and mass shifts for the ion with m/z 141, the mechanism shown in Figure 3-9 is proposed. Reaction of triplet oxygen and the radical molecular anion ***(a)*** occurs at the radical site at C5 along the side chain of the molecular anion. Initially, an unstable peroxy intermediate ***(b)*** is formed. The proposed mechanisms suggests that this adduct with m/z 310 decomposes to transfer an oxygen to C1', forming a neutral radical fragment and the enolate anion of m/z 141 with structure ***(c)***. This product ion of m/z 141, which contains one of the oxygens from O_2, has a highly resonance-stabilized enolate structure, as shown in Figure 3-9, which resists further fragmentation. In collisions with argon at an energy of 25 eV_{Lab}, the ion with m/z 141 yields a daughter ion represented

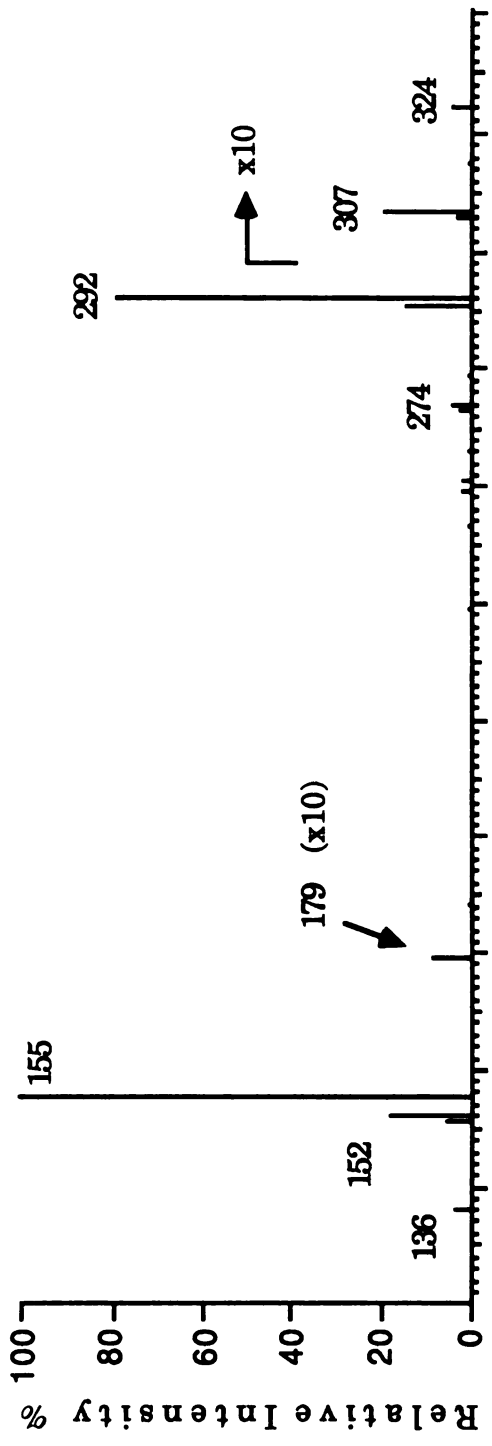

Figure 3-8: Product ion mass spectrum of the molecular anion of ABA-ethyl ester (m/z 292) and molecular oxygen at a pressure of 1 mtorr and a collision energy of 1 eV_{Lab}.

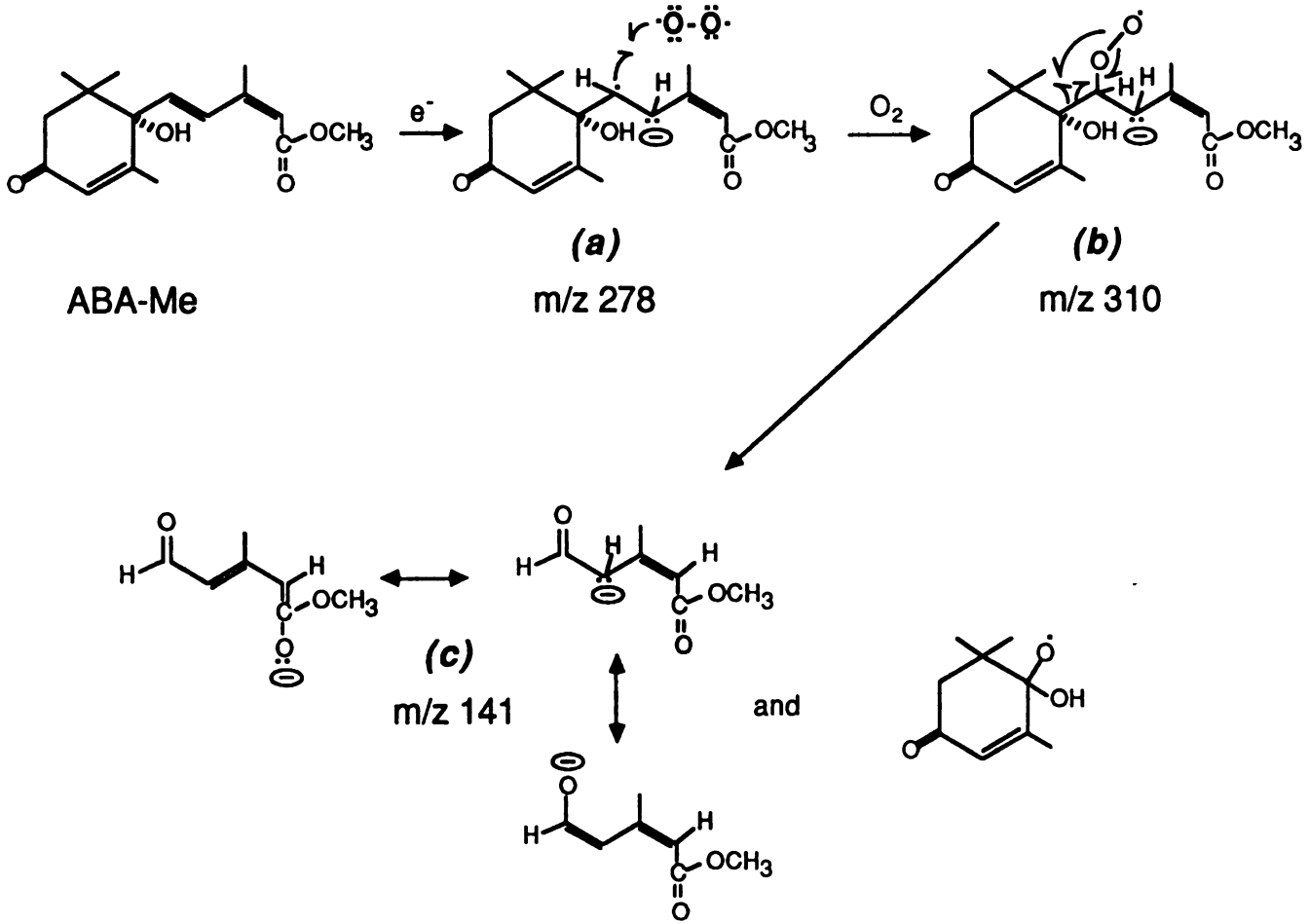

Figure 3-9: Ion/molecule reaction mechanism accounting for the formation of the ion of m/z141 following the reaction of the molecular anion of ABA-Me and O_2.

by a minor peak at m/z 109. Examination of the CID daughter ion mass spectra of labeled analogues reveals that when one ^{18}O atom is located in the carbomethoxyl group of the side chain, the ion of m/z 143 yields fragments upon CID with m/z 109 and m/z 111 in a 1:1 ratio. This indicates that the fragment ion of m/z 109 results from expulsion of methanol (32 u) from one of the equivalent (prior to methylation) carbomethoxyl oxygen atoms.

Although the ion with m/z 179 is represented by only a minor peak in the product ion mass spectrum obtained during reaction of $M^{-\cdot}$ with oxygen (Figure 3-4B), it is of interest due to incorporation of an oxygen atom from collision with O_2 as demonstrated by a shift in its peak to m/z 181 when $^{18}O_2$ is the reactant gas (Figure 3-6). Mass spectra of structural analogues of ABA-Me containing ^{18}O also show that the ion of m/z 179 contains both ring oxygens. The fragmentation sequence of the intermediate ion with m/z 310 decomposing to the ion with m/z 179 proceeds by a two-step process as represented in Figure 3-10. The conventional negative ion mass spectrum shown in Figure 3-2A indicates a minor peak is found at m/z 293 which represents loss of ·OH from the $(M+O_2)^{-\cdot}$ of m/z 310; we postulate that the loss of ·OH involves the distal oxygen of the peroxy moiety and a hydrogen atom from C5'. The CID daughter ion mass spectrum was obtained for the ion of m/z 293; it revealed that the ion with m/z 179 is a daughter of the ion of m/z 293 as the mechanism of Figure 3-10 suggests. As indicated in the product ion mass spectrum resulting from reaction of the molecular anion with $^{18}O_2$ (Figure 3-6), the peak at m/z 295 corresponds to loss of a single ^{18}O atom from the intermediate (m/z 314). In this mechanism forming the ion of m/z 179 as shown in Figure 3-10, it is suggested that molecular oxygen reacts with the charged site at C4, rather than at the radical site (C5), to form once again, a peroxy intermediate of m/z 310, but with an alternative structure

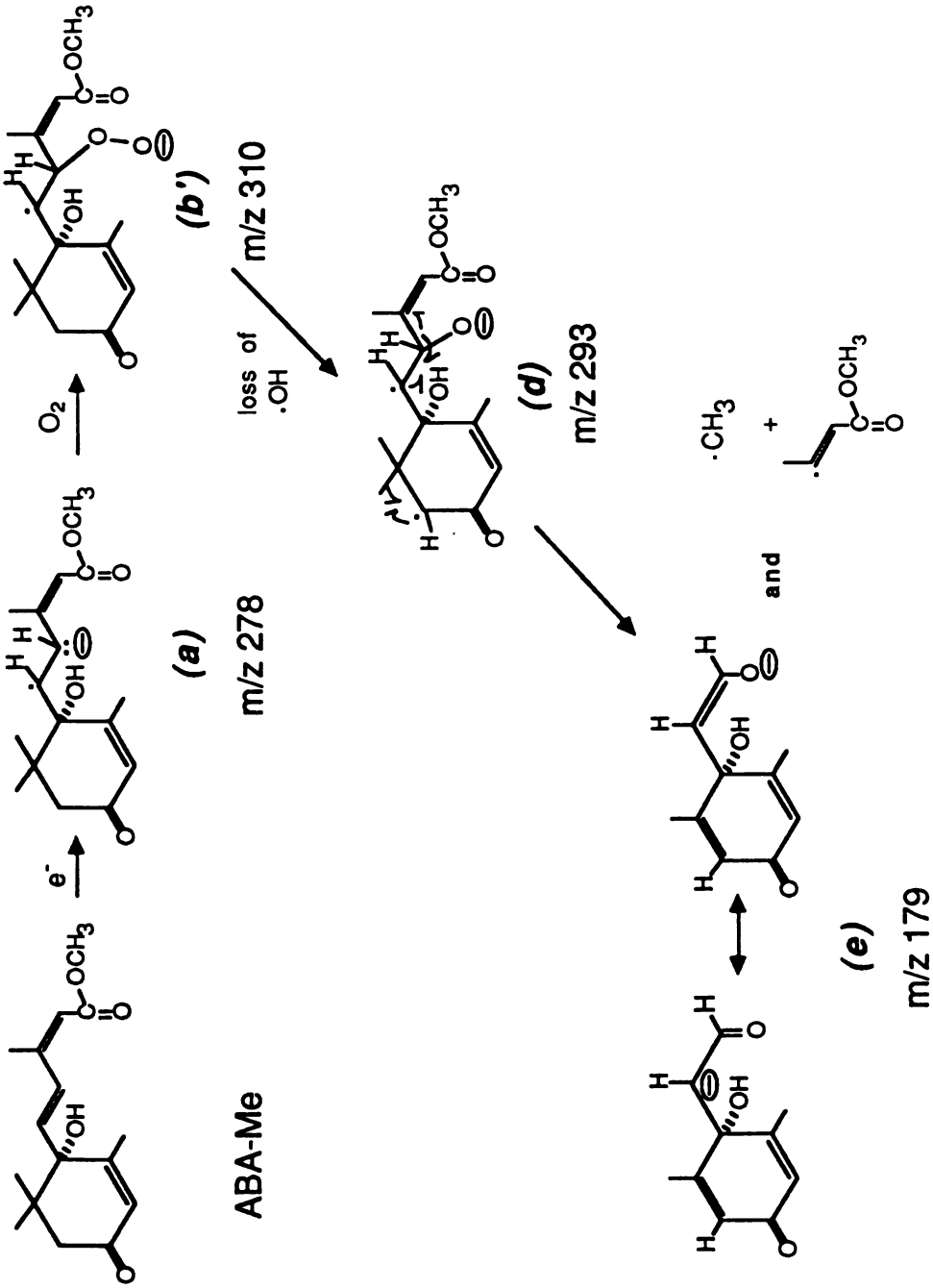

Figure 3-10: Ion/molecule reaction mechanism accounting for the product ion of m/z 179.

(b'). Following the formation of intermediate ***(b')***, sequential losses occur initially to form first the ion of m/z 293 ***(d)***, then an enolate anion with m/z 179 ***(e)*** as illustrated in Figure 3-10. Two radical species are postulated as the neutral products in the formation of the ion of m/z 179 from the ion of m/z 293 ***(d)*** . No ion current is detected at m/z 141 or at m/z 152 upon CID of the ion of m/z 293 indicating that these product ions do not form via this pathway involving the intermediate with m/z 293.

Formation of the ionic reaction products of m/z 152 ***(f)*** and 136 ***(g)***, as shown in Figure 3-11, also requires activation of the molecular anion with oxygen. However, these do not retain an oxygen atom from the adduct, as is evident from the product ion mass spectrum with $^{18}O_2$ shown in Figure 3-6. Analysis of the isotopically-labeled compounds lend support to the structure of m/z 152 as was originally proposed by Netting *et. al.* (136), but formed via the mechanism shown in Figure 3-11 which indicates the role of oxygen in activating the fragmentation process. After initial formation of ***(b)***, m/z 310, the peroxy moiety abstracts a hydrogen from the acidic hydroxyl group at C1'. Subsequently, the charged site initiates cleavage of the C1'-C5 bond. The oxygen-activated product ions of m/z 152 and m/z 136 always co-occur which suggests sequential decomposition pathways from the common intermediate of m/z 310 ***(b)***. The ion with m/z 136 has the stable quinoid structure, ***(g)***, which results from the net loss of CH_4 (a methyl radical is eliminated from one of the *gem*-dimethyls along with a hydrogen radical from the ring) from the ion of m/z 152. This was confirmed by the CID daughter ion mass spectrum of the ion of m/z 152. Analogous CID experiments with ring deuterated ABA-Me ([$^2H_3$]-C7', [$^2H_1$]-C3', [$^2H_2$]-C5') indicate that the hydrogen lost is from the ring, most likely the 5' position.

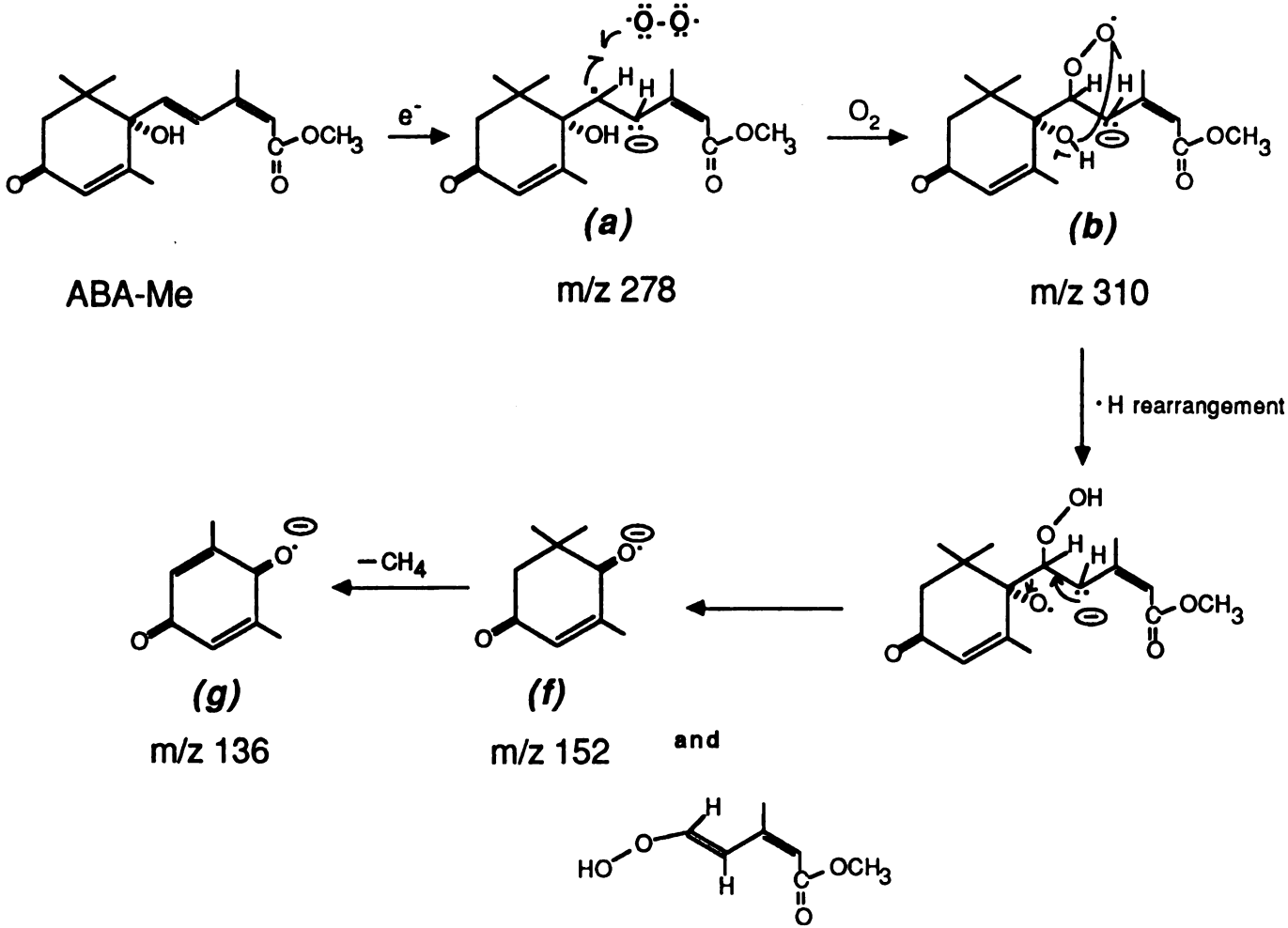

Figure 3-11: Mechanism for formation of the ions of m/z 152 and 136 following the ion/molecule reaction of $M^{-\cdot}$ of ABA-Me and O_2.

The molecular anion of ABA-Me was the only ion in the mass spectrum observed to undergo reaction with molecular oxygen. Other anions, including the radical anion with m/z 260, which represents the loss of H_2O from ABA-Me, and the even-electron species with m/z 277 and m/z 245, were selected by Q_1 and reacted with molecular oxygen in the collision cell, but no reaction products were observed. The anion with m/z 277 may not react because it lacks the radical site necessary for attack by triplet oxygen. The ion with m/z 260, although a radical anion, lacks the 1'-OH which precludes hydrogen abstraction by the peroxy intermediate, a process that would lead to the formation of the ion with m/z 152 (see Figure 3-11). Stable isotope studies indicated, in contrast to what had previously been suggested (136), that the water loss does not abstract a ring hydrogen (at C5'), but most likely removes a hydrogen from C5 of the side chain as illustrated in Figure 3-12. MS/MS studies revealed that in the formation of the dehydration product, the molecular anion with m/z 284 of ring-deuterated ABA-Me ([$^2H_3$]-C7', [$^2H_1$]-C3', [$^2H_2$]-C5') eliminates H_2O, rather than H^2HO, resulting in a peak at m/z 266. In addition, the loss of H_2O allows the charge in this fragment ion ***(h)*** to be more delocalized which may preclude the reaction of O_2 at C5 to form the ion with m/z 141. Finally, as might be expected, the anion with m/z 245, which lacks a radical site and the 1'-OH group, also is not reactive with oxygen. In these studies, the minor quantities of product ions, which were generated in collision with O_2, could be attributed to CID processes, as similar experiments with argon in the collision cell resulted in peaks at identical m/z values. This conclusion is supported by the fact that the abundance of these fragment ions increased as the collision energy was raised.

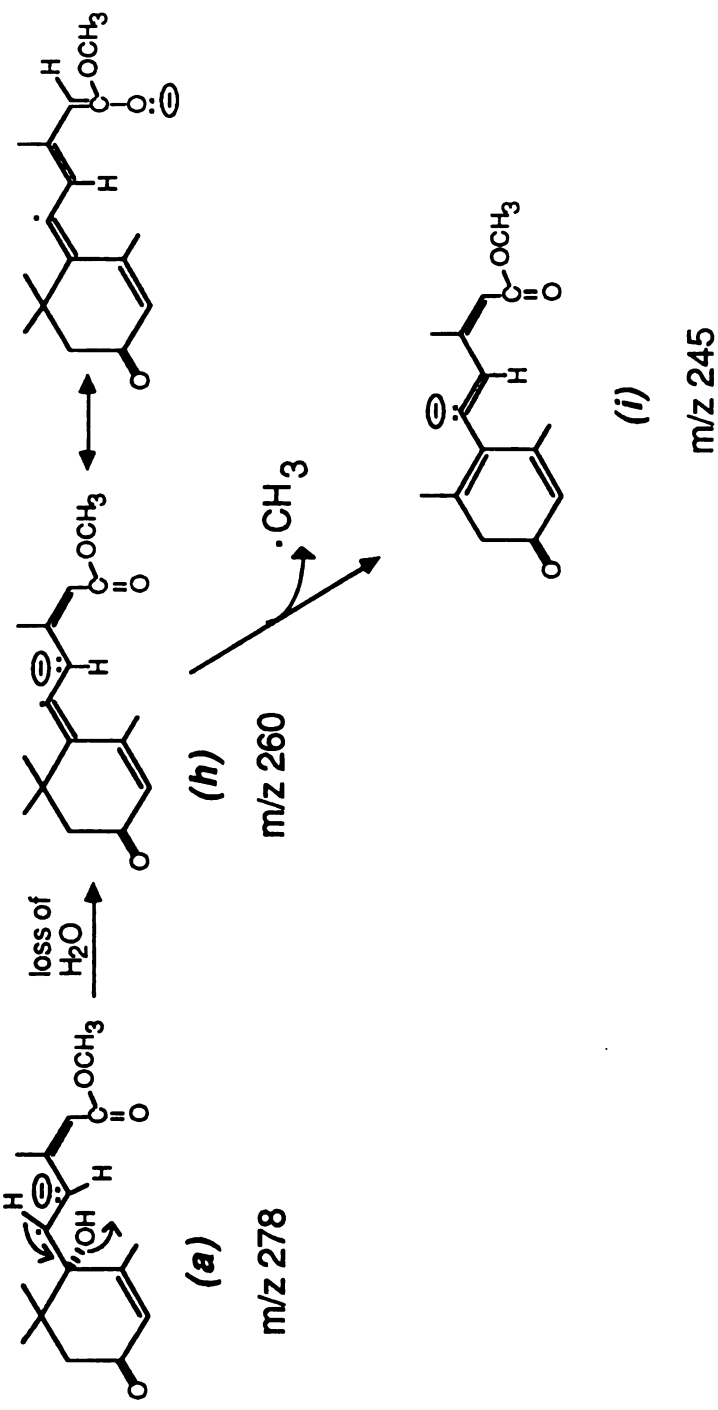

Figure 3-12: Fragmentation of $M^{\cdot}$ of ABA-Me (m/z 278) to yield ions with m/z 260 and 245.

Parenthetically, the MS/MS studies of ABA-Me indicated that there are two possible structures and mechanisms for the formation of the ion of m/z 245. The first structure being that suggested by Netting *et al.* (136) shown in Figure 3-3, which results from a primary loss of ·H at C5' followed by a concerted loss of CH_3OH from the tertiary hydroxyl and one of the *gem*-dimethyl groups. A second structure ***(i)***, shown in Figure 3-12, results from elimination of a methyl radical from the dehydration product formed by the mechanism described above. The CID daughter ion mass spectrum of the dehydration fragment ion of m/z 266 from ring-deuterated ABA-Me ([$^2H_3$]-C7', [$^2H_1$]-C3', [$^2H_2$]-C5') indicated that a methyl radical may be eliminated resulting in a fragment ion peak at m/z 251. This fragment ion with m/z 251 must contain all the ring deuterium atoms, including [$^2H_1$]-C5'. The CID daughter ion mass spectrum of the ion of m/z 284 for this ring-deuterated analogue results in a major fragment peak at m/z 250 due to loss of a deuterium atom and methanol (Figure 3-3), and a minor peak at m/z 251 ***(i)***, which represents the loss of H_2O and a methyl radical. The results of these CID experiments are consistent with the formation of the fragment ion of m/z 245 formed via two separate decomposition pathways.

4. *Analysis of structurally-similar compounds*

a) ABA metabolites

Several metabolites shown in Figure 3-13 were available for analysis and analogous fragment ions requiring oxygen-activation also were observed for these compounds. When the parent ion of abscisic aldehyde ($M^{-\cdot}$ at m/z 248) reacts with oxygen in the collision cell, oxygen-activated fragment ions result in peaks at m/z 111, 152, and 136. The ion with m/z 111 corresponds to

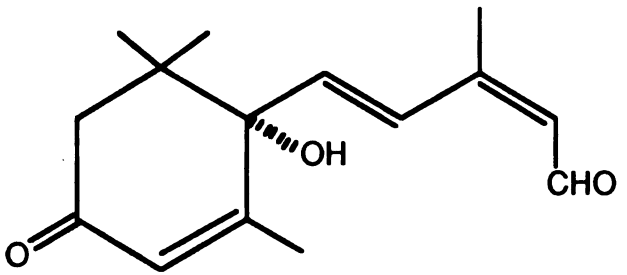

Abscisic Aldehyde

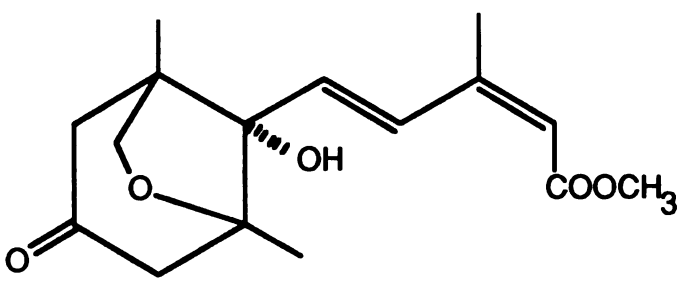

Phaseic Acid Methyl Ester (PA-Me)

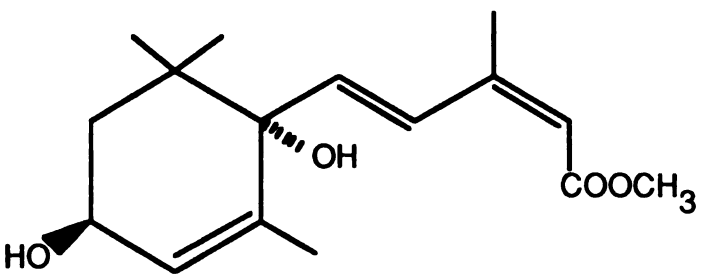

1',4'-trans-diol Abscisic Acid Methyl Ester

Figure 3-13: Structure of ABA metabolites.

the enolate anion containing the side chain portion of the molecule after incorporation of an oxygen atom from O_2. When $^{18}O_2$ is introduced into Q_2, the peak shifts to m/z 113 indicating its formation is likely from the same mechanism that produces the ion with m/z 141 in ABA-Me. Ions with m/z 152, 136, and 179 also form during reaction with abscisic aldehyde, and they are thought to be identical in structure to the ions represented in Figures 3-10 and Figure 3-11. Likewise, when methylated phaseic acid was the analyte, the parent ion of m/z 294 yielded oxygen-activated fragments with m/z 141 and m/z 168, representing the side chain and ring portion of the methyl ester of phaseic acid, respectively. The structure of the ion with m/z 168 is shown in Figure 3-14. When the molecular anion of *trans*-diol abscisic acid methyl ester is reacted with O_2, the predicted side-chain fragment ion peak at m/z 141 is observed. The ring fragment ion of *trans*-diol ABA-Me is represented by a minor peak at m/z 153. Apparently loss of ·H from the predicted ring fragment of m/z 154 results in a more stable even-electron quinoid anion with m/z 153. Reaction of the molecular anion of these metabolites with oxygen does not appear to be as efficient as that with ABA-Me. Under identical conditions (O_2 pressure at 1.4 mtorr and collision energy at 2 eV_{Lab}), the intensity of the oxygen-activated fragment ion peak at m/z 111 from abscisic aldehyde, for example, is on the order of 30 percent of the base peak, whereas with ABA-Me, the corresponding peak at m/z 141 is the base peak in the product ion mass spectrum.

b) Analysis of α and β ionone

Over the course of the investigation of the fragmentation of ABA-Me, a few additional compounds structurally similar to ABA were analyzed by ECNI, and anions were selected for analysis with O_2 in the collision cell. The

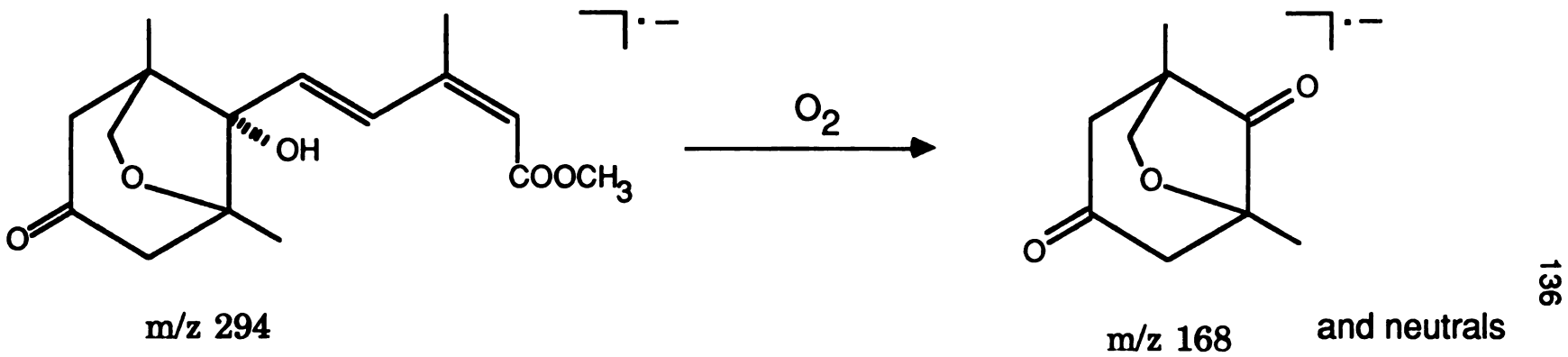

Figure 3-14: Formation of ion with m/z 168 from the ion/molecule reaction of the molecular anion of phaseic acid-Me and O_2 .

first two compounds analyzed were α- and β- ionone, whose structures are shown in Figure 3-15. Prior to analysis by ECNI, the purity of the compounds was checked by EI, and the mass spectra were in good agreement with those reported in the literature (109). The ECNI mass spectra for both α- and β- ionone with ammonia as the buffering reagent gas to generate the thermal electrons are shown in Figure 3-16. Unlike the case with ABA-Me, the base peak in the mass spectrum represents $(M-H)^-$, an even-electron anion. When this ion was selected for reaction with molecular oxygen, there were no product ion peaks obtained in the product ion mass spectrum. Further investigation of these two isomeric compounds did reveal some interesting results, not related, however, to oxygen-induced fragmentation. The ECNI mass spectra of α- and β- ionone with methane as the buffering gas are shown in Figure 3-17. A striking difference is observed in the mass spectra if methane is used as the modifying gas. As seen in Figure 3-17, both isomers show an unusually abundant MH^- ion at m/z 193. In fact, with the β-isomer, this unusual ion, MH^-, is represented by the base peak. The mass spectrum of the α- isomer shows an intense peak at m/z 136 when methane is used, whereas this peak is minor when ammonia is the buffering gas. These isomers were introduced by the GC, and β–ionone eluted 20 seconds later than the α-isomer. Introduction of the sample by GC ensured that the source conditions were identical. Recently, it was reported that MH^- ions were observed in the methane ECNI mass spectra of chlorprothixene and aromatic sulfur compounds (152). This MH^- ion was accounted for by electron capture followed by $H\cdot$ transfer from the reagent gas (152). This process likely accounts for what was observed in the ECNI mass spectrometry of α and β ionone, and is presented here as a curious phenomenon.

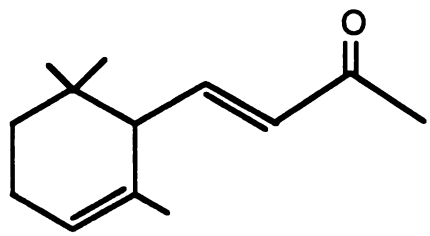

α–Ionone

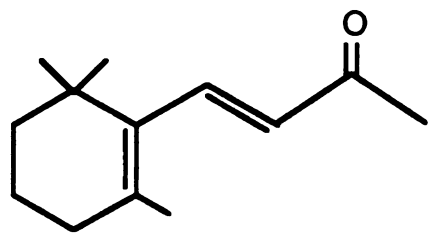

β– Ionone

Figure 3-15: Structures of the isomeric forms of ionone (MW=192).

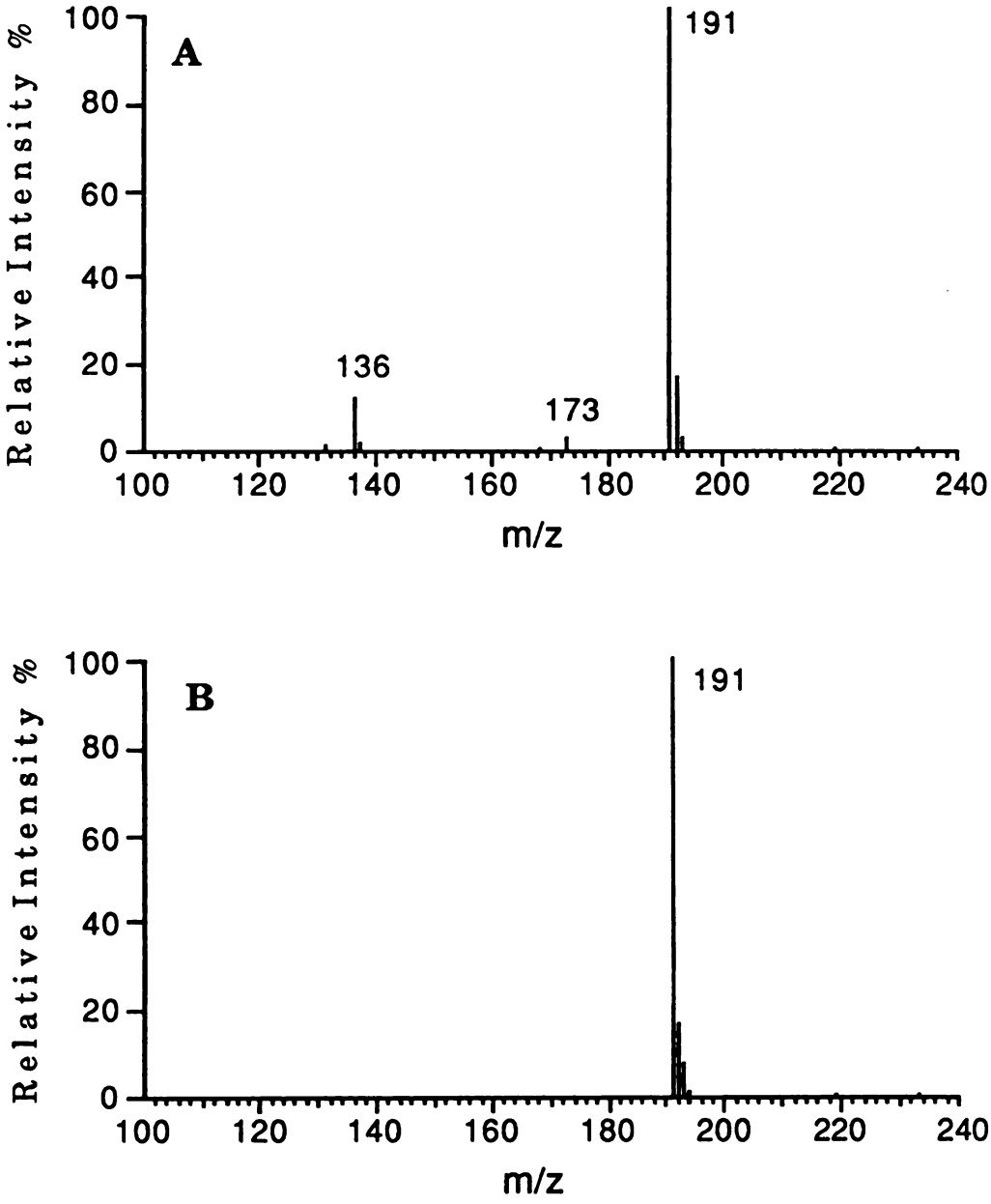

Figure 3-16: ECNI mass spectrum of (A) α-ionone and (B) β-ionone with ammonia as the buffering reagent.

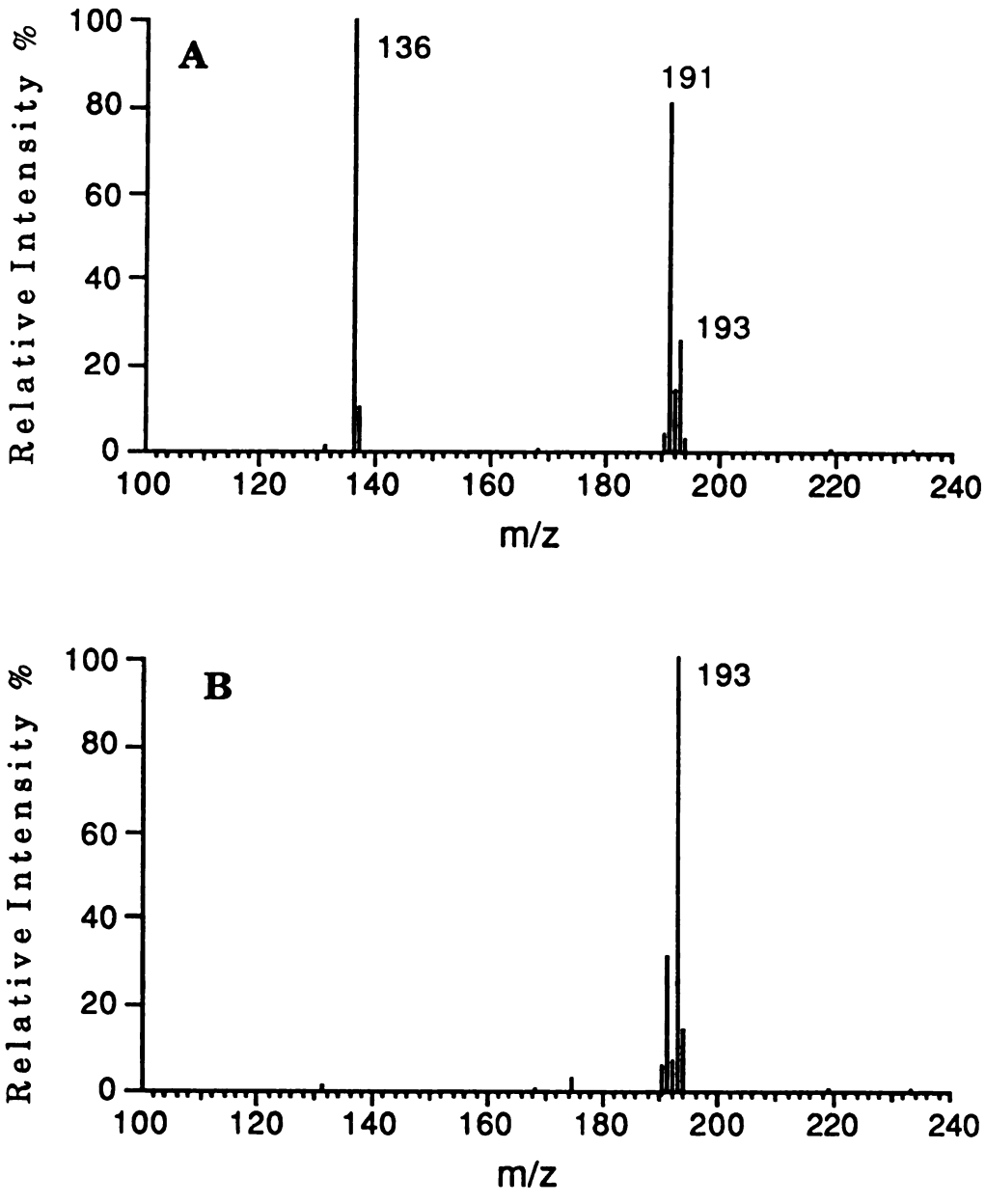

Figure 3-17: ECNI mass spectrum of (A) α-ionone and (B) β-ionone with methane as the buffering reagent.

c) Analysis of 2,4-hexadiene

A second compound which was investigated in this study was 2,4 hexadiene. The ion/molecule reaction of the molecular anion of ABA-Me and oxygen is postulated to occur along the side chain which contains a conjugated diene system. As mentioned above, reactions of even-electron anions containing a conjugated diene system with oxygen in flow tube studies, resulted in the formation of enolate anions (149-151). Perhaps similar reactions could be observed in a TQMS to provide further insight on the reaction of ABA-Me with oxygen. The ECNI mass spectrum of 2,4-hexadiene showed the base peak at m/z 81, representing the $(M-H)^-$ anion. Even though this ion is not a radical anion, the product ion mass spectrum of the $(M-H)^-$ of 2,4-hexadiene and O_2 at a pressure of 1.5 mtorr was obtained and is shown in Figure 3-18. Peaks are seen in the product ion mass spectrum at identical m/z values to those reported in the flowing afterglow study when 2,4-hexadiene was analyzed (151). It seems likely that these ions represent enolate anions, with reaction mechanisms shown in Figure 3-19. These results indicate that it is possible to observe ion/molecule reactions of even-electron anions with oxygen in the collision cell of a TQMS. Isomeric carbanions were distinguished by ion/molecule reactions with oxygen in the flow-tube studies; maybe a TQMS could be utilized in similar fashion for probing the structure of anions.

5. *Wall-catalyzed reactions*

One oxygen-related ion that stands in contrast to the gas-phase ion/molecule reaction products of ABA-Me and O_2 is that with m/z 165. This peak at m/z 165, as seen in Figure 3-2A, appears in the ECNI mass spectrum

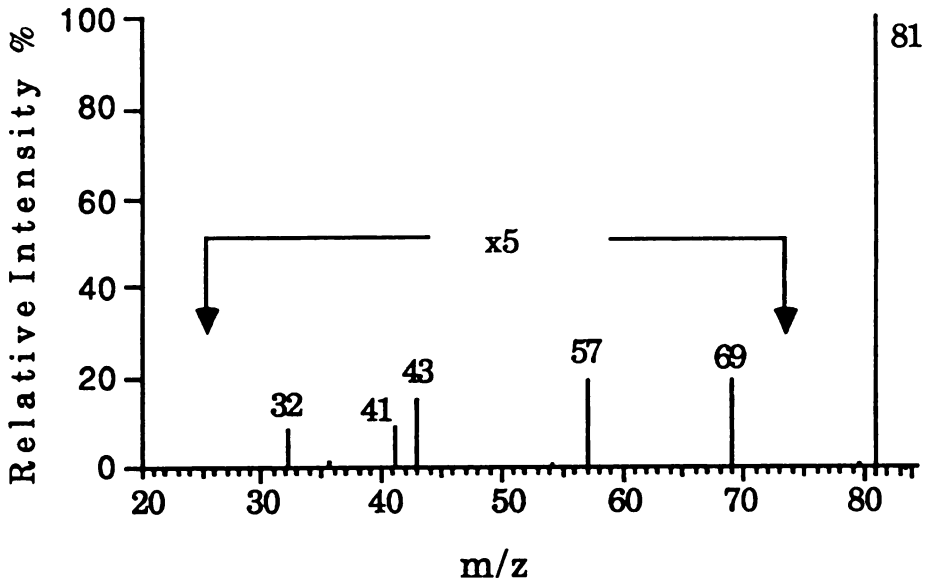

Figure 3-18: Product ion mass spectrum of $(M-H)^-$ of trans, trans-2,4-hexadiene (MW=82) with molecular oxygen at a pressure of 1.5 mtorr and a collision energy of 1 eV_{Lab}.

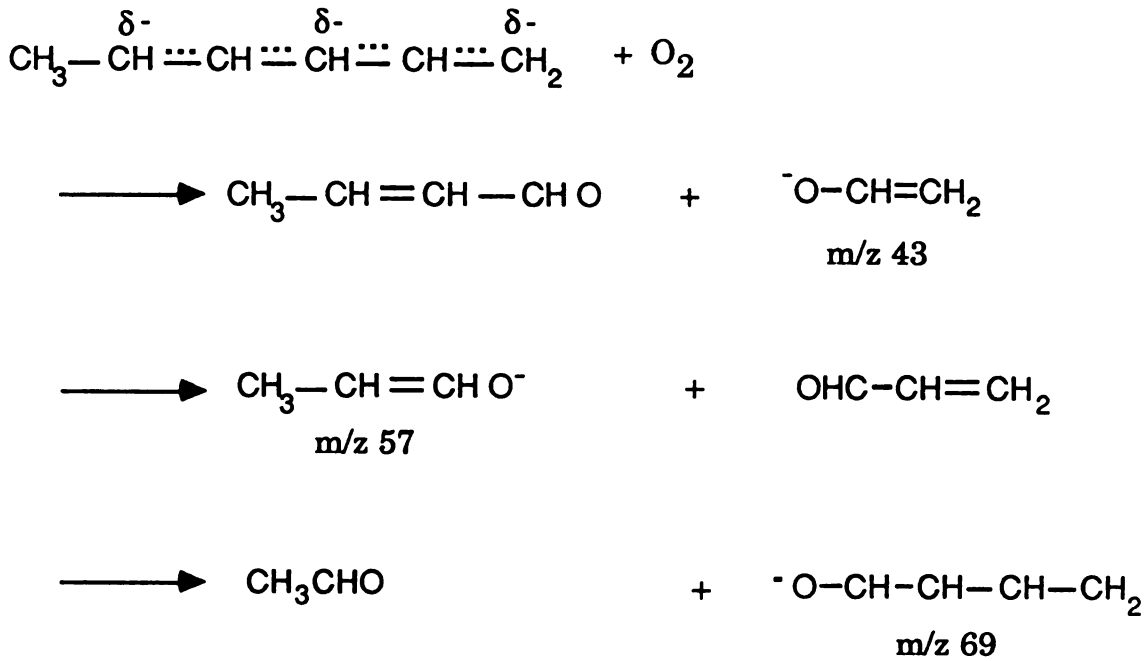

Figure 3-19: Ion/molecule reactions of $(M-H)^-$ of trans,trans-2,4-hexadiene in reaction with molecular oxygen to form enolate anions. (Adapted from reference 151).

when oxygen-activated product ions are present, yet it is not observed in any MS/MS study using oxygen or argon. It appears that this reaction product may be attributed to wall-catalyzed source reactions (153). Examination of reconstructed mass chromatograms shown in Figure 3-20 for the ions in the mass spectrum shown in Figure 3-2A indicates that the ion current at m/z 165 lags in time behind that for other ions, including those ions which are due to gas-phase ion/molecule reactions with O_2. These observations are consistent with the results of the study by Stemmler *et al.* where wall-catalyzed reactions resulted in tailing in the mass chromatogram for the mass of interest (137). Isotope labeling studies indicate that this fragment ion contains the ring portion of the ABA molecule, including both ring oxygen atoms, yet the structure remains undetermined.

D. Application

With the interpretation of the fragmentation pattern of ABA-Me obtained under ECNI conditions following reactions of the molecular anion with molecular oxygen, the ^{18}O atoms may be readily assigned to the ring or side chain of ABA-Me. In labeling studies of ABA with $^{18}O_2$, the conventional ECNI mass spectrum provides the isotopic enrichment information, while the MS/MS approach can be used to quantitatively determine isotopic enrichment at the various positions of ^{18}O-labeled ABA-Me from different plant tissues. For example, in the MS/MS analysis of single ^{18}O-labeled ABA-Me (m/z 280), the presence of an ion with m/z 260 indicates that the ^{18}O-label is at the OH-C1'. If, however, ion current is detected at m/z 262, then the label is located elsewhere, yet could be determined precisely from the pattern of the peaks surrounding m/z 141 and 152.

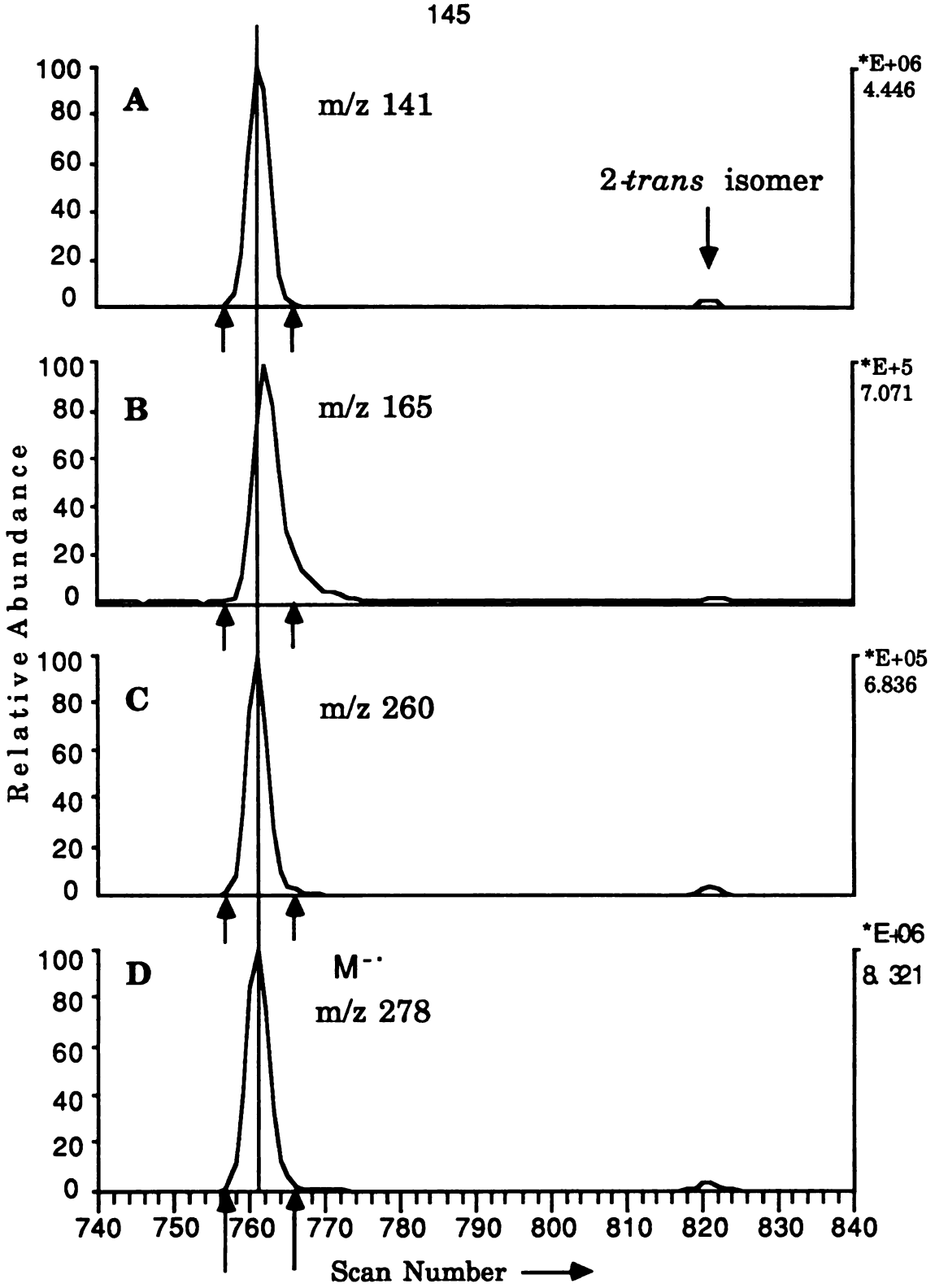

Figure 3-20: Mass chromatograms at m/z 141 (A), m/z 165 (B), m/z 260 (C), and m/z 278 (D) reconstructed from mass spectra obtained during ECNI with sample introduction via the GC inlet.

The conventional ECNI mass spectrum of ABA-Me extracted from plant tissue, which was stress-induced and then exposed to an $^{18}O_2$ environment, is shown in Figure 3-21. The need for an MS/MS approach is obvious as a mixture of single-, double-, and triple-labeled analogues are present. Provided that there is oxygen present in the ion source, the diagnostic fragment ions are observed as peaks in the mass spectrum. However, it would be difficult to determine the specific location of the isotopic label. Figure 3-22 shows three MS/MS mass spectra of ABA-Me which contains one ^{18}O atom, but extracted from different plant tissue. In these product ion mass spectra shown in Figure 3-22, the collision energy was 5 eV, resulting in less intense peaks at m/z 141 and 152, while increasing the abundance of the CID peaks at m/z 260 and 245. This figure serves to illustrate the analytical utility of the ion/molecule reaction approach. The relative abundance of ion current representing the diagnostic ions is different in each spectrum, yet in all the spectra the parent ion is monolabeled ABA-Me. The peak ratios provide information concerning the biosynthesis of ABA in the respective tissue, pointing out the location of the isotopic label in the labeled material containing a single ^{18}O atom. This approach was used extensively in the investigation of ABA with the results indicating that a universal pathway exists for biosynthesis of ABA in higher plants (134). The intent of this chapter is not to describe in detail the biosynthesis of ABA, but rather to demonstrate how this novel ion/molecule reaction approach, once the role of oxygen activation was elucidated, was useful in probing the biosynthetic mechanism of ABA.

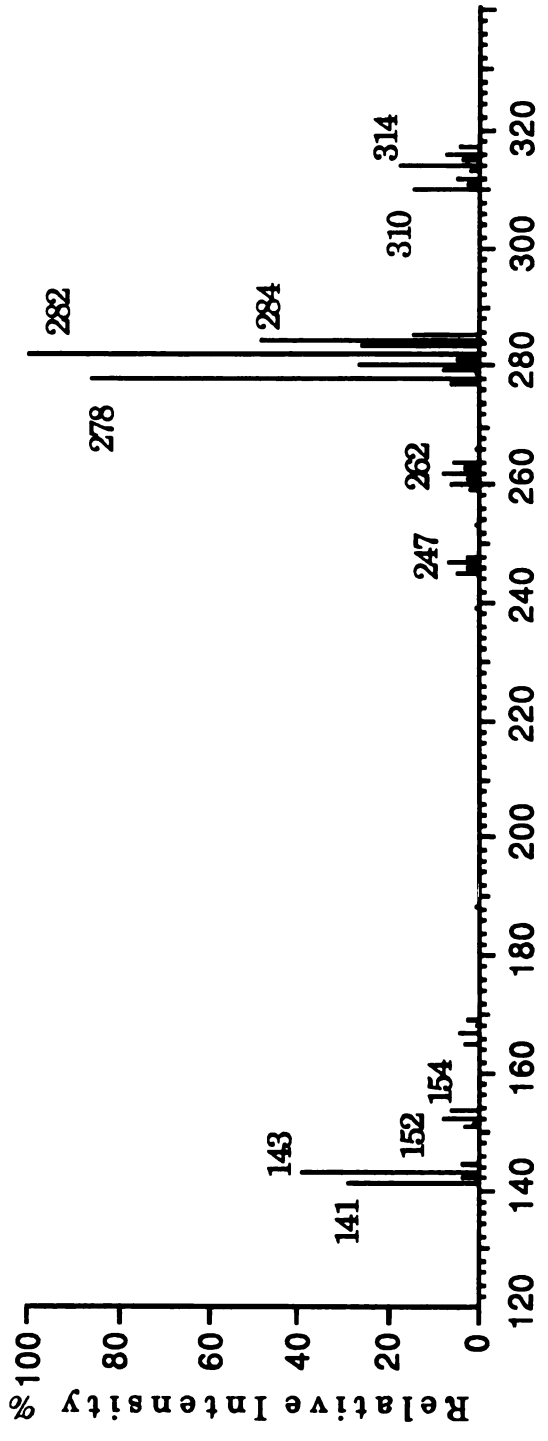

Figure 3-21: ECNI mass spectrum of a mixture of isotopically labeled ABA-Me

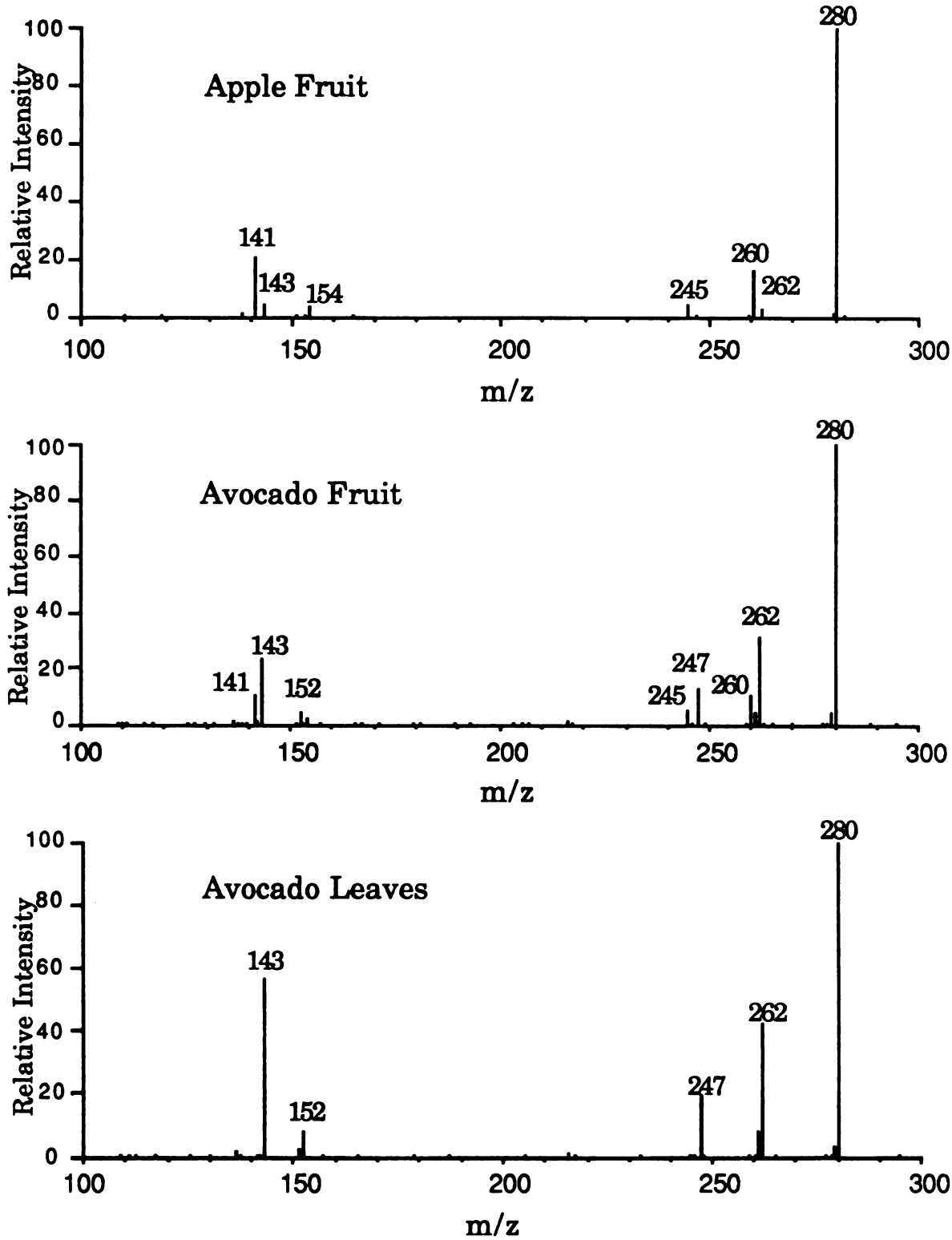

Figure 3-22: Product ion mass spectra of mono-labeled ABA-Me (m/z 280) with molecular oxygen at a collision energy of 5 eV_{Lab} .

E. Conclusion

The gas-phase reactions between molecular oxygen and odd-electron molecular anions of the methyl ester derivative of the plant growth regulator abscisic acid and several of its metabolites are unprecedented in that they represent the first case where a non-aromatic radical anion reacts with molecular oxygen, promoting fragmentation. It is postulated that the radical site has a decisive role in directing the fragmentation process, as this is the site of initial attack by O_2. Mechanisms are suggested to rationalize the formation of ions generated by the reaction with oxygen. These ion/molecule reactions have a dramatic effect on the appearance of the mass spectrum, and thus, could cause problems for the unsuspecting spectroscopist who operates with an intermittent and minor air leak, and who relies on pattern recognition for identifying compounds similar in structure to ABA. On the other hand, ions formed in this process enable the site of oxygen isotope enrichment to be precisely located within the molecule, an observation which has provided invaluable insight into the mechanism of biosynthesis of these compounds, as evidenced by recent publications for which this technique has played a prominent role (134,135,154). In the case of these particular compounds, CID-MS/MS with argon does not allow the position of the isotope label to be determined precisely. Although low-energy ion/molecule reactions in a TQMS have been used previously to investigate the structure of gas-phase ions, these have been nearly exclusively in positive ion mode. This chapter demonstrates the potential analytical utility of oxygen as a reagent gas for possibly probing the structure of some anions, specifically radical anions.

CHAPTER IV

COLLABORATIVE RESEARCH PROJECTS

A. Introduction

The opportunity for collaborations with other researchers provided the author with a great deal of enjoyment. In certain cases, the combined research efforts resulted in the completion of a project, while in other instances, preliminary studies demonstrated some interesting chemistry which may eventually lead to a full-fledged research topic for an incoming graduate student. This chapter describes four collaborative projects in which the author played a significant role, and these projects are summarized below.

The first project involved a study which was undertaken with Kathleen Kayganich, a former graduate student in the Department of Chemistry under the direction of Dr. J.T. Watson. Her research involved developing methodology for the determination of dexamethasone and other synthetic steroidal drugs in physiological fluids (60). The novel aspect of this research involved the unique sample preparation of dexamethasone prior to mass spectral analysis. Chemical oxidation was used to transform dexamethasone to a highly electrophilic compound which may be detected by electron capture negative ionization mass spectrometry (ECNI-MS). A collaborative effort was made to determine if an MS/MS approach could provide an alternative method for detection and quantitation of chemically oxidized dexamethasone in human plasma by electron capture negative ionization (155). Although

this project did not involve the study of gas-phase ion/molecule reactions, it was of interest to the author as it involved analytical applications of TQMS.

Unlike the project involving the analysis of dexamethasone, the second project described was unique in that the genesis of this investigation was begun at Michigan State University by Gregory Dolnikowski (106). However, the culmination of this project which involved the study of a gas-phase ion/molecule reaction between protonated acetaldehyde and methanol, occurred following his departure. Greg continued his efforts in unraveling this reaction mechanism while he was completing a post-doctoral assignment in England. Dr. J.T. Watson studied this ion/molecule reaction on a penta-quadrupole mass spectrometer while he was on sabbatical leave in France. Finally, many experiments were carried out by the author at Michigan State, which were important in determining the ion/molecule reaction mechanism of this gas-phase ion/molecule reaction (156).

The final two projects which will be described, fall under the heading of collaborations, as both studies were begun by a different investigator, yet later, some experiments were performed by the author on the Finnigan TSQ instrument. Both of these studies can be classified as being in their preliminary stage, as much more work needs to be accomplished by future graduate students. The first of these involves the reactions of protonated esters and alcohols. This study was prompted by the reports of Greg Dolnikowski describing the condensation reaction of protonated ethyl acetate and propanol yielding an acetal ion (106). Some additional experiments were performed mixing ethyl acetate (EtOAc) with other alcohols (Alc) in the ion source and subjecting the observed product ion representing the $(EtOAc*Alc*H - H_2O)^+$ ion to CID. The last section describes some experiments in which protonated molecules were reacted with

hexamethyldisilazane (HMDS) in Q_2 to determine if silylation would occur in the gas-phase. Once again, the initial experiments of this type were carried out by Dr. Watson while he was in France on sabbatical leave. Experiments were done on the TQMS in the Mass Spectrometry Facility to determine if the author could reproduce the results obtained in France where a penta-quadrupole mass spectrometer was used. The results suggest that silylation may occur in the gas-phase, yet future experiments need to be performed to determine the selectivity of this silylation reaction for protonated molecules.

B. ECNI-MS/MS analysis of oxidized dexamethasone

1. *Introduction*

It has been demonstrated previously in our laboratory that dexamethasone, a synthetic steroid, can be oxidized chemically to a ketonic steroid structure which can be readily detected by ECNI-MS (60,157). The structures of dexamethasone and oxidized dexamethasone are shown in Figure 4-1. The conventional approach for detection of dexamethasone in biological matrixes has been to prepare the 11,17,21-tris-trimethylsilyl ether-20-enol-trimethylsilyl ether (tetra-TMS) (158). By using this approach, Kasuya *et al.* were able to detect an on-column injection of 100 pg of dexamethasone-tetra-TMS with a signal-to-noise (S/N) of 2.5, from 1mL of plasma spiked to a concentration of 300 pg/mL (158). On the other hand, Kayganich *et al.* were able to detect an injection of 30 pg of oxidized dexamethasone (S/N=11) from 1 mL of plasma spiked with 209 pg of dexamethasone and 35 ng of internal standard (60). In addition, extensive isolation procedures were not required in the sample preparation, as they

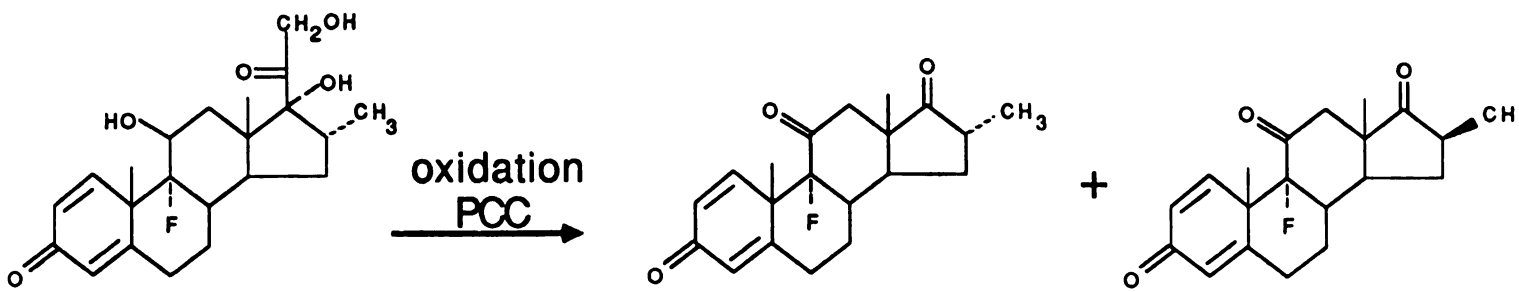

Dexamethasone

(9α-fluoro-16α-methyl-11β,17α,21-triol-1,4-pregnadien-3,20-dione)

16α-methyl-11,17-keto "Dexamethasone"

(9α-fluoro-16α-methyl-1,4-androstadiene-3,11,17-trione)

16β-methyl-11,17-keto "Dexamethasone"

(9α-fluoro-16β-methyl-1,4-androstadiene-3,11,17-trione)

Figure 4-1: Conversion of dexamethasone to its 11,17-keto analogue by chemical oxidation.

were in the Kasuya method. This is attributed to the selectivity of the oxidation reaction and the ionization by electron capture. The ECNI mass spectrum of oxidized dexamethasone is shown in Figure 4-2. This spectrum consists primarily of a peak at m/z 330 representing the molecular anion and a base peak at m/z 310 representing the $(M-HF)^{-\cdot}$ ion. It was expected that upon CID, the molecular anion with m/z 330 would eliminate HF yielding a daughter peak at m/z 310 and this was confirmed experimentally as seen in the CID daughter ion mass spectrum shown in Figure 4-3. Few endogenous compounds contain fluorine, so the loss of 20 u (loss of HF) appeared to be a selective transition to monitor in a selected reaction monitoring (SRM) analysis as interfering substances from a plasma matrix are unlikely to undergo loss of HF. The attempt to further simplify the analysis of oxidized dexamethasone by using tandem mass spectrometry, and perhaps shorten the analysis time by introducing the sample by means of a direct insertion probe (DIP), was investigated and the results are presented in this section.

2. *Experimental*

a) Instrumentation

All experiments were performed on the Finnigan TSQ-70 triple quadrupole mass spectrometer which was equipped with a Varian 3400 gas chromatograph. Samples were introduced into the ion source via a DB-5 capillary column directly interfaced to the mass spectrometer. Helium was used as the carrier gas at a flow rate of 1 mL/min. The column was operated with a splitless injector and, following an injection, the GC oven temperature was ramped from 60 or 120° C to 260° C at 40 °C/min and from 260°C to 280 °C at 4 °C/min. For samples which were introduced via the DIP, after

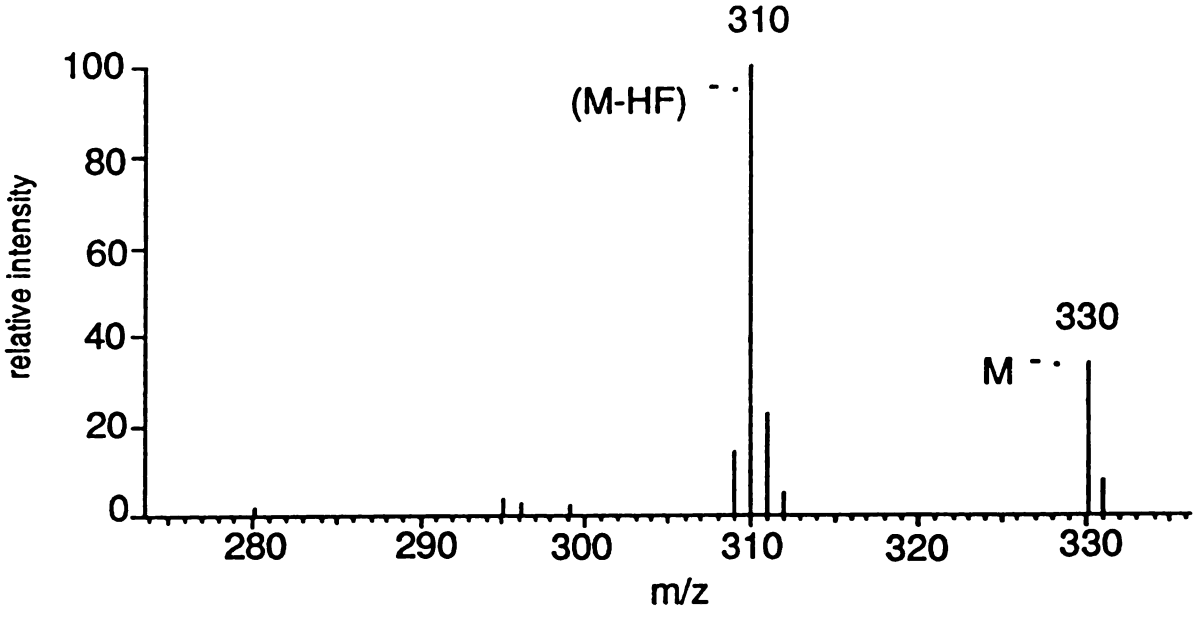

Figure 4-2: ECNI mass spectrum of 11,17-keto-dexamethasone.

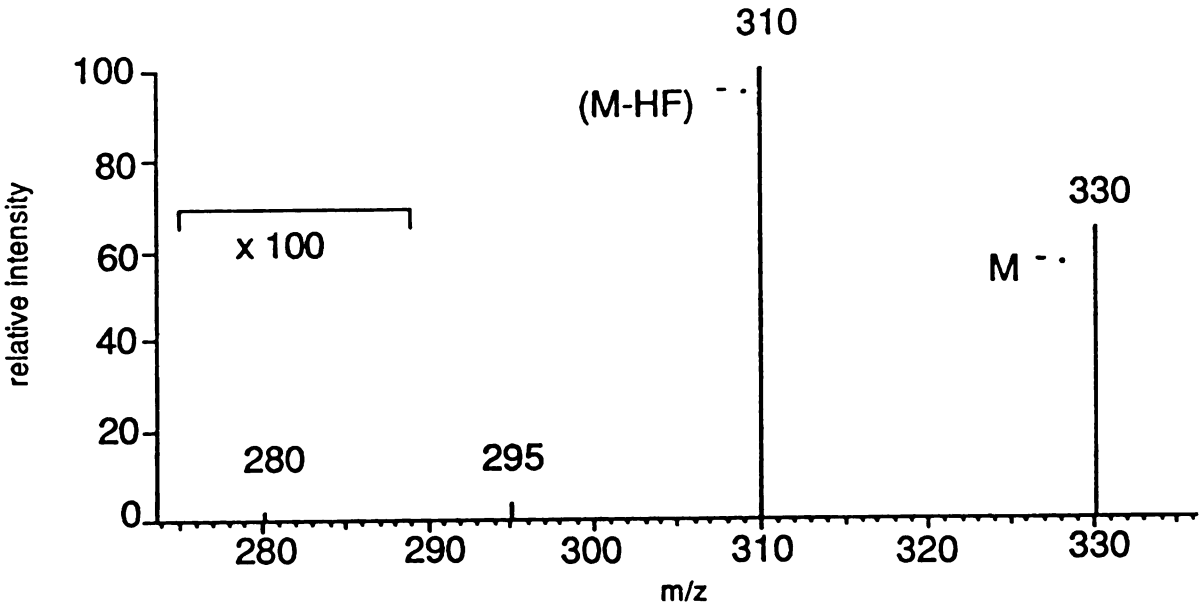

Figure 4-3: CID daughter ion mass spectrum of the molecular anion (m/z 330) of 11,17-keto-dexamethasone.

insertion of the probe, the temperature was ramped from 35 to 200 °C at a rate of 70 °C/min and held at 200 °C for 2 minutes. Regardless of the method used to introduce the sample, (GC or DIP) the ion source conditions were established to maximize the abundance of the parent ion, $M^{-\cdot}$, for analysis by MS/MS. The molecular anion of oxidized dexamethasone was at the greatest absolute abundance when ammonia was used as the ECNI modifying gas at a pressure of about 1 torr. The electron energy was 100 eV, and the primary electron beam current was 300 μA. The ion source temperature was maintained at 100°C.

b) Collision energy and pressure studies

The conditions for the MS/MS experiments were optimized by varying both the collision gas pressure and the collision energy. Conditions for these parameters were sought which would provide for the greatest detection of the daughter ion peak at m/z 310, following CID of the molecular anion. In order to determine these optimal values, 3.56 ng of oxidized dexamethasone was introduced via the direct insertion probe (DIP). The probe was held at 40 °C for 1 minute and then ramped to 200°C at 30 °C/min and held at 200°C for 2 minutes. This temperature program yielded a level plateau region in the desorption profile over which the total ion current (TIC) was relatively constant. Over the course of this constant TIC region, repetitive daughter ion spectra of m/z 330 were obtained at different collision energies. The parent ion current at m/z 330 was selected by the first quadrupole Q_1, and the third quadrupole, Q_3, was scanned from m/z 275 to m/z 345 at 0.1 sec/scan. The full daughter ion mass spectrum indicated no fragments below m/z 275. Consecutive daughter ion scans were acquired at collision energies of 1,3,5,12, and 25 eV_{Lab}; this cycle was repeated many times during the course

of the desorption profile. Five scans at each collision energy, collected during the period of relatively constant parent ion current in the desorption profile, were averaged to provide a representative daughter ion mass spectrum. Replicate experiments were performed for each collision gas pressure. This protocol permitted a reliable assessment of the fragmentation and collection efficiency as a function of collision energy at a given pressure of collision gas in Q_2.

c) Selected reaction monitoring studies

For the determination of dexamethasone in plasma by selected reaction monitoring (SRM), the ion currents corresponding to the transition of m/z 330 to m/z 310 (for oxidized dexamethasone) and m/z 339 to m/z 319 (for the internal standard, oxidized $^{13}C_6$,$^{2}H_3$-dexamethasone) were monitored with a 1.0 u window. Dwell times were 50 ms and the electron multiplier was set at 1400 eV.

d) Methods

The sample preparation based on the oxidation method consisted of three steps: plasma extraction, chemical oxidation, and removal of excess oxidation reagent. The author was not involved in this aspect of the research, and since the intent was not to demonstrate the value of the chemical oxidation procedure, the details concerning these procedures are not presented. These sample preparation methods are described in references 60 and 155.

3. *Results and discussion*

The goal of this study was to determine if an assay for oxidized dexamethasone could be developed utilizing MS/MS. There have been reports of improvements by the tandem mass spectrometry approach to the detection of targeted compounds using ECNI with sample introduction by GC (59, 159-161). Recently, a quantitative assay for leukotriene-B_4 (as the butyldimethylsilyl ether derivative) in synovial fluid was reported (56). The selectivity of ECNI in combination with MS/MS, allowed quantitation of lower levels of LTB_4 in the matrix than would have been possible using selected ion monitoring (SIM) with a conventional single-stage mass spectrometer.

a) Optimization of MS/MS parameters

In order to determine the optimal parameters which would provide maximum detection of the daughter ion with m/z 310, the experimental protocol described above was performed. Two essential MS/MS parameters affecting fragmentation efficiency, $\Sigma F_i/(\Sigma F_i+P)$, and collection efficiency, $((\Sigma F_i+P)/P_0)$, where ΣF_i is the sum of the fragment ion intensity, P is the remaining parent ion intensity, and P_0 is the parent ion intensity without collision gas, are collision gas pressure and collision energy. The experiments were designed to dissect out interactive parameters of the CID process that could be adjusted individually.

First, the ion collection efficiency was assessed as a function of collision energy. The reconstructed TIC, shown in Figure 4-4A, is presented as a function of collision energy at argon pressures of 0.4, 0.9, and 1.3 mtorr in Q_2. When argon was present at these pressures in Q_2, the collection efficiency

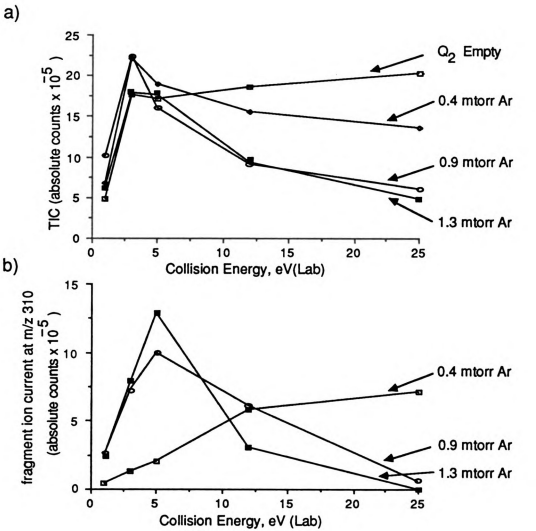

Figure 4-4: (A) Reconstructed TIC from CID of the $M^{+\cdot}$ of oxidized dexamethasone as a function of collision energy at different collision gas (argon) pressures in Q_2 . (B) Magnitude of daughter ion (m/z 310) current as a function of collision energy at three pressures of argon in Q_2.

decreased at collision energies above 3 eV_{Lab}. A similar attenuation of the TIC at higher collision energy has been noted by other researchers (56). The poorest collection of ions is observed at the lowest collision energy examined, 1 eV_{Lab}. This is attributed to the low kinetic energy of the parent ion. The highest collection efficiency occurred with a collision energy of 3 eV_{Lab} for each of the pressures examined. As is evident from Figure 4-4A, the maximum TIC at 3 eV_{Lab} was approximately the same for the three pressures of argon except at 1.3 mtorr, where there was slight attenuation of the ion beam (about 15%) due to higher collision gas pressure. No reasonable explanation is offered for the TIC results from experiments with no collision gas in Q_2 being lower than those when Q_2 is pressurized at collision energies below 5 eV_{Lab}; the precision of results (+ or - 15% relative standard deviation) is too poor. A very accurate assessment may be made in comparing the TIC at constant pressure, but different energy, as all these values are obtained over the course of a single experiment and during the nearly constant desorption region. However, in comparing different pressures, separate experiments are required. Fluctuations in parent ion intensity may occur as a result of (i) different desorption profiles, (ii) slight variations in ion source conditions which may alter the ionization efficiency, and (iii) error in loading the sample onto the probe tip.

The interdependency of various instrumental parameters involved in an MS/MS experiment makes it difficult to determine what causes the decrease in collection efficiency as collision energy is raised. Of the several variables, greater collision energy increases the fragmentation efficiency, and these daughter ions may be confined with varying degrees of efficiency in the RF-only field of Q_2 (162,163). Mass-discriminatory effects are generally pronounced when the daughter ion mass is much lower than the parent ion

mass. In this case, however, the most abundant daughter ion of m/z 310 is 94% of the parent mass (m/z 330); therefore losses due to disparities in the efficiency with which ions are contained in Q_2 should be minimal. Alexander and Boyd (163) have noted that for a hybrid BEQQ instrument, there are variations in the transmission of ions as a function of collision energy. In their study, the maximum and minimum transmission of protonated Leu-enkephalin (MH^+, m/z 556), without collision gas present, varied by a factor of 2 over the collision energy range of 10-30 eV_{Lab} (163). Although this study by Alexander and Boyd was performed on a BEQQ instrument, fluctuations in the transmission curve for both parent and daughter ions as E_{Lab} increases could account for the apparent losses of ion current in the studies of oxidized dexamethasone using a TQMS. However, the constant parent ion flux with Q_2 empty (Figure 4-4A), which is quite independent of collision energy, seems to indicate that the losses observed are not due to the instrumental dependency reported by Alexander and Boyd. Thus, by default, target gas pressure factors appear to cause the decrease in collection efficiency as E_{Lab} increases. Scattering of both parent and daughter ions may lead to lower transmission in the acceptance region of Q_3 (22), but the tandem quadrupole configuration is generally considered to be a good focusing device for scattered ions, so scattering losses probably are not the major factor. Finally, with increased pressure and higher collision energies, collision-induced electron detachment (23) may compete with the CID processes, resulting in formation of undetectable neutral species. All the factors described probably contribute to ion losses, but electron detachment is most likely the predominant factor causing the decrease in collection efficiency as collision energy is raised.

The primary function of the optimization studies was to determine the conditions for which the daughter ion current at m/z 310 is greatest. The magnitude of fragment ion current at m/z 310 as a function of collision energy is represented in Figure 4-4B. At the lowest pressure examined, 0.4 mtorr argon, collision at 25 eV_{Lab} provides the greatest amount of $(M-HF)^{-\cdot}$. At increased pressures, lower energies were required for maximal formation of $(M-HF)^{-\cdot}$; optimal energy for CID at 0.9 mtorr and 1.3 mtorr was 5 eV_{Lab}, and the ion current detected at m/z 310 for these conditions is greater than at a collision energy of 25 eV_{Lab} at lower pressure (0.4 mtorr). More effective transfer of kinetic energy to internal energy occurs with higher collision frequency (23,162,164); thus, less translational energy is required at higher gas pressures than at low pressure to induce similar fragmentation. Secondary dissociation of $(M-HF)^{-\cdot}$ also may occur at higher pressures, primarily due to successive losses of $CH_3\cdot$. This results in an increase in abundance for ions with m/z 295 and 280 when the collision energy is raised at argon pressures of 0.9 mtorr and 1.3 mtorr.

As a result of the optimization studies, a pressure of approximately 1.3 mtorr argon in Q_2 and a collision energy of 4 eV_{Lab} were employed to ensure both high ion collection efficiency and extensive fragmentation of the parent ion of m/z 330, resulting in optimal detectability of the daughter ion with m/z 310 during the analysis of plasma samples.

b) SRM vs SIM

The improved selectivity of the GC/SRM analysis over GC/SIM is shown in Figure 4-5, which is a composite of results from the analysis of a plasma extract for dexamethasone. Shown in Figure 4-5A are the selected ion current profiles for $M^{-\cdot}$ and $(M-HF)^{-\cdot}$ of 11,17-keto-dexamethasone (top

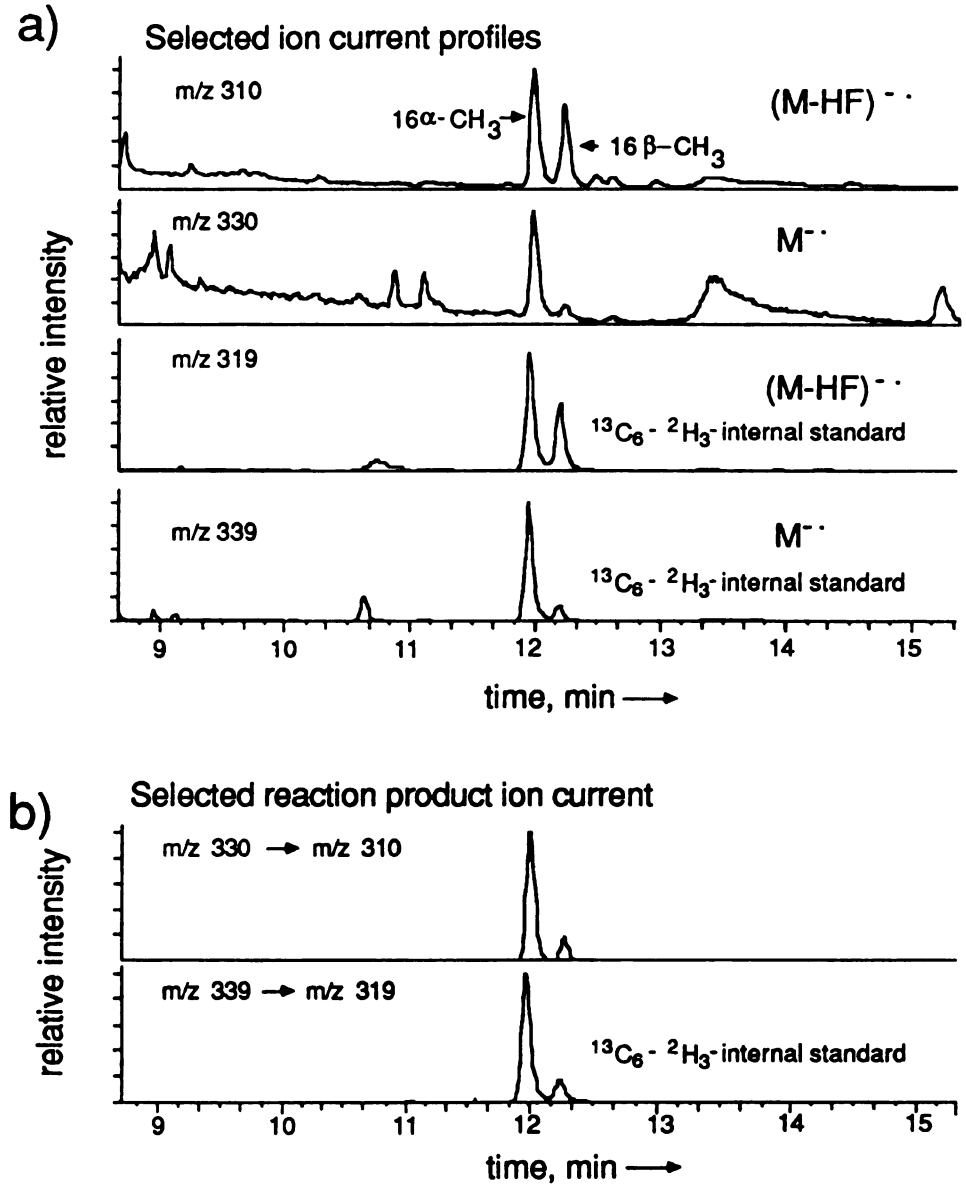

Figure 4-5: Comparison of selected ion current profiles obtained by GC/ECNI with (A) selected ion monitoring (top two panels for oxidized dexamethasone; bottom two panels for internal standard) and (B) selected reaction monitoring (top panel for oxidized dexamethasone; bottom panel for internal standard).

two panels) and 11,17-keto-$^{13}C_6$,$^{2}H_3$-dexamethasone (bottom two panels); the latter was used as an internal standard during analysis of this plasma sample. The quantities injected on-column to obtain the data shown in Figure 4-5A correspond to approximately 20 pg of oxidized dexamethasone and 0.7 ng of the oxidized isotopically labeled dexamethasone. Shown in Figure 4-5B are the selected reaction current profiles obtained from another aliquot of the same sample as analyzed by GC/SRM with CID of the molecular anions of oxidized dexamethasone (m/z 330), and the isotopically labeled internal standard (m/z 339). Figure 4-5B demonstrates the inherent selectivity of MS/MS as all the interfering ion current in GC/MS has been eliminated by the MS/MS process. The only signal detected is that from the 11,17-keto-dexamethasone and its 16β-CH_3 epimer (peak at longer retention time). This 16β-CH_3 epimer is formed during the chemical oxidation procedure. The absence of background makes the determination of peak height or peak area straightforward and increases the precision of replicate analyses. It is more difficult to determine the baseline position in quantitation measurements obtained from the GC/SIM analysis.

The additional selectivity provided by the MS/MS approach, along with the inherent selectivity of the assay resulting from the chemical oxidation and ECNI detection, led to the investigation of the use of the direct insertion probe (DIP) as an alternative method of introducing the sample. Other researchers have reported that a chromatographic step in the sample preparation is necessary in methodology based on ECNI/MS/MS when a general derivatization reagent is used to prepare an electrophilic derivative of the sample (160). The chromatographic step is required because the electron capture cross sections of many matrix components also are enhanced by the derivatization. The electrophilic matrix components can deplete the

concentration of thermal electrons in the ion source (160,165). Without sufficient chromatographic separation, the low level of analyte cannot compete with the excess matrix for the pool of thermal electrons in the ion source. However, as suggested by Figure 4-6 which shows the calibration curves for the determination of dexamethasone in plasma by GC/SIM, GC/SRM, and DIP/SRM, the chemical oxidation procedure provides sufficient selectivity in the conversion of the dexamethasone to the electrophilic oxidation product without enhancing the electrophilic character of the matrix. The calibration curves are all similar. Therefore, the results obtained by DIP/SRM are in good agreement with those obtained when the GC is used to introduce the sample. The additional selectivity of SRM allows the direct insertion probe sample inlet to be used for analysis of dexamethasone due to the selectivity achieved by the chemical oxidation and subsequent ECNI. This significantly simplifies and shortens the analysis. Comparison of the values obtained for the concentration of dexamethasone in plasma were in good agreement for most of the samples analyzed by the three techniques (155).

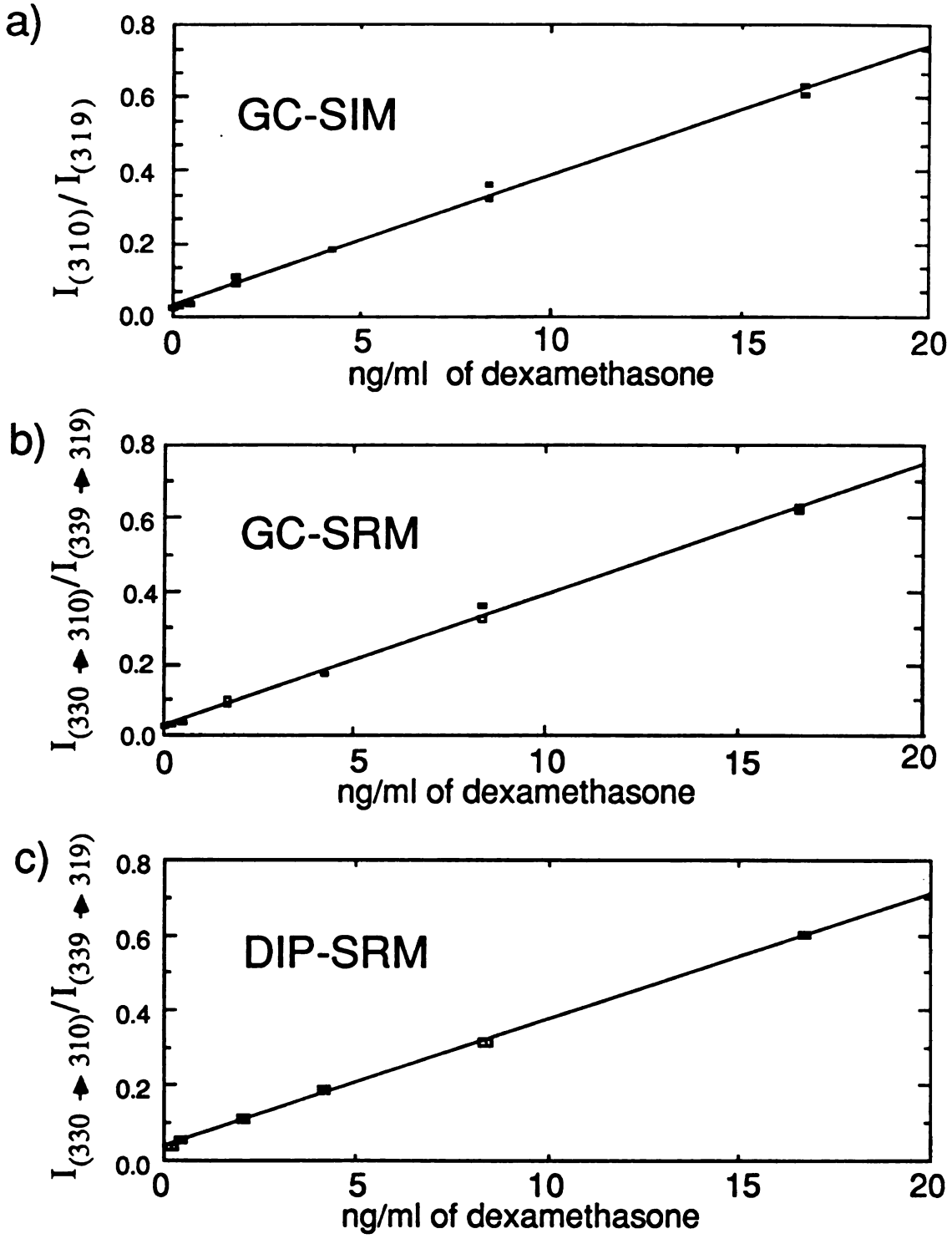

Figure 4-6: Calibration curves for the determination of dexamethasone in plasma by (A) GC/ECNI/MS with selected ion monitoring, (B) GC/ECNI/MS/MS with selected reaction monitoring, and (C) DIP/ECNI/MS/MS with selected reaction monitoring. The quantities introduced into the ion source represent a range of 4-200 pg of dexamethasone and 700 pg of internal standard.

C. Study of the gas-phase reaction between protonated acetaldehyde and methanol

1. *Introduction*

The study of the ion/molecule reaction between protonated acetaldehyde and methanol in a TQMS was begun by Greg Dolnikowski (106). If protonated acetaldehyde (m/z 45) is selected by Q_1 and reacted with methanol in the collision cell, a product ion mass spectrum is obtained as shown in Figure 4-7, which shows the presence of a peak at m/z 59. This experiment was performed on the Extrel TQMS and also on the Finnigan TSQ-70, and the product ion mass spectra were similar. It is clear that following the formation of a collision complex with m/z 77, dehydration occurs to form the ion with m/z 59. However, it was originally postulated that the structure of this ion with m/z 59 was that of protonated acetone (106). Further studies on three different types of mass spectrometers (BEQQ, TQMS, and a penta-quadrupole instrument) were performed in pursuit of determining whether C-alklylation (166,167) or the anticipated O-alkylation (168-172) was involved in the formation of the covalently bonded product ions (Figure 4-8). The culmination of this odyssey occurred following experiments performed in England, France, and at Michigan State University. Comparison of the CID daughter ion mass spectrum of the product ion of m/z 59 formed in the ion source, with known ionic structures at identical mass, enabled us to determine the structure (156). This chapter describes the role of the TQMS in determining the ionic structure of the product ion of m/z 59, and in unraveling the ion/molecule reaction mechanism which accounts for its formation.

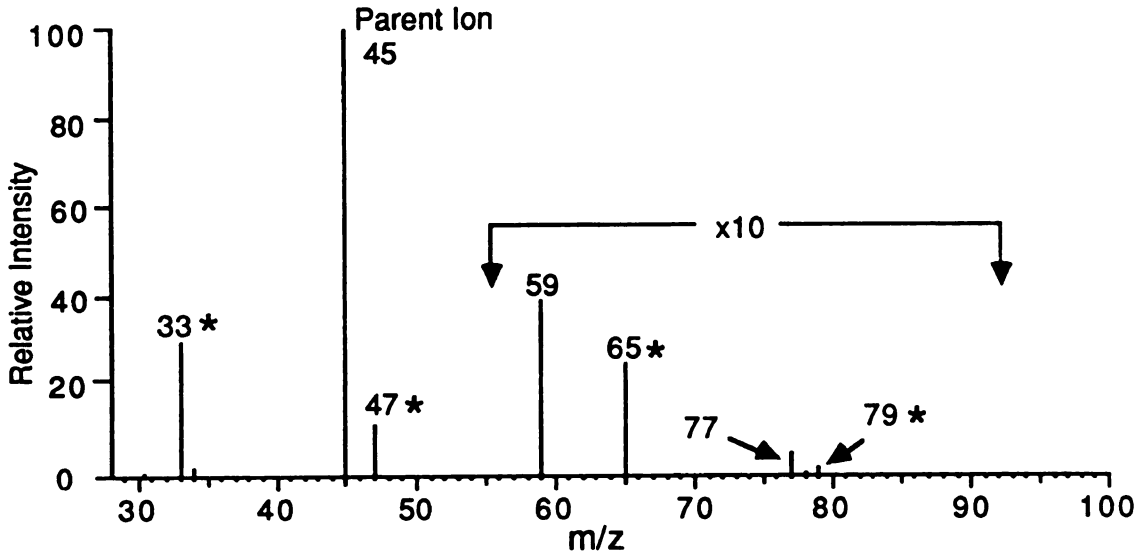

Figure 4-7: Product ion mass spectrum of ions produced during ion/molecule reactions of protonated acetaldehyde with methanol in Q_2 at a pressure of 2 mtorr. Those peaks marked by an asterisk represent known product ions in the ion/molecule reaction between protonated methanol (generated by proton transfer in this case) and methanol.

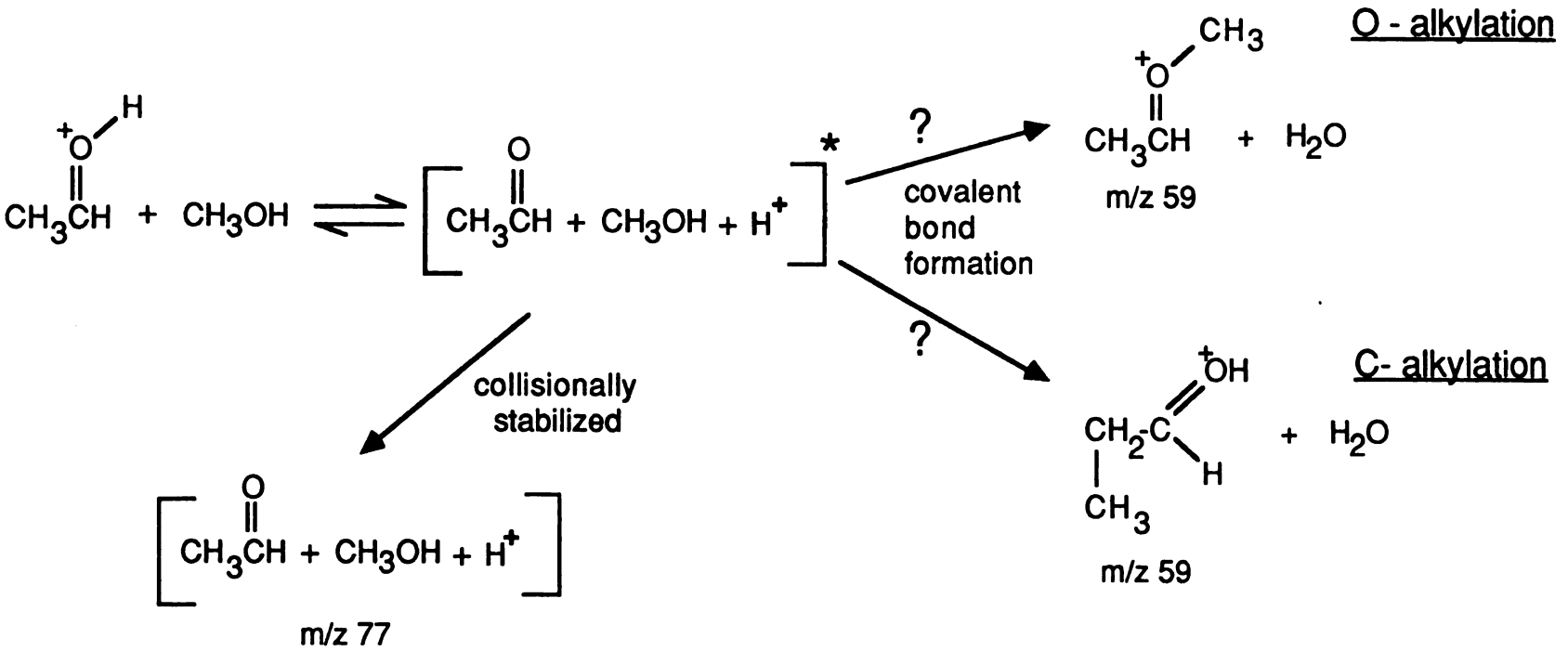

Figure 4-8: C-alkylation or O-alkylation for the formation of the ion of m/z 59.

2. *Experimental*

The experiments carried out by the author were performed on the Finnigan TSQ-70 instrument equipped with a Varian 3400 gas chromatograph. The ion source was maintained at 150°C; the ionizing current was 200 μA at 70 eV. Ion/molecule reactions between molecules and ions of methanol and acetaldehyde in the ion source were conducted by introducing two microliters of both compounds (neat) through the GC inlet, thereby providing transitory high pressure conditions as the two compounds coeluted into a CI volume (without CI gas). The other chemicals used throughout this study were either introduced into the GC, or introduced through a fixed gas reservoir that was connected to the ion source via a valve with a variable leak. In all cases, the parent ion of m/z 59 was selected by Q_1 for CID in the collision cell, with argon at 0.1 mtorr. The CID daughter ion mass spectra were collected with a collision energy of 25 eV_{Lab}. To obtain the product ion mass spectrum of protonated acetaldehyde and methanol, methanol vapors were introduced into the collision cell via a controlled variable leak valve to a pressure of 2 mtorr and protonated acetaldehyde was introduced at a collision energy of 1 eV_{Lab}.

3. *Results and discussion*

a) Formation of the product ion with m/z 59

The product ion mass spectrum shown in Figure 4-7 was obtained when protonated acetaldehyde at low kinetic energy reacted with methanol in the collision cell of the TQMS at a pressure of 2 mtorr. Product ion peaks at m/z 59 and m/z 77 are observed along with peaks that may be attributed to

the proton transfer reaction to methanol (m/z 33), and peaks from subsequent ion/molecule reactions in methanol (173,187). The product ion with m/z 59 is not obtained if protonated methanol is allowed to react with acetaldehyde. This is in contrast to results obtained on the penta-quadrupole instrument when protonated methanol reacted with acetaldehyde; the ion with m/z 59 was observed if ion confinement was used (156). This is attributed to proton affinity (PA) differences. The PA of acetaldehyde (780.8 kJ/mol) is greater than that of methanol (761.0 kJ/mol) (108). In the TQMS, the only reaction that proceeds when protonated methanol interacts with acetaldehyde is a proton transfer reaction. However, in the penta-quadrupole instrument using ion confinement which provides more time for reactions, proton transfer may occur and the protonated acetaldehyde then may react with methanol vapor which has leaked from the ion source into the collision region. This sequence of reactions requires more time which is provided by the ion confinement technique. A second possibility may be that the formation of a proton-bound complex (m/z 77) generated from protonated methanol and acetaldehyde may require transfer of the proton within the collision-complex prior to forming the covalently bound species of m/z 59. This transfer may be sufficiently slow (173), so that formation of the product ion (m/z 59) occurs after an extended time, as is available with ion confinement in the penta-quadrupole instrument.

The structure of the ion/molecule reaction product (m/z 59) was characterized by CID. The ion of m/z 59 is formed when acetaldehyde and methanol are mixed in the ion source and ionized by EI, as is shown in Figure 4-9. The CID daughter ion mass spectrum of the product ion with m/z 59 formed when methanol and acetaldehyde were simultaneously introduced into the ion source is shown in Figure 4-10A. The CID daughter ion mass

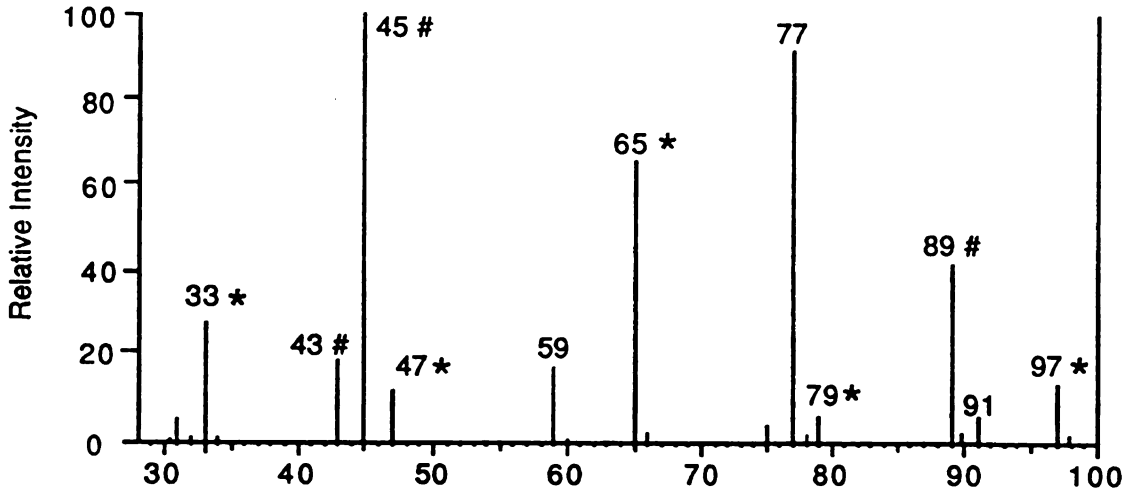

Figure 4-9: Reaction product mass spectrum of ions produced during ion/molecule reactions following EI of methanol and acetaldehyde in a high pressure ion source of the TSQ-70. Those peaks marked by an asterisk represent known product ions of methanol self-CI. Those peaks marked with a # represent known product ions of acetaldehyde self-CI.

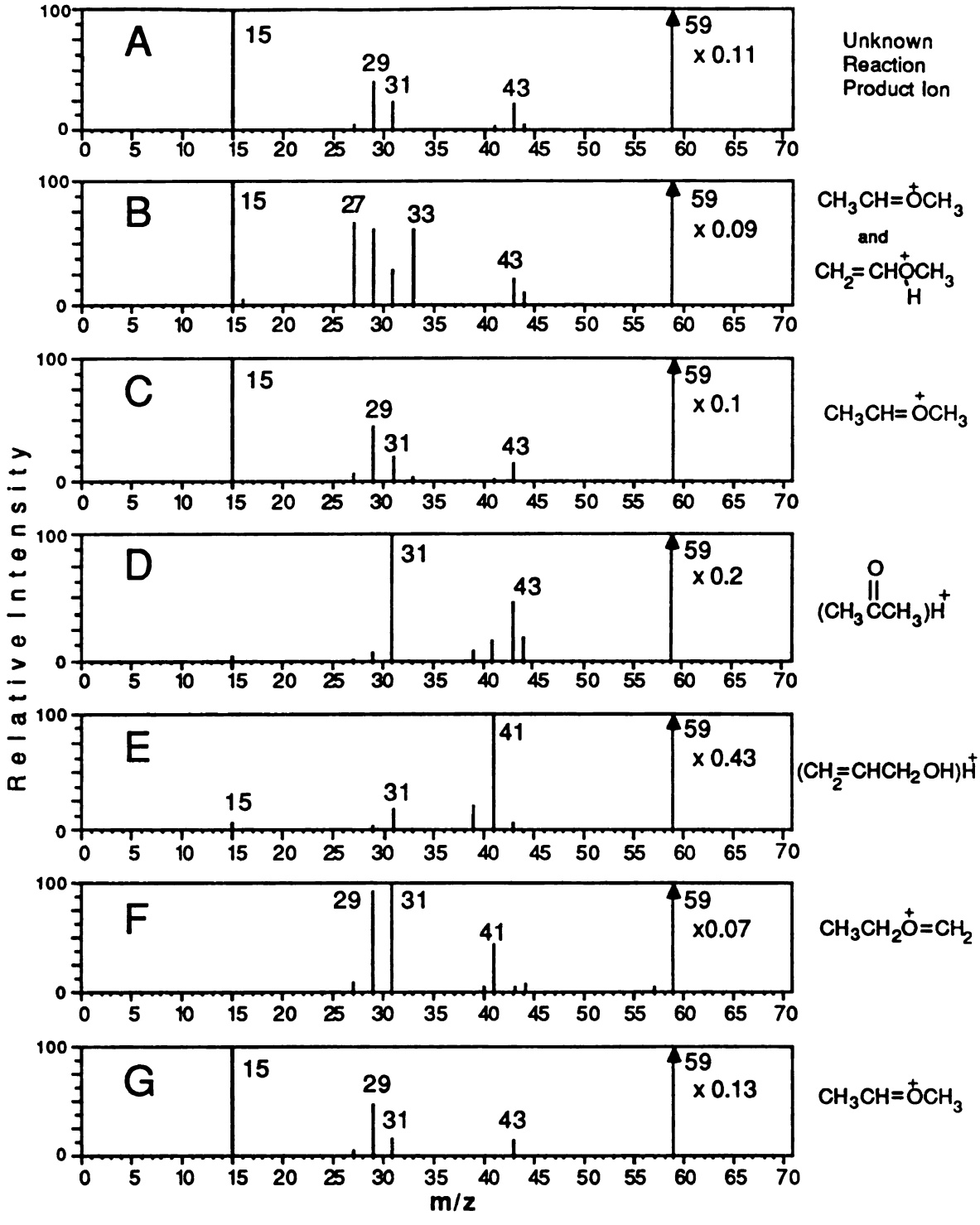

Figure 4-10: Daughter ion mass spectra obtained during CID in Q_2 of TQMS of a parent ion of mass 59 corresponding to: (A) product ion from high pressure ion source containing methanol and acetaldehyde; (B) protonated methyl vinyl ether (self-CI at lower pressure); (C) protonated methyl vinyl ether (self-CI at higher pressure); (D) protonated acetone; (E) protonated allyl alcohol; (F) fragment ion from diethyl ether following EI; and (G) fragment ion from acetaldehyde dimethylacetal following EI.

spectra of several isomeric ions of m/z 59 were obtained with the TSQ-70 in a comparative effort to identify the structure of the product ion with m/z 59 generated from the ion/molecule reaction of methanol and protonated acetaldehyde. Isomeric $C_3H_7O^+$ ion structures have been extensively investigated (25,174-183). If thermochemistry were the determining factor in the formation of the $C_3H_7O^+$ product ion structure, then a variety of candidate structures must be considered as is shown in Figure 4-11. A composite of low energy CID daughter ion mass spectra of protonated forms of methyl vinyl ether, acetone, allyl alcohol and fragment ions of diethyl ether and acetaldehyde dimethyl acetal, is shown in Figure 4-10. Two spectra in this composite, C and G match the daughter ion mass spectrum of Figure 4-10A. Figure 4-10G is the CID daughter ion mass spectrum of the fragment ion of m/z 59 formed by homolytic cleavage in the molecular ion of acetaldehyde dimethylacetal following ionization by EI, with the structure shown in Figure 4-12. The results provide evidence that the product ion of m/z 59 from the reaction of protonated acetaldehyde and methanol results from methylation of the oxygen atom on the acetaldehyde. The structure of the ion/molecule reaction product ion clearly is identical with this structure represented in Figure 4-12, as seen by the similar CID daughter ion mass spectra. Both Figure 4-10B and Figure 4-10C are the CID daughter ion mass spectra of protonated vinyl methyl ether (VME), however, Figure 10C is obtained with a higher source pressure of VME. At the higher pressure conditions, there are sufficient collisions to drive the protonation reaction to the thermodynamically favored (182,184) C-protonated product (structure shown in Figure 4-12); at lower pressures, a mixture of O-protonated (kinetically favored) and C-protonated ions is produced.

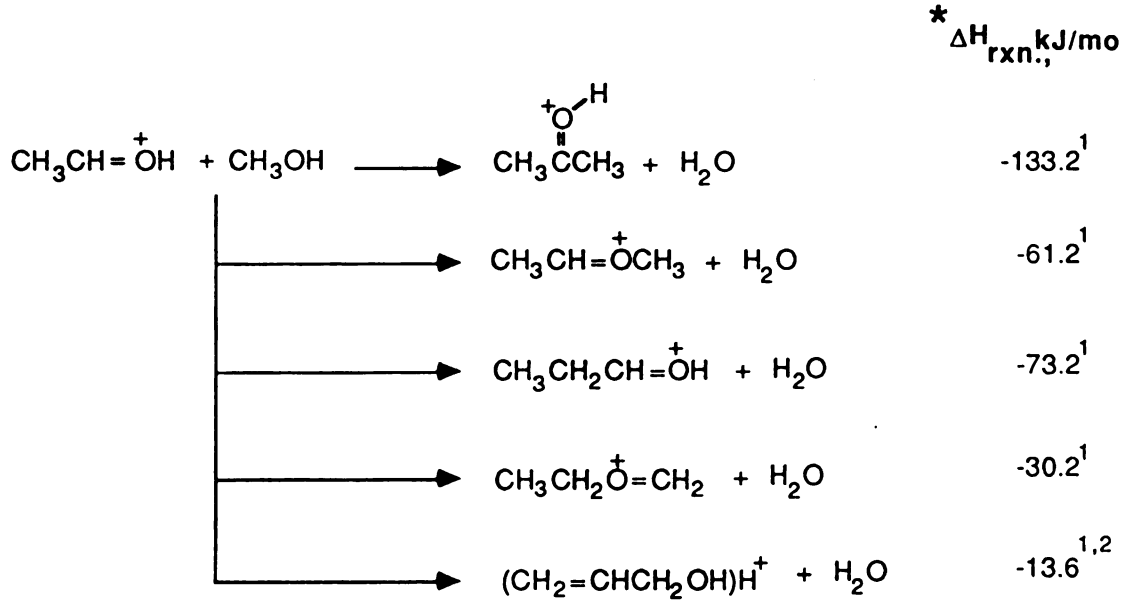

* [1] Reaction enthalpies calculated from ionic and neutral heats of formation found in reference 108.

[2] P.A. of allyl alcohol, estimated in reference 176, used in calculation of $\Delta H_{rxn.}$

Figure 4-11: Candidate structures for product ion with m/z 59.

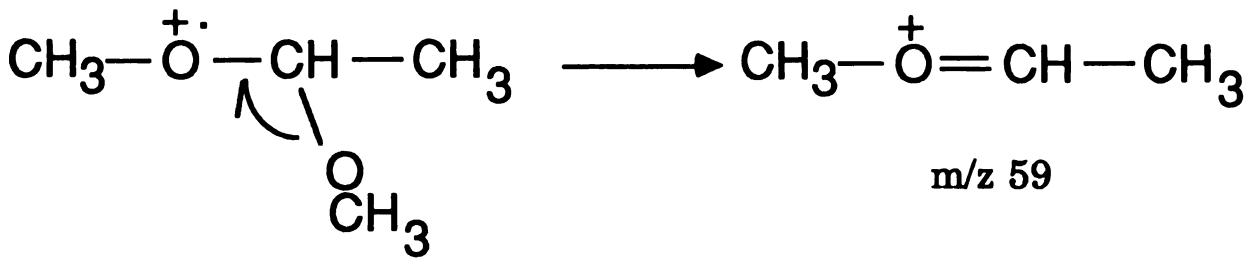

acetaldehyde dimethylacetal

Figure 4-12: Structure of m/z 59 formed by homolytic cleavage of the molecular ion of acetaldehyde dimethylacetal.

Not only were CID experiments performed on the TQMS, but they were carried out on BEQQ (in England) and penta-quadrupole instruments. Although the data from these instruments are not shown, as the experiments were not carried out by the author, it deserves mention that all of the daughter ion mass spectra were remarkably similar. In spite of the different source conditions and different collision conditions, the CID daughter ion mass spectra were qualitatively in accord, and all the data point to the structure of m/z 59 from the reaction of protonated acetaldehyde and methanol being that shown in Figure 4-12 which represents O-methylation of protonated acetaldehyde.

Having established the identity of the ion with m/z 59, we wished to determine the mechanism or mechanisms for its production in the high pressure ion source and to determine the structure of the intermediate. A proposed mechanism is shown in Figure 4-13. As shown by the mechanism, it is postulated that there are two structures for the ion of m/z 77, each which are formed at thermal energies in either the ion source or in the quadrupole reaction chamber. The different location of the charge in protonated acetaldehyde, the reactant ion, accounts for the formation of different ionic structures with m/z 77. For the O-charged form of acetaldehyde, the proton becomes "sandwiched" between the oxygens of the acetaldehyde and the methanol. Upon CID, this proton-bound "sandwich" form falls apart into either protonated methanol or protonated acetaldehyde (as shown in pathway (i) in Figure 4-13). On the other hand, for the C-charged form of protonated acetaldehyde, the intermediate involves close encounter of the oxygen atom of methanol with the positively charged carbon in protonated acetaldehyde due to electrostatic forces, and also close contact between the oxygen of protonated acetaldehyde and the methyl carbon of methanol. This "close

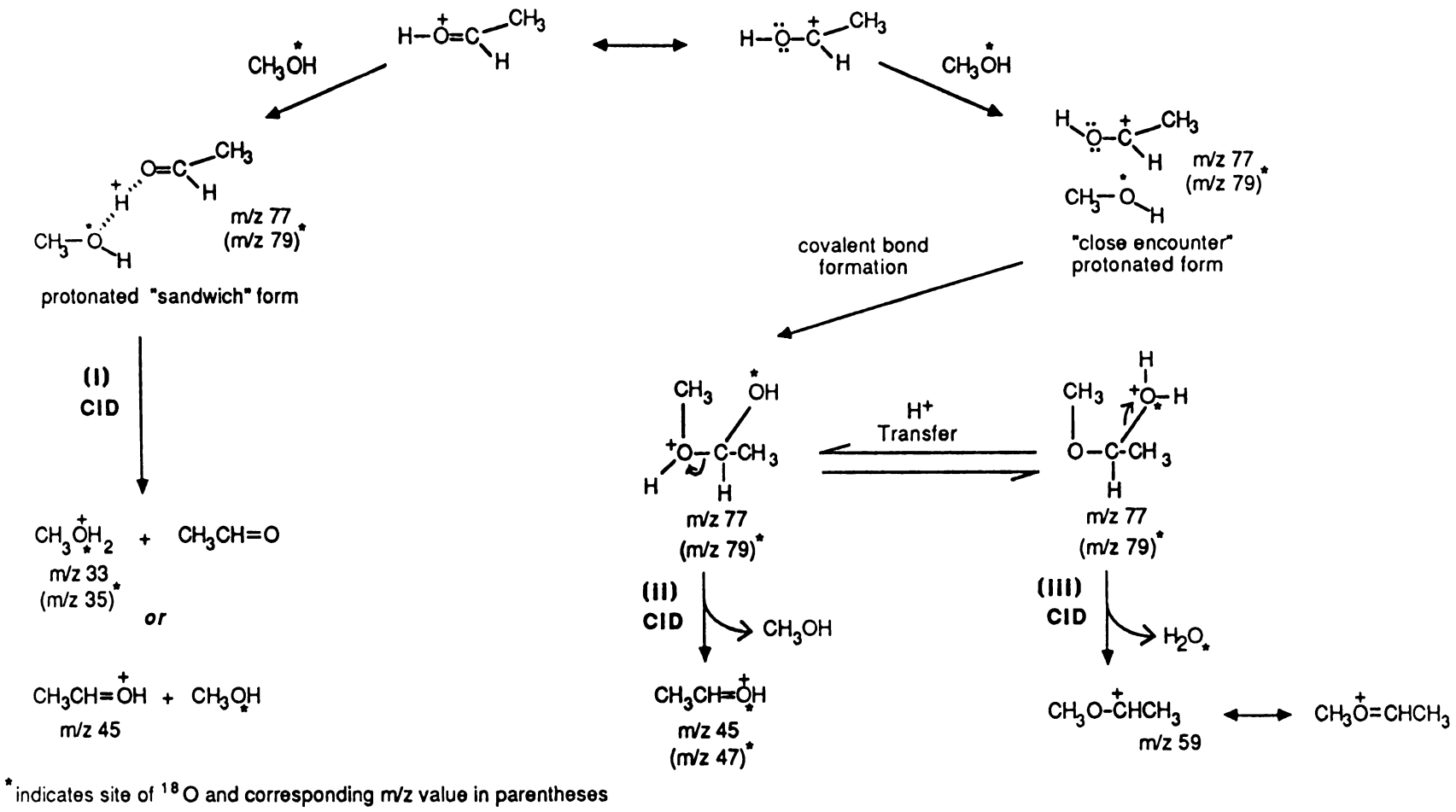

Figure 4-13: Proposed mechanism for the formation of the ion of m/z 59 from the collision-complex intermediate of m/z 77 following the ion/molecule reaction of protonated acetaldehyde and methanol.

encounter" form of the intermediate permits covalent bond formation (as indicated in the middle of Figure 4-13), thereby producing a protonated molecular species with m/z 77. This ion of m/z 77 decomposes promptly by elimination of methanol to form an ion with m/z 45, or rapidly undergoes hydrogen transfer (as indicated at the right of Figure 4-13) and abruptly eliminates water to form the product ion with m/z 59. The CID daughter ion mass spectrum of m/z 77 is shown in Figure 4-14A, and supports the validity of the proposed reaction mechanism. At low eV collision energy, some of the ions with m/z 77 expel water to form a daughter ion with m/z 59. However, at collision energies above 5 eV, no peak is observed at m/z 59. The "close encounter" adduct which leads to the covalent bound formation yielding the ion of m/z 59, may be interrupted before covalent bond formation can be accomplished, if the collision energy is greater than 5 eV. This kinetic energy should readily disrupt the electrostatic forces holding two of the four critical atoms together.

The majority of the ions with m/z 77 exist as the traditional proton-bound adduct of methanol and acetaldehyde as the dominant CID daughter ions (Figure 4-14A) are protonated methanol (m/z 33) or protonated acetaldehyde (m/z 45). Isotopic labeling studies helped clarify the reaction mechanism. With the introduction of ^{18}O-methanol and acetaldehyde in the ion source, the intermediate shifts to m/z 79. The CID daughter ion mass spectrum of the ion with m/z 79, shown in Figure 4-14B, indicates that this collision complex intermediate loses CH_3OH to give a peak at m/z 47 representing protonated ^{18}O acetaldehyde (pathway (ii) of Figure 4-13). The proton-bound adduct form of the intermediate still generates a daughter ion of m/z 45 upon CID as demonstrated in Figure 4-14B. After hydrogen transfer within the intermediate, the ion of m/z 79 may eliminate $H_2{}^{18}O$ upon

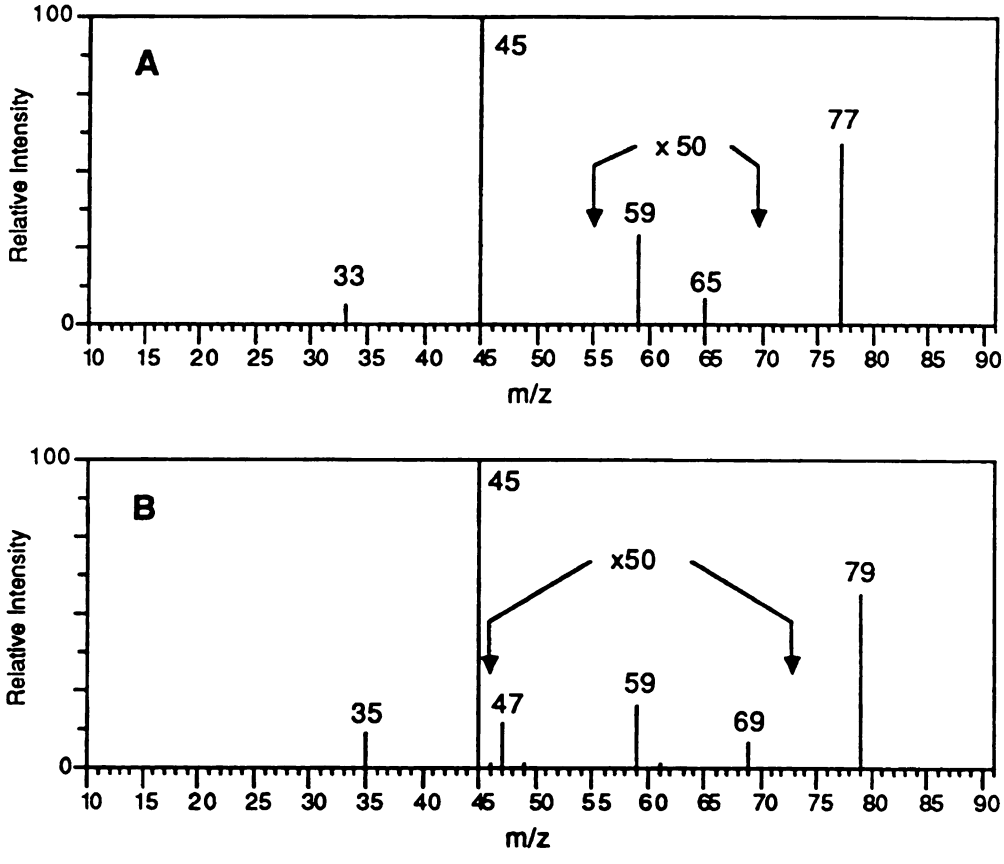

Figure 4-14: (A) CID (E_{Lab} = 4 eV) daughter ion mass spectrum of the adduct ion of m/z 77 formed by ion/molecule reactions occurring after methanol and acetaldehyde were placed in the high pressure ion source. (B) Daughter ion mass spectrum of m/z 79 formed when $CH_3{}^{18}OH$ and acetaldehyde were placed in the ion source.

CID to give the reaction product ion of m/z 59 (pathway (iii) of Figure 4-13). The peak at m/z 65 in Figure 4-14A appears to represent a proton-bound dimer of methanol due to leakage of methanol into the collision cell from the ion source. This is supported by the fact that the peak shifts to m/z 69 when ^{18}O-methanol is admitted into the ion source (Figure 4-14B). It is postulated that a molecular beam of methanol dimers (185,186) from the ion source enters the collision cell where it captures a proton from the intermediate of m/z 77 to form a protonated dimer of methanol.

A parent ion scan of m/z 59 was obtained following the introduction of acetaldehyde and methanol into the ion source, to determine if there were other intermediates which may account for the formation of the product ion of m/z 59. The results indicated the ion with m/z 59 arises not only from the intermediate of m/z 77, but from an intermediate with m/z 91; this second reaction sequence is illustrated in Figure 4-15. Ion/molecule reactions in methanol have been studied previously, and one of the ionic products is protonated dimethyl ether (173,187). Protonated dimethyl ether reacts with acetaldehyde to give a collision complex of m/z 91, some of which represents a protonated acetaldehyde dimethyl acetal intermediate. The CID daughter ion mass spectrum of m/z 91 at low-energy collisions with argon in the TQMS gives a daughter ion of m/z 59, which is accounted for by pathway (ii) or (iii) of Figure 4-15. When ^{18}O methanol is introduced into the ion source, the peak for the intermediate shifts to m/z 93. The CID daughter ion mass spectrum of m/z 93, shown in Figure 4-16, indicates fragment peaks at m/z 59 and m/z 61 in a 1:1 ratio. This corresponds to loss of $CH_3{}^{18}OH$ and CH_3OH, respectively, as would be expected statistically from the equivalent structures in equilibrium through proton transfer, as indicated in Figure 4-15. This daughter ion spectrum also shows a large peak at m/z 49 which represents

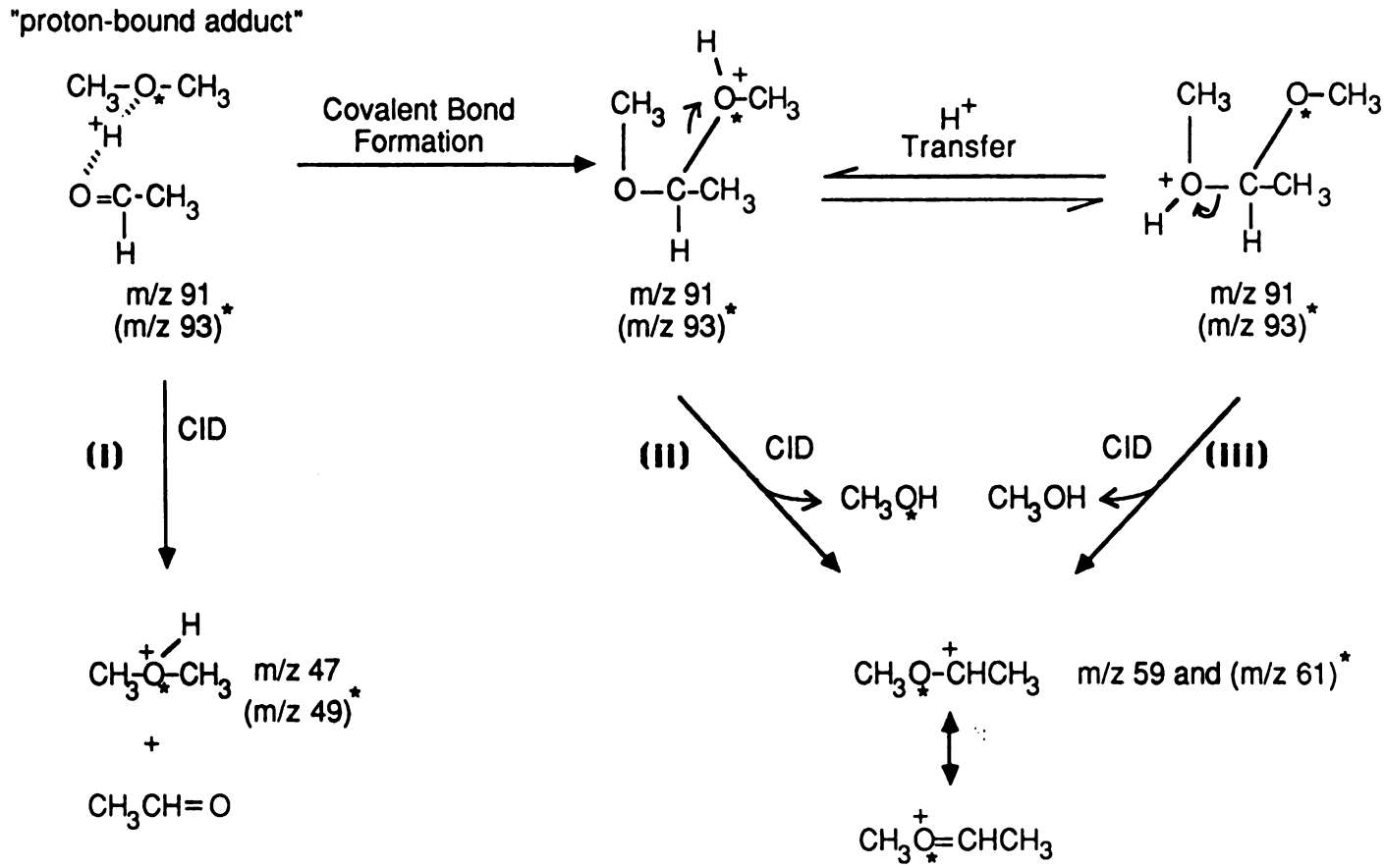

*indicates site of ^{18}O and corresponding m/z value in parentheses

Figure 4-15: Proposed mechanism for the formation of the ion of m/z 59 from the intermediate of m/z 91 following the ion/molecule reactions occurring in a mixture of methanol and acetaldehyde.

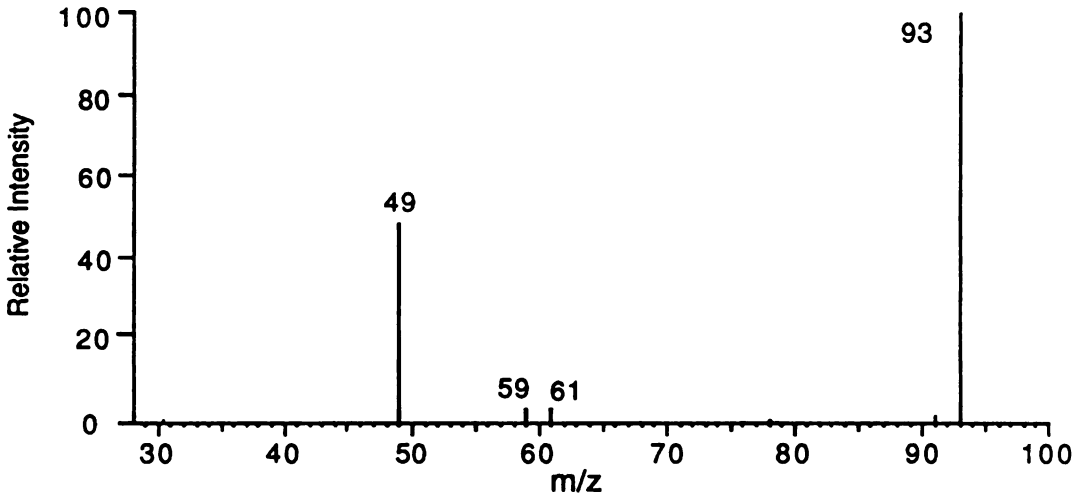

Figure 4-16: CID (E_{Lab} = 2 eV) daughter ion mass spectrum of m/z 93 formed by ion/molecule reaction occuring after acetaldehyde and ^{18}O methanol were introduced into the ion source.

the protonated ^{18}O-dimethyl ether. This daughter ion spectrum is consistent with the proposed mechanism. If the ion with m/z 93 only represented a proton-bound adduct consisting of m/z 59 (formed in source) and ^{18}O-methanol, then the daughter ion spectrum would lack a peak at m/z 61 representing the ^{18}O-labeled product ion. The presence of m/z 59 and m/z 61 is anticipated due to the H^+ transfer that can occur prior to the expulsion of methanol (or ^{18}O-methanol). When [$^2H_4$]-methanol is used, the intermediate of m/z 98 upon CID yields the product ion of m/z 62, which is consistent with the proposed mechanism.

b) Reactions of acetaldehyde and dimethyl ether

Some further experiments were performed in the continued effort to verify this mechanism accounting for the formation of the ion with m/z 59. Dimethyl ether and acetaldehyde were simultaneously introduced into the ion source at approximately equal pressures totalling ~0.6 mtorr to determine if the product ion (m/z 59) is detected in the mass spectrum. The mass spectrum of this mixture is shown in Figure 4-17. The peak at m/z 59 is observed in this spectrum, and again the mechanism shown in Figure 4-15 is postulated to account for its formation. The ion with m/z 91 could have two structures, the first resulting from ion/molecule reactions in dimethyl ether (188) (m/z 45 cluster to DME), and the second representing the protonated DME-acetaldehyde species. Before the CID daughter ion mass spectrum of the ion of m/z 91 was obtained with both DME and acetaldehyde in the ion source, the daughter ion mass spectrum of the ion with m/z 91 formed with DME only in the ion source was obtained. There were two fragment peaks detected, the major peak representing the oxonium ion with m/z 45 (DME-H)$^+$, and a peak at m/z 61 which represents the elimination of CH_2O.

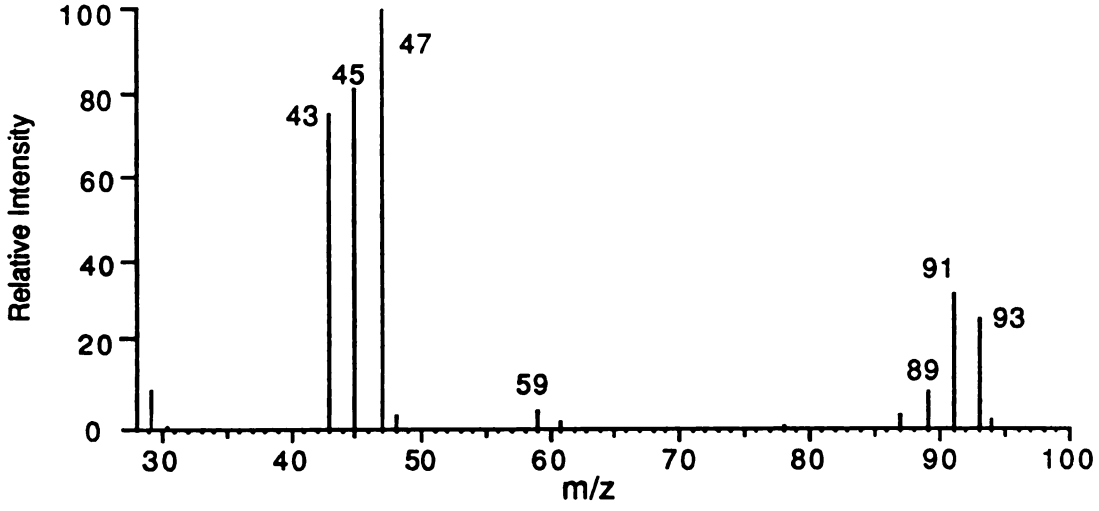

Figure 4-17: Partial reaction product spectrum of ions produced during ion/molecule reactions following EI of acetaldehyde and dimethyl ether in a high pressure ion source.

Following this experiment, the daughter ion mass spectrum of the ion with m/z 91 was obtained when DME and acetaldehyde were mixed in the source. Not only were peaks detected at m/z 45 and m/z 61, but peaks were observed at m/z 59 and m/z 47. The ion of m/z 59 has the structure shown in Figure 4-12, and m/z 47 represents protonated dimethyl ether. Based on these additional experiments it seems likely that the ion/molecule reaction mechanism postulated in Figure 4-15 accounts for at least some of the formation of the covalently bound product ion of m/z 59.

c) Reaction of benzaldehyde and dimethyl ether

The results described above indicate that O-alkylation is occurring in the reaction of protonated acetaldehyde with methanol (and protonated DME with acetaldehyde). For all the reactions described, the molecular weights of the compounds were similar, which can make it difficult to determine the reactant species in the formation of higher-mass product ions. Product ions may represent a mixture of ionic structures. A system where the difference in molecular weights of the reactant species is great may facilitate determining the reactants involved in formation of product ions as the possibility of different ionic structures of identical mass is reduced. This led to the investigation of benzaldehyde and dimethyl ether. Would an O-alkylated product ion be observed in the ion/molecule reactions occurring in mixtures of these components? Initially, benzaldehyde and dimethyl ether were mixed in the ion source, and the reaction product mass spectrum was obtained. This spectrum (with the self-CI peaks from DME subtracted) is shown in Figure 4-18. Of interest is the peak at m/z 121 which represents [(benzaldehyde-DME)H - CH_3OH]$^+$. The CID daughter ion mass spectrum of the ion of m/z 153 was obtained to determine if this ion, representing the

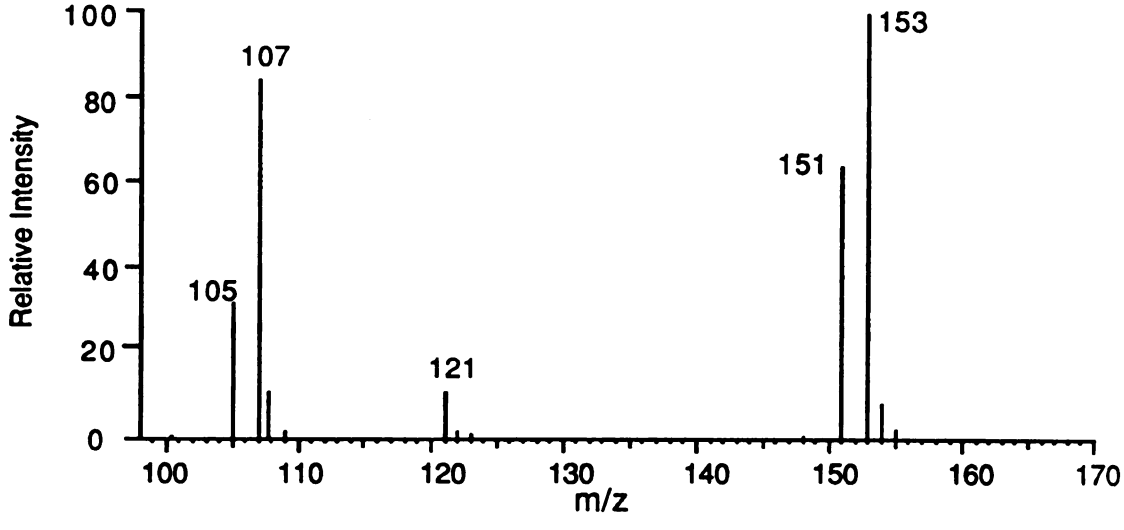

Figure 4-18: Partial reaction product spectrum of ions produced during ion/molecule reactions following EI of benzaldehyde and dimethyl ether in a high pressure ion source. Peaks produced from self-CI of dimethyl ether were subracted.

protonated collision-complex, is the intermediate in the formation of the ion of m/z 121. Following CID of m/z 153, no ion current was detected at m/z 121, only at m/z 107 which represents protonated benzaldehyde, formed by elimination of dimethyl ether. The parent ion mass spectrum of the product ion of m/z 121 showed that the precursor is the ion with m/z 151. A proposed reaction mechanism is shown in Figure 4-19. It would be necessary to perform stable isotope labeling studies to determine the source of the oxygen and CH_3 in the acetal product ion having m/z 121. The mechanism shown in Figure 4-19 suggests that the methoxy groups prior to the elimination of methanol are identical, yet this would need to be confirmed experimentally.

d) Ion trapping

Over the course of the studies involving the ion/molecule reaction of protonated acetaldehyde and methanol, an attempt was made to implement the ion/trapping technique of Dolnikowski *et al.* (72,106). If a large voltage is applied to the Q_2 exit lens, the lens may function as a gate and trap reactant ions in the collision chamber in the presence of the neutral reagent. This provides more time for the ion to react with the neutral vapors in Q_2. After trapping the ions for a designated amount of time (usually milliseconds), the ions in the collision chamber can be pulsed out by applying a large negative potential to the Q_2 exit lens. This serves to extract the ionic reaction products from the collision chamber, and may provide greater detectability for some ion/molecule reaction product ions. This technique was implemented on the Extrel TQMS, and was called the trap and pulse method (72,106). If the parent ions are admitted into Q_2 for a designated period of time, and the entrance lens to Q_2 is then gated with a large potential so that no more parent ions may enter, the phrase "inject, trap and pulse" is used.

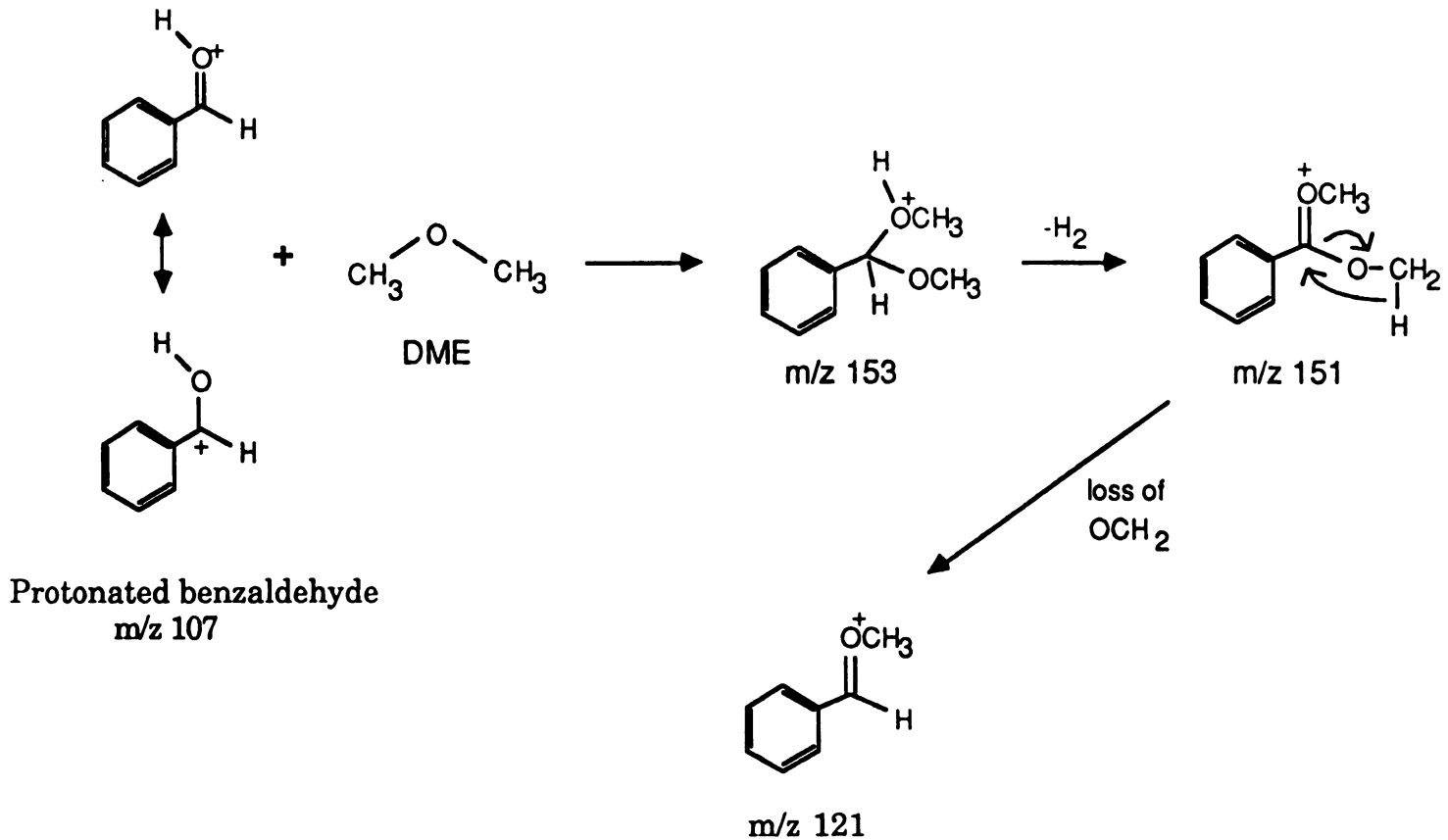

Figure 4-19: Proposed mechanism for the formation of the ion of m/z 121 following ion/molecule reactions in mixture of benzaldehyde and dimethyl ether.

The trap and pulse method admits parent ions continuously; only the voltage on the exit lens following Q_2 is varied. In the inject, trap and pulse method, only a discrete packet of ions is admitted into the collision cell (72,106). After the ions are introduced into the reaction region, the Q_2 exit lens performs the ion containment and ion extraction functions. A similar approach was used by Beaugrand and coworkers on a penta-quadrupole instrument which provided access to kinetic and thermodynamic parameters in ion/molecule reactions (189).

The ion/trapping technique did not prove to be very fruitful on the TSQ-70. The Finnigan instrument requires that at least one of the two mass-analyzing quadrupoles be in a scan mode; that is, each quad cannot be set to pass one fixed mass. This eliminates the possibility of monitoring ion current in real time as it is always necessary to implement a mass scan to obtain the data. In the attempt to overcome this difficulty, extremely fast scans were used over a narrow mass window. The first quadrupole was allowed to scan over a narrow mass range (0.4 u) which served to introduce the reactant ion into the reaction chamber, while Q_3 passed ion current at one fixed mass value. A diagram of the instrument is shown in Figure 4-20 which also summarizes how the inject, trap and pulse technique was attempted on the TSQ-70. The user output voltage was connected to lens 2-3 to provide better control of this voltage, and enable it to be adjusted quickly. A procedure was written as shown in Table 4-1, which would allow adjustment of the user output voltage and lens 3-1 voltage for altering the potential applied to the Q_2 entrance and exit lenses. The number of scans multiplied by the scan rate (scan rate is 0.001 sec/scan), will determine the approximate length of time for the filling of the collision cell. During the filling time, the Q_2 exit lens voltage was 100 volts; no positive ions could leave Q_2 at this voltage. After

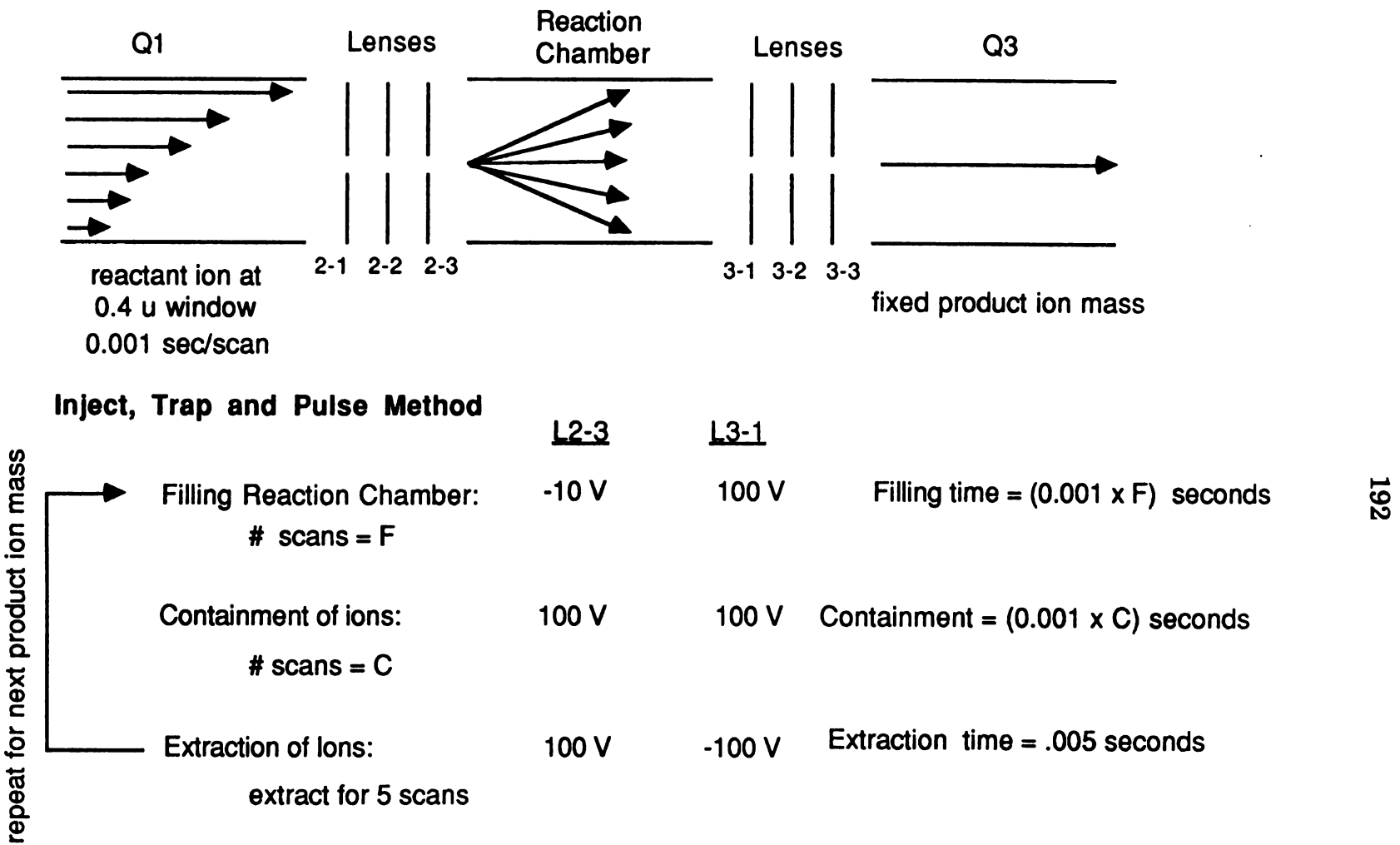

Figure 4-20: Implementation of inject, trap and pulse methodology on TSQ-70.

Table 4-1: Procedure used to implement inject, trap and pulse on the TSQ-70 triple quadrupole mass spectrometer.

```
N=9
PAR N, 44.8,45.2,.001      ! Sets parent ion scan, so Q3 mass is fixed at m/z N.
                             Q1 is scanned from 44.8 to 45.2 u at 0.001 sec/scan
                             to introduce reactant ion (m/z 45) into Q2.

REPEAT 80

  N=N+1;PAR N              !Selection of fixed product ion (Q3) mass.
  U01=-5;L23=-10           !User output connected to L31 and will cause L31 to
                             be +100 V

    REPEAT 50
      GO;STOP              ! Fill reaction chamber for 50 scans of Q1.
    END

L23=100
C=5
REPEAT C                   ! Containment in reaction chamber for 5 scans.
  GO
  STOP
END

UO1=5                      ! L23 set to -100 V to extract the ions from Q2

REPEAT 5
  GO;STOP                  ! Collect 5 scans of data (ions detected)
END

END                        ! Repeats cycle 80 times so product ion mass
                         Mass spectrum from m/z 10 to m/z 90 is obtained

UO1=0.5;L23=-10            ! Sets L1-3 and L3-1 to typical values.

ASTOP                      ! End of procedure.
```

the entrance gate is 'closed', the number of scans times the scan time defines the confinement time for the inject, trap, and pulse method. Following the confinement, the Q_2 exit lens is biased with -100 volts, and the ion current at the fixed m/z value is monitored for 5 scans (0.005 seconds). Generally, ion current was detected only for the first two scans. This whole procedure is repeated for the entire product ion mass range of interest.

The procedure was attempted when protonated acetaldehyde was selected to react with methanol in the collision cell. The reconstructed mass chromatogram could essentially be interpreted as a mass spectrum, as each mass scan represents the ion current detected at a fixed mass when Q_1 is scanning over essentially one m/z value. Most of the scans are obtained during the filling time or containment time; no ion current is detected during this time. When the exit lens to Q_2 is pulsed, it is expected that ion current would be detected for at least one scan or as long as it takes the ions to reach the detector. The product ion mass spectrum for reaction of protonated acetaldehyde and methanol for the inject, trap and pulse method is shown in Figure 4-21 for a filling time of 50 milliseconds (50 scans 1 msec/scan). After filling the chamber for 50 milliseconds, the entrance lens was gated so no more parent ions could enter and, immediately, the exit lens was pulsed to extract the ions in the collision cell with the data collected for 5 scans. This was repeated for each mass to obtain the product ion mass spectrum. The TIC chromatogram shows 'peaks' at m/z 45, m/z 47 and m/z 59 representing the parent ion, protonated dimethyl ether, and the product ion, respectively. If the same procedure is followed, but with ion confinement for 5 milliseconds following admittance of the reactant ion into the collision chamber, the product ion mass spectrum shown in Figure 4-22 is obtained. This spectrum shows an increase in the product ions (m/z 47 and m/z 59) as compared to

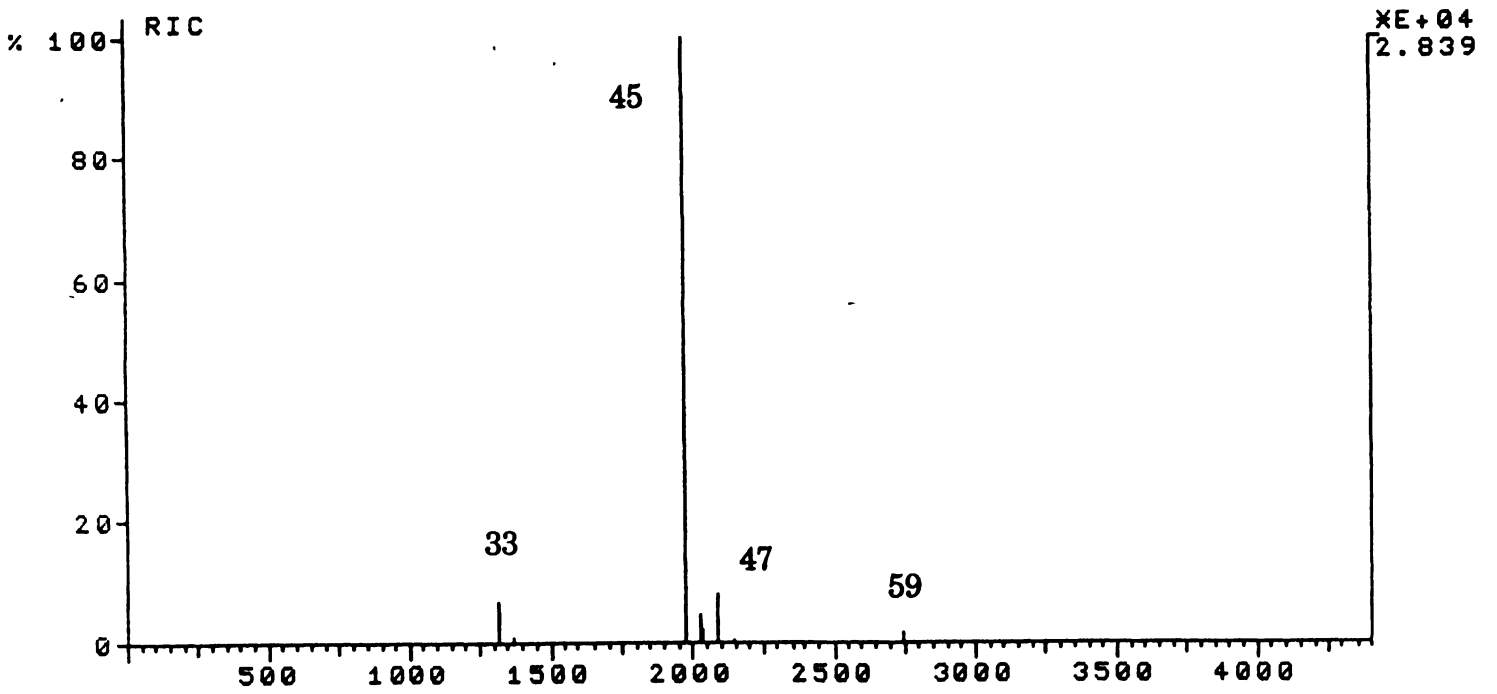

Figure 4-21: Product ion mass spectrum obtained when the inject, trap and pulse method was implemented on the TSQ-70. The collision cell, containing methanol vapors, was filled for 50 msec with protonated acetaldehyde. Immediately after L23 was gated, the ions were extracted by L31.

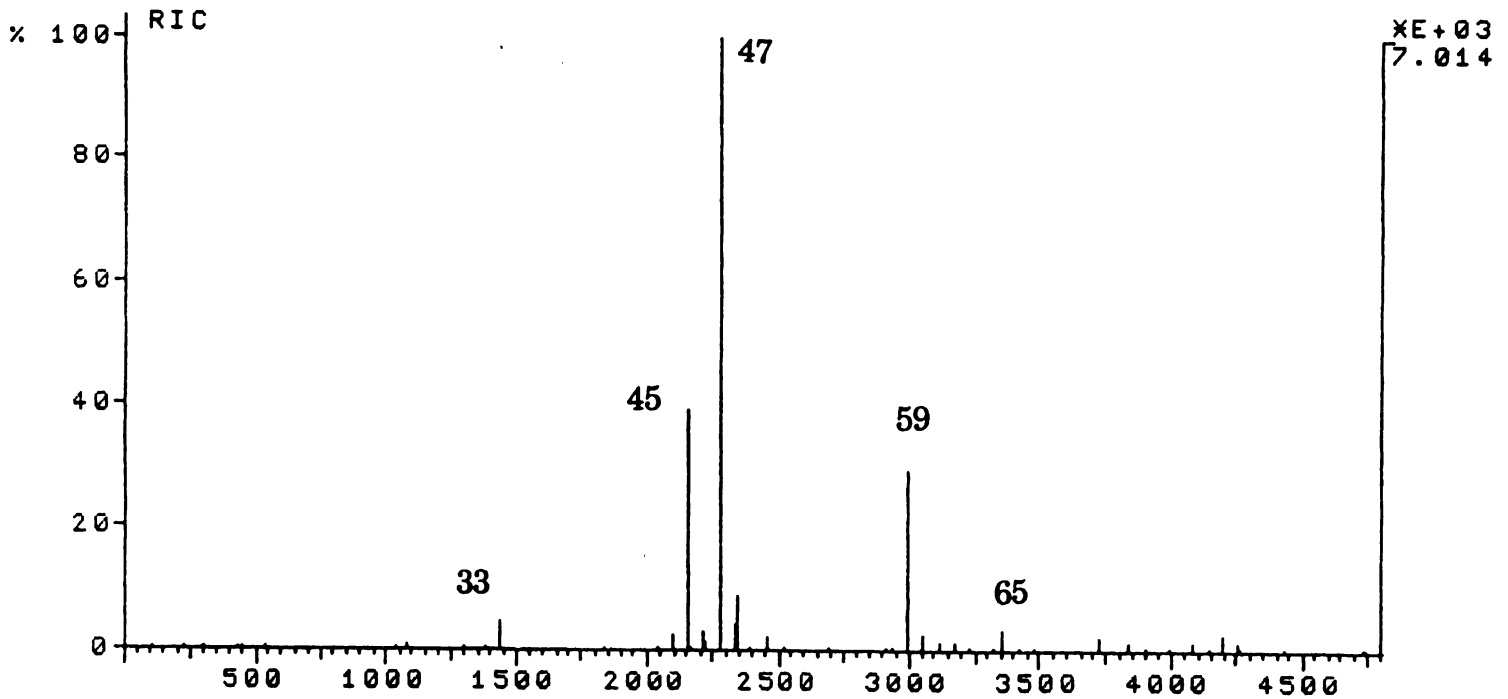

Figure 4-22: Product ion mass spectrum obtained when the inject, trap and pulse method was implemented on the TSQ-70. The collision cell, containing methanol vapors, was filled for 50 msec with protonated acetaldehyde. Ions were extracted after a containment period of 5 msec.

when no confinement is used. In both experiments, the methanol pressure in Q_2 was 0.5 mtorr and the collision energy was 1 eV. Although the signal-to-background appears to have improved when there is ion confinement, the total current detected is quite low indicating that the procedure does not contain or extract ions very efficiently. The ion current detected for a steady state signal (no trapping procedures) is on the order of 1000 times greater than the signal detected implementing the trap and pulse method. Over the course of the research, the author did not have difficulty in detecting ionic products following ion/molecule reactions in Q_2, therefore, the trap and pulse methodology was not pursued any further. Much work needs to be done before one may accurately assess the feasibility of performing ion-confinement experiments in the Finnigan TSQ-70.

4. *Summary*

The results of this study provide direct evidence by CID mass spectrometry for O-alkylation in the gas phase reaction between protonated acetaldehyde and methanol (156). A second reaction mechanism was elucidated involving protonated dimethyl ether and acetaldehyde. Some additional experiments were performed suggesting that ion/molecule reactions of dimethyl ether and aldehydes result in O-alkylation of the aldehyde. Perhaps O-alkylation is a general phenomena for reactions of aldehydes and ethers in the gas phase, yet further experiments need to be done to verify this claim. The trap and pulse methodology was difficult to implement on the TSQ and at this time it is not known whether it would provide advantages in detection of product ions as compared to the conventional 'steady state' approach.

D. Reactions of protonated alcohols and ethyl acetate

Condensation reactions involving protonated esters and alcohols have been studied in the gas-phase by other researchers (106,190). It had been shown by Dolnikowski that the product ion mass spectrum of protonated ethyl acetate and propanol in the collision cell of a TQMS shows peaks at m/z 131 and m/z 149. These peaks also were observed when protonated propanol was reacted with ethyl acetate. The ion with m/z 149 represents the proton-bound adduct of ethyl acetate and propanol, whereas the ion with m/z 131 represents the dehydration product ion. Similar dehydration ion/molecule reactions involving esters and alcohols also have been reported from studies with an ICR instrument (190). This brief section describes a few additional experiments where the product ion, formed via a condensation reaction, was made in the ion source and selected for CID.

1. *Experimental*

All experiments were performed on the Finnigan TSQ-70 triple quadrupole mass spectrometer. A direct inlet was constructed which was used to introduce vapors of one of the neutral compounds (the alcohol) into the high pressure CI ion source. Vapor from the second reagent (ethyl acetate) was introduced via the CI gas lines. This allowed mixture of the vapors to occur in the ion source for ionization by EI. It also provided some control over the partial pressures of the individual components. A mass spectrum was generated which showed peaks representing ion/molecule reactions involving both reagents. For the CID studies, the ion formed from

dehydration of the proton-bound collision complex, was selected for CID with argon introduced into the collision cell at a pressure of 0.6 mtorr and a collision energy of 20 eV_{Lab}.

2. *Results and discussion*

The ion/molecule reaction between protonated ethyl acetate and propanol has been studied previously in an ICR instrument (190) and in a TQMS (95). In the TQMS study, the CID daughter ion mass spectrum of the ion with m/z 131, which represents [(Propanol•ethyl acetate)H^+ - H_2O]$^+$, showed elimination of 60 u ($CH_3CH_2CH_2OH$). This result led to the suggestion that the product ion has the structure of an acetal ion as shown in Figure 4-23, as loss of propanol may be envisioned from this ionic structure (106).

One of the difficulties in studying this reaction is that ion/molecule reactions in ethyl acetate produce an ion of m/z 131 with structure shown in Figure 4-24. This ion is identical in mass to that of the reaction involving propanol and ethyl acetate, and this fact needs to be considered while evaluating the CID results. Both ionic structures are likely to be formed in the ethyl acetate-alcohol mixture. The CID daughter ion mass spectrum of m/z 131 produced when only ethyl acetate was in the ion source lacks the fragment peak at m/z 71 which represents loss of ($CH_3CH_2CH_2OH$). In the effort to clarify the ion/molecule reaction mechanism, deuterated analogues of the ethyl ester, including $^2H_5$-ethyl acetate ($C_2{}^2H_5COOCH_3$) and $^2H_3$-ethyl acetate ($C_2H_5COOC^2H_3$) were reacted with propanol. When the deuterated analogues of ethyl acetate were introduced into the ion source along with propanol, in all cases, a peak was detected in the mass spectrum which

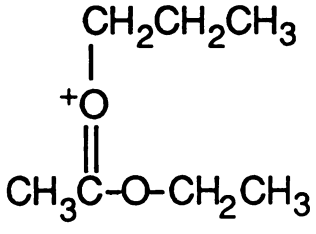

$C_7H_{15}O_2^+$

acetal ion

Figure 4-23: Acetal ion formed in reaction of protonated propanol and ethyl acetate.

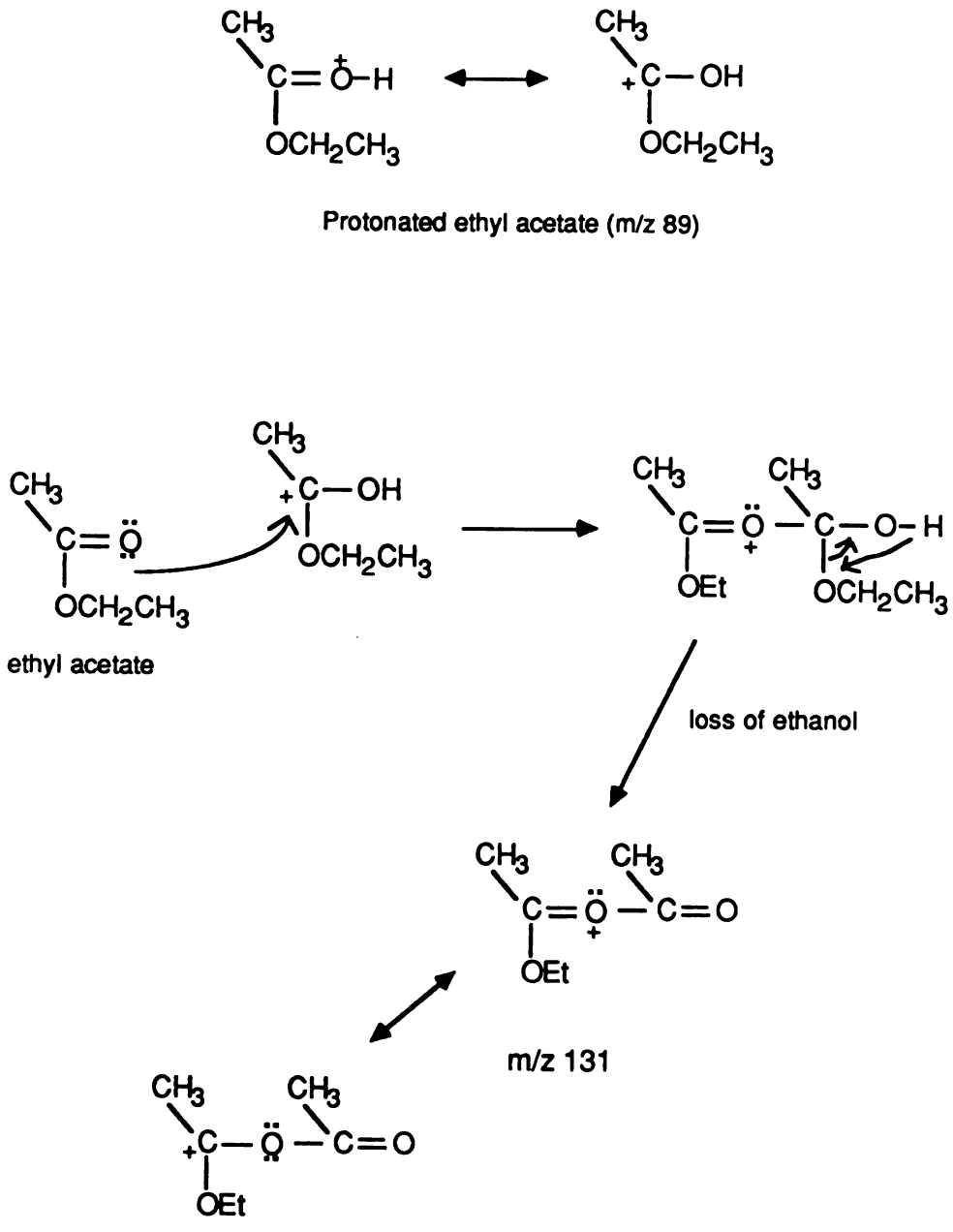

Figure 4-24: Ion/molecule reaction of protonated ethyl acetate with ethyl acetate to form the product ion of m/z 131.

represented the addition of 43 u ($C_3H_7^+$) to ethyl acetate. It can only be presumed that this represents the ion formed in the reaction of protonated ethyl acetate and propanol, followed by loss of water. The CID daughter ion mass spectrum of the ion of m/z 134 formed when $^2H_3$-ethyl acetate and propanol are mixed in the ion source is shown in Figure 4-25. With $^2H_3$-ethyl acetate, the self-CI peak shifts to m/z 136, eliminating the interference from the ethyl acetate ion. Once again, the daughter ion spectrum of the dehydration product ion shows a peak at m/z 76 which is from the loss of propanol. Based on the structure of the acetal ion (Figure 4-23), it might be expected that ethanol could be eliminated as well. However, the daughter ion mass spectrum which lacks a peak representing loss of ethanol suggests that this process does not take place. Other peaks detected in the CID of m/z 134 include: m/z 92 which represents protonated ethyl acetate formed by the loss of the C_3H_6 olefin, m/z 64 which is protonated acetic acid (with three ^2H atoms), and m/z 43 which is the $C_3H_7^+$ cation.

Butanol was also simultaneously introduced with ethyl acetate into the ion source and the anticipated acetal ion was detected as a peak at m/z 145. The CID daughter ion mass spectrum of the product ion of m/z 145 is shown in Figure 4-26. The dominant fragmentations include elimination of C_4H_8 and loss of butanol. Once again, the daughter ion spectrum does not show a peak which would indicate that the acetal ion may eliminate ethanol.

Finally, ethyl acetate and ethanol were mixed in the ion source, and the product ion representing the addition of $C_2H_5^+$ to ethyl acetate with m/z 117 was selected for CID. The acetal product ion can eliminate C_2H_4 to give a peak at m/z 89, or ethanol forming an ion with m/z 71. Labeling studies with $CH_3O_2C_2{}^2H_5$ indicate that the product ion, shifted to m/z 122, eliminates both C_2H_4 and $C_2{}^2H_4$ as seen in the CID spectrum shown in

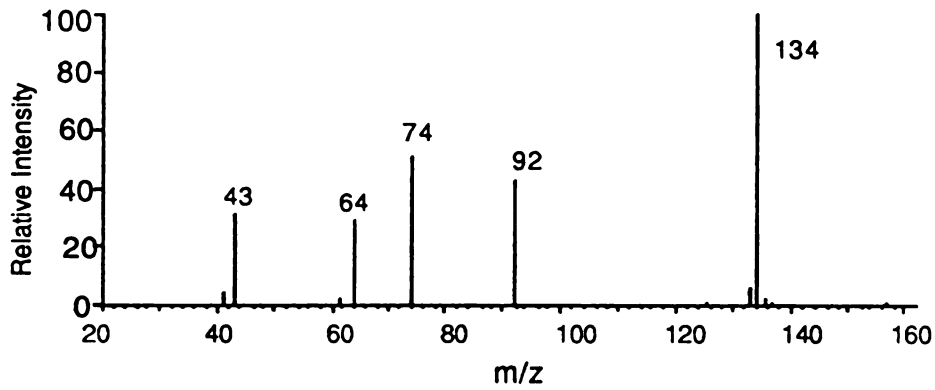

Figure 4-25 : CID daughter ion mass spectrum of the ion of m/z 134 formed when propanol and $C^2H_3COOC_2H_5$ are introduced into the ion source.

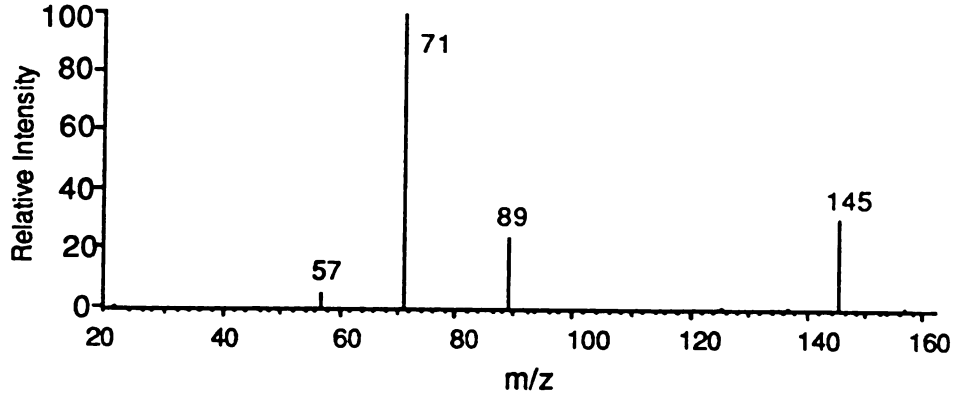

Figure 4-26: CID daughter ion mass spectrum of the product ion of m/z 145 formed when ethyl acetate and butanol are introduced into the ion source.

Figure 4-27. The ratio of m/z 94 (loss of C_2H_4) to m/z 90 (loss of $C_2{}^2H_4$) from the acetal ion is 2.1 : 1. This can be attributed to an isotope effect favoring H transfer over ^2H transfer (191). In high energy CA studies, Harrison obtained a ratio of 2.3 : 1 for the losses of C_2H_4 and $C_2{}^2H_4$ from ion with m/z 122 formed in the reaction of $C_2{}^2H_5{}^+$ with ethyl acetate (191).

A general scheme for the fragmentation mechanism of the acetal ion is shown in Figure 4-28. The acetal ion may eliminate the larger alcohol moiety and the larger olefin. It should be noted that for both primary alcohols and olefins, the heat of formation for the neutral species decreases with increasing chain length, so the acetal ion preferentially eliminates the most stable neutral. For example, the acetal ion of m/z 131 formed in reaction of protonated propanol and ethyl acetate can eliminate C_3H_6 to form protonated ethyl acetate (Figure 4-25); it does not eliminate C_2H_4 to form protonated propyl acetate. The difference in heat of formation for C_3H_6 (ΔH_f =20.2 kJ/mol) and C_2H_4 (ΔH_f = 52.2 kJ/mol) is 32 kJ/mol, whereas the difference is only 6kJ/mol between protonated ethyl acetate (ΔH_f = 247kJ/mol) and protonated propyl acetate ((ΔH_f =241 kJ/mol). Therefore, loss of the larger olefin is thermodynamically favored, and this same trend holds for elimination of the alcohol moiety. In the reaction involving ethyl acetate and ethanol, the alkoxy groups within the ion are identical, so that both groups are included in the fragmentation process.

These CID studies lend support to the structure of the product ion involving reaction of alcohols and ethyl acetate being an acetal ion. It has been suggested that this reaction mechanism involves the formation of a collision-complex, followed by elimination of water. However, these studies described do not provide definitive information on the reaction mechanism forming the acetal ion. The results only support the premise that the product

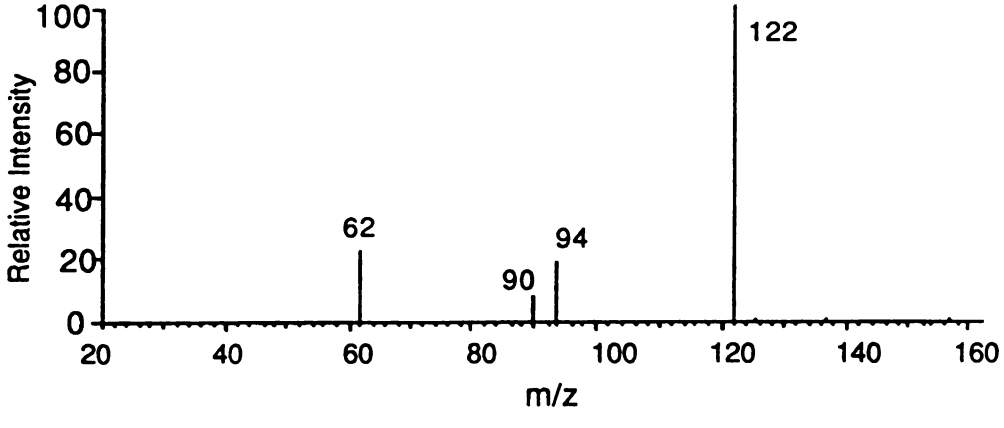

Figure 4-27: CID daughter ion mass spectrum of the ion of m/z 122 formed when $CH_3COOC_2{}^2H_5$ and ethanol are introduced into the ion source.

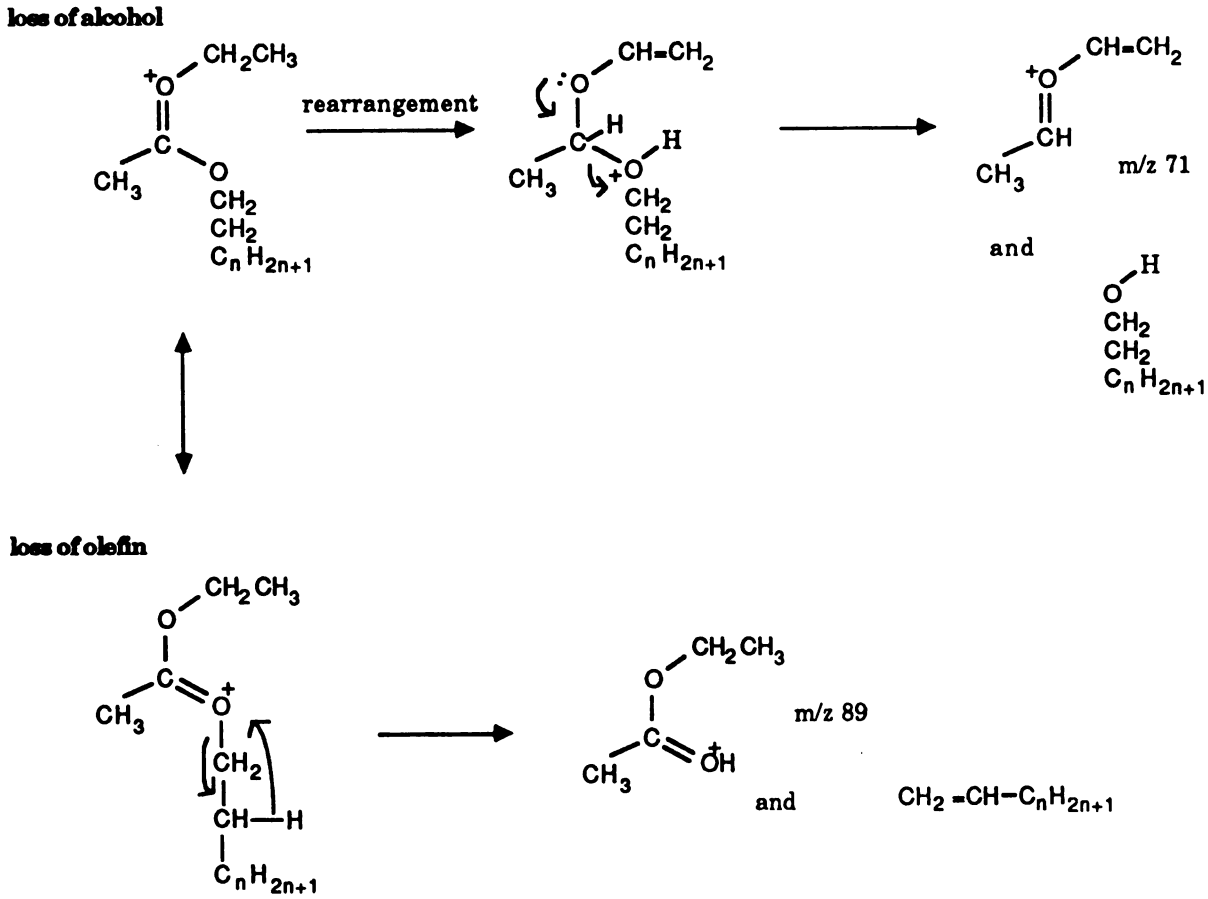

Figure 4-28: General scheme showing the elimination of an alcohol or olefin molecule from the acetal ion formed in ion/molecule reactions of alcohols and ethyl acetate.

ion has the acetal structure. A few product ion mass spectra were obtained for reaction of protonated propanol and esters in Q_2. The esters which where introduced into the collision cell included ethyl acetate, methyl acetate, and methyl propionate. In these product ion mass spectra obtained at low collision energy (1 eV_{Lab}), peaks were detected representing loss of H_2O from the proton-bound adduct. However, in all cases, a prominent peak was also detected at m/z 43 ($C_3H_7^+$) which is a CID fragment ion (loss of H_2O) from protonated propanol. At the high Q_2 pressures, multiple collisions occur. Second order reactions involving the $C_3H_7^+$ ion and the neutral ester may account for the formation of the acetal product ion. It may be that alkyl attachment to the carbonyl oxygen of the ester is the reaction occurring and not a condensation reaction. Furthermore, in CID studies of the various (ester-alcohol)H^+ complexes formed in the ion source, elimination of H_2O was not observed. It is clear from the TQMS studies where the neutral and ionized reactants were isolated, a product ion corresponding to dehydration of the original protonated collision-complex is formed, however, the author believes that many more detailed studies need to be carried out before the mechanism is unraveled.

E. Ion/molecule reactions of protonated molecules and hexamethyldisilazane

There are many analytical tests to determine the functional groups present in an organic molecule in solution (192). Most of them use a specific reagent such as 2,4-phenylhydrazine for detecting ketones. It would be useful to extend this strategy to characterize gas phase ionic species. Preliminary experimental results performed on the penta-quadrupole mass

spectrometer in Paris involving ion/molecule reactions of protonated molecules and hexamethyldisilazane (HMDS) suggested that a silicon-hydrogen exchange reaction was selective for the amino group as is shown in Figure 4-29. When protonated amines were reacted with HMDS, a product ion was observed which represented the addition of 72 u. Silylation was occurring in the gas-phase. Protonated alcohols and protonated ketones did not appear to undergo the silicon exchange reaction. These preliminary experiments were carried out by Dr. J.T. Watson while he was on sabbatical in France.

$$RNH_3^+ + (CH_3)_3SiNHSi(CH_3)_3 \text{ -----> } RNH_2Si(CH_3)_3^+ \quad (CH_3)_3SiNH_2$$

Figure 4-29: Proposed reaction of protonated amines with HMDS.

In January 1989, Dr. Christian Rolando from Ecole Normale Superieure, Paris France, visited the Mass Spectrometry Facility. Dr. Watson and Dr. Rolando were the researchers who initially studied this ion/molecule reaction on the penta-quadrupole mass spectrometer. While Dr. Rolando was visiting Michigan State, some experiments were performed to determine if the results obtained on the penta-quadrupole mass spectrometer which had ion-confinement capabilities, could be reproduced on the Finnigan TSQ-70 instrument. A few experiments were carried out where protonated molecules were chosen for reaction with HMDS, and this section describes some of the results.

1. *Experimental*

All experiments were performed on the Finnigan TSQ-70 mass spectrometer. Hexamethyldisilazane (HMDS), a liquid at STP, was introduced into a glass reservoir which was connected to the CID gas lines. The needle valve was adjusted so that the pressure in the collision cell was approximately 3 mtorr. Liquid samples which were chosen for reaction with HMDS were introduced via the glass reservoir directly into the ion source. The pressure in the ion source was adjusted so that the base peak in the mass spectrum was the protonated molecule. Solid samples were introduced by the direct insertion probe. Later in the studies, a few small peptides were placed on the probe tip in a droplet of glycerol, and ionized by fast atom bombardment (FAB). In all the experiments the protonated molecule was selected as the reactant ion and introduced into the collision cell with a collision energy ranging from 1-4 eV_{Lab}. For each reaction, the collision energy was adjusted to provide optimal detection of a reaction products, either the silylation product ion or the ion with m/z 162 which represents protonated HMDS.

2. *Results and discussion*

The preliminary results obtained in France suggested that the derivatization reaction involving HMDS was selective for protonated amines. The first compound chosen for investigation was aniline, with a molecular weight of 93. When protonated aniline was reacted with HMDS, two major peaks were detected in the product ion mass spectrum. The first peak was at m/z 162 which represents protonated HMDS. The second peak was at m/z

166, which represents the net addition of 72 u. A trimethyl silyl group was exchanged with a hydrogen atom to form the product ion and $(CH_3)_3SiNH_2$. Ion confinement was not necessary for detection of the product ion peaks representing the silylation ion/molecule reaction.

Next, acetone was introduced into the ion source, and protonated acetone with m/z 59 was chosen for reaction with HMDS. This reaction was attempted in France, and the silylation reaction was not observed. However, on the Finnigan TSQ-70, the reaction was observed to occur quite readily as can be seen by the product ion mass spectrum shown in Figure 4-30. A few other protonated ketones, including cyclohexanone and 4-heptanone were selected to react with HMDS, and all gave a product peak which represented the net addition of 72 u

Table 4-2 lists the compounds that were investigated and indicates those for which a successful reaction was observed. In all cases, the intensity of the product ion was low, yet the distinctive isotopic pattern of silicon indicated that the peak was not just noise. Although not much is known about the ion/molecule reaction mechanism, a few points may be made from the experimental results. Protonated leucine was one of the compounds analyzed, and it reacted with HMDS to give a product ion with m/z 204. When ^{15}N -leucine is protonated, the protonated molecule also yields a product ion representing the addition of 72 u. This result indicates that the amino nitrogen remains in the product ion; it is not replaced by the nitrogen from the neutral reagent. Although our results conflict with those obtained on the penta-quadrupole, indicating that this ion/molecule reaction is not selective for amines, this reaction is worth pursuing further and suggests that gas-phase derivatization may be performed in the collision cell of a TQMS.

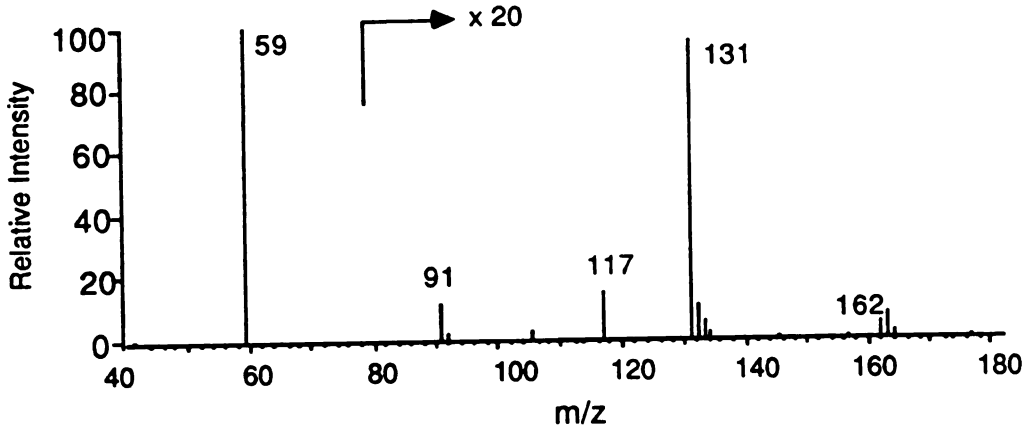

Figure 4-30: Product ion mass spectrum following ion/molecule reactions of protonated acetone (m/z 59) with HMDS at a pressure of 3 mtorr and a collision energy of 1 eV_{Lab}.

Table 4-2: Protonated compounds which were reacted with HMDS in the collision cell of the TQMS.

Compound	m/z of MH^+	Dectection of peak at $(MH+72)^+$
aniline	94	yes
N,N, dimethyl aniline	122	no
L-leucine	132	yes
isoleucine	132	yes
β- alanine	90	?
L-tryptophan	205	yes
6-aminohexanol	118	yes
glycyl L-isoleucine	189	yes
alanyl leucylglycine	260	yes
L-tryptophyl L-alanine	276	yes
acetone	59	yes
cyclohexanone	99	yes
4-heptanone	115	yes

? *Product ion peak would be at m/z 162 which also may represent protonated HMDS.*

The fact that reaction products are observed for some protonated molecules with HMDS, suggest that those reactions are exothermic. If excess energy is generated during the formation of the product ion, this energy may be redistributed among the bonds within the product ion. Given sufficient energy, bond fragmentation could take place. It would be worthwhile to continue the investigation of ion/molecule reactions with hexamethyldisilazane. A major thrust in mass spectrometry is peptide sequencing (193). Protonation of peptides occurs at the basic amino terminus. The results suggest that the protonated peptide may be able to undergo the derivatization reaction in the gas-phase. Perhaps reaction-induced fragmentation may occur, thereby provided a novel system for analysis of peptides.

CHAPTER V

SUMMARY AND FUTURE WORK

This dissertation describes gas-phase ion/molecule chemistry studied by triple quadrupole mass spectrometry. The principal theme is pursuit of developing analytical methodology based on selective gas-phase ion/molecule chemistry. Two reactive regions are available with the TQMS, the ion source and the second quadrupole collision chamber. The collision chamber provides a region where the ionic and neutral species may react in an isolated environment. On the other hand, ion/molecule reactions may occur in the ion source with the ionic products being selected for conventional MS/MS analysis using CID. Over the course of this research, both methods were utilized providing complementary information. Throughout this research, thermochemistry was examined along with experimental results obtained with the TQMS, in the attempt to clarify the gas-phase chemistry.

The gas-phase chemistry of aryl cations with nucleophilic reagents was investigated by TQMS. These studies led to the development of new methodology for distinguishing $C_7H_7^+$ isomers. Of the three isomers investigated, the tolyl, benzyl, and tropylium cations, only the tolyl cation undergoes a ring addition reaction with methanol or dimethyl ether. The benzyl and tropylium isomers do not undergo this reaction. Examination of the thermochemistry revealed that in the reaction with dimethyl ether, methoxylation of $C_7H_7^+$ is exothermic for the tolyl cation, but endothermic with benzyl or tropylium. The results suggest that quantitation of the tolyl cation in $C_7H_7^+$ mixtures may be possible using this low-energy analytical approach. Future efforts in this area should focus on continuing to search for

ion/molecule reactions which may be selective for either the benzyl cation or tropylium cation. Gas-phase ion/molecule studies using ICR instruments have previously demonstrated the reactivity of the benzyl cation. In order for a reagent molecule to be reactive with the benzyl cation, but not with the tolyl cation, the stability of the reaction products must overcome the 157 kJ/mol difference in the ΔH_f of the tolyl and benzyl reactants. If such a reaction is found and the reaction enthalpy with the benzyl cation is exothermic, but endothermic for the tolyl cation, then perhaps this ion/molecule reaction could be accomplished in the center quadrupole of a TQMS. This may enable complete quantification of $C_7H_7^+$ mixtures to be made by the low-energy ion/molecule reaction approach.

Not only have the studies involving aryl cations led to a method for selectively detecting the tolyl cation, but the results suggest that methods could be developed for rapidly screening aromatics in mixtures. The preliminary results indicate that only aromatic ions with a vacant charged site on the ring react with dimethyl ether to give the methoxylation product ion. By utilizing a neutral gain scan mode in a GC/MS/MS analysis, it may be possible to selectively detect those compounds in a complex mixture which are aromatic. This was demonstrated for a simple five-component mixture, but it would be necessary to analyze a more complex mixture to determine the utility of this approach for rapidly screening aromatics.

The results of other studies indicate that molecular oxygen is involved in some of the major fragmentation processes of molecular anions of methylated abscisic acid (ABA-Me). It is proposed that O_2 attacks at the radical site, forming a peroxy anion intermediate. This intermediate anion readily decomposes yielding predominant fragment ions. Molecular anions of structurally similar ABA metabolites also were shown to undergo an

analogous reaction with molecular oxygen. These results are unprecedented in that they represent the first case using a TQMS where a non-aromatic radical anion reacts with molecular oxygen, promoting fragmentation. The ions formed in this process enable the site of oxygen isotope enrichment to be precisely located within the molecule, an observation which has provided invaluable insight into the mechanism of biosynthesis of these compounds.

Electron capture negative ionization mass spectrometry is a rapidly expanding field, yet not much attention has been devoted to the study of ion/molecule reactions of anions. Flowing afterglow studies have shown that anionic conjugated dienes undergo reactions with molecular oxygen to form enolate anions. The reaction of 2,4 hexadiene with O_2 was examined with the triple quadrupole mass spectrometer, and the ionic products detected are thought to represent enolate ions. It would be interesting to perform this experiment with $^{18}O_2$ in the center quadrupole to verify that the product ions have incorporated an atom from molecular oxygen. It would be worthwhile for future investigators to engage in research involving reactions of anions and O_2 to determine if oxygen-induced fragmentation has analytical utility. The location of double bonds in fatty acids, for example, is an important area of research, and perhaps reactions of oxygen could be used for analytical purposes with anions which contain a conjugated diene moiety. Also, other reactions of anions with neutral reagents have been characterized in a flowing afterglow apparatus, and it would be worthwhile to investigate similar model systems on a TQMS to determine if the same chemistry is observed. Some interesting results in this dissertation show that the buffering gas used in electron capture ionization of α- and β-ionone affects the appearance of the mass spectrum. These results suggest that ion/molecule

reactions or reactions involving radicals may be occurring in the ion source, and exploring these phenomena in a systematic study would be interesting.

One of the collaborative studies described in this dissertation involves the MS/MS analysis of dexamethasone. Sufficient selectivity is provided by the chemical oxidation procedure along with ionization by electron capture to permit sample introduction into the mass spectrometer via the direct insertion probe when selected reaction monitoring is employed. Use of the direct insertion probe rather than the gas chromatograph significantly simplifies and shortens the analysis of dexamethasone in plasma. Where applicable, the selected reaction monitoring approach will continue to provide a simple and rapid alternative to the selected ion monitoring approach for the analysis of low-level analytes in complex biological matrices.

Other studies include those involving ion/molecule reactions of carbonyl compounds and alcohols. Evidence for alkylation occurring on the carbonyl oxygen is presented. A detailed study of the ion/molecule reaction of protonated acetaldehyde and methanol is described. Although structural studies of these types did not lead to analytical applications, they demonstrate the versatility of the TQMS in the determination of ionic structures. It is important that the chemistry be understood before attempting to find analytical applications for the chemistry. Further work needs to be carried out in the study of protonated carbonyl compounds with alcohols before assessing the analytical utility for such reactions. Perhaps, in general, protonated carbonyls are methylated on the carbonyl oxygen in reaction with methanol. This may be useful in developing methodology for selectively detecting these compounds. Also, these types of studies may be useful in the study of larger protonated species where the location of the proton is not known. Once reactions of this sort are characterized with

smaller molecules, a potential application for this reaction is in probing the location of a proton in multifunctional-group compounds.

Finally, some results are described which demonstrate that certain protonated molecules undergo a silicon-hydrogen exchange reaction with hexamethyldisilazane (HMDS). These preliminary studies indicate that gas-phase derivatization forming a silylated product ion can be observed in a TQMS, but the selectivity of HMDS for protonated molecules remains unknown. It appears that HMDS reacts with protonated ketones and protonated amines. This gas-phase silylation reaction may be useful in peptide sequencing studies, as the site of protonation on a peptide is usually at the amino terminal group. Formation of the silylated product ion intermediate may produce excess energy which perhaps could be expended and redistributed, directing the cleavage of the peptide in a reaction-induced fragmentation sequence.

In closing, the data shown in this dissertation give a glimpse of the variety of analytical applications offered by implementing gas-phase ion/molecule reactions on a triple quadrupole mass spectrometer. Certainly, as future researchers are engaged in the study of ion/molecule reactions, this exciting field will supply the mass spectrometry community with many more analytical applications based on the unique chemistry ions exhibit in reaction with selected neutral reagents.

LIST OF REFERENCES

LIST OF REFERENCES

1. K.L. Busch, G.L. Glish, S.A. McLuckey, *Mass Spectrometry / Mass Spectrometry* , VCH Publishers: Deerfield, FL, 1988.

2. F.W. McLafferty, Ed. *Tandem Mass Spectrometry* Wiley: New York, 1983.

3. R.A. Yost and C.G. Enke, *Anal. Chem.* , **51**, 1251A (1979).

4. R.A. Yost, C.G. Enke, D.C. McGilvery, D. Smith and J.D. Morrison, *Int. J. Mass Spectrom. Ion Phys.*, **30**, 127 (1979).

5. R.A. Yost and C.G. Enke, *J. Am. Chem. Soc.* **100**, 2274 (1978).

6. P.H. Dawson, Ed. *Quadrupole Mass Spectrometry and Its Applications,* Elsevier: NY, 1976.

7. P.H. Dawson and Y. Bingqi, *Int. J. Mass Spectrom. Ion Processes,* **56**, 25 (1984).

8. P.E. Miller and M.B. Denton, *J. of Chem. Educat.* **63**, 617 (1986).

9. P.E. Miller and M.B. Denton, *Int. J. Mass Spectrom. Ion Processes,* **72**, 223 (1986).

10. J.E.P. Syka and A.E. Schoen, *Int. J. Mass Spectrom. Ion Processes,* **96**, 97 (1990).

11. A.G. Harrison, *Chemical Ionization Mass Spectrometry*, CRC Press, Inc.:Boca Raton, Florida, 1983.

12. H. Mestdagh, N. Morin and C. Rolando, *Org. Mass Spectrom.*, **21**, 321 (1986).

13. R.M. Caprioli, *Anal. Chem.*, **62**, 477A (1990).

14. E.C. Huang, T. Wachs, J.J. Conboy and J.D. Henion, *Anal. Chem.*, **62**, 713A (1990).

15. R.D. Smith, C.J. Barinaga and H.R. Udseth, *J. Phys. Chem.* **93**, 5019 (1989).

16. S.F. Wong, C.K. Meng and J.B. Fenn, *J. Phys. Chem.* , **92**, 546 (1988).

17. TSQ-70 Operator's Manual, Finnigan MAT, 1984.

18. M. Vincenti, J. Schwartz, R.G. Cooks, A.P. Wade and C.G. Enke, *Org. Mass Spectrom.* **23**, 579 (1988).

19. J.C. Schwartz, A.P. Wade, C.G. Enke and R.G. Cooks, *Anal. Chem.* **62**, 1809 (1990).

20. K. Levsen and H. Schwarz, *Mass Spec. Reviews,* **2**, 77 (1983).

21. P.H. Dawson, *Int. J. Mass Spectrom. Ion Phys.*, **50**, 287 (1983).

22. K.L. Schey, H.I. Kenttamaa, V.H. Wysocki and R.G. Cooks, *Int. J. Mass Spectrom. Ion Processes,* **90**, 71 (1989).

23. V.H. Wysocki, H.I. Kenttamaa and R.G. Cooks, *Int. J. Mass Spectrom. Ion Processes,* **75**, 181 (1987).

24. S. Naylor and J.H. Lamb, *Rapid Commun. Mass Spectrom.* **4**, 251 (1990).

25. J.S. Brodbelt-Lustig and R.G. Cooks, *Int. J. Mass Spectrom. Ion Processes,* **86**, 253 (1988).

26. H.I. Kenttamaa and R.G. Cooks, *Int. J. Mass Spectrom. Ion Processes,* **64**, 79 (1985).

27. H.I. Kenttamaa and R.G. Cooks, *J. Am. Chem. Soc.*, **107**, 1881 (1985).

28. H.I. Kenttamaa, *Org. Mass Spectrom.*, **20**, 703 (1985).

29. J.L. Holmes, *Org. Mass Spectrom.*, **20,** 169 (1985).

30. MD. A. Mabud, M.J. DeKrey and R.G. Cooks, *Int. J. Mass Spectrom. Ion Processes,* **67**, 285 (1985).

31. MD. A. Mabud, T. Ast and R.G. Cooks, *Org. Mass Spectrom.*, **22**, 418 (1987).

32. M.E. Bier, J.W. Amy, R.G. Cooks, J.E.P. Syka, P. Ceja and G. Stafford, *Int. J. Mass Spectrom. Ion Processes,* **77**, 31 (1987).

33. J.H. Callahan, F.L. King, M.M. Ross, V.H. Wysocki, Surface-Induced Dissociation (SID) In Tandem Quadrupole Mass Spectrometers; Proceedings of the 38th ASMS Conference on Mass Spectrometry and Allied Topics, Tucson, Arizona, June 3-8, 1990.

34. R.E. Tecklenburg Jr. and D.H. Russell, *Mass Spectrom. Reviews*, **9**, 405 (1990).

35. D.F. Hunt, J. Shabanowitz and J.R. Yates III, *J. Chem. Soc. Chem. Commun.*, 548-550 (1987).

36. H. Michel, D.F. Hunt, J. Shabanowitz and J. Bennett *J. Biol. Chem* **263**, 1123 (1988).

37. D.C. McGilvery and J.D. Morrison, *Int. J. Mass Spectrom. Ion Phys.*, **28**, 81 (1978).

38. M.L. Gross and D.C. Rempel, *Science*, **226**, 261 (1984).

39. N.M.M. Nibbering, *Adv. Phys. Org. Chem.* **24**, 1 (1988).

40. E.E. Ferguson, F.C. Fehsenfeld and A.L. Schmeltekopf, *Adv. At. Mol. Phys.*, **5**, 1 (1969).

41. J.M. Van Doren, S. E. Barlow, C.H. DePuy and V.M. Bierbaum, *Int. J. Mass Spectrom. Ion Processes,* **81**, 85 (1987).

42. V.M. Bierbaum, G.B. Ellison, S.R. Leone, in M.T. Bowers, (Ed.) *Gas Phase Ion Chemistry* Vol. 3 Academic Press, Orlando, 1984, Ch. 17.

43. K.M. Ervin, S. Groner, S.E. Barlow, M.K. Gilles, A.G. Harrison, V.M. Bierbaum, C.H. DePuy, W.C. Lineberger and G.B. Ellison, *J. Am. Chem. Soc.*, **112**, 5750 (1990).

44. R. Orlando, D.P. Ridge and B. Munson, *J. Am. Soc. Mass Spectrom.*, **1**, 144 (1990).

45. M. Henchman, *Ion Molecule Reactions*, Franklin, J.L. Ed. Plenum: NY, 1972.

46. T.C. Cairns and E.G. Siegmund, *Rapid Commun. Mass Spectrom.*, **3**, 68 (1989).

47. S.N. Ketkar, J.G. Dulak, W.L. Fite, J.D. Buchnar and S. Dheandhanoo, *Anal. Chem.*, **61**, 260 (1989).

48. K.W.M. Siu, G.J. Gardner and S.S. Berman, *Anal. Chem.*, **61**, 2320 (1989).

49. R. Guevremont, R.A. Yost and W.D. Jamieson, *Biomed. Environ. Mass Spectrom.* **14**, 435 (1987).

50. W.C. Brumley, B.J. Canas, G.A. Perfetti, M.M. Mossoba, J.A. Sphon and P.E. Corneliussen, *Anal. Chem.*, **60**, 975 (1988).

51. M.S. Lee and R.A. Yost, *Biomed. Environ. Mass Spectrom.* , **15**, 193 (1988).

52. W.M. Draper, F.R. Brown, R. Bethen and M.J. Miille, *Biomed. Environ. Mass Spectrom.*, **18**, 767 (1989).

53. M.C. Pumasia and E. Houghton, *Biomed. Environ. Mass Spectrom.*, **18**, 1030 (1989).

54. J. Roboz, E. Nieves, J.F. Holland, M. McCamish and C. Smith, *Biomed. Environ. Mass Spectrom.*, **16**, 67 (1988).

55. W.E. Seifert Jr., A. Ballatore and R.M. Caprioli, *Rapid Commun. Mass Spectrom.*, **3**, 117 (1989).

56. M. Dawson, C.M. McGee, P.M. Brooks, J.H. Vine and T.R. Watson, *Biomed. Environ. Mass Spectrom.*, **17**, 205 (1988).

57. H. Schweer, D. Groessl, S. Gund, K. Soeding and H.W. Seyberth, *Prog. Clin. Biochem. Res.*, **301**, 107 (1989).

58. R. Lorenz, P. Helmer, W. Vedelhover, B. Zimmer and P.C. Weber, *Prostaglandins*, **38**, 157 (1989).

59. T. Krishnaumurthy and E.W. Sarver, *Biomed. Environ. Mass Spectrom,* **15**, 13 (1988).

60. K.Kayganich, J.T. Watson and C. Kilts, J. Ritchie,*Biomed. Environ. Mass Spectrom.*, **19**, 341 (1990).

61. M. Barber and G.B.N. Green, *Rapid Commun. Mass Spectrom.*, **1**, 80 (1987).

62. E.C. Huang and J.D. Henion, *J. Am. Soc. Mass Spectrom.*, **1**, 158 (1990).

63. R.D. Smith, J.A. Loo, C.J. Barinaga, C.G. Edmonds and H.R. Udseth, *J. Am. Soc. Mass Spectrom.*, **1**, 53 (1990).

64. D.F. Hunt, J.R. Yates, J. Shabanowitz, S. Winston and C.R. Hauer, *Proc. Natl. Acad. Sci. USA,* **83**, 6233 (1986).

65. D.F. Hunt, N.Z. Zhu and J. Shabanowitz, *Rapid Commun. Mass Spectrom,* **3**, 122 (1989).

66. K.J. Volk, R.A. Yost and A.B.-Toth, *Anal. Chem.*, **61**, 1709 (1989).

67. K.J. Volk, M.S. Lee, R.A. Yost and A.B.-Toth, *Anal. Chem.*, **60**, 722 (1988).

68. R.D. Smith, J.A. Loo, C.G. Edmonds, C.J. Barinaga and H.R. Udseth, *Anal. Chem.*, **62**, 882 (1990).

69. H. Mestdagh, N. Morin and C. Rolando, *Org. Mass Spectrom.*, **23**, 246 (1988).

70. N.H. Mahle, R.G. Cooks and R.W. Korzeniowski, *Anal. Chem.*, **55**, 2272 (1983).

71. G.G. Dolnikowski, J. Allison and J.T. Watson, *Org. Mass Spectrom.*, **25**, 119 (1990).

72. G.G. Dolnikowski, M.J. Kristo, C.G. Enke and J.T. Watson, *Int. J. Mass Spectrom. Ion Processes,* **82**, 1 (1988).

73. M.T. Kinter and M.M. Bursey, *J. Am. Chem. Soc.*, **108**, 1797 (1986).

74. M.T. Kinter and M.M Bursey, *Org. Mass Spectrom.*, **22**, 775 (1987).

75. M.M Bursey, T.R. Blackburn,W.J. Meyerhoffer and W.A. Mattson; *Org. Mass Spectrom* . **25**, 232 (1990).

76. E.L. White, J.C. Tabet and M.M. Bursey, *Org. Mass Spectrom.*, **22**, 132 (1987).

77. J.-P. Schmit, S. Beaudet and A. Brisson, *Org. Mass Spectrom.* , **21**, 493 (1986).

78. D.D. Fetterolf, R.A. Yost and J.R. Eyler, *Org. Mass Spectrom.*, **19**, 104 (1984).

79. J. Jalonen, *J. Chem. Soc., Chem. Commun.* 872 (1985).

80. J.H. Batey and J.M. Tedder, *J. Chem. Soc. Perkin Trans. II* 1283 (1983).

81. A.L. Mitchel and J.M. Tedder, *J. Chem. Soc. Perkin Trans. II* 667 (1984).

82. A.L. Mitchel and J.M. Tedder, *J. Chem. Soc. Perkin Trans. II* 1197 (1986).

83. J.P. Schmit, P.H. Dawson and N. Beaulieu, *Org. Mass Spectrom.*, **20**, 269 (1985).

84. R.R. Pachuta, H.I. Kenttamaa, R.G. Cooks, T.M. Zennie, C. Ping, C-j Chang and J.M. Cassady, *Org. Mass Spectrom.*, **23**, 413 (1988).

85. E.L. White and M.M. Bursey, *Biomed. Environ. Mass Spectrom.* , **18**, 413 (1989).

86. W.J. Meyerhoffer and M.M. Bursey, *Org. Mass Spectrom.*, **24**, 169 (1989).

87. W.J. Meyerhoffer and M.M. Bursey,. *Org. Mass Spectrom.*, **24**, 246 (1989).

88. G.L. Glish, P.H. Hemberger and R.G. Cooks, *Analytica Chimica Acta,* **119**, 137 (1980).

89. M.T. Kinter and M.M Bursey, *Biomed. Environ. Mass Spectrom.,* **15**, 583 (1988).

90. R. Kostiainen, *Biomed. Environ. Mass Spectrom.,* **16**, 197 (1988).

91. R. Kostiainen, *Biomed. Environ. Mass Spectrom.,* **18**, 116 (1989).

92. D.R. Mueller, B. Domon, W. Blum, W.J. Richter, H. Reiner, R. Keller and P. Fischer, *Org. Mass Spectrom.*, **24**, 157 (1989).

93. R. Kostiainen and S. Auriola, *Rapid Commun. Mass Spectrom.,* **2**, 135 (1988).

94. R. Kostiainen and S. Auriola, *Org. Mass Spectrom.*, **25**, 255 (1990).

95. E. Schroder, *Org. Mass Spectrom.*, **24**, 205 (1989).

96. D.W. Berberich, M.E. Hail, J.V. Johnson and R.A. Yost, *Int. J. Mass Spectrom. Ion Processes,* **94**, 115 (1989).

97. M.E. Hail, D.W. Berberich and R.A. Yost, *Anal. Chem.*, **61**, 1874 (1989).

98. R. Orlando, C. Fenselau and R.J. Cotter, *Org. Mass Spectrom.*, **24**, 1033 (1989).

99. R. Orlando, C. Murphy, C. Fenselau, G. Hansen and R.J. Cotter, *Anal. Chem.*, **62**, 125 (1990).

100. R. Orlando, C. Fenselau and R.J. Cotter, *Rapid Commun. Mass Spectrom,* **4**, 259 (1990).

101. R. Orlando, C. Fenselau and R.J. Cotter, *J. Am. Chem. Soc.*, **112**, 5747 (1990).

102. R. Orlando, C. Fenselau and R.J. Cotter, *Org. Mass Spectrom.*, **25**, 485 (1990).

103. R. Orlando, Private Communication, June, 1990.

104. A. Bjarnason, J.W. Taylor, J.A. Kinsinger, R.B. Cody and D.A. Weil, *Anal. Chem.* **61**, 1889 (1989).

105. D. Kuck, *Mass Spectrom. Reviews*, **9**, 187 (1990).

106. G.G. Dolnikowski, PhD Dissertation, Michigan State University (1987).

107. J.C. Tabet and C. Guenat, *Adv. Mass Spectrom,* 1985 Part B, 831.

108. S.G. Lias, J.E. Barmess, J.F. Liebman, J.L. Holmes, R.D. Levin, W.G. Mallard, *J. Phys. Chem. Ref. Data* 1988, **17**, Suppl. 1.

109. F.W. McLafferty, *Interpretation of Mass Spectra* University Science Books: Mill Valley, California, 1980.

110. M. Karni and A. Mandelbaum,*Org. Mass Spectrom.* **15**, 53 (1980).

111. T. Keough, *Anal. Chem.*, **54**, 2540 (1982).

112 J.-L. M. Abboud, W.J. Hehre and R.W. Taft, *J. Am. Chem. Soc.*, **98**, 6072 (1976).

113. P. N. Rylander, S. Meyerson and H.M Grubb, *J. Am. Chem. Soc.*, **79**, 842 (1957).

114. F. McLafferty and F. Bockhoff, *Org. Mass Spectrom.*, **14**, 181 (1979).

115. F. McLafferty and J.J. Winkler, *J. Am. Chem. Soc.*, **96**, 5182 (1974).

116. P.P. Dymerski and F. McLafferty, *J. Am. Chem. Soc.*, **98**, 6070 (1976).

117. J.M. Buschek, J.J. Ridal and J.L. Holmes, *Org. Mass Spectrom.*, **23**, 543 (1988).

118. S. Olesik, T. Baer, J.C. Morrow, J.J. Ridal, J. Buschek and J.L. Holmes, *Org. Mass Spectrom.*, **24**, 1008 (1989).

119. J.-A. A. Jackson, S.G. Lias and P.J. Ausloos, *J. Am. Chem. Soc.*, **99**, 515 (1977).

120. R.C. Dunbar, *J. Am. Chem. Soc.*, **97**, 1382 (1975).

121. J.Shen, R.C. Dunbar and G.A. Olah, *J. Am. Chem. Soc.*, **96**, 6227 (1974).

122. P. Ausloos, J.A. Jackson and S.G. Lias *Int. J. Mass Spectrom. Ion Phys,* **33**, 269 (1980).

123. R.D. Wieting, R.H. Staley and J.L. Beauchamp, *J. Am. Chem. Soc.*, **96**, 7552 (1974).

124. H.W. Leung, H. Ichikawa, Y.-H. Li and A.G. Harrison, *J. Am. Chem. Soc.*, **100**, 2479 (1978).

125. T. Baer, J.C. Morrow, J.D. Shao and S. Olesik, *J. Am. Chem. Soc.*, **110**, 5633 (1988).

126. V.H. Wysocki and H.I. Kenttamaa, *J. Am. Chem. Soc.*, **112**, 5110 (1990).

127. S. Hammerum, *Mass Spectrom Reviews* , **7**, 123 (1988).

128. R.C. Dougherty, M.J. Whitaker, L.M. Smith, D.L. Stalling and D.W. Kuehl, *Environ. Health Perspec.*, **36**, 103 (1980).

129. F.I. Onuska and K.A. Terry, *Anal. Chem.*, **57**, 801 (1985).

130. R.G. McLoughlin, J.D. Morrison and J.C. Traeger, *Org. Mass Spectrom.*, **14**, 104 (1979).

131. J.A.D. Zeevaart and R.A. Creelman, *Annu. Rev. Plant Physiol. Plant Mol. Biol.*, **39**, 439 (1988).

132. R.A. Creelman, D.A. Gage, J.T. Stults and J.A.D. Zeevart, *Plant Physiol.*, **85**, 726 (1987).

133. D.A. Gage, F. Fong and J.A.D. Zeevart, *Plant Physiol.*, **89**, 1039 (1989).

134. J.A.D. Zeevaart, T.G. Heath and D.A. Gage, *Plant Physiol.*, **91**, 1594 (1989).

135. C.D. Rock and J.A.D. Zeevaart, *Plant Physiol.*, **93**, 915 (1990).

136. A.G. Netting, B.V. Milborrow, G.T. Vaughan and R.O. Lidgard, *Biomed. Environ. Mass Spectrom.* **15**, 375 (1988).

137. E.A. Stemmler and M.V. Buchanan, *Org. Mass Spectrom.*, **24**, 94 (1989).

138. E.A. Stemmler and M.V. Buchanan, *Org. Mass Spectrom.*, **24**, 705 (1989).

139. J.R. Hass, M.D. Friesen and M. Hoffman, *Org. Mass Spectrom.*, **14**, 9 (1979).

140. W.F. Miles, N.P. Gurprasad and G.P. Malis, *Anal. Chem.*, **57**, 1133 (1985).

141. D. Fung, R.K. Boyd, S. Safe and B.G. Chittim, *Biomed. Environ. Mass Spectrom.*, **12**, 247 (1985).

142. K.L. Busch, A. Norstrom, M.M Bursey, J.R. Hass and C.A. Nilsson, *Biomed. Environ. Mass Spectrom.* **6**, 157 (1979).

143. D.F. Hunt, T.M. Harvey and J.W. Russell, *J. Chem. Soc. Chem. Commun.* 151 (1975).

144. B. Arbogast, W.L. Budde, M. Deinzer, R.C. Dougherty, J. Eichelberger, R.P. Foltz, C.C. Grimm, R.A. Hites, C. Sakashita and E. Stemmler, *Org. Mass Spectrom.*, **25**, 191 (1990).

145. B.V. Milborrow, *Chem. Commun.* 966 (1969).

146. S.J. Neill, R. Horgan. In: *Principles and Practice of Plant Hormone Analysis,* Vol. 1, eds, L. Rivier and A. Crosier, pp. 111-167. Academic, London (1988).

147. R.T. Gray, R. Mallaby, G. Ryback and V.P. Williams, *J. Chem. Soc. Perkins Trans.* **2**, 919 (1974).

148. R.A. Creelman and J.A.D. Zeevaart, *Plant Physiol.* **75**, 166 (1984).

149. A.H. Andrist, C.H. DuPuy and R.R. Squires, *J. Am. Chem. Soc.*, **106**, 845 (1984).

150. R.J. Schmitt, V.M. Bierbaum and C.H. DePuy, *J. Am. Chem. Soc.*, **101**, 6443 (1979).

151. V.M. Bierbaum, R.T. Schmitt and C.H. DePuy, *Environ. Health Perspect.* **36**, 119 (1980).

152. P.S. Callery, W.A. Garland and E.K. Fukuda,*Org. Mass Spectrom.*, **24**, 385 (1989).

153. L.J. Sears, J.A. Campbell and E.P. Grimsrud, *Biomed. Environ. Mass Spectrom.* **14**, 401 (1987).

154. C.D. Rock and J.A.D. Zeevaart, *Plant Physiol.* **89**, S-113 (1989).

155. K. Kayganich, T.G. Heath and J.T. Watson, *J. Am. Soc. Mass Spectrom.* **1**, 341 (1990).

156. G. G. Dolnikowski, T.G. Heath, J.T. Watson, J.H. Scrivens and C.H. Rolando *J. Am. Soc. Mass Spectrom.*, in press (1990).

157. G.R. Her and J.T. Watson, *Biomed. Environ. Mass Spectrom,* **13**, 57 (1986).

158. Y. Kasuya, J.R. Althaus, J.P. Freeman, R.K. Mitchum and J.P. Skelly, *J. Pharm. Sci.*, **73**, 446 (1984).

159. R.A. Yost, D.D. Fetterolf, J.R. Hass, D. J. Harvan. A. F. Weston, P.A. Skotnicki and N.M. Simon, *Anal. Chem.*, **56**, 2223 (1984).

160. J.V. Johnson, R.Yost and K.F. Faull, *Anal. Chem.*, **56**, 1655 (1984).

161. H. Schweer, H. W. Seyberth, C.O. Meese and O. Furst, *Biomed. and Environ. Mass Spectrom.*, **15**, 143 (1988).

162. P.H. Dawson, J.B. French, J.A. Buckley, D.J. Douglass and D. Simmons, *Org. Mass Spectrom.*, **17**, 205 (1982).

163. A.J. Alexander and R.K. Boyd, *Int. J. Mass Spectrom. Ion Processes,* **90**, 211 (1989).

164. P.H. Dawson, *Int. J. Mass Spectrom. Ion Phys.*, **43**, 195 (1982).

165. D. F. Hunt and F.W. Crow, *Anal. Chem.*, **50**, 1781 (1978).

166. G. Bouchoux, Y. Hoppilliard and R. Houriet, *New J. Chem.* **11**, 225 (1987).

167. H.E. Audier, C. Monteiro and D. Robin, *Org. Mass Spectrom.*, **24**, 353 (1989).

168. H.E. Audier, D. Berthomieu, P. Hudhomme, C. Monteiro and P. Mourgues, *Org. Mass Spectrom.*, **25**, 87 (1990).

169. J.-P. Morizur, I. Martigny, J. Tortajada and S. Geribaldi, *Org. Mass Spectrom.*, **25**, 89 (1990).

170. C. Wesdemiotis and F.W. McLafferty, *Tetrahedron,* **37**, 3111 (1981).

171. C. Wesdemiotis and F.W. McLafferty, *Org. Mass Spectrom.*, **16**, 381 (1981).

172. A. Maquestiau, C. Jortay, D. Beugnies, R. Flammang, R. Houriet, E. Rolli and G. Bouchoux, *Int. J. Mass Spectrom. Ion Processes,* **82**, 33 (1988).

173. J.C. Kleingeld and N.M.M. Nibbering, *Org. Mass Spectrom.*, **17**, 136 (1982).

174. G. Hvistendahl and D.H. Williams, *J. Am. Chem. Soc.*, **97**, 3097 (1975).

175. R.D. Bowen and A.G. Harrison, *Org. Mass Spectrom.*, **16**, 159 (1981).

176. R.D. Bowen, D.H. Williams, G. Hvistendahl and J.R. Kalman, *Org. Mass Spectrom.*, **13**, 721 (1978).

177. G. Hvistendah. R.D. Bowen and D.H. Williams, *J. Chem. Soc. Chem. Commun.* 294 (1976).

178. F. W. McLafferty and I. Sakai, *Org. Mass Spectrom.*, **7**, 971 (1973).

179. W. Wagner, H. Heimbach and K. Levsen, *Int. J. Mass Spectrom. Ion Phys.*, **36**, 125 (1980).

180. A.G. Harrison, T. Gaumann and D. Stahl, *Org. Mass Spectrom.*, **18**, 517 (1983).

181. S.J.A. Curtis and A.G. Harrison, *J. Am. Soc. Mass Spectrom.*, **1**, 301 (1990).

182. R.H. Nobes and L. Radom, *Org. Mass Spectrom.*, **19**, 385 (1984).

183. D.J. McAdoo and C.E. Hudson, *Int. J. Mass Spectrom Ion Processes,* **88**, 133 (1989).

184. G. Bouchoux, F. Djazi, Y. Hoppilliard, R. Houriet and E. Rolli, *Org. Mass Spectrom.*, **21**, 209 (1986).

185. U. Buck; X. Gu, C. Lauenstein and A. Rudolph, *J. Phys. Chem.* **92**, 5561 (1988).

186. S. Morgan and A.W. Castleman, *J. Phys. Chem.* **93**, 4544 (1989).

187. J.M.S. Henis, *J. Am. Chem. Soc.*, **90**, 844 (1968).

188. A. J. Illies, *Org. Mass Spectrom.*, **25**, 73 (1990).

189. C. Beaugrand, D. Jaouen, H. Mestdagh and C. Rolando, *Anal. Chem.*, **61**, 1447 (1989).

190. P.W. Tiedemann and J.M. Riveros, *J. Am. Chem. Soc.*, **96**, 185 (1974).

191. A.G. Harrison, *Can. J. Chem.* **64**, 1051 (1986).

192. T.W.G. Solomons, *Organic Chemistry,* Wiley: New York, 1980.

193. K. Beimann, *Biomed. Environ. Mass Spectrom.*, **16**, 99 (1988).